PALAEOCLIMATE RECONSTRUCTION OF THE LAST GREENHOUSE-ICEHOUSE TRANSITION BASED ON GEOCHEMICAL AND MICROPALAEONTOLOGICAL RECORDS FROM CENTRAL MISSISSIPPI, US GULF COASTAL PLAIN

By

Marcelo Augusto De Lira Mota

A thesis submitted to the University of Birmingham

for the degree of DOCTOR OF PHILOSOPHY

School of Geography, Earth

and Environmental Sciences

College of Life and Environmental

Sciences

University of Birmingham

July 2019

UNIVERSITY OF
BIRMINGHAM

University of Birmingham Research Archive

e-theses repository

This unpublished thesis/dissertation is copyright of the author and/or third parties. The intellectual property rights of the author or third parties in respect of this work are as defined by The Copyright Designs and Patents Act 1988 or as modified by any successor legislation.

Any use made of information contained in this thesis/dissertation must be in accordance with that legislation and must be properly acknowledged. Further distribution or reproduction in any format is prohibited without the permission of the copyright holder.

ABSTRACT

During the Eocene-Oligocene Transition (EOT; ~34.4-33.7 Ma), the Earth experienced a major shift in climate state, from so called “greenhouse” to “icehouse” conditions, with the first formation of the modern continental-scale ice sheet on Antarctica (Oi-1 event: ~33.7 Ma). This transition was associated with deep-sea cooling, glacioeustatic sea level fall, worldwide regressions, along with major disturbances in the global carbon cycle and ecosystems. To investigate this climatic disruption, high-resolution coccolith fraction (<20 μm) carbonate stable oxygen ($\delta^{18}O$) and carbon ($\delta^{13}C$) isotope records (~7 ka resolution), palynological and calcareous nannofossil assemblage (~26 ka resolution) records, and bulk sediment X-ray fluorescence analyses (<10 ka resolution) have been generated from a continuously cored (~137 m) and substantially expanded (~4.7 cm ka^{-1}) succession of upper Eocene-lower Oligocene (~4 Ma) mid-shelf marine clays from the central Mississippi, US Gulf Coastal Plain – the Mossy Grove Core (MGC). Based on a refined age-depth model, this multiproxy analysis revealed that the increasing export of nutrients from the Southern Ocean to the tropical and sub-tropical oceans enhanced marine primary production in these regions, further leading to increased sequestration of atmospheric CO_2 through an invigorated biological pump. We also found evidence that extraterrestrial impacts may have induced sulfate-aerosol-driven climate forcing, triggering positive feedback mechanisms, and intensifying and/or sustaining the cooling. Further analysis also demonstrated that a significant sea level fall (~34.5 Ma) preceded the Oi-1 event by ~800 ka and represents the first stage of large-scale expansion of the East Antarctica Ice Sheet. This challenges the current view that the dynamics of the EOT are dominated by global cooling during the earliest stages, which then precondition the system to continental-scale ice-sheet expansion in the later stages. We

also propose that the earliest stages of the major EOT eustatic sea-level fall had a disproportionate effect on global biogeochemistry, by causing the first major incision of organic- and nutrient-rich coastal low lands that had been accreting under warm, high sea-level greenhouse conditions for tens of millions of years.

RESUMO

Durante a Transição Eoceno-Oligoceno (EOT; ~34,4-33,7 Ma), a Terra passou por uma importante mudança no estado climático, das chamadas condições de "*greenhouse*" para as condições de "*icehouse*", ocorrendo então a primeira formação da moderna camada de gelo em escala continental na Antártida (evento Oi-1: ~33,7 Ma). Essa transição esteve associada ao resfriamento do mar profundo, à queda glacio-eustática do nível do mar, a regressões em escala global, além de importantes distúrbios no ciclo global do carbono e nos ecossistemas. Para investigar esta perturbação climática, registros em alta resolução (~7 ka) de isótopos estáveis de oxigênio ($\delta^{18}O$) e carbono ($\delta^{13}C$) da fração de cocólitos (<20 μm) de carbonatos, registros de associações palinológicas e de nanofósseis calcários (resolução: ~26 ka) e análises de fluorescência de raios-X de rocha total (resolução: <10 ka) foram gerados a partir de uma sucessão continuamente testemunhada (~137 m) e substancialmente expandida (~4,7 $cm.ka^{-1}$) de argilas marinhas de plataforma média do Eoceno superior ao Oligoceno inferior (~4 Ma), região central do Mississippi, Planície Costeira do Golfo dos EUA – o "Mossy Grove Core" (MGC). Com base em um refinado modelo de idade-profundidade, essa análise *multiproxy* revelou que a crescente exportação de nutrientes do Oceano Austral para os oceanos tropicais e sub-tropicais aumentou a produção primaria marinha nestas regiões, levando ainda a elevado sequestro de CO_2 atmosferico por meio de uma bomba biológica revigorada. Tambem encontramos evidencias de que impactos extra-terrestres podem ter induzido forçamento climático por aerossóis de sulfato, desencadeando mecanismos de retroalimentação positivos e intensificando ou sustentando o resfriamento. Analises adicionais demonstraram ainda que significativa queda no nivel do mar (~34,5 Ma) precedeu o evento Oi-1 em ~800 ka e representa o primeiro estagio de expansão em larga escala da

Calota de Gelo da Antartida Oriental. Isto desafia a atual visão de que a dinâmica do EOT é dominada por resfriamento global nos primeiros estágios, que então precondiciona o sistema para expansão de calotas de gelo em escala continental nos estágios finais. Tambem propomos que os estágios iniciais da principal queda no nível eustático do mar tiveram um efeito desproporcional na biogeoquímica global, causando a primeira importante incisão das terras costeiras baixas e ricas em nutrientes e matéria orgânica, acumuladas sob condições "*greehouse*" quentes e com nível do mar elevado por dezenas de milhões de anos.

To my parents and wife

[It] is the little causes, long continued, which are considered as bringing about the greatest changes of the Earth.

James Hutton

ACKNOWLEDGEMENTS

In the last four years, it was not only in Earth Sciences that I discovered new branches and expanded knowledge and experience. In the field of human relationships, I have rediscovered the meaning of Gratitude. After all, developing a study of this magnitude and complexity alone would be humanly impossible. That is why I want to thank all those who contributed to me to reach the scope of this task. I thus give my thanks to:

My Sponsor, The National Council for Scientific and Technological Development (CNPq), for providing me a nearly 4-year scholarship to study abroad and for performing efforts to accurately address all my needs, NEVER delaying payments and ALWAYS answering my requests;

My Lead Supervisor, Dr Tom Dunkley Jones, who I first met between the 25th and the 27th of November 2013 during a short course on Micropalaeontology promoted by the Federal University of Pernambuco (UFPE), for being so patient in waiting for me to transpose all the bureaucratic processes that brought me to the UK, and ever since, for teaching me how to make science with focus, devotion, excellence, and ethics;

My Co-supervisors for supporting me at different stages of my PhD – Dr Haydon Mort, who introduced me to the practical English language, motivating me to perform my first academic presentation in this language (still in Brazil), and for helping me to build up my "bridge" to the UK; Dr Guy Harrington and Dr James Bendle, for initiating me into the fields of Palynology and Palaeoclimatology, key topics of my thesis;

Dr Carlos D'Apolito, for introducing me to the United Kingdom, Birmingham and the School of Earth Sciences of the University of Birmingham, and for giving me the initial support during my adaptation in my new land and Institution;

Dr Kirsty Edgar, for accepting the role of examining this thesis and for following my research with so much interest and attention since nearly the first months, always providing wise and helpful suggestions;

Dr Fabienne Marret-Davies, for accepting the role of examining this thesis, which honors me, since it is from her co-authorship one of the first and most important works I read in my PhD and that founded this thesis;

All my officemates and colleagues, Amy Jones, Andy Jones, Asrin Azmi, Dan Cashmore, Dana Ridha, Emma Dunne, Emma Hanson, Frederike Wittkopp, Jack Richardson, Juan Benito, Juan Pablo, Kate Ashley, Mike McKnight, Nursufiah Sulaiman, Ulrike Baranowski, and Zainab Al Rawahi, for all the support, fellowship, and countless scientific and technical aids;

Aruna and Gretchel, for providing all department-related help;

Dr James Wheeley and Dr Ian Boomer, for reintroducing me to the field geology;

Dr Sarah Greene, for leading me to the gratifying public engagement activities I participated in my PhD life;

The University of Birmingham, for providing me all necessary infrastructure, facilities and resources for me to fulfil my duties;

All my instructors and colleagues from the Urbino Summer School in Paleoclimatology (Italy, July 2018), where I learned the fundamentals and applications of this branch of the Earth Sciences;

All my instructors and colleagues from the MagellanPlus Workshop, held in Southampton (UK, August 2018), where I experienced the challenges of preparing a deep ocean drilling proposal;

All new friends from the Utrecht University (The Netherlands), Frida Hoem, Dr Appy Sluijs, Dr Peter Bijl, and Natasja Welters, for expanding my experience as a Palynologist;

All friends from the IODP Expedition 379 (January-March 2019), with whom I learned that teamwork made with effort, focus and patient can provide great results;

And last, but no least, I thank God, my wife, family, and friends for all support!

To you all: MUITO OBRIGADO!

LIST OF CONTENTS

CHAPTER 1:INTRODUCTION 1

CHAPTER 2:THE EOCENE-OLIGOCENE TRANSITION: UNDERSTANDING THE DYNAMICS OF THE ANTARCTIC CRYOSPHERE 8

2.1. OVERVIEW 8

2.2. CAUSAL MECHANISMS 10

2.3. CONSEQUENCES OF THE EOT 14

2.4. WHY WAS THE EOT A UNIQUE EVENT? 22

CHAPTER 3:MATERIALS AND METHODS 25

3.1. REGIONAL GEOLOGICAL CONTEXT 25

3.2. MOSSY GROVE BOREHOLE 28

3.3. PALYNOLOGICAL PREPARATION TECHNIQUES 29

3.4. PALYNOMORPH ASSEMBLAGE CHARACTERIZATION 31

3.5. PALYNOMORPH-BASED PALAEOENVIRONMENTAL ANALYSIS 31

3.6. CALCAREOUS NANNOFOSSIL ASSEMBLAGE CHARACTERIZATION 38

3.7. BULK STABLE-ISOTOPE DATA 39

3.8. X-RAY FLUORESCENCE (XRF) DATA 40

CHAPTER 4:ORGANIC-WALLED DINOFLAGELLATE CYST BIOSTRATIGRAPHY OF THE UPPER EOCENE TO LOWER OLIGOCENE YAZOO FORMATION, US GULF COAST 42

4.1. INTRODUCTION 42

4.2. REGIONAL GEOLOGICAL CONTEXT 47

4.3. MATERIALS AND METHODS 53

4.3.1. Mossy Grove Borehole *53*

4.3.2. Palynological preparation techniques *55*

4.3.3. Dinocyst assemblage characterisation *56*

4.3.4. Nannofossil assemblage characterisation *56*

4.4. RESULTS 57

4.4.1. Dinocyst distribution *57*

4.4.2. Nannofossil biostratigraphy *59*

4.4.3. Dinocyst biostratigraphic framework *60*

4.4.4. Integrated age model *69*

4.5. CONCLUSIONS 72

CHAPTER 5:SEA-LEVEL FALL AND CARBON CYCLE PERTURBATIONS AT THE ONSET OF ANTARCTIC GLACIATION **73**

CHAPTER 6:ECOSYSTEM RESPONSE TO LATE EOCENE CLIMATIC AND IMPACT EVENTS **87**

6.1. INTRODUCTION 87

6.2. MATERIALS AND METHODS 92

6.3. RESULTS 95

6.4. DISCUSSION 102

6.4.1. Implications for the North Atlantic circulation patterns *102*

Regime 1 (R1; ~37.6-36.2 Ma): Reconfiguration of oceanic gateways? *104*

Regime 2 (R2; ~36.2-34.9 Ma): Evidence of a late Eocene AMOC-like system? *106*

Regime 3 (R3; ~34.9-34.1 Ma): An early-stage EOT-1 sea-surface cooling? *110*

6.4.2. Implications for extraterrestrial impacts *112*

6.4.3. Concluding remarks *113*

CHAPTER 7:CONCLUSION **117**

APPENDICES **121**

Total word count: 28,525

(excluding tables and captions)

LIST OF ILLUSTRATIONS

Figure 1. Summary figure of the EOT. 9

Figure 2. Schematic illustration of factors influencing the distribution of dinocysts and typical palynomorphs. 32

Figure 3. Photomicrographs of selected palynomorphs found at MGC and used for palaeoenvironmental reconstruction purposes. 34

Figure 4. Palaeogeographic reconstruction showing location of the Mossy Grove, #1 Wayne and #1 Young cores, as well as St. Stephens Quarry outcrop. 48

Figure 5. Simplified stratigraphic correlation chart of upper Eocene to lower Oligocene sedimentary rocks in the Mississippi-Alabama area. 50

Figure 6. Stratigraphic correlation between the Mossy Grove Core and other three sections from Mississippi and Alabama. 52

Figure 7. Semiquantitative range chart of dinocyst taxa encountered at the Mossy Grove core, central Mississippi, US Gulf Coastal Plain, including calcareous nannoplankton zonation. 58

Figure 8. Refined age-depth model of the Mossy Grove Core. 70

Figure 9. Palaeogeography and lithology of Mississippi and Alabama sector of the US Gulf Coastal Plain according to Tew and Mancini (1995). 77

Figure 10. Geochemical and micropalaeontological records of the MGC (Part 1). 80

Figure 11. Geochemical and micropalaeontological records of the MGC (Part 2). 81

Figure 12. Scatter plot of genera ordination from principal component analysis (PCA). 98

Figure 13. Geochemical and micrpalaeontological records of the MGC (Part 3). 101

Figure 14. Late Eocene to early Oligocene geochemical and micropalaeontological records from the MGC compared to Northern and Southern Hemisphere multiproxy records. 103

Figure 15. Palaeogeographic reconstruction of the North Atlantic showing oceanic circulation patterns and expected/inferred temperature trends under two distinct scenarios. 107

LIST OF TABLES

Table 1. List of bioevents, biohorizons and calibrated ages, updated to the Timescale of Westerhold et al. (2014). 59

Table 2. List of dinocyst bioevents recorded in the section. 61

Table 3. Age assignments of the major late Eocene impact structures. 91

Table 4. Empirically established palaeoecological affinities of selected dinocyst genera found at MGC. 96

LIST OF ABBREVIATIONS

ACC: Antarctic Circumpolar Current.

AMOC: Atlantic Meridional Overturning Circulation.

$CaCO_3$: calcium carbonate.

CCD: calcite compensation depth.

CO_2: carbon dioxide.

CO_3^{2-}: carbonate.

Dinocysts: organic-walled dinoflagellate cysts.

DIC: dissolved inorganic carbon.

EAIS: East Antarctic Ice Sheet.

EECO: early Eocene Climatic Optimum.

EOB: Eocene-Oligocene Boundary.

EOGM: early Oligocene Glacial Maximum.

EOT: Eocene-Oligocene Transition.

ETM2: Eocene Thermal Maximum 2.

IPCC: Intergovernmental Panel on Climate Change.

LOW: late Oligocene Warming.

MECO: middle Eocene Climatic Optimum.

MGC: Mossy Grove Core.

Mi-1: Miocene Isotopic Event 1.

MMCO: middle Miocene Climatic Optimum.

MMCT: middle Miocene Climate Transition.

NADW: North Atlantic Deep Water.

PAL: pre-industrial atmospheric levels.

PETM: Paleocene-Eocene Thermal Maximum.

Ple: Pleistocene.

Pli: Pliocene.

Priabon.: Priabonian.

ppmv: parts per million by volume.

SSQ: Saint Stephens Quarry.

SST: sea-surface temperature.

VPDB: “Vienna Pee Dee Belemnite”, i.e., the standard established based on a Cretaceous marine fossil, *Belemnitella americana*, which was from the Peedee Formation in South Carolina.

WAIS: West Antarctic Ice Sheet.

$\delta^{13}C$: carbon isotope ratio.

$\delta^{13}C_{bf}$: benthic foraminiferal carbon isotope ratio.

$\delta^{18}O$: oxygen isotope ratio.

$\delta^{18}O_{bf}$: benthic foraminiferal oxygen isotope ratio.

$\delta^{18}O_{sw}$: seawater oxygen isotope ratio.

CHAPTER 1: INTRODUCTION

By the year 2100, it is predicted the concentration of carbon dioxide (CO_2) will rise to values between ~790 and 1,150 parts per million by volume (ppmv), if anthropogenic carbon emissions to the atmosphere continue to grow at the same rate as in recent years (IPCC, 2013). This represents an increase of ~2.8 to 4.1 times pre-industrial levels of atmospheric CO_2 (280 ppmv). Multiproxy reconstructions of CO_2 records (Anagnostou et al., 2016; Pagani et al., 2005, 2011; Pearson et al., 2009; Zhang et al., 2013) show that the last time in Earth's history the concentration of carbon dioxide in the atmosphere reached values as high as these predicted values for 2100, was ~34 Ma ago, during the late Eocene. The late Eocene is a key interval in the climate history of the past hundred million years or more, as after a multi-million year decline in atmospheric CO_2 concentrations (Anagnostou et al., 2016; Pagani et al., 2005, 2011; Pearson et al., 2009; Zhang et al., 2013) and associated planetary cooling, East Antarctic continental-scale ice sheets formed for the first time in the Cenozoic (Zachos et al., 2001, 2008). It has been argued, therefore, that there is a threshold in atmospheric CO_2 concentration, on the order of ~750 ppmv, below which a descending snowline intersects high-elevation regions of Antarctica, permitting the coalescence of large ice caps into a more permanent feature – the East Antarctic Ice Sheet (EAIS) – almost insensitive to orbital forcing and seasonal melting (DeConto et al., 2008; DeConto and Pollard, 2003; Pearson et al., 2009). Although there is likely strong hysteresis in this system, with warmer (and higher CO_2) climate conditions required for ice sheet melting than for growth, the same feedbacks that cause this hysteresis (e.g. ice – albedo / ice – elevation feedbacks) also pre-conditions the system for rapid non-linear changes in state (DeConto et al., 2008; DeConto and Pollard, 2003). If anthropogenic carbon emissions do not change in a dramatic way, by the end of

the century, atmospheric CO_2 concentrations will approach the levels of greenhouse gas forcing at which the EAIS first formed (DeConto et al., 2008; DeConto and Pollard, 2003). Understanding and predicting the behaviour of the EAIS around these thresholds of climate forcing, and its role in the wider Earth System, should provide strong cautionary evidence to support the mitigation of 21st century anthropogenic climate change. These thresholds concern the first growth of the EAIS, but both data and models show that the West Antarctic Ice Sheet (WAIS) is vulnerable at lower CO_2 levels (~250-300 ppmv) and a threshold leading to its collapse may have been passed already (Joughin et al., 2014; McKay et al., 2016b; Tripati et al., 2009).

Studies of global change are required to try and consider the Earth's climate as a complex system, with interacting components represented by the atmosphere (air), the biosphere (ecosystems, biomes), the cryosphere (polar ice caps, sea ice, permafrost, seasonal snow cover, mountain glaciers), the hydrosphere (oceans, lakes, rivers) and the lithosphere (tectonic and magmatic processes), which are all related through the dynamic exchange of matter and energy through multiple processes (Wild et al., 2013). Through changes in surface albedo and atmospheric radiative absorption, these components ultimately affect the planetary energy budget (Wild et al., 2013). The climate system is thus under the continuous action of external forcing (orbital changes in insolation; greenhouse gas concentrations) and internal feedback mechanisms (vegetation-ice-albedo feedbacks; biosphere responses; weathering; ocean dynamics). While the external forcing tends to "push" the planet into warmer or colder climate states, feedbacks either amplify or attenuate the effects of this climate forcing. Both aspects play an important role in understanding equilibrium climate sensitivity and predicting future climate states (Rohling et al., 2012; Skinner, 2012).

Understanding the complexity of these systems has long been a challenge for geoscientists (Shackleton and Kennett, 1975), and the motivation for efforts to establish long-term records of climate proxies. Especially successful has been the development of stable isotope records of oxygen ($\delta^{18}O$) and carbon ($\delta^{13}C$) from benthic foraminifera (Zachos et al., 1996), which provide insights into the long-term evolution of the Earth's climate, cryosphere and global carbon cycling (Zachos et al., 2001). Benthic foraminiferal oxygen isotope records ($\delta^{18}O_{bf}$) record seafloor conditions and are strongly controlled by global ice volume and temperatures at the site of growth (Pearson, 2012). Since most of these records come from deep ocean sediments, at intermediate or deeper water depths, and assuming that high-latitude deep-water formation prevailed over the last 50 Ma, this proxy is considered a better indicator of long-term global temperature changes, than surface ocean or continental records, which are more susceptible to seasonal, latitudinal and geographical variations (Lear et al., 2000). The deconvolution of the impacts of global ice volume – through changes in local seawater $\delta^{18}O_{sw}$ - from water temperature effects on $\delta^{18}O_{bf}$ requires an independent assessment of deep-water temperature, which is typically from Mg/Ca palaeothermometry undertaken on the same benthic foraminiferal calcite (Lear et al., 2000). Recent efforts have generated long-term paired records of $\delta^{18}O_{bf}$ and Mg/Ca, which have provided unprecedented records of deep-water temperature and ice volume since the Late Cretaceous (Cramer et al. 2011).

Similar long-term benthic foraminiferal $\delta^{13}C$ records are widely used to track first-order shifts in the global carbon cycle, especially the movement of carbon between the lithosphere and readily exchangeable reservoirs on the planetary surface – the hydrosphere (ocean), atmosphere, and biosphere (marine and terrestrial biomass and soils) (Ridgwell and Edwards, 2009). Carbon isotopic fractionation that occurs during

exchange between these reservoirs – especially between inorganic and organic components – combined with the relative flux between the lithospheric (long-term storage) and exchangeable reservoirs, drives variations in the carbon isotopic composition ($\delta^{13}C$) of oceanic dissolved inorganic carbon (DIC) through time (Ridgwell and Edwards, 2009). In general, $\delta^{13}C$ values are highly negative in terrestrial vegetation and soils (-22 to -25‰), moderately negative in the atmosphere (-6.5‰), to slightly positive in surface ocean DIC (2‰) (Ridgwell and Edwards, 2009). As with terrestrial plants, phytoplankton discriminates against the heavier carbon isotope (^{13}C) during photosynthesis (Rau et al., 1996). This ultimately enriches the surface ocean DIC in ^{13}C, to a degree dependent on the strength of primary production and export of this production from surface to deeper waters (Sarmiento and Gruber, 2002). Conversely, deep waters tend to be depleted in ^{13}C (lower $\delta^{13}C$ than surface waters) to an extent that is dependent on water mass source, age and overlying productivity (Sarmiento and Gruber, 2002).

The compilation of benthic foraminiferal oxygen and carbon isotope data from over forty deep-sea sites is the fundamental reference point for understanding long-term Cenozoic climate evolution (Zachos et al., 2001, 1996, 2008). These compiled isotope records have been constantly improved (Cramer et al., 2011), and even extended back through the Late Cretaceous (Cramer et al., 2011; Friedrich et al., 2012). These records reveal the intricate path of Earth's climate evolution, from short-term, orbital-scale variability to multi-million-year trends driven by long-term tectonic and greenhouse gas forcing. There are also rapid transient events and abrupt transitions, which stand out well above "normal" background variability in terms of their rate and/or amplitude of change, and are normally accompanied by a major perturbation in the global carbon cycle as inferred from carbon isotope data (Zachos et al., 2001). One of these aberrations, in fact

the most sudden and prominent in the last 112 Ma (Cramer et al., 2011; Friedrich et al., 2012), occurred ~34 Ma, between the Eocene and the Oligocene epochs, and shifted Earth's climate into a new mode that has persisted ever since. This thesis focuses on generating new high-resolution climate and biotic records of this event to better understand the rates of change and mechanisms operating during these non-linear transitions involving the Antarctic cryosphere. As part of wider palaeoclimate research into the past dynamics of the Antarctic ice sheets, I hope the analyses of this event may inform wider society about the risks of approaching critical thresholds in the climate system.

To reach its scope, this thesis content was split into five major chapters, each of which concerns a particular aspect of this study. Whereas Chapters 2 and 3 were dedicated to literature review on key topics and methodological approaches covered by this study, Chapters 4, 5 and 6 present detailed results and discussion that address the aims of this work. Data for the entire thesis are provided in Supplementary Material (SM). Furthermore, Chapter 4 was published in the *Journal of Micropalaeontology* (39, 1–26, 2020) and Chapter 5 was prepared for submission to a short-format journal but has not yet been submitted. All ages in this work were calibrated from the literature to the timescale of Westerhold et al. (2014); where necessary the original quoted age from within a publication, and consistent with the timescale originally used, is given in brackets.

In order to emphasize the importance of the climate transition between the late Eocene and the early Oligocene and the mechanisms and sensitivities of Cenozoic climate, **Chapter 2** provides a review on its causes and consequences, along with a summary on

the current state of understanding based on fossils and palaeoclimatic proxies for the Eocene–Oligocene climate change.

Chapter 3, presents a detailed description of the Materials and Methods used in this work, starting with a brief discussion on the upper Eocene-lower Oligocene sucession of the Gulf Coastal Plain, followed by a chronostratigraphic characterisation of the study site. Preparation protocol and assemblage characterization of organic-walled and carbonate microfossils are also presented, along with summaries of proxy analysis applied to the thesis, i.e., palynomorph-based palaeoenvironmental reconstruction, and data generation from bulk-stable isotopes and X-ray fluorescence.

Chapter 4 presents new dinocyst biostratigraphic data from the study site, the Mossy Grove Core, Jackson, Mississippi, and, since sediments yielded well-preserved and highly abundant palynomorph assemblages, this chapter includes illustrated descriptions of these assemblages. This chapter was published in the *Journal of Micropalaeontology* (39, 1–26, 2020).

New high-resolution (~6 ka) fine-fraction (<20μm) carbonate stable oxygen ($\delta^{18}O$) and carbon ($\delta^{13}C$) isotope analyses, bulk sediment X-ray fluorescence (<10 ka) data and palynological (~26 ka) analyses are presented in **Chapter 5**, in order to generate a multiproxy record through the late Eocene-early Oligocene. These ultimately provided an entirely new sea-level change record across the critical late Eocene-early Oligocene interval, with unequivocal linkages with coeval large-scale ice-sheet expansion on Antarctica.

Chapter 6 aims to document potential changes in sub-tropical North Atlantic surface waters associated with proposed late Eocene variations in Atlantic Meridional Overturning Circulation (AMOC). It uses plankton-based biotic records from the same

study site on the US Gulf Coast to assess water mass changes through the late Eocene. It also interrogates the effects of major late Eocene impact events and their potential role in the onset of the Eocene-Oligocene Transition.

Finally, through the convergence of the results exposed in the previous three chapters, the **Conclusion** of this Thesis integrates the data provided by all the proxies adopted throughout the entire chronostratigraphic range of the studied section in order to assess the dynamics of the EOT from a more general perspective, in a deep-time context.

CHAPTER 2: THE EOCENE-OLIGOCENE TRANSITION: UNDERSTANDING THE DYNAMICS OF THE ANTARCTIC CRYOSPHERE

2.1. Overview

The relatively rapid, widespread glaciation of Antarctica during the Eocene-Oligocene Transition (EOT: ~34.4-33.7 Ma) marks the climax of a shift from the warmer Cretaceous and early Paleogene climates towards the typical colder climate state that prevails since the Oligocene (Westerhold et al., 2014; Zachos et al., 2001) (Figure 1). This greenhouse-to-icehouse climate transition was first recognised by an abrupt ~1.0-1.5±0.1‰ increase in benthic foraminifera oxygen stable isotope ratio ($\delta^{18}O_{bf}$) close to the Eocene-Oligocene boundary (Coxall et al., 2005; Kennett and Shackleton, 1976; Miller et al., 1987). The presence of distinct rapid positive "steps" in the first high-resolution benthic foraminiferal oxygen isotope ($\delta^{18}O$) records across this event (Figure 1) was initially interpreted as representing at least two pulses of accelerated ice-sheet growth (Coxall et al., 2005). These steps appear to be orbitally paced, with a duration of 40 ka, separated by a ~250 ka interval of relative stability, or "plateau" (Coxall et al., 2005; Scher et al., 2011; Westerhold et al., 2014). The first step in $\delta^{18}O$ records (EOT-1) is thought to be associated with relatively limited ice-sheet growth (Katz et al., 2008; Lear et al., 2008), being mainly driven by significant global cooling (Houben et al., 2018; Katz et al., 2008; Miller et al., 2008; Wade et al., 2012). The second step in $\delta^{18}O$ (EOT-2) is thought to be dominated by ice-volume expansion (Katz et al., 2008; Lear et al., 2008), a sharp deepening of the ocean carbonate saturation depth (Coxall et al., 2005) and a massive and abrupt increase in weathering flux from East Antarctica (Scher et al., 2011). However, based on evidences from a sequence boundary at Saint Stephens Quarry, Alabama, and increased glacial weathering fluxes from Prydz Bay, Antarctica, some authors proposed an early-stage

onset of the large-scale expansion of the East Antarctic Ice Sheet in the late Eocene (Miller, 2005; Passchier et al., 2017). For the purpose of this work, we adopted an EOT defined between the extinction of nannofossil species *Discoaster saipanensis* (~34.4 Ma) and the beginning of the early Oligocene glacial maximum (EOGM: ~33.7 Ma) (Pearson et al., 2008; Westerhold et al., 2014).

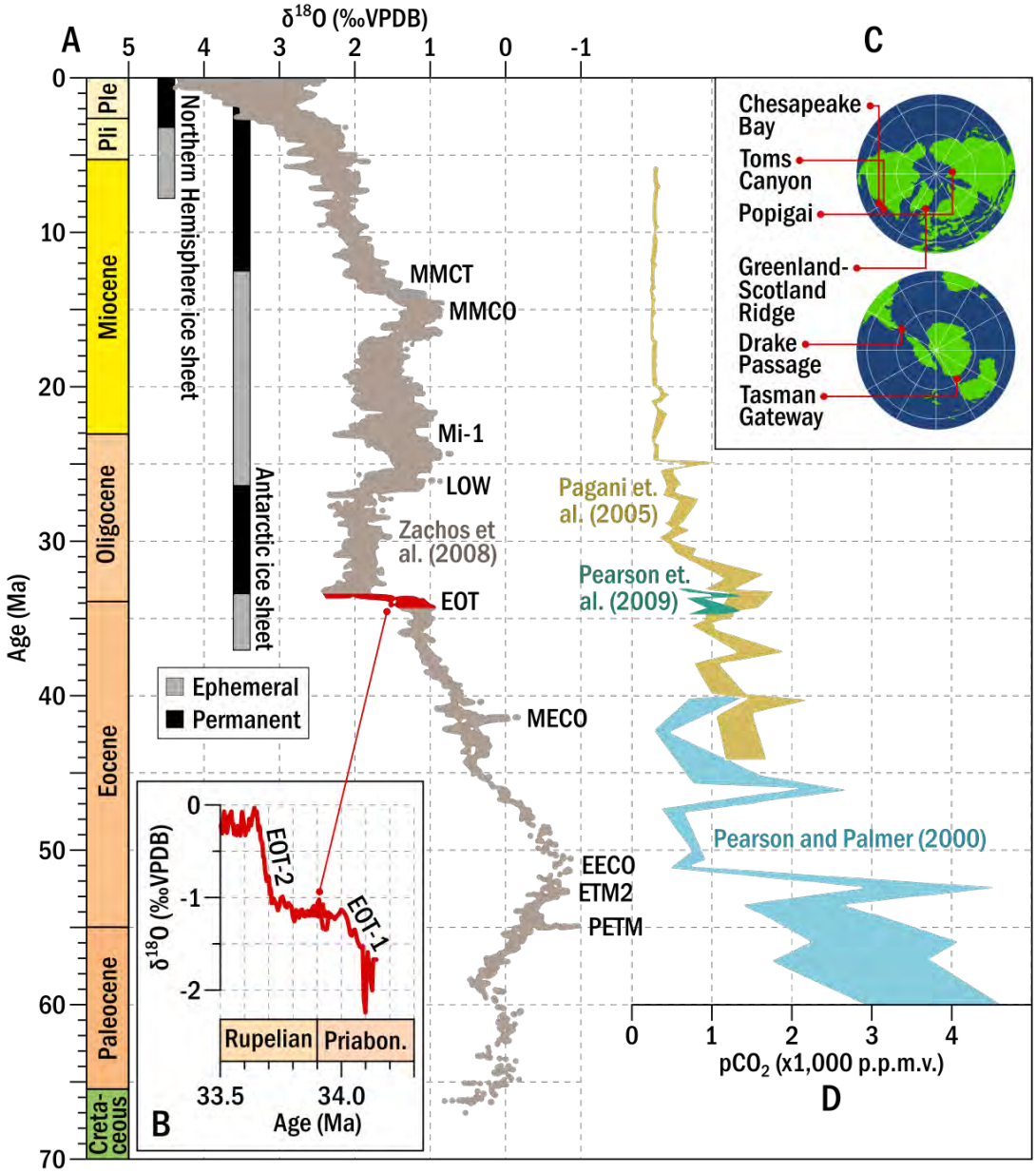


Figure 1. Summary figure of the EOT. A: Long-term benthic foraminifera oxygen isotope record during the Cenozoic. B: High-resolution benthic foraminifera oxygen isotope record from Equatorial Pacific

(Coxall et al., 2005). C: Location of key geological features (see explanation in Section 2.2). D: Multiproxy-based long-term atmospheric CO_2 concentration. Legend: Pli – Pliocene; Ple – Pleistocene; Priabon. – Priabonian; PETM – Paleocene-Eocene Thermal Maximum; ETM2 – Eocene Thermal Maximum 2; EECO – early Eocene Climatic Optimum; MECO – middle Eocene Climatic Optimum; LOW – late Oligocene Warming; Mi-1 – Miocene Isotopic Event 1; MMCO – middle Miocene Climatic Optimum; MMCT – middle Miocene Climate Transition.

2.2. Causal mechanisms

Two main hypotheses have been proposed to explain the onset of the EOT: Antarctic cooling related to changes in the geometry of Southern Ocean gateways (Kennett, 1977) and global cooling linked to declining greenhouse gas concentration (DeConto and Pollard, 2003; Pagani et al., 2005). More recent work has focused on an understanding of the interaction between these two processes, especially the role of the developing Antarctic Circumpolar Current (ACC) on global biogeochemistry and carbon dioxide drawdown through the middle to late Eocene (Coxall et al., 2018; Elsworth et al., 2017). Other causal mechanisms, however, have been proposed as minor drivers of this climate transition and may have played important roles in the timing and dynamics of the onset of the EOT. We briefly discuss each of these mechanisms below (Figure 1).

Geometry of oceanic gateways. The tectonic opening of Southern Ocean gateways (Drake Passage and Tasmanian Gateway; Figure 1) would have reduced southward oceanic heat transport and facilitated cooling of Southern Ocean sea-surface temperatures (Nong et al., 2000; Toggweiler and Bjornsson, 2000), allowing the formation of the Antarctic Circumpolar Current (ACC), the thermal isolation of the Antarctic continent (Kennett, 1977; Scher and Martin, 2006; Stickley et al., 2004b) and a less arid maritime climate (Lear et al., 2000).

However, coupled ocean-atmosphere models suggested that warm waters did not penetrate to high latitudes (Huber et al., 2004) and the rise of Antarctic glaciation enhanced northward transport of Antarctic intermediate water and invigorated the

formation of Antarctic bottom water, reorganising ocean circulation and better explaining the oceanographic changes (Goldner et al., 2014). This ultimately demonstrates that the existence of a continuous ACC and the colder SSTs were an effect of glaciation rather than the cause. Moreover, multiproxy records from the Drake Passage and the Tasman Gateway show that they initiated a deepening and widening process much earlier than the onset EOT, with estimates varying from ~1 to more than 15 Ma (Bijl et al., 2013; Scher and Martin, 2006; Stickley et al., 2004b). And using a general circulation model with coupled components for atmosphere, ocean, ice sheet and sediment, other authors advocate a secondary role for the opening of continental gateways in the EOT (DeConto and Pollard, 2003; Pagani et al., 2005) and invoked an alternative explanation for this climate transition.

Greenhouse gases. This second hypothesis argues that a long-term decline of atmospheric CO_2 concentration from ~1,000-2,000 parts per million by volume (ppmv) typical in the Paleocene-early Eocene (Pagani et al., 2005; Pearson and Palmer, 2000) towards a critical threshold (~750-760 ppmv) (Figure 1) (DeConto et al., 2008; DeConto and Pollard, 2003; Pearson et al., 2009) would have permitted orbital forcing (Coxall et al., 2005; Pälike et al., 2006) and ice-climate feedbacks (DeConto et al., 2008; DeConto and Pollard, 2003) to drive cooler high-latitude summers during times of low summer insolation. These combined factors may have allowed a descending snowline to intersect high elevation regions on Antarctica and permit large-scale ice growth during the EOT (Pearson et al., 2009). This hypothesis was tested with a coupled ice sheet and general circulation climate model for glacial inception and early growth of the East Antarctic ice sheet, including scenarios with closed gateways and an unobstructed Southern Ocean (DeConto and Pollard, 2003). As a result, it was observed that declining Cenozoic CO_2

led to the formation of initially small and highly dynamic ice caps on high Antarctic plateaux. However, once a CO_2 threshold was crossed, ice-sheet height/mass-balance feedbacks caused the ice caps to expand rapidly, paced by large orbital variations, and eventually coalescing into a continental-scale ice sheet (DeConto and Pollard, 2003).

Enhanced overturning circulation. The recent studies (Coxall et al., 2018; Elsworth et al., 2017) of multiple Atlantic Ocean sites proposed a third mechanism to explain the origins of the EOT, by means of a link between tectonic movements and CO_2 drawdown. They argue for a strong role of the Atlantic Meridional Overturning Circulation (AMOC) in pre-conditioning the late Eocene Earth for the greenhouse-icehouse transition. As a major component of the ocean circulation system, the AMOC is responsible for redistributing heat, influencing the global carbon cycle and therefore impacting Earth's climate evolution. The strength of the AMOC depends on a delicate balance between temperature and salinity and comprises northward transport of warm and salty surface waters that cool and sink at high latitudes and perform a deep southward return flow to lower latitudes. As a consequence, the AMOC can affect not only the North Atlantic and surrounding landmasses, but also global-scale ocean circulation.

The formation and strengthening of a late Eocene North Atlantic Deep Water (NADW) component at ~35.9 Ma, i.e., ~1.5 Ma prior to the EOT, would have enhanced northward ocean heat transport, and is suggested to be linked to a significant increase in rainfall over land and silicate weathering (Coxall et al., 2018). This increased weathering is then proposed as a driver of long-term CO_2 drawdown through CO_2-weathering feedback loops (Coxall et al., 2018; Elsworth et al., 2017), which culminated with the Antarctic glaciation. Nevertheless, the cause of such an enhanced AMOC is under discussion. One view suggests that, as the tectonics deepened the Drake Passage below a critical threshold,

the newly formed Southern Ocean isolated Antarctica from warm and salty subtropical waters, initiating strong overturning circulation in the North Atlantic (Elsworth et al., 2017). The other hypothesis argues that tectonic adjustments in subarctic seas enabled an increased exchange across the Greenland-Scotland Ridge (GSR; Figure 1), which created a considerable salinity and temperature gradient between cooler and more brackish Arctic waters and warmer saltier North Atlantic surface waters (Coxall et al., 2018). This ultimately permitted sinking and a progressive increase in NADW export (Coxall et al., 2018).

Extra-terrestrial impact events. An additional hypothesis invokes the role of extra-terrestrial impact events as a further forcing mechanism behind the EOT. These phenomena can trigger climate cooling by blocking sunlight due to dust loading of the atmosphere, shock formation of nitrogen oxides, and atmospheric injection of sulfur dioxide (Toon et al., 1994). Moreover, feedback mechanisms could have extended impact-induced climate cooling (Vonhof et al., 2000). This is partly supported by the discovery of multiple layers of breccia and ejecta deposits in late Eocene strata, especially of the Northern Hemisphere (Figure 1) (Bottomley et al., 1997; Koeberl et al., 1996; Poag et al., 2002; Poag and Poppe, 1998). Three of the identified impact craters are bigger than 10 km in diameter and have well-constrained ages (error <1.0 Ma). These are the Popigai crater (diameter: ~100 km) in central Siberia, and the Chesapeake Bay (diameter: ~90 km) and Toms Canyon (diameter: ~20 km) craters, on the Atlantic margin of North America. Biochronology, magnetostratigraphy, and radiometric dating methods provided an age assignment to these events of ~36.1-35.5 Ma (Bottomley et al., 1997; Koeberl et al., 1996; Liu et al., 2009a; Poag, 2012; Poag et al., 2002; Pusz et al., 2009), which places them ~1.1-1.7 Ma prior to the EOT. Although some biotic turnover episodes are

associated with these late Eocene impacts (Coccioni et al., 2009; Keller, 1986; Pusz et al., 2009; Vonhof et al., 2000), it has been widely considered that the impact events in general could not be invoked as a possible cause of long-term climatic evolution (Coxall and Pearson, 2007; Pusz et al., 2009).

2.3. Consequences of the EOT

A growing body of evidence, built up worldwide in the course of the last five decades through a range of multiproxy studies (Coxall and Pearson, 2007) have demonstrated that the abrupt, global-scale climatic shift through the EOT was responsible for major disruptions in many components of the Earth System, including atmospheric circulation (Xiao et al., 2010) and hydrological cycling (Robert and Kennett, 1997; Wolfe, 1995), the biosphere (Coxall and Pearson, 2007; Prothero, 1994a) and cryosphere (Kennett, 1977; Scher et al., 2011; Zachos et al., 1992). These are discussed in more detail below.

Global cooling. The EOT is characterised by global cooling, with falling temperatures in the deep sea (Cramer et al., 2011; Lear et al., 2008), sea surface (Katz et al., 2008; Lear et al., 2008; Liu et al., 2009b; Wade et al., 2012), and continental environments (Schouten et al., 2008; Zanazzi et al., 2007). Although some authors argue that temperature change was negligible (Grimes et al., 2005; Ivany et al., 2000; Kobashi et al., 2001; Kohn et al., 2004; Sheldon, 2009), other workers point to a ~4° C deep-sea cooling (Cramer et al., 2011; Lear et al., 2008), ~2.5-5° C sea-surface cooling (Katz et al., 2008; Lear et al., 2008; Liu et al., 2009b; Wade et al., 2012), and a decrease in ~8° C of tropospheric temperatures (Dupont-Nivet et al., 2007; Zanazzi et al., 2007). Although this pattern did not follow a uniform path across the globe, with high-latitude regions cooling more than the Equatorial zone (Liu et al., 2009b; Zachos et al., 1994), geochemical and micropalaeontological evidence indicate that even subtropical realms, such as the Gulf of

Mexico, underwent substantial cooling during the EOT, especially in surface waters (Houben et al., 2018; Katz et al., 2008; Wade et al., 2012).

Antarctic ice-sheet growth and glacioeustatic sea-level fall. The apex of the EOT was undoubtedly the rapid expansion of the first permanent continental-scale ice sheets on Antarctica (Kennett, 1977; Scher et al., 2011; Zachos et al., 1992), associated with a glacioeustatic sea-level fall and regressions worldwide (Kominz and Pekar, 2001; Miller et al., 2008; Pekar et al., 2002; Pekar and Christie-Blick, 2008). The assessment of significant expansion/retraction of Earth's cryosphere is performed by means of the benthic foraminiferal oxygen stable isotope ($\delta^{18}O_{bf}$) records (Zachos et al., 2001, 1996), which represent a combination of local temperature-dependent isotopic fractionation during calcification and the isotopic composition of seawater in which the organism calcified ($\delta^{18}O_{sw}$) (Zachos et al., 2001). Changes in the $\delta^{18}O_{sw}$ composition of deep-waters are largely a function of global ice volume (Zachos et al., 2001), since the hydrological cycle concentrates ^{16}O in ice sheets, leaving the oceans more enriched in ^{18}O during glaciated climate states (Hays et al., 1976). Quantifying this global ice volume component within $\delta^{18}O_{bf}$, therefore, requires an independent assessment of deep-water temperature, typically from Mg/Ca palaeothermometry (Lear et al., 2000).

Through the EOT, however, deep-water foraminiferal Mg/Ca ratio is likely affected by the dramatic increase in the deep ocean carbonate saturation state (Coxall et al., 2005), which substantially reduces Mg/Ca-derived estimates of cooling (Lear et al., 2000, 2004, 2008) and makes the accurate quantification of ice growth across the EOT challenging. The best estimates to date indicate total ice-sheet expansion to a volume equivalent to 70% of the present Antarctic ice sheet (Cramer et al., 2011; Lear et al., 2008), assuming the same mean isotopic composition of modern Antarctic ice (Shackleton and Kennett,

1975). The maximum ice-sheet expansion in the EOT led to a glacioeustatic sea-level fall on the order of ~70±20 m (Kominz and Pekar, 2001; Miller et al., 2008; Pekar et al., 2002; Pekar and Christie-Blick, 2008), which considers the isostatic response of the oceanic lithosphere to the change in weight of the overlying water (hydroisostasy). This is based on the fact that an eustatic sea-level change is fixed relative to the centre of the Earth and is due to actual variations in the volume of Earth's ocean water, whereas apparent sea-level change is the observed fluctuations in water depth relative to the ocean floor during an eustatic sea-level change (Kominz and Pekar, 2001; Pekar et al., 2002). Therefore, apparent sea-level changes observed through sequence stratigraphy must be calibrated against oxygen isotope records by a factor of 0.68 to obtain the equivalent glacioeustatic change (Pekar et al., 2002).

The current view of East Antarctic Ice Sheet (EAIS) dynamics suggests that, as atmospheric CO_2 concentration declined, initial glaciation formed relatively small ice caps in the East Antarctic interior (Barrett, 1996) and in the highest elevations of Dronning Maud Land (DeConto and Pollard, 2003) driven by orographically lifted maritime moisture. High winter snowfall rates would have enabled isolated ice caps over the high elevations of the Gamburtsev Mountain region and along the Transantarctic Mountains (DeConto and Pollard, 2003). Discharge mainly occurred via the Lambert Graben to Prydz Bay (Barrett, 1996; Passchier et al., 2017). As CO_2 concentration continued to fall, height/mass-balance feedbacks suddenly initiated, and larger dynamic ice sheets coalesced until the EAIS became a more permanent feature (DeConto and Pollard, 2003). Accumulation zones eventually reached sea level around most of the continent and a massive ice sheet, almost insensitive to orbital forcing (little summer

melting), was formed by the early Oligocene (Barrett, 1996), paced by Milankovitch orbital parameters (Naish et al., 2001; Pälike et al., 2006; Zachos et al., 1996).

The best direct evidence for massive ice-sheet growth on Antarctica comes from the wide spectrum of proximal glacial-related deposits produced by surges of erosion that carried weathering products to depocentres around the continent. These include glaciomarine sequences on the continental shelves (Barrett, 1996; Cooper and O'Brien, 2004), coarse grains of ice-rafted debris (IRD) in pelagic sediments of the circum-Antarctic and Southern Ocean (Barrett, 1996; Zachos et al., 1992), weathering flux inferred from fossil fish teeth radiogenic Neodymium from the Kerguelen Plateau (Southern Ocean) (Scher et al., 2011), and a shift from smectite- to illite-dominated clay mineral assemblages, interpreted as the transition from a chemical weathering regime to one of mechanical weathering by ice sheets (Ehrmann and Mackensen, 1992).

Although estimates of ice volume growth and deep-ocean cooling through the EOT could be accommodated on Antarctica alone (DeConto et al., 2008; Larsen et al., 1994; Lear et al., 2008; Liu et al., 2009b; Pearson et al., 2009; Shackleton et al., 1984), some studies (Coxall et al., 2005; Lear et al., 2004) argue for a "bipolar glaciation hypothesis", i.e., for some coeval Northern Hemisphere continental-scale ice-sheet growth. Evidence for this has now come from records of continental cooling (Zanazzi et al., 2007) and IRD deposits in the Greenland Sea (Eldrett et al., 2007; Tripati et al., 2008) and the Arctic Ocean (Tripati et al., 2008), although likely associated with isolated ice caps and/or alpine outlet glaciers. Considering that even the lowest estimates of the threshold for Antarctic ice-sheet growth, i.e., ~450 ppmv (Pearson et al., 2009), is nearly twice the modelled value for widespread Northern Hemisphere continental glaciation, i.e., ~280 ppmv (DeConto et al., 2008), and since there is a lack of direct evidence for significant and

consistent Northern Hemisphere ice sheets before ~3.0 Ma (Shackleton et al., 1984; Larsen et al., 1994), we assume that the Eocene-Oligocene climate transition is dominated by continental-scale ice-sheet growth only on Antarctica.

Global carbon cycle perturbations. An abrupt positive shift in benthic foraminiferal carbon stable isotope ratio ($\delta^{13}C_{bf}$) coeval with the $\delta^{18}O_{bf}$ signal suggests that a major disturbance in the global carbon cycle is also associated with this climate transition (Zachos et al., 1996). This idea was reinforced by reconstructions showing a deepening of the calcite compensation depth (CCD) of more than 1 km near the EOT (van Andel and Moore Jr, 1974; Coxall et al., 2005), which raised speculations on potential relationships between the Antarctic glaciation and the global carbon cycle, including a large-scale perturbation to oceanic carbonate chemistry (Pälike, 2012). A number of hypotheses have been proposed to explain the coupled shifts in marine carbon isotopes and oceanic carbonate chemistry during the EOT, including an increase in organic carbon burial rates (Olivarez Lyle and Lyle, 2006; Salamy and Zachos, 1999; Zachos et al., 1996; Zachos and Kump, 2005), an increase in global silicate weathering rates (Ravizza and Peucker-Ehrenbrink, 2003; Zachos et al., 1999; Zachos and Kump, 2005), an increase in global siliceous (versus calcareous) plankton export production (Coxall et al., 2005), and a shift of global calcium carbonate ($CaCO_3$) burial/sedimentation from shallow shelf seas to deep ocean basins coupled with a temporary increase in carbonate weathering from freshly exposed, fast-weathering, and ^{13}C-enriched carbonate shelves (Coxall et al., 2005; Kump and Arthur, 1997; Merico et al., 2008; Opdyke and Wilkinson, 1988).

Attempts to model these processes (Merico et al., 2008) indicate that Antarctic ice-sheet growth and concomitant glacioeustatic sea-level fall exposed widespread shallow-shelf limestone platforms to erosion, inducing a one-off discharge of dissolved inorganic

carbon and alkalinity into the ocean. This eventually increased oceanic carbonate (CO_3^{2-}), deepened the CCD and increased seawater $\delta^{13}C$. The reduction in shelf habitat for neritic benthic calcifiers would also have led to a large reduction in $CaCO_3$ burial state in shallow seas. To balance river inputs of dissolved $CaCO_3$ with global $CaCO_3$ burial, the decline in shallow-sea burial forces a compensating increase in deep-sea carbonate burial through a deepening of the CCD. However, critics of this hypothesis suggest that the sea-level fall across the EOT is insufficiently large or so unique as to cause such a large and permanent change in both shelf carbonate burial and weathering (Miller et al., 2009; Rea and Lyle, 2005). An alternative proposed mechanism (McKay et al., 2016a) suggested that the rapidity of the two steps in the $\delta^{13}C_{bf}$ palaeorecord can best be attributed to the net sequestration of ~1,000 Pg of organic carbon during the EOT by "carbon capacitors" through processes such as permafrost and peatland expansion. Even in this scenario, a large repartitioning of carbonate burial from the shelves to the deep ocean is required in order to explain the long-term deepening of the CCD observed across the EOT (McKay et al., 2016a).

Biotic turnovers. The EOT is associated with biotic turnovers and biogeographic reorganisation in plants and animals across a range of latitudes (Prothero, 1994a), as well as substantial extinction and ecological reorganisation in the marine microplankton. Although not comparable to the "Big Five" mass extinction events (Raup and Sepkoski, 1982), EOT-related strata contain records of major turnover and/or influx of molluscs in North America and Europe (Dockery III, 1986; Dockery III and Lozouet, 2003; Hickman, 2003; Nesbitt, 2003; Squires, 2003), disappearance of tropical taxa and declining diversity of amphibians and turtles (Hutchison, 1992; Rage, 1986), radiation of passerine birds (Mayr, 2005), turnover in mammalian faunas in Europe and Asia (Meng and

McKenna, 1998; Stehlin, 1909), extinction of the archeocete whales (Fordyce, 1992, 2003; Manning, 2003), and diversification of cat-like carnivores (Bryant, 1996). Remarkable biogeographic reorganisation was also observed in plant groups: in North America, widespread replacement of subtropical vegetation by cooler, deciduous forms, regional extinctions (Wolfe, 1992, 1994), and diversification of desert species in the continental interior as aridity increased (Moore and Jansen, 2006; Yancey et al., 2003); in Europe, replacement of tropical and subtropical taxa by a more seasonal temperate flora (Collinson, 1992); in South America, rapid changes in floral (pollen and spores) records (Jaramillo et al., 2006); in Australia, a shift to lower diversity, higher seasonality and a spread of cool-temperate plants (Kemp, 1978); in Asia, diversity reduction (Leopold et al., 1992); and in Antarctica, a change from evergreen forest to sparse tundra on the Antarctic peninsula and Seymour island (Francis, 1999; Francis and Poole, 2002).

Detailed micropalaeontological records also show that substantial extinction and ecological reorganization are closely coupled to the EOT (Cotton and Pearson, 2012; Coxall and Pearson, 2007; Dunkley Jones et al., 2008; Houben et al., 2013a; Moore et al., 2015; Pearson et al., 2008, 2009). These include extinctions in the **planktonic foraminifera** with the worldwide last occurrence of the planktonic foraminiferal Family Hantkeninidae (five species and two genera – *Hantkenina* and *Cribrohantkenina*), which is the marker of the Eocene-Oligocene Boundary (EOB: 33.89 Ma) (Nocchi et al., 1988; Premoli Silva and Jenkins, 1993; Westerhold et al., 2014). The EOB extinction event is slightly preceded by the extinction of the widespread *Turborotalia cerroazulensis* group at ~34.0 Ma (Pearson et al., 2006) and followed by the extinction of the dwarfing *Pseudohastigerina naguewichiensis* at ~32.1 Ma (Wade and Pearson, 2008). Among the **benthic foraminifera**, there was a sudden increase in worldwide, deep-sea accumulation

rate (Diester-Haass et al., 2003; Diester-Haass and Zahn, 2001), decline of deep-sea benthic diversity and subsequent increase in dominance of opportunistic species (Thomas and Gooday, 1996), acme of deep-water agglutinated species in the North Atlantic and Western Tethys (Kaminski, 2005), abrupt turnover of neritic benthic foraminifera in Australia (McGowran et al., 1992; McGowran and Beecroft, 1986) and in the U.S. Gulf Coast (Fluegeman, 2003), mass extinction of some important long-ranging genera and species, notably *Asterocyclina*, *Discocyclina* and some species of *Nummulites* (Adams et al., 1986), and rapid decline in larger foraminifera in the Caribbean that may be associated with the boundary interval (Cotton and Pearson, 2012; Robinson, 2004). **Calcareous nannofossils** present major turnovers (Bordiga et al., 2015a; Dunkley Jones et al., 2008; Persico and Villa, 2004; Villa et al., 2008), long-term decline in diversity (Aubry, 1992; Bown et al., 2004; Perch-Nielsen et al., 1986), and extinctions of *Discoaster saipanensis* (Berggren et al., 1995) and *Pemma papillatum* (Varol, 1998). Significant drop in **ostracode** diversity has been recorded (Schellenberg, 1998; Yamaguchi et al., 2014). Other major biotic event was the increase in cold-adapted **diatom** species in Antarctica (Olney et al., 2005), and increase in the diversity of benthic diatoms associated with the increasing influence of the Antarctic polar current (Rabosky and Sorhannus, 2009; Whitehead, 2005). The **radiolaria** group also records major turnover of tropical species in the Pacific (Funakawa et al., 2006) and North Atlantic (Kamikuri and Wade, 2012), including extinction of several taxa, sudden drop in diversity and radiolarian accumulation rates, and expansion of cool-water cosmopolitan taxa. Among **organic-walled dinoflagellate cysts**, two successive influxes of high-latitude species have been observed in Italy (Brinkhuis & Biffi 1993), along with decreasing diversity in the Wedell Sea and off Dronning Maud Land, Antarctic margin (Mohr, 1990), and significant

turnover and biotic reorganisation in the Gulf of Mexico (Houben et al., 2018) and Southern Ocean (Houben et al., 2013a).

Other consequences. Evidence of a significant increase in primary productivity have been reported from several deep-sea sites in the Southern Ocean (Anderson and Delaney, 2005; Diester-Haass et al., 1996; Latimer and Filippelli, 2002; Salamy and Zachos, 1999) and may be associated with upwelling of nutrient-rich waters driven by cooling-induced increases in surface-ocean divergence and/or enhanced fluxes of weathering derived nutrients during rapid sea-level fall (Nilsen et al., 2003; Salamy and Zachos, 1999; Zachos and Kump, 2005). Other important disturbances caused during the EOT include changes in atmospheric circulation (Xiao et al., 2010), increased aridification (Dupont-Nivet et al., 2007), and increased seasonality (Eldrett and Harding, 2009; Ivany et al., 2000; Wade et al., 2012).

2.4. Why was the EOT a unique event?

Studying the EOT climate transition provides important information about two major questions for Earth Scientists: [1] what are the driving mechanisms and feedbacks that generate rapid changes of state in the Earth's Climate System and [2] how does this understanding translate into predictions of future climate conditions in response to rapid greenhouse gas climate forcing?

[1] Although substantial efforts have focused on modelling the dynamic growth of the Antarctic ice sheets, and the potential for non-linear positive feedbacks within the cryosphere that could contribute to the observed step-change into the modern icehouse climate state in the earliest Oligocene (DeConto et al., 2008; DeConto and Pollard, 2003), there is substantial evidence for contemporaneous increases in the carbonate saturation state of the global oceans (Coxall et al., 2005; Pälike et al., 2006) and significant

acceleration of the marine biological pump (McKay et al., 2016a; Merico et al., 2008; Salamy and Zachos, 1999), the causes and effects of which are poorly known. Long-term records of atmospheric CO_2 levels estimate late Eocene values close to the threshold for Antarctic ice-sheet growth (Anagnostou et al., 2016; Pagani et al., 2005), whilst the only available record of the transition itself, indicates a transient drawdown of CO_2 closely coupled to the main phase of ice-sheet expansion (Pearson et al., 2009). Modelling studies show that changes in the partitioning of organic and inorganic carbon burial from continental margins to the deep ocean, as well as the magnitude of nutrient trapping within shelf systems and weathering fluxes from rapidly exposed coastal environments are essential drivers of the observed global carbon cycles perturbations (McKay et al., 2016a; Merico et al., 2008). Within the dynamics of the EOT itself, however, the timing of changes in these sea-level controlled shelf-ocean partitioning and nutrient / carbon fluxes is, however, very poorly known.

[2] By the year 2100, it is predicted that the CO_2 concentration in the atmosphere will rise to values between ~790 and 1,150 ppmv if anthropogenic carbon emissions to the atmosphere continue to grow at the same rate as in recent years (IPCC, 2013). This represents an increase of ~2.8 to 4.1x PAL (pre-industrial atmospheric levels) CO_2. Multiproxy reconstructions of atmospheric CO_2 concentrations through the Cenozoic (Anagnostou et al., 2016; Pagani et al., 2005, 2011; Pearson et al., 2009; Zhang et al., 2013) show that the last time in Earth's history the concentration of carbon dioxide in the atmosphere reached values that high was ~34 Ma, after a long-term (10^6-to-10^7-year scale) decline (Pagani et al., 2005). As a result, descending snowline would have lowered enough to intersect high elevation regions in Antarctica, thus permitting the formation of its first continental-scale ice sheets (DeConto et al., 2008; DeConto and Pollard, 2003).

It has been argued, therefore, that there is a threshold in atmospheric CO_2 concentrations, ~750-760 ppmv, below which stable and large ice caps coalesce and become a more permanent feature, which are less sensitive to orbital forcing and seasonal melting (DeConto et al., 2008; DeConto and Pollard, 2003; Pearson et al., 2009). Following from this premise and assuming that anthropogenic carbon emissions do not change in a dramatic way, we recognise that, by the end of the century, atmospheric CO_2 concentrations will be approaching the threshold levels for stability for the EAIS. Furthermore, modelling studies proposed a hysteresis effect associated with ice-sheet height mass balance feedbacks, where CO_2 levels need to rise slightly above 3x PAL to induce drastic retreat of a pre-existing EAIS, and need to drop slightly below 3x PAL to grow a large ice sheet from no ice (McKay et al., 2016a; Pollard and DeConto, 2005). When albedo feedback is added, the hysteresis between forward and reverse runs results in even more sudden transitions occuring at 3x and 4x PAL CO_2 (Pollard and DeConto, 2005).

CHAPTER 3: MATERIALS AND METHODS

3.1. Regional geological context

The Gulf Coastal Plain is one of the largest physiographic provinces in North America. In the subsurface the Mississippi embayment consists of a structurally complex basin with thick Jurassic-to-Holocene deposits (Cushing et al., 1964; Hosman, 1996). Within these sequences, the most continuous Paleogene successions are found between central and southern Mississippi and Alabama (Cushing et al., 1964; Hosman, 1996).

The upper Eocene to lower Oligocene stratigraphy of the US Gulf Coast is split into two groups – the Jackson (~ upper Eocene) and Vicksburg (~ lower Oligocene) groups (Cushing et al., 1964; Hosman, 1996). The contact between these groups is commonly indistinguishable on a lithologic basis, but they have distinct faunal assemblages (Hosman, 1996). The lithology, and constituent formations within these groups, also varies geographically across Mississippi and Alabama, reflecting relative positions along the palaeoshelf and proximity to river outflows. The upper middle Eocene of Mississippi consists of discontinuous and lenticular beds of lignitic-to-carbonaceous fine-to-medium quartz sand, silt, and clay. These sediments constitute the non-marine Cockfield Formation, the youngest continental deposits of the Eocene on the Gulf Coastal Plain (Cushing et al., 1964; Hosman, 1996). The upper Eocene Jackson Group overlies the Cockfield Formation, and it represents the last extensive marine inundation within the Mississippi embayment (Cushing et al., 1964; Hosman, 1996). The Jackson Group consists of two major facies: to the west of the Gulf Coastal Plain, towards Texas, a shallow-water marine facies with beach sands, clays, and occasional volcanic tuffs, whilst to the east, in the central part of the Gulf Coastal Plain (Mississippi and Alabama), the group becomes more fossiliferous and argillaceous as deeper-water clays dominate

(Cushing et al., 1964; Hosman, 1996). The two main lithostratigraphic units within the Jackson Group are the highly fossiliferous glauconitic sandy marls of the basal Moodys Branch Formation and the calcareous fossiliferous dark-grey to blue clays of the Yazoo Formation (Cushing et al., 1964; Hosman, 1996). The Yazoo Formation has four well-characterized members in eastern Mississippi and Alabama: the North Twistwood Creek Member (marl and calcareous clay), the Coccoa Sand Member (sandy marl), Pachuta Marl Member (glauconitic fossiliferous marls and sandy hard limestones), and the Shubuta Member (calcareous clays with concretions) (Cushing et al., 1964; Hosman, 1996). In central Mississippi, in the region of the Mossy Grove core, the entire Yazoo Formation is represented by an undifferentiated marine clay unit – the Yazoo Formation (Dockery III et al., 1991). Towards northern Mississippi this group occurs as a non-marine clastic facies, with evidence of lacustrine, palustrine, and lagoonal sedimentation, and the Yazoo Formation becomes undifferentiated and relatively homogeneous (Cushing et al., 1964; Hosman, 1996). The Oligocene series begins with the marine fossiliferous glauconitic clay and sandy clay of the Red Bluff Formation, overlain by the fossiliferous and laminated sands of the Forest Hill Formation. Westward, this unit presents some lenses of lignite and lignitic clay. Above the Forest Hill Formation is the fossiliferous, granular, white crumbly limestone of the Bumpnose Formation (Cushing et al., 1964; Hosman, 1996). The Bumpnose Formation in Alabama and Florida is the equivalent of the Red Bluff-Forest Hill sequence in central and southern Mississippi (Hosman, 1996). Finally, overlying all these units is the Marianna-Mint Spring Formation, which consists of fossiliferous and porous limestone, glauconitic marl, and calcareous clay (Cushing et al., 1964; Hosman, 1996). In northern Mississippi, no evidence of Oligocene sedimentation is observed (Cushing et al., 1964; Hosman, 1996).

The upper Eocene to lower Oligocene lithostratigraphy outlined above has been interpreted within two distinct sequence stratigraphic models. The first argues that the Yazoo-Bumpnose contact coincides with a maximum flooding surface throughout the region (Baum and Vail, 1988; Echols et al., 2003; Jaramillo and Oboh-Ikuenobe, 1999; Loutit et al., 1988; Mancini and Tew, 1991; Tew, 1992). The second, and more recent (Miller et al., 2008), supports the association of the Yazoo-Bumpnose contact (Dockery, 1982) with a low stand sequence boundary, which is linked to the increasing $\delta^{18}O$ (Zachos et al., 2001, 1996, 2008) and global eustatic sea level fall (Coxall et al., 2005; Pekar et al., 2002) during the EOT. Sequence stratigraphic interpretations are difficult because of the depositional and lithologic variability across this region, and the difficulties in establishing robust, mostly biostratigraphic, tie points between key sections (Miller et al., 2008). Some of the key sections, from both outcrops and cores, which have been used for regional stratigraphic correlation, chronostratigraphy, and sequence stratigraphy, are shown in Figure 6.

Even at the St. Stephens Quarry section, southwestern Alabama, which is a widely studied reference for the EOT (Katz et al., 2008; Miller et al., 2008; Wade et al., 2012), establishing a robust biostratigraphy and sequence stratigraphy has been difficult (Miller et al., 2008). The low abundance and generally poor preservation of hantkeninids in the shallow-water Gulf Coast successions make the accurate placement of their last occurrence (LO) problematic (Miller et al., 2008). This difficulty is further aggravated by the reworking of upper Eocene calcareous microfossils up into lowest Oligocene sediments as a result of the major regression across the EOT (Bybell and Poore, 1983). Nevertheless, a middle-to-late Priabonian age was assigned to the Pachuta Member at SSQ, based on the LO of *R. reticulata*, upper part of nannofossil zone NP19-20 (Miller

et al., 2008). The Shubuta Member has a late Priabonian age correlated to the lower part of NP21 zone, the interval between E16 and the lower part of O1 zones, and the upper part of magnetochron C13r (Miller et al., 2008). The Red Bluff-Bumpnose sequence was dated as late Priabonian to early Rupelian age and can be correlated to the middle part of NP21 zone, the lower to middle part of O1 zone and the upper part of C13n magnetochron (Miller et al., 2008).

3.2. Mossy Grove borehole

The Mossy Grove borehole was drilled in September 1991 at Mossy Grove, Hinds County, Mississippi, to investigate the clay mineralogy and geologic history of a complete section of the Yazoo Formation in central Mississippi where this unit has a thickness greater than ~120 m (>400 ft) (Dockery III et al., 1991). It consists of a 161.6 m (530 ft) continuously cored succession, with near full recovery (Dockery III et al., 1991). At its base it recovered ~5.5 m of the upper Cockfield Formation (161.6 to 156.1 m; 530 to 512 ft, 18 ft thick), overlain by ~3.7 m of the Moodys Branch Formation (156.1 to 152.4 m; 512 to 500 ft, 12 ft thick), and then a thick 140.9 m succession of the Yazoo Formation (152.4 to 11.6 m; 500 to 38 ft, 462 ft thick). At the top of the core, overlaying the Yazoo Formation, 3.0 m of terrestrial lignites of the Forest Hill Formation were recovered (11.6 to 8.5 m; 38 to 28 ft, 10 ft thick), which in turn was overlain by a 8.5 m thick (28 ft) cover of Pleistocene loess. To improve the chronology of the upper Yazoo Formation, $^{40}Ar/^{39}Ar$ absolute dating was undertaken from a number of bentonite layers at four sites (Obradovich et al., 1993; Priddy, 1960), including seven layers within the Mossy Grove core, from which two dates were recovered (Obradovich et al., 1993; Obradovich and Dockery III, 1996). Establishing a robust age model for the Mossy Grove core has required significant effort and the integration of dinocyst, calcareous nannofossil, and

radiometric dating techniques. Initial age models were based on planktonic foraminifera assemblage data (Fluegeman, 1996; Fluegeman et al., 2009), but due to low planktonic foraminifera abundances, especially in the upper part of the core (<91.4 m; 300 ft), this age model relied upon poorly calibrated secondary markers. For instance, the direct placement of the EOB, based on the last occurrence of the Hantkeninidae, is problematic as the record of *Hantknenina alabamensis*, the only hantkeninid species found in the core, is poor and discontinuous above ~86.6 m (284 ft). The last occurrence of *Turborotalia cerroazulensis*, expected to be ~0.1 Ma older than the EOB and the Hantkeninidae extinction, occurs ~7.3 m (24 ft) higher than the last occurrence of *H. alabamensis*. Radiometric $^{40}Ar/^{39}Ar$ dating is significantly offset from the existing planktonic foraminifera biochronology. Bentonite layers at ~26.5 m (87 ft) and ~84.4 m (277 ft) were dated to 33.40 and 34.36 Ma, respectively (Obradovich and Dockery III, 1996), whereas foraminifera biochronology places these bentonites at ~33.87 and 35.33 Ma, respectively (Fluegeman et al., 2009), an offset of between 0.5 and 1.0 Ma. This mismatch has implications for the accurate placement of the EOB in this section; assuming a constant sedimentation rate within the interval between the bentonites, radiometric dating would place the boundary at ~56.7 m (186 ft), which is ~30.2 m (99 ft) lower than the existing foraminiferal estimate of ~26.5 m (87 ft) (Fluegeman et al., 2009). For a complete sample list with methods applied in this work, see Appendix 1.

3.3. Palynological preparation techniques

Samples were processed at PetroStrat Ltd. by Dr Roger Burgess with support of PetroStrat staff members Gary Smith, Marcel Polling, Neil Campion, and Paul Cornick, and followed standard techniques. Altogether, 112 sediment samples were collected from the Mossy Grove core at ~1.2 m (4 ft) intervals, between ~17 and 152 m deep (55 and

499 ft). A mass of 20 g from each sediment sample was broken into pieces, ~5 mm in diameter, using a pestle and mortar. This was followed by a set of acid treatments, including (1) 40% HCl for 30 min to remove carbonates; (2) 60% HF for 24 h to disaggregate the rock matrix; (3) sieving of the residues at 10 μm through a nylon mesh sieve to retain the HF effluent from the material; (4) a second HCl treatment to remove any precipitate formed during stage 2; and (5) a final sieving, as per stage 3. The material was then subjected to oxidation (70% HNO_3 for exactly 2 min) to remove pyrite, inorganic debris, and any unstructured organic material from the residues. Another sieving step was done to remove any HNO_3 effluent. A final cleaning treatment was undertaken with a combination of domestic and industrial detergents. Using a glass swirling dish and centrifugal swirling techniques, palynomorphs in each sample were subsequently concentrated and Bismark brown was added to make them more visible with light microscopy. Finally, the samples were sieved into two size fractions, 10-30 μm (concentrating spores and pollen) and >30 μm (concentrating dinocysts), and then mounted on separate 22x22 mm coverslips, which were glued to a glass slide using Norland optical adhesive. In this work, only the coarse fraction content of each slide was analysed. A pilot survey of these slides revealed that the acid and oxidizing technique yielded higher diversity than their non-acid and non-oxidizing counterparts (Burgess, 2015). The coarse/fine-fraction sorting follows the premise that pollen and spores size mostly ranges between 11 and 44 μm, whereas dinocysts range between 20 and150 μm (Tyson, 1995). All slides were stored in the collection of the School of Geography, Earth and Environmental Sciences, University of Birmingham.

3.4. Palynomorph assemblage characterization

The number of cysts which should be counted in order to obtain reliable data for the assessment of diversity and absolute abundance has been a matter of debate for decades. Some authors (Traverse, 2007; Tyson, 1995) assert that 200-300 palynomorph counts might be viewed as sufficient for determining the overall nature of the palynomorph population, unless a few of these counts were plankton. Recent interlaboratory calibration exercise concluded that an additional 100 cysts in the counting technique shows insignificant disparities in the results (Mertens et al., 2009). In this sense, with a Zeiss transmitted-light microscope, at least 200 dinocyst specimens were counted in each sample, along with the respective number of spores, pollen, algae (Prasinophyceae and Chlorophyceae), zoomorphs/zooclasts, phytoclasts, and amorphous organic matter. Once 200 specimens were counted, the remaining fields of the coverslip were scanned for very rare dinocysts. Only palynomorphs that were more than 50% complete and not obscured either by air bubbles or organic debris were considered (Clowes et al., 2016). We used the following abundance scheme: 0% – barren (B); 0-1% – trace (T); 1-10% – few (F); 10-25% – common (C); >25% – abundant (A). Preservation was qualitatively categorized as good (G), moderate (M) or poor (P). Reworked acritarchs and amorphous organic matter were excluded from the final sum of palynomorphs and thereby from the percentage calculations (SM2, SM3).

3.5. Palynomorph-based palaeoenvironmental analysis

Excluding the component of dispersed organic matter contents that derives from reworking processes, newly-formed organic matter can be classified as either continent-derived (e.g. spores and pollen, *Pediastrum*, phytoclasts) or ocean-derived (e.g.

prasinophyte algae, acritarchs, dinoflagellate cysts, zoomorphs, zooclasts, AOM) (Figure 2) (Traverse, 2007; Tyson, 1995).

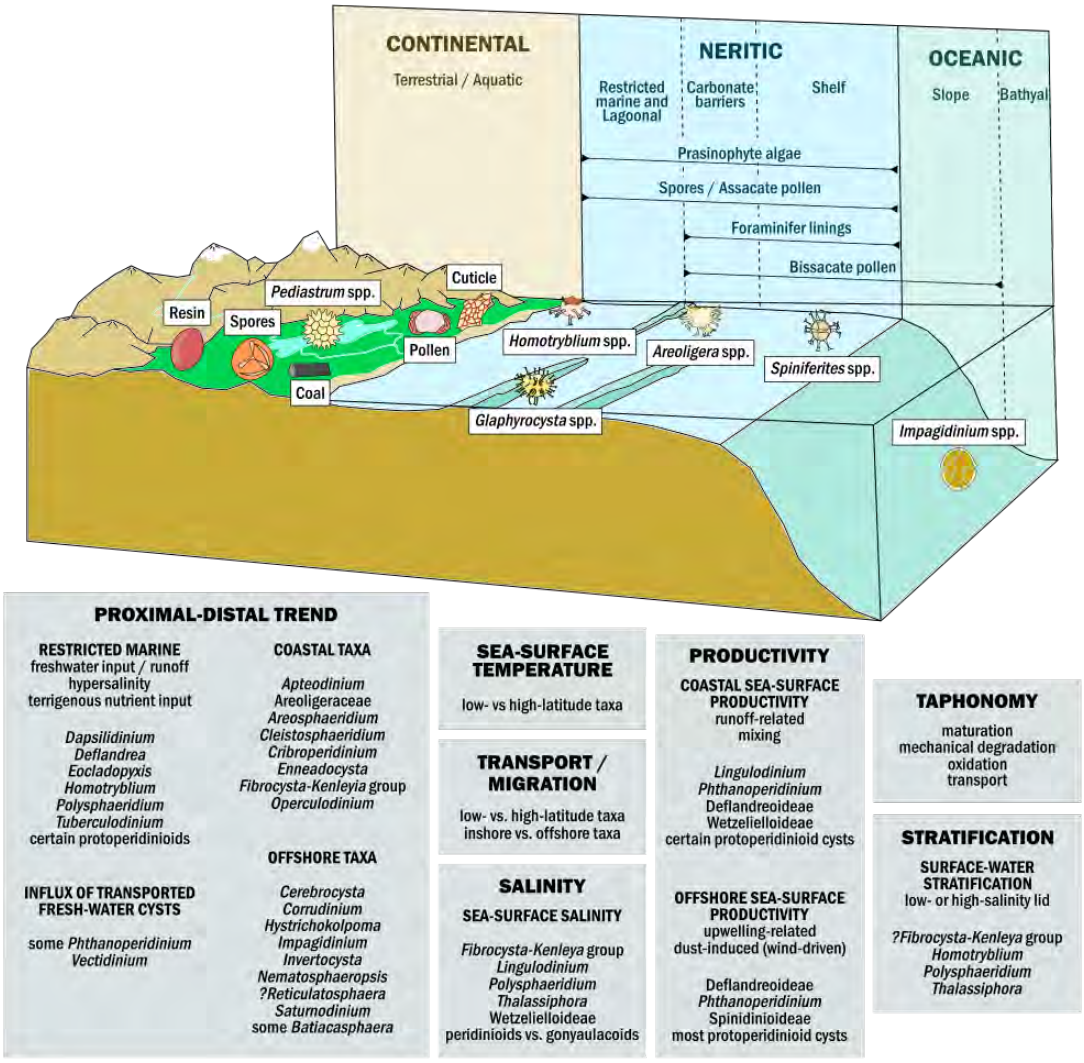


Figure 2. Schematic illustration of factors influencing the distribution of dinocysts and typical palynomorphs. Dinocyst genera indicative of specific environmental conditions are also shown (Brinkhuis, 1994; Pross and Brinkhuis, 2005; Sluijs et al., 2005; Tyson, 1995; de Vernal and Marret, 2007).

It is worth mentioning that rich and diverse organic matter content of a single palynological slide can provide a broad and relatively complete palaeoenvironmental assessment, either from continental or shallow/deep marine sediments, and from Paleozoic to Recent strata (Tyson, 1995). Relative abundance of individual organic matter

components can be used to infer palaeoenvironmental conditions, such as shifts in proximal-distal trend (Brinkhuis, 1994; Pross and Brinkhuis, 2005; Sluijs et al., 2005; Tyson, 1995; de Vernal and Marret, 2007). Therefore, relative abundances of dinocysts, plant cuticle, plant resin, and *Pediastrum* spp. have been calculated based on the overall counts of organic matter components of each sample. The palynomorphs and palynodebris discussed below are shown in Figure 3.

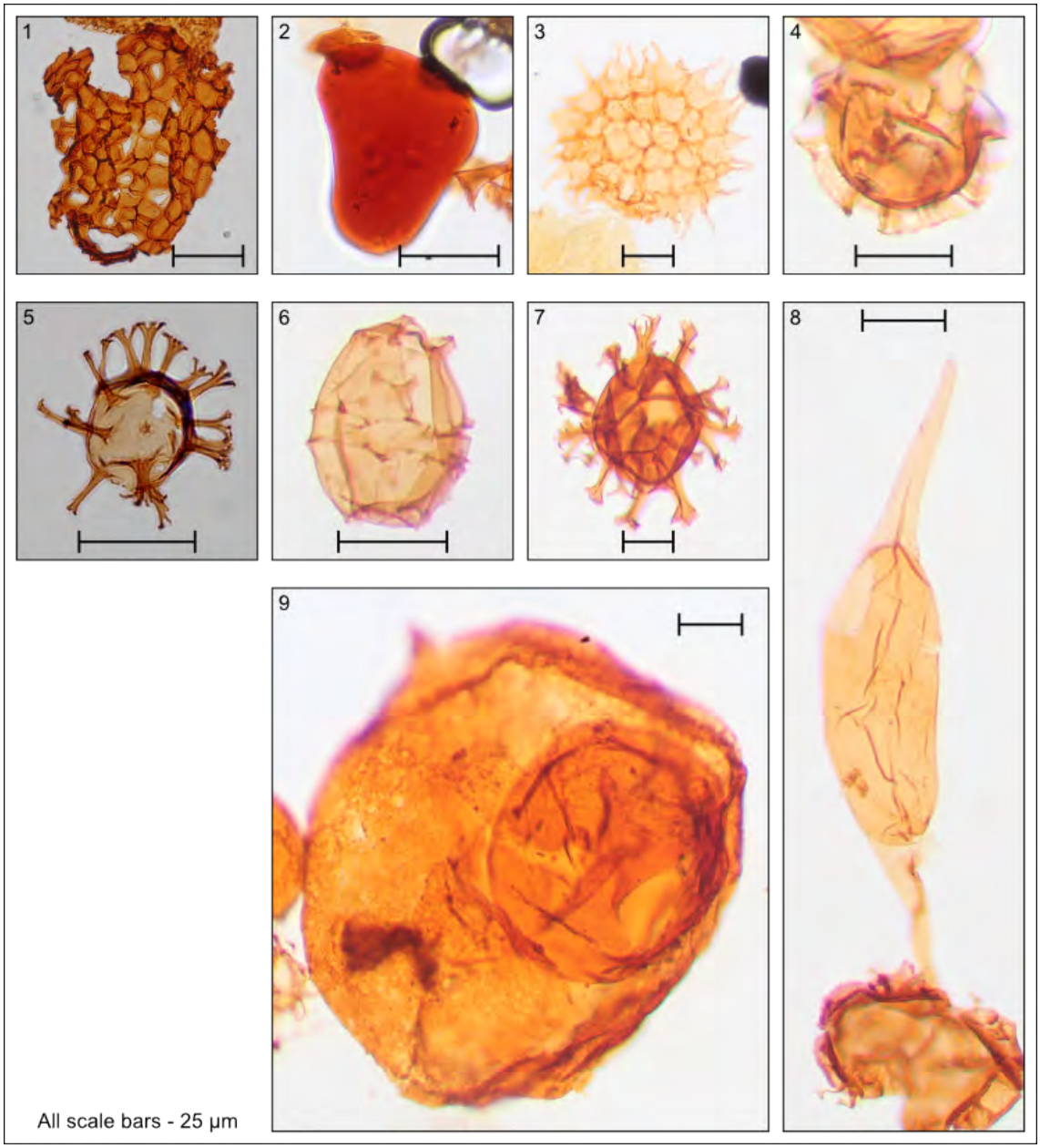


Figure 3. Photomicrographs of selected palynomorphs found at MGC and used for palaeoenvironmental reconstruction purposes. Legend: 1 – plant cuticle fragmente; 2 – plant resin fragmente; 3 – *Pediastrum* sp.; 4 – *Hemiplacophora semilunifera*; 5 – *Homotryblium floripes*; 6 – "short-process" *Spiniferites bentori*; 7 – "long-process" *Spiniferites pseudofurcatus*; 8 – *Svalbardella partimtabulata*; 9 – *Talassiphora fenestrata*.

Dinocysts are fossilized remnants produced by single-celled flagellate eukaryotes and preserved in the geological record (Head, 1996). Of all living dinoflagellate species, only 10-20% are known to produce cysts (Dale, 1976; Dodge and Harland, 1991; Evitt, 1985; Head, 1996), and less than 70% of these may produce cysts that are preserved as fossils

(Dale, 1976). These percentages also vary according to the species, and might range from <3% in *Spiniferites* spp. to 50-85% in *Operculodinium* spp. (Dodge and Harland, 1991). Dinoflagellates are rarely found below 100 m depth and their abundance is strongly controlled by the hydrographic stability, which determines the distribution of nutrients and efficiency with which available light can be utilized (Dodge and Harland, 1991; Margalef, 1978; Raine et al., 2002). This in turn provides the basis for several environmental proxies, including surface water temperature, salinity, productivity, and shoreline proximity (Brinkhuis, 1994; Brinkhuis et al., 1992; Brinkhuis and Biffi, 1993; Chateaneuf and Reyre, 1974; Dale, 1996; Kothe, 1990; Pross and Brinkhuis, 2005; Sluijs et al., 2005; de Vernal and Marret, 2007; Wall et al., 1977; Zevenboom et al., 1994).

Although dinoflagellates have a relatively broad temperature tolerance (1-35 ºC), temperature can control patterns of dinocyst abundance, with most species associated with optimum temperatures of 18 to 25 ºC. For instance, *Thalassiphora* spp. has been associated with cooling of surface waters in Central Italy (Coccioni et al., 2000; Vonhof et al., 2000), whereas the absence of low latitude *Hemiplacophora semilunifera* was reported as a response to major cooling events (Brinkhuis and Biffi, 1993). Recent study (Frieling and Sluijs, 2018) tested empiral relations between extinct dinocysts and high-quality geochemical data in order to extract more quantitative information of ecological signals from a wide range of taxa (Brinkhuis, 1994; Brinkhuis and Biffi, 1993; Pross, 2001). Their findings suggest a strong control of sea-surface temperature on some dinocyst genera: *Lentinia* spp., and *Phthanoperidinium* spp., are associated with 15-30 ºC; whereas *Heteraulacacysta* spp., and *Homotryblium* spp. are commonly found at 25-40 ºC (Frieling and Sluijs, 2018). Most dinocyst species show optimal growth at 10-20 practical salinity units, even though in some species the size and morphology of the cyst

may vary considerably with salinity (Pross and Brinkhuis, 2005; Sluijs et al., 2005; de Vernal and Marret, 2007). Many studies have corroborated that process length in various chorate dinocysts, such as *Spiniferites* spp., can be determined by salinity (Dale, 1996; Ellegaard, 2000; Lewis et al., 1999; Mudie et al., 2018). Although salinity is not the only factor controlling these morphological changes (Kokinos and Anderson, 1995), other works have demonstrated that process lengths tend to reduce at lower salinities, (e.g. Lewis and Hallett, 1997). Additionally, recent study supports the premise that long-process *S. ramosus* and short-process *S. bentorii* had very distinct ecological preferences (de Vernal et al., 2018). At MGC, we approached this assumption by assessing the long-short process ratio in the genus *Spiniferites*. This was obtained by the relative abundance of long-process species (*S. mirabilis*, *S. pseudofurcatus*, and *S. ramosus*) divided by the relative abundance of all the species of the same genus, which included the short-process *S. bentori*. Furthermore, the generally sharp separation between peridinioid- and gonyaulacoid-dominated dinoflagellate assemblages led to the development of the gonyaulacacean ratio (Harland, 1973), or peridinioid:gonyaulacoid cyst ratio (P:G ratio) (Downie et al., 1971), as an environmental index. This ratio is calculated between gonyaulacoid and peridinioid cysts, either applying actual cyst abundance or species diversity (Powell et al., 1990). This index has been interpreted as being indicative of brackish-to-open marine environments, palaeo-salinity, or productivity variations (Harland, 1973; Kothe, 1990; Sluijs et al., 2005; de Vernal and Marret, 2007).

The abundance, i.e., the number of cysts per gram of sediment, and diversity of dinocysts increase in the unstable seasonal temperate latitudes and in shelf sediments, which is reflected in the fossil record (Dodge and Harland, 1991; Harland, 1983; Sluijs et al., 2005; de Vernal and Marret, 2007; Wall et al., 1977). Besides, the abundance of

dinocysts may not be directly linked to primary productivity, since the distribution of cysts can be modified by sedimentological and hydrographic factors (Wall et al., 1977). They generally have two abundance maxima in onshore-offshore profiles: nearshore and on the upper part of the continental slope, with declining numbers with increased water depth and distance offshore (Davey, 1970; Davey and Rogers, 1975; Farr et al., 1989; McMinn, 1990; de Vernal and Giroux, 1991). Regional surveys have shown an effective absence within 15 km of a delta front (Muller, 1959), scarcity in sandy nearshore sediments (Rossignol, 1961, 1969; White and Lewis, 1982), but high abundance in silt- and clay-rich shelf sediments (Dale, 1976; Wall et al., 1977). In semi-restricted conditions, for instance in the Gulf of St Lawrence, dinocyst abundance in sediments increases dramatically from the upper estuary into more open marine conditions (de Vernal and Giroux, 1991), which is a combination of reduced sediment accumulation rates and salinity and turbidity-controlled variations in primary productivity. This is part of a consistent pattern of increasing abundance from the head to the mouth of estuaries (Anderson et al., 1982; Balch et al., 1983; Tyler et al., 1982) and then out to the continental slope (Wall et al., 1977). In Mesozoic deep-sea sediments deposited during periods of high sea-level – when most terrigenous material was trapped on wider continental shelves – dinocysts tend to be abundant relative to low concentrations of total palynomorphs (Habib, 1983).

Other palynological components such as plant debris and freshwater algae are widely assigned as continent-derived sedimentation (Carvalho et al., 2006; Clowes et al., 2016; Tyson, 1995). Plant cuticle or epidermal tissue remains is a non-opaque phytoclast mostly derived from leaves (Carvalho et al., 2006; Clowes et al., 2016; Tyson, 1995). Plant resin is a particular kind of amorphous material, but is a natural product of higher plants that

forms a physical surface barrier against infections (Carvalho et al., 2006; Clowes et al., 2016; Tyson, 1995) or is a result of fast-growing healthy trees (Larsson, 1978). Resins are strongly resistant to decay and are typically best preserved when deposited in subaqueous or waterlogged environments (Larsson, 1978). Atmospheric weathering often produces opaque surface crusts and oxidation rims, and may result in an overall darkening of the resin grains (Murchison and Jones, 1964). *Pediastrum* spp. is a genus of colonial algae and one of the most common forms of fossilizing Chlorococcale (green) algae (Carvalho et al., 2006; Clowes et al., 2016; Tyson, 1995). They are the dominant structured algal component of Cenozoic lacustrine oil shale and source rock facies, and are commonly associated with hard water lakes (Chu, 1942; Crisman, 1978; Prescott and Vinyard, 1965; Reynolds and Allen, 1968), the periphyton (Cronberg, 1982; Tyson, 1995), hyper-eutrophic lakes with unstable water columns (Hutchinson, 1967; Reynolds, 1980, 1984), and even swamps (Korde, 1960; Prescott, 1951), but is absent or rare in bog or deep waters (Korde, 1960; Pentecost, 1984; Prescott, 1951). In fact, it has been observed that increases in the absolute abundance of *Pediastrum* are associated with increase in the abundance of cuticle debris (Hultberg, 1987), which further confirms their continental origin.

3.6. Calcareous nannofossil assemblage characterization

Samples for the analysis of calcareous nannofossils were taken at ~1.2 m (~4 ft) intervals throughout the MGC, and prepared using the simple smear slide technique (Bown and Young, 1998). Calcareous nannofossil assemblages were observed and quantified with standard transmitted cross-polarized light (XPL) microscopy (Zeiss AxioScope at 1250x magnification). A total of 135 simple smear slides were prepared from raw samples and within each slide individual taxa were quantified by the counting

of at least 400 specimens. The relative abundance of each taxa was reported as a percentage of the total number of nannofossils observed in each sample. Calcareous nannofossil preservation and abundances were logged for all samples with taxonomy following Dunkley Jones et al. (2009). Major biohorizons were identified based on the presence and absence of key marker taxa following the biostratigraphic scheme of Agnini et al. (2014). This work was undertaken by Dr Nursufiah Sulaiman as part of her doctoral thesis (Sulaiman, 2017), but is unpublished and is included and re-interpreted here with the aim of providing the basis for an integrated micropalaeontological and palaeoenvironmental analysis of the MGC.

3.7. Bulk stable-isotope data

The MGC sediments contain exceptionally well-preserved calcareous nannofossil assemblages and light microscopy demonstrated that coccolith carbonate dominates the fine (<20 μm size) fraction carbonates (Sulaiman, 2017). Therefore, this size-fraction was targeted for bulk isotope analyses to reduce noise from the mixing of planktonic and benthic foraminifera, ostracod carbonate, or other allochthonous carbonate which could affect the geochemical signals. Coccolithophores dwell and secrete coccolith plates within the photic zone (Okada and Honjo, 1973). The chemical compositions of coccoliths are thus considered to record signals in the shallow mixed layer (Dudley et al., 1980, 1986; Goodney et al., 1980). Further comparative studies on planktic calcareous microfossils have demonstrated that nannofossil $\delta^{18}O$ values vary in parallel to those of planktic foraminifers (Ennyu et al., 2002). This technique is particularly useful for Cretaceous and Tertiary pelagic nannofossil oozes and chalks that rarely or do not contain planktic foraminiferal tests and allows more rapid assay of variability in a record than does washing and picking individual foraminifers (Ennyu et al., 2002).

In this sense, a total of 444 bulk sediment samples, taken at ~30 cm spacing from the MGC, were processed at the University of Birmingham (SM1). The sediment was sieved over a 20 μm stainless steel mesh, with the fine-fraction passing through the sieve captured on ultra-fine-grade filter paper and air dried. The sediment residue was then transferred to 50 ml centrifuge tubes and organic matter within this fine fraction removed by overnight reaction with 5% sodium hypochlorite (NaClO) solution. The sample was then spun down at 4,500 rpm and the supernatant discarded. The sample was then washed 2-3 times with de-ionized water – each wash consisting of resuspension, agitation and then centrifuging and disgarding of the solution as above - until a neutral pH was established. Stable isotope measurements were performed at the NERC Isotope Geochemistry Laboratory (NIGL) at the British Geological Survey, Keyworth, on a dual inlet, triple collector, gas source mass spectrometer which is capable of simultaneously determining mass ratios 44/45 ($^{12}C/^{13}C$) and 46/44 ($^{16}O/^{18}O$). The carbonate analysis method involves reacting the carbonate sample with anhydrous phosphoric acid to liberate CO_2. All data are reported against VPDB after calibration of the in-house standard with NBS-19.

3.8. X-ray fluorescence (XRF) data

Several elements and element ratios have been reported as process and environmental proxies (Rothwell, 2015). To assess major changes in sedimentation patterns, we used combined ratios between calcium (Ca), silicon (Si), iron (Fe), and titanium (Ti). Whereas Ca reflects biogenic carbonate content, Si, Fe, and Ti provide evidence for rainfall, runoff, sediment density, and terrigenous sediment delivery (Ingram et al., 2010; Itambi et al., 2009; Rothwell, 2015). Therefore, Ca/Si, Ca/Fe, and Ca/Ti ratios can be used as a proxy

for biogenic versus lithogenic sedimentation, inputs from terrestrial sources, and ultimately continental influence (Rothwell, 2015).

We analyzed the elemental composition of the sediment core using two XRF techniques. 179 samples collected every 20-30 cm downcore, spanning the interval 106.8-151.6 m, were finely ground and dried before analysis as pressed powders in wax pellets. Pellets were analysed with a Bruker S8 TIGER XRF spectrometer with 8 min analysis time, at the School of Chemistry, University of Birmingham. Another 2,098 intervals on the original core section were analysed at a resolution of ~1.2 cm across the interval 17.1-109.4 m, directly with a hand-held XRF analyser at the core store of the Mississippi Department of Environmental Quality, in Jackson, Mississippi, by Dr Tatsuhiko Yamaguchi (Kochi University, Japan). The two methodologies were cross-calibrated over an interval of overlap between 106.8 and 109.4 m, with a total of ~80 samples, spanning a range of compositions, cross-correlated from both analysis methods (SM4).

CHAPTER 4: ORGANIC-WALLED DINOFLAGELLATE CYST BIOSTRATIGRAPHY OF THE UPPER EOCENE TO LOWER OLIGOCENE YAZOO FORMATION, US GULF COAST

(Author contributions: Marcelo A. De Lira Mota conceived the study, processed and analysed samples, interpreted results, and wrote and edited the article; Guy Harrington analysed the samples and participated in interpretation of the article; Tom Dunkley Jones collected samples and participated in interpretation, writing, and editing of the article.)

4.1. Introduction

The Eocene-Oligocene transition (EOT: ~34.0 Ma; Westerhold et al., 2014) represents a phase of accelerated climatic and biotic change that began before and ended after the Eocene-Oligocene boundary (EOB: 33.89 Ma). It is one of the most significant changes in the long-term background climate state over the past 110 Ma (Friedrich et al., 2012; Zachos et al., 2001). Across the whole EOT there is a ~1.2-1.5‰ increase in benthic $\delta^{18}O$ (e.g. Coxall et al., 2005; Kennett, 1977; Kennett and Shackleton, 1976b; Lear et al., 2000; Miller et al., 1987; Zachos et al., 2001, 1996, 1999), interpreted to represent ice expansion equivalent to 60% to 110% of the present Antarctic ice-sheet volume (Cramer et al., 2011) and a 3-4 ° C deep-water cooling (Cramer et al., 2011; Lear et al., 2003b). This ice expansion resulted in ~50-60 m of eustatic sea level fall (Cramer et al., 2011; Pekar et al., 2002), and it is associated with an estimated 3-6 ° C cooling across latitudes (Lear et al., 2008; Liu et al., 2009b). The presence of distinct rapid positive steps in high-resolution benthic foraminiferal oxygen isotope ($\delta^{18}O$) records are interpreted as representing at least two pulses of accelerated ice-sheet growth (Coxall et al., 2005; Scher

et al., 2011). These steps appear to be orbitally paced, with a duration of 40 ka, separated by a 300-400 ka interval of relative stability, or plateau (Coxall et al., 2005; Scher et al., 2011; Westerhold et al., 2014). The first step in $\delta^{18}O$ records is thought to be associated with relatively limited ice-sheet growth (Katz et al., 2008; Lear et al., 2008), being mainly driven by significant global cooling (Houben et al., 2018; Katz et al., 2008; Miller et al., 2008; Wade et al., 2012). The second step in $\delta^{18}O$ is thought to be dominated by ice-volume expansion (Katz et al., 2008; Lear et al., 2008), a sharp deepening of the ocean carbonate saturation depth (Coxall et al., 2005), and a massive and abrupt increase in weathering flux from East Antarctica (Scher et al., 2011). The geological rapidity of the EOT is, most likely, driven by the non-linear dynamics of Antarctic ice-sheet growth in response to a gradual decline in atmospheric greenhouse gas (carbon dioxide, CO_2) forcing (DeConto et al., 2008; DeConto and Pollard, 2003; Pagani et al., 2011; Pearson et al., 2009). These same positive feedbacks also resulted in a strong hysteresis, with the climate state becoming locked into a long-term icehouse state with large continental-scale ice sheets on Antarctica since the earliest Oligocene (Cramer et al., 2011; Lear et al., 2003a; Zachos et al., 2001). Furthermore, the EOT is associated with biotic turnover in plants and animals across a range of latitudes and environments (Prothero, 1994b). Although not comparable to the "big five" mass extinction events (Raup and Sepkoski, 1982), detailed micropalaeontological records show that substantial extinction and ecological reorganization is closely coupled to the EOT (Cotton and Pearson, 2012; Coxall and Pearson, 2007; Dunkley Jones et al., 2008; Houben et al., 2013b; Moore et al., 2015; Pearson et al., 2008, 2009). These include the extinction of the planktonic foraminiferal Family Hantkeninidae, which marks the EOB (Nocchi et al., 1988; Pearson et al., 2008; Premoli Silva and Jenkins, 1993), significant extinction in shallow-water

benthic foraminifera (Cotton and Pearson, 2012; Pearson et al., 2008), radiolarian (Kamikuri and Wade, 2012), and community overturning in the calcareous phytoplankton (Bordiga et al., 2015a; Dunkley Jones et al., 2008; Persico and Villa, 2004; Villa et al., 2008).

Dinocysts have been widely used in biostratigraphic and palaeoenvironmental studies (e.g. Bujak and Williams, 1985; Duxbury and Vieira, 2018; Kothe, 1990; Powell, 1992; Pross et al., 2010; Stover et al., 1996; Vieira et al., 2018), including several detailed studies of the EOT (e.g. Brinkhuis, 1994; Brinkhuis and Biffi, 1993; Houben et al., 2012, 2013b, 2018b; Jaramillo and Oboh-Ikuenobe, 1999; Van Mourik et al., 2001; Oboh-Ikuenobe and Jaramillo, 2003). A major compilation of Late Cretaceous–Neogene calibrated dinocyst bioevents, from both Northern Hemisphere and Southern Hemisphere, demonstrates a strong climatic control on the timing of bioevents, which are commonly diachronous (Williams et al., 2004). Dinocyst biostratigraphic studies thus need to consider comparable realms in similar climatic zones when selecting appropriate dinocyst bioevents (Williams and Bujak, 1985). There are existing dinocyst biostratigraphic studies of the Eocene-Oligocene from both the Northern Hemisphere (Brinkhuis and Biffi, 1993; Bujak and Mudge, 1994; Egger et al., 2016; Mudge and Bujak, 1994; Śliwińska et al., 2012; Thomsen et al., 2012; Wilpshaar et al., 1996) and the Southern Hemisphere (Bijl et al., 2018; Wilson, 1988). At the Massignano Eocene-Oligocene Global Stratotype Section and Point (GSSP), there are two successive influxes of cool-water high-latitude organic-walled dinoflagellate cyst (dinocyst) species (Brinkhuis and Biffi, 1993), the first of which correlates directly with the EOB and the second with the onset of a more severe cold episode and inferred sea level lowstand. In parallel, quantitative analysis of dinocyst distribution patterns from the “Massicore”, central Italy

(Van Mourik and Brinkhuis, 2005), revealed biotic turnover potentially associated with latitudinal and climatic zone changes through the Eocene-Oligocene transition. In the Massicore, dinocyst assemblages are interpreted to represent substantial cooling on the first step, with little subsequent change on the second step (Houben et al., 2012). Records from the Antarctic Margin show decreasing dinocyst species diversity through the Eocene and at the EOB (Mohr, 1990), interpreted as the progressive development of cold surface waters. More recent dinocyst studies (Houben et al., 2013b) document a sudden regime shift in zooplankton-phytoplankton interactions in the Southern Ocean associated with the earliest Oligocene glaciation of Antarctica, likely triggered by cooling, ice-sheet expansion, and sea-ice formation.

Eocene to Oligocene strata are well represented in outcrop and the shallow subsurface across the Gulf Coastal Plain of Mississippi and Alabama, as well as in the offshore systems of the northern Gulf of Mexico (Hosman, 1996). In these areas, dinocyst assemblages have an instrumental importance for site-to-site stratigraphic correlation and biochronology (Jaramillo and Oboh-Ikuenobe, 1999). Existing palynological work from five sites across southern Mississippi and Alabama allowed the correlation of stratigraphic sequences through the upper Eocene and the lower Oligocene (Jaramillo and Oboh-Ikuenobe, 1999). They observed a maximum flooding surface, estimated to be ~100 ka older than the EOB and a lower Oligocene lowstand system tract, most likely correlated to the global eustatic sea level lowstand coincident with the Earliest Oligocene Glacial Maximum (EOGM; Jaramillo and Oboh-Ikuenobe, 1999). However, this study is not well integrated into biostratigraphic schemes based on the calcareous plankton or detailed oxygen isotope stratigraphy, both of which are important in generating robust correlations of dinocyst biohorizons into global records of the EOT. More recently,

coupled sea level and palaeotemperature records from the neritic succession of the Saint Stephens Quarry (SSQ), Alabama (Houben et al., 2018), are interpreted to show cooling, minor ice-sheet expansion, and temperature-driven turnover in dinocysts in the first step, while the second step is characterized by a significant hiatus, potentially associated with a major sea level fall, with no meaningful change in palynological assemblages. Here we seek to extend this work by adding new biostratigraphic data from a site, the Mossy Grove core, Jackson, Mississippi, which recovered a continuous stratigraphic succession through the uppermost Eocene and into the lower Oligocene. This core recovered a complete sequence through the marine clays of the Yazoo Formation, central Mississippi (Dockery III et al., 1991). This clay yields palynomorph assemblages with high abundance and diversity, as well as an exceptional preservation. The Mossy Grove core is also substantially expanded compared to the St. Stephens Quarry section, with sedimentation rates estimated to be more than 10 times higher through the EOT (St. Stephens Quarry ~0.4 cm ka^{-1}; Mossy Grove ~4.7 cm ka^{-1}). This current study includes illustrated descriptions of the assemblages from the Mossy Grove core and dinocyst stratigraphic range data for the purpose of establishing a more resolved regional biostratigraphic scheme for the Gulf of Mexico and the US Gulf Coast.

While considerable attention has focused on EOT sections in southwestern Alabama (Jaramillo and Oboh-Ikuenobe, 1999; Katz et al., 2008; Mancini, 1979; Miller et al., 1993, 2008; Quaijtaal and Brinkhuis, 2012; Tew and Mancini, 1995; Wade et al., 2012) and southeastern Mississippi (Jaramillo and Oboh-Ikuenobe, 1999; Quaijtaal and Brinkhuis, 2012; Tew and Mancini, 1995), where the Yazoo Formation is lithologically heterogenous and divided into multiple constituent members, in central and western Mississippi the Yazoo Formation is a thick and relatively homogeneous succession of

calcareous clays. For micropalaeontological and palaeoenvironmental studies, these successions have the potential to yield some of the best marine records of the late Eocene in all of North America, if not globally. The relative lack of study of these successions appears to stem from early problems in determining a robust chronostratigraphic framework and the failure to constrain the EOB within the upper Yazoo Formation (Obradovich et al., 1993). The purpose of this study is to provide a detailed dinocyst biostratigraphic framework through an expanded EOT succession from the US Gulf Coast, as the basis for future studies of community change, extinction, and palaeoenvironments based on these assemblages. Such studies of the response of organic-walled cyst-producing dinoflagellate communities across this interval are important for an understanding of the nature of the reorganization of planktonic ecosystems through this major transition.

4.2. Regional geological context

The Gulf Coastal Plain (Figure 4) is one of the largest physiographic provinces in North America. In the subsurface the Mississippi embayment consists of a structurally complex basin with thick Jurassic-to-Holocene deposits (Cushing et al., 1964; Hosman, 1996). Within these sequences, the most continuous Paleogene successions are found between central and southern Mississippi and Alabama (Cushing et al., 1964; Hosman, 1996).

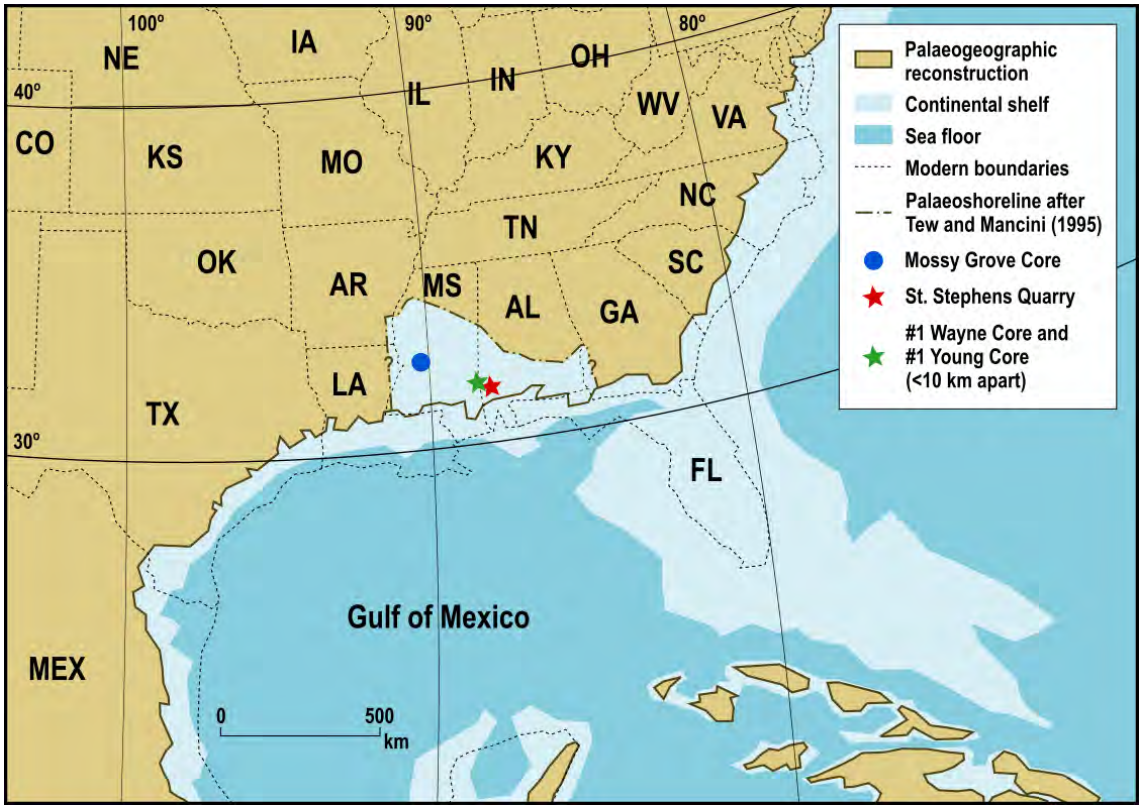


Figure 4. Palaeogeographic reconstruction showing location of the Mossy Grove, #1 Wayne and #1 Young cores, as well as St. Stephens Quarry outcrop. Main North American palaeogeography at ~35 Ma follows Deep Time Maps™ (https://deeptimemaps.com/, last access: 16 October 2018).

The upper Eocene to lower Oligocene stratigraphy of the US Gulf Coast is split into two groups (Figure 5): the Jackson (~ upper Eocene) and Vicksburg (~ lower Oligocene) groups (Cushing et al., 1964; Hosman, 1996). The contact between these groups is commonly indistinguishable on a lithologic basis, but they have distinct faunal assemblages (Hosman, 1996). The lithology, and constituent formations within these groups, also varies geographically across Mississippi and Alabama, reflecting relative positions along the palaeoshelf and proximity to river outflows. The upper middle Eocene of Mississippi consists of discontinuous and lenticular beds of lignitic-to-carbonaceous fine-to-medium quartz sand, silt, and clay. These sediments constitute the non-marine Cockfield Formation, the youngest continental deposits of the Eocene on the Gulf Coastal

Plain (Cushing et al., 1964; Hosman, 1996). The upper Eocene Jackson Group overlies the Cockfield Formation, and it represents the last extensive marine inundation within the Mississippi embayment (Cushing et al., 1964; Hosman, 1996). The Jackson Group consists of two major facies: to the west of the Gulf Coastal Plain, towards Texas, a shallow-water marine facies with beach sands, clays, and occasional volcanic tuffs, whilst to the east, in the central part of the Gulf Coastal Plain (Mississippi and Alabama), the group becomes more fossiliferous and argillaceous as deeper-water clays dominate (Cushing et al., 1964; Hosman, 1996). The two main lithostratigraphic units within the Jackson Group are the highly fossiliferous glauconitic sandy marls of the basal Moodys Branch Formation and the calcareous fossiliferous dark-grey to blue clays of the Yazoo Formation (Cushing et al., 1964; Hosman, 1996). The Yazoo Formation has four well-characterized members in eastern Mississippi and Alabama: the North Twistwood Creek Member (marl and calcareous clay), the Coccoa Sand Member (sandy marl), Pachuta Marl Member (glauconitic fossiliferous marls and sandy hard limestones), and the Shubuta Member (calcareous clays with concretions) (Cushing et al., 1964; Hosman, 1996). In central Mississippi, in the region of the Mossy Grove core, the entire Yazoo Formation is represented by an undifferentiated marine clay unit – the Yazoo Formation (Dockery III et al., 1991). Towards northern Mississippi this group occurs as a non-marine clastic facies, with evidence of lacustrine, palustrine, and lagoonal sedimentation, and the Yazoo Formation becomes undifferentiated and relatively homogeneous (Cushing et al., 1964; Hosman, 1996). The Oligocene series begins with the marine fossiliferous glauconitic clay and sandy clay of the Red Bluff Formation, overlain by the fossiliferous and laminated sands of the Forest Hill Formation. Westward, this unit presents some lenses of lignite and lignitic clay. Above the Forest Hill Formation is the

fossiliferous, granular, white crumbly limestone of the Bumpnose Formation (Cushing et al., 1964; Hosman, 1996). The Bumpnose Formation in Alabama and Florida is the equivalent of the Red Bluff-Forest Hill sequence in central and southern Mississippi (Hosman, 1996). Finally, overlying all these units is the Marianna-Mint Spring Formation, which consists of fossiliferous and porous limestone, glauconitic marl, and calcareous clay (Cushing et al., 1964; Hosman, 1996). In northern Mississippi, no evidence of Oligocene sedimentation is observed (Cushing et al., 1964; Hosman, 1996).

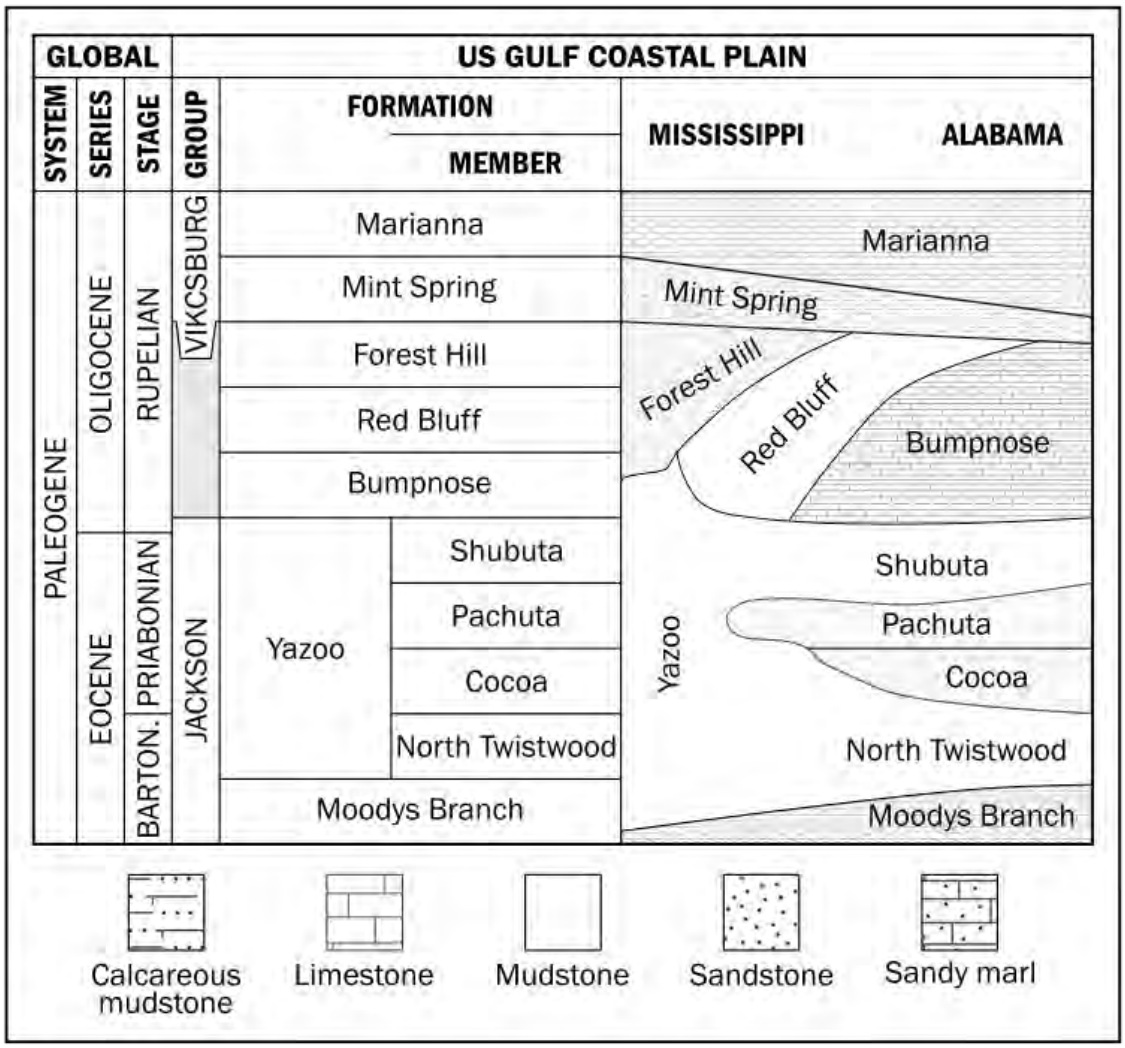


Figure 5. Simplified stratigraphic correlation chart of upper Eocene to lower Oligocene sedimentary rocks in the Mississippi-Alabama area (modified from Pasley and Hazel, 1995; Tew and Mancini, 1995; Hosman, 1996).

The upper Eocene to lower Oligocene lithostratigraphy outlined above has been interpreted within two distinct sequence stratigraphic models. The first argues that the Yazoo-Bumpnose contact coincides with a maximum flooding surface throughout the region (Baum and Vail, 1988; Echols et al., 2003; Jaramillo and Oboh-Ikuenobe, 1999; Loutit et al., 1988; Mancini and Tew, 1991; Tew, 1992). The second, and more recent (Miller et al., 2008), supports the association of the Yazoo-Bumpnose contact (Dockery, 1982) with a low stand sequence boundary, which is linked to the increasing $\delta^{18}O$ (Zachos et al., 2001, 1996, 2008) and global eustatic sea level fall (Coxall et al., 2005; Pekar et al., 2002) during the EOT. Sequence stratigraphic interpretations are difficult because of the depositional and lithologic variability across this region, and the difficulties in establishing robust, mostly biostratigraphic, tie points between key sections (Miller et al., 2008). Some of the key sections, from both outcrops and cores, which have been used for regional stratigraphic correlation, chronostratigraphy, and sequence stratigraphy, are shown in Figure 6.

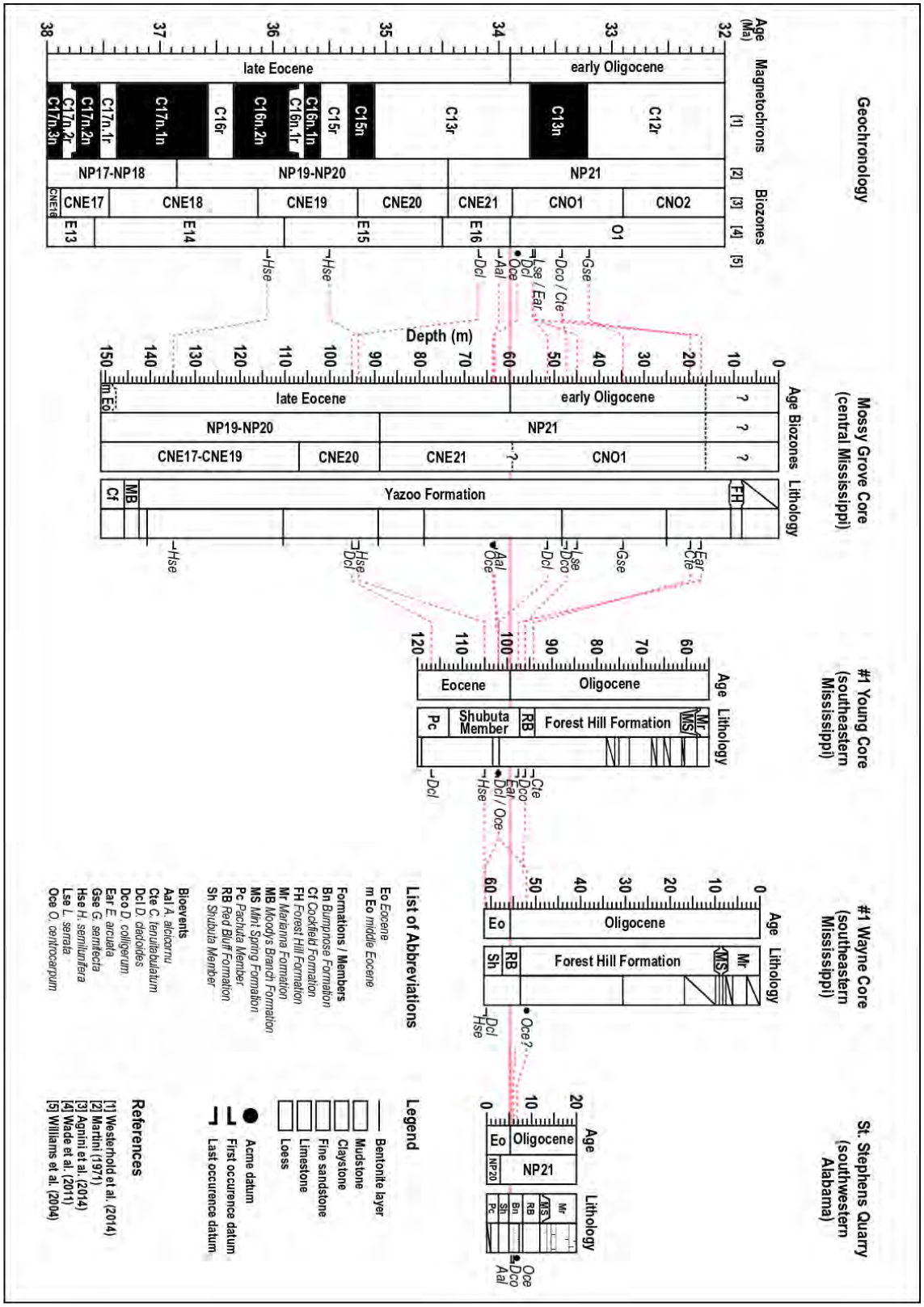


Figure 6. Stratigraphic correlation between the Mossy Grove Core and other three sections from Mississippi and Alabama (Jaramillo and Oboh-Ikuenobe, 1999). Lithology at the Mossy Grove follows Dockery III *et al.* (1991) and timescale for all sections follows Westerhold *et al.* (2014). See discussion about dinocyst bioevents in section 4.4.3.

Even at the St. Stephens Quarry section, southwestern Alabama, which is a widely studied reference for the EOT (Katz et al., 2008; Miller et al., 2008; Wade et al., 2012), establishing a robust biostratigraphy and sequence stratigraphy has been difficult (Miller et al., 2008). The low abundance and generally poor preservation of hantkeninids in the shallow-water Gulf Coast successions make the accurate placement of their last occurrence (LO) problematic (Miller et al., 2008). This difficulty is further aggravated by the reworking of upper Eocene calcareous microfossils up into lowest Oligocene sediments as a result of the major regression across the EOT (Bybell and Poore, 1983). Nevertheless, a middle-to-late Priabonian age was assigned to the Pachuta Member at SSQ, based on the LO of *R. reticulata*, upper part of nannofossil zone NP19-20 (Miller et al., 2008). The Shubuta Member has a late Priabonian age correlated to the lower part of NP21 zone, the interval between E16 and the lower part of O1 zones, and the upper part of magnetochron C13r (Miller et al., 2008). The Red Bluff-Bumpnose sequence was dated as late Priabonian to early Rupelian age and can be correlated to the middle part of NP21 zone, the lower to middle part of O1 zone and the upper part of C13n magnetochron (Miller et al., 2008).

4.3. Materials and methods

4.3.1. Mossy Grove Borehole

The Mossy Grove borehole was drilled in September 1991 at Mossy Grove, Hinds County, Mississippi. It consists of a 161.6 m (530 ft) continuously cored succession, with near full recovery (Dockery III et al., 1991). At its base it recovered ~5.5 m of the upper Cockfield Formation (161.6 to 156.1 m; 530 to 512 ft, 18 ft thick), overlain by ~3.7 m of

the Moodys Branch Formation (156.1 to 152.4 m; 512 to 500 ft, 12 ft thick), and then a thick 140.9 m succession of the Yazoo Formation (152.4 to 11.6 m; 500 to 38 ft, 462 ft thick). At the top of the core, overlaying the Yazoo Formation, 3.0 m of terrestrial lignites of the Forest Hill Formation were recovered (11.6 to 8.5 m; 38 to 28 ft, 10 ft thick), which in turn was overlain by a 8.5 m thick (28 ft) cover of Pleistocene loess. To improve the chronology of the upper Yazoo Formation, $^{40}Ar/^{39}Ar$ absolute dating was undertaken from a number of bentonite layers at four sites (Obradovich et al., 1993; Priddy, 1960), including seven layers within the Mossy Grove core, from which two dates were recovered (Obradovich et al., 1993; Obradovich and Dockery III, 1996).

Establishing a robust age model for the Mossy Grove core has required significant effort and the integration of dinocyst, calcareous nannofossil, and radiometric dating techniques. Initial age models were based on planktonic foraminifera assemblage data (Fluegeman, 1996; Fluegeman et al., 2009), but due to low planktonic foraminifera abundances, especially in the upper part of the core (<91.4 m; 300 ft), this age model relied upon poorly calibrated secondary markers. For instance, the direct placement of the EOB, based on the last occurrence of the Hantkeninidae, is problematic as the record of *Hantknenina alabamensis*, the only hantkeninid species found in the core, is poor and discontinuous above ~86.6 m (284 ft). The last occurrence of *Turborotalia cerroazulensis*, expected to be ~0.1 Ma older than the EOB and the Hantkeninidae extinction, occurs ~7.3 m (24 ft) higher than the last occurrence of *H. alabamensis.*

Radiometric $^{40}Ar/^{39}Ar$ dating is significantly offset from the existing planktonic foraminifera biochronology. Bentonite layers at ~26.5 m (87 ft) and ~84.4 m (277 ft) were dated to 33.40 and 34.36 Ma, respectively (Obradovich and Dockery III, 1996), whereas foraminifera biochronology places these bentonites at ~33.87 and 35.33 Ma,

respectively (Fluegeman et al., 2009), an offset of between ~0.5 and 1 Ma. This mismatch has implications for the accurate placement of the EOB in this section; assuming a constant sedimentation rate within the interval between the bentonites, radiometric dating would place the boundary at ~56.7 m (186 ft), which is ~30.2 m (99 ft) lower than the existing foraminiferal estimate of ~26.5 m (87 ft) (Fluegeman et al., 2009).

4.3.2. Palynological preparation techniques

Altogether, 112 sediment samples were collected from the Mossy Grove core at ~1.2 m (4 ft) intervals, between ~17 and 152 m deep (55 and 499 ft). A mass of 20 g from each sediment sample was broken into pieces, ~5 mm in diameter, using a pestle and mortar. This was followed by a set of acid treatments, including (1) 40% HCl for 30 min to remove carbonates; (2) 60% HF for 24 h to disaggregate the rock matrix; (3) sieving of the residues at 10 μm through a nylon mesh sieve to retain the HF effluent from the material; (4) a second HCl treatment to remove any precipitate formed during stage 2; and (5) a final sieving, as per stage 3. The material was then subjected to oxidation (70% HNO_3 for exactly 2 min) to remove pyrite, inorganic debris, and any unstructured organic material from the residues. Another sieving step was done to remove any HNO_3 effluent. A final cleaning treatment was undertaken with a combination of domestic and industrial detergents. Using a glass swirling dish and centrifugal swirling techniques, palynomorphs in each sample were subsequently concentrated and Bismark brown was added to make them more visible with light microscopy. Finally, the samples were sieved into two size fractions, 10-30 μm (concentrating spores and pollen) and >30 μm (concentrating dinocysts), and then mounted on separate 22 mm × 22 mm coverslips, which were glued to a glass slide using Norland optical adhesive. In this work, only the coarse fraction content of each slide was analysed. A pilot survey of these slides revealed that the acid

and oxidizing technique yielded higher diversity than their non-acid and non-oxidizing counterparts (Burgess, 2015). All slides were stored in the collection of the School of Geography, Earth and Environmental Sciences, University of Birmingham.

4.3.3. Dinocyst assemblage characterisation

With a Zeiss transmitted-light microscope, at least 200 dinocyst specimens were counted in each sample, along with the respective number of spores, pollen, algae (Prasinophyceae and Chlorophyceae), zoomorphs/zooclasts, phytoclasts, and amorphous organic matter. Once 200 specimens were counted, the remaining fields of the coverslip were scanned for very rare dinocysts. Only palynomorphs that were more than 50% complete and not obscured either by air bubbles or organic debris were considered. We used the following abundance scheme: 0% – barren (B); 0%-1% – trace (T); 1 %-10% – few (F); 10 %-25% – common (C); >25% – abundant (A). Preservation was qualitatively categorized as good (G), moderate (M) or poor (P).

4.3.4. Nannofossil assemblage characterisation

Samples for the analysis of calcareous nannofossils were taken at ~1.2 m (~4 ft) intervals throughout the Mossy Grove core. Samples were prepared using the simple smear slide technique (Bown and Young, 1998) and observed with standard transmitted cross-polarized light (XPL) microscopy (Zeiss AxioScope at 1250x magnification). Calcareous nannofossil preservation and abundances were logged for all samples with taxonomy following Dunkley Jones et al. (2009). Major biohorizons were identified based on the presence and absence of key marker taxa following the biostratigraphic scheme of Agnini et al. (2014).

4.4. Results

4.4.1. Dinocyst distribution

Nearly all the core samples contain abundant and very well-preserved dinocysts, with only a few samples being scarce or rare. A semiquantitative distribution of all dinocysts recognized in the investigated section is shown in Figure 7. *Spiniferites* species dominate in most samples and account for ~50% of the overall count, followed by *Hystrichokolpoma* (mainly *H. rigaudiae* and *H. salacia*) and *Operculodinium* (mainly *O. centrocarpum*) (~6% each); *Charlesdowniea* (*C. coleothrypta*) (~4 %); *Heteraulacacysta* (mainly *H. porosa*); *Lingulodinium* (mainly *L. machaerophorum*) and *Cleistosphaeridium* (mainly *C. ancyreum*) (3% each); and *Cordosphaeridium*, *Dinopterygium* (*D. cladoides*), *Glaphyrocysta*, *Homotryblium* (mainly *H. floripes*), *Saturnodinium* (*S. pansum*), and *Thalassiphora* (mainly *T. fenestrata*) (~2% each). These genera account for nearly 90% of all dinocysts counted in the section, although there are other significant occurrences of *Achomosphaera alcicornu*, *Dapsilidinium pastielsii*, *Enneadocysta arcuata*, and *Hystrichosphaeridium tubiferum*. Several influxes of relative abundances higher than 25% are observed: *C. fibrospinosum* (~142.3 m depth; 467 ft), *D. cladoides* (~94.8 m depth; 311 ft), *H. leptalea* (~66.8 m depth; 219 ft), *H. porosa* (~58.4 m depth; 191.5 ft), *H. floripes* (~118.0 m depth; 387 ft), *H. tubiferum* (~91.1 m depth; 299 ft), *L. machaerophorum* (~107.0 m depth; 351ft), *O. centrocarpum* (~68.0 and ~75.3 m depth; 223 and 247 ft), *T. fenestrata* (~83.8 and ~85.0 m depth; 275 and 279 ft), and *W. articulata* (~102.1 m depth; 335 ft).

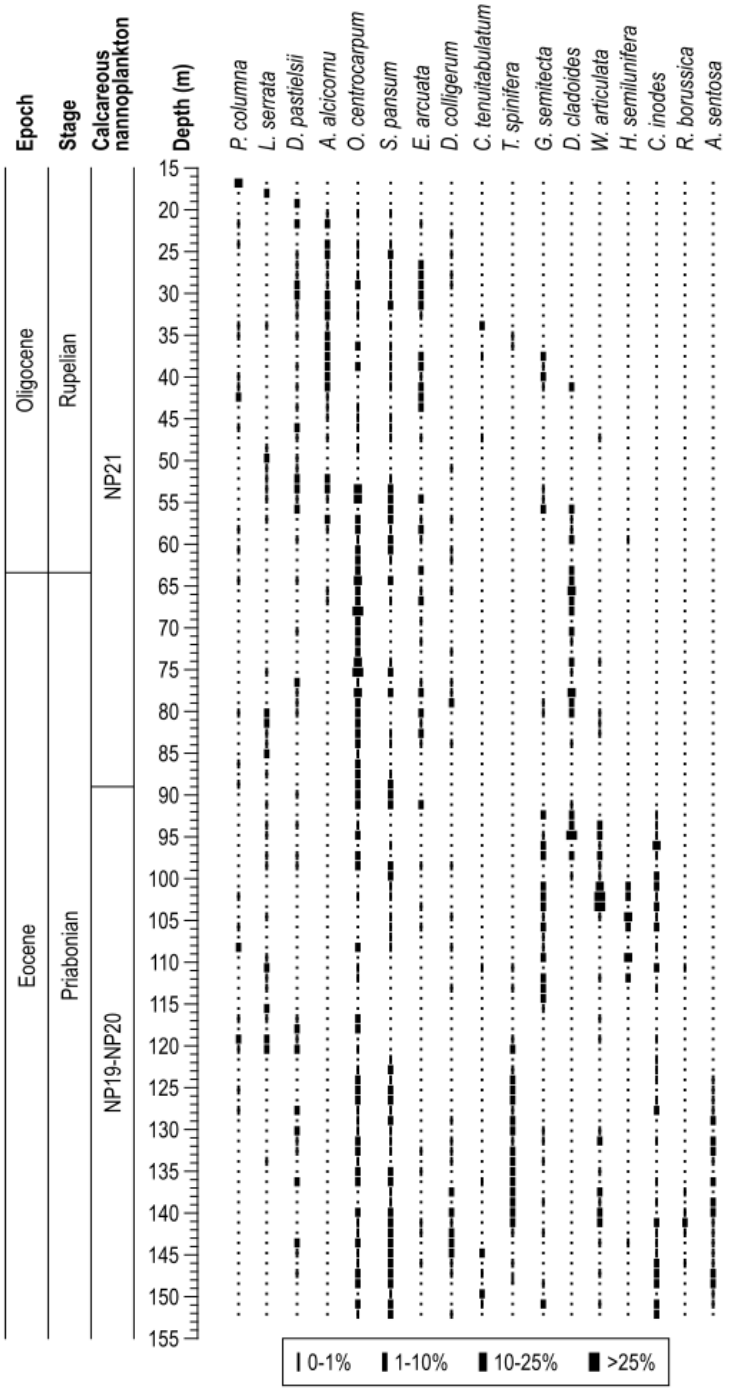


Figure 7. Semiquantitative range chart of dinocyst taxa encountered at the Mossy Grove core, central Mississippi, US Gulf Coastal Plain, including calcareous nannoplankton zonation.

4.4.2. Nannofossil biostratigraphy

For this study we present the first calcareous nannofossil biostratigraphy of the Mossy Grove core, with biohorizons calibrated to the global zonation scheme of Agnini et al. (2014). We updated these absolute ages (Agnini et al., 2014) to the timescale of (Westerhold et al., 2014). Three of these bioevents constrain the base and top of the core: the absence of *Sphenolithus obtusus* at the base of the core indicates that the section bottom (152.1 m; 499 ft) is younger than 38.24 Ma; the first common occurrence (FCO) of *Isthmolithus recurvus* was identified at ~136.9 m (449 ft), which corresponds to 36.74 Ma; and the LO of *Coccolithus formosus*, whose occurrence spans from ~50.0 m (164 ft) to ~16.8 m (55 ft), indicates that the top of the section is older than 32.90 Ma. Moreover, two other LO events have been detected within the core: *Discoaster saipanensis* (~89.2 m; 292.5 ft) and *Reticulofenestra reticulata* (~107.6 m; 353 ft), indicating ages of 34.44 and 35.31 Ma, respectively. All biostratigraphic and radiometric ages are presented in Table 1.

Table 1. List of bioevents, biohorizons and calibrated ages, updated to the Timescale of Westerhold et al. (2014). Legend: CN – calcareous nannofossils (this tudy); PF – planktonic foraminifera (Fluegeman, 1996; Fluegeman et al., 2009); RD – radiometric dating (Obradovich and Dockery III, 1996).

Type	Event	Depth		Age
		m	ft	(Ma)
CN	LO *C. formosus* (constrain)	16.8	55.0	32.90
RD	$^{40}Ar/^{39}Ar$	26.5	87.0	33.40
PF	E16/O1 boundary	29.0	95.0	33.82
PF	E15/E16 boundary	56.4	185.0	34.50
RD	$^{40}Ar/^{39}Ar$	84.4	277.0	34.36
CN	LO *D. saipanensis*	89.2	292.5	34.44
PF	E14/E15 boundary	100.3	329.0	35.90

CN	LO *R. reticulata*	107.6	353.0	35.31
PF	E13/E14 boundary	124.1	407.0	38.02
CN	FCO *I. recurvus*	136.9	449.0	36.74
CN	LO *Sphenoliths obtusus* (constrain)	152.1	499.0	38.24

4.4.3. Dinocyst biostratigraphic framework

Dinocysts dominate the palynological assemblages in the studied material. In total, we identified 52 genera and 70 species, with nomenclature following Williams et al. (2017) and references therein. A full species list and plates are provided in Appendices 2 an 3. The rich and well-preserved dinocyst assemblages provide the basis for a detailed assessment of upper Eocene dinoflagellate biostratigraphy in this succession, which is developed with reference to dinocyst biostratigraphic data from offshore eastern Canada (Egger et al., 2016; Williams, 1975, 1977), the Gulf Coastal Plain (Houben et al., 2018; Jaramillo and Oboh-Ikuenobe, 1999), offshore Florida (Van Mourik et al., 2001), the Norwegian and Greenland seas (Eldrett et al., 2004; Manum, 1976; Manum et al., 1989; Williams and Manum, 1999), the North Sea (Bujak and Mudge, 1994; Gradstein et al., 1992; Hansen, 1977; Heilmann-Clausen and Van Simaeys, 2005; Mudge and Bujak, 1996; Śliwińska et al., 2012), the Hampshire Basin (Costa et al., 1976), the central Mediterranean region (Brinkhuis, 1994; Brinkhuis and Biffi, 1993; Van Mourik and Brinkhuis, 2005; Wilpshaar et al., 1996), northwestern Europe (England, Belgium, and Germany; Costa and Downie, 1979; Kothe, 1990), the Tasmanian Gateway (Stickley et al., 2004a), and the wider Northern Hemisphere (Williams, 1993). Although there have been studies of dinocyst biohorizons across the EOB interval in Gulf Coast sections from Alabama (e.g. Houben et al., 2018; Jaramillo and Oboh-Ikuenobe, 1999), these do not

have the stratigraphic coverage of the upper Eocene or the quality of dinocyst preservation provided by the Mossy Grove core material. Age assignments are based on the global compilation of age-calibrated bioevents (Williams et al., 2004), with a total of 23 potentially useful dinocyst biohorizons recognized in the Mossy Grove succession (Table 2), including 7 first occurrences (FO), 1 first common occurrence (FCO), 14 last occurrences (LO), and 1 last common occurrence (LCO) event.

Table 2. List of dinocyst bioevents recorded in the section. Reliability rating and absolute ages were assigned for selected events. Timescale (GPTS) follows Westerhold et al. (2014). The last column presents ages calculated from the age-depth model provided by this study (see section 4.4.4). Legend: FO represents first occurrence; LO represents last occurrence; FCO represents first common occurrence; LCO represents last common occurrence; A represents acme; * represents age available only after the timescale of Pälike et al. (2006); H represents high reliability; L represents low reliability; and M represents moderate reliability. References for chosen ages: a – Brinkhuis and Biffi (1993), b – Brinkhuis et al. (2003), c – Bujak and Mudge (1994), d – Eldrett et al. (2004), e – Jaramillo and Oboh-Ikuenobe (1999), f – Williams et al. (2004), g – Williams and Manum (1999).

Type	Event	Mean-Depth		Uncertainty		Chosen Age (Ma)	Reliability	Age at Mossy Grove (Ma)
		m	ft	m	ft			
LO	*Dapsilidinium pastielsii*	18.6	61.0	0.6	2.0	-	-	32.94
LO	*Enneadocysta arcuata*	18.6	61.0	0.6	2.0	33.68[a]	M	32.94
LO	*Saturnodinium pansum*	19.8	65.0	0.6	2.0	30.20*[g]	L	32.97
LO	*Cribroperidinium tenuitabulatum*	21.0	69.0	0.6	2.0	33.43[e]	M	32.99
LCO	*Enneadocysta arcuata*	25.9	85.0	0.6	2.0	-	-	33.09
LO	*Glaphyrocysta semitecta*	36.9	121.0	0.6	2.0	33.21[a]	H	33.33
LO	*Lentinia serrata*	48.0	157.5	0.6	2.0	33.68[f]	H	33.57
LO	*Diphyes colligerum*	50.3	165.0	0.6	2.0	33.44[f]	H	33.61
LO	*Dinopterygium cladoides*	55.2	181.0	0.6	2.0	33.70[e]	M	33.72
FO	*Achomosphaera alcicornu*	67.4	221.0	0.6	2.0	33.99[f]	H	33.98
A	*Operculodinium centrocarpum*	68.0	223.0	-	-	33.83[e]	M	33.99
LO	*Wetzeliella articulata*	73.5	241.0	0.6	2.0	-	-	34.11
LO	*Cordosphaeridium inodes*	91.8	301.0	0.6	2.0	-	-	34.55
FCO	*Dinopterygium cladoides*	95.4	313.0	0.6	2.0	-	-	34.71
FO	*Dinopterygium cladoides*	100.3	329.0	0.6	2.0	34.18[e]	M	34.92
LO	*Hemiplacophora semilunifera*	100.3	329.0	0.6	2.0	35.49[f]	M	34.92
LO	*Thalassiphora spinifera*	110.0	361.0	0.6	2.0	-	-	35.37
LO	*Rottnestia borussica*	110.0	361.0	0.6	2.0	39.00[d]	L	35.37
LO	*Areoligera sentosa*	123.5	405.0	0.6	2.0	38.84[c]	M	36.11

FO	*Piladinium columna*	128.3	421.0	0.6	2.0	-	-	36.37
FO	*Lentinia serrata*	134.4	441.0	0.6	2.0	39.97[f]	L	36.71
FO	*Hemiplacophora semilunifera*	144.2	473.0	0.6	2.0	36.05[f]	M	37.24
FO	*Thalassiphora spinifera*	146.6	481.0	0.6	2.0	-	-	37.37

At least 15 of the 23 biohorizons within the Mossy Grove succession could be correlated to other mid-latitude areas in the Northern Hemisphere, and we discuss each of these – from the base of the succession upwards – in the text below. Our estimation of the reliability of each bioevent as highly, moderately, or lowly reliable; it is based on a combination of the clarity of taxonomic definition of a species or genus, as well as the number of reports of the associated biohorizon at other localities, and the consistency of stratigraphic position between them. The estimated age of each bioevent is also given, along with a rationale for the chosen calibration. Ages are first provided according to the original assignment and timescale but then, for consistency, are all updated to the Westerhold et al. (2014) timescale, which is given in brackets. Where there is evidence for latitudinal diachroneity of an event, we preferentially choose age calibrations from locations closest to the study site. Standard nannoplankton (Agnini et al., 2014; Martini, 1971) and foraminiferal (Berggren et al., 1995; Berggren and Pearson, 2005; Wade et al., 2011) biozonation schemes were used when discussing selected dinocyst bioevents.

The palynological assemblages of the Mossy Grove core show strong evidence for sea level fall associated with the EOT interval manifest in the form of increased flux of terrestrial plant material but also in the influx of clearly weathered and reworked acritarchs and continental palynomorphs towards the top of the succession. This includes reworked Late Cretaceous taxa such as *Achomosphaera ramulifera*, *Cannosphaeropsis* sp., *Chatangiella* sp., *Cymososphaeridium phoenix*. *Dinogymnium sibiricum*, *Litosphaeridium siphoniphorum*, and *Palaeohystrichophora infusorioides*, as well as

early and middle Eocene dinocyst taxa *Hystrichosphaeridium tubiferum* (Bujak and Mudge, 1994; Mudge and Bujak, 1996), *Wetzeliella articulata* (Bujak and Mudge, 1994; Mudge and Bujak, 1996), *Piladinium columna* (Bujak and Mudge, 1994; Mudge and Bujak, 1996), and *Diphyes ficusoides* (Gradstein et al., 1992). The distribution patterns of Eocene dinocysts through the core indicate local reworking of older middle and lower Eocene marine sediments from around the margin of the Mississippi embayment, especially through the EOT and towards the top of the succession. This reworking makes the confident placement of some last occurrences difficult, especially where there is some existing discrepancy between published age assessments of these bioevents as being either late Eocene or early Oligocene. Here we interpret consistent presence of a taxa, followed by a continuous stratigraphic absence or sporadic occurrences, as representing a genuine LO event. Sporadic occurrences are reported as local reworking from exposed middle to upper Eocene sediments during regional sea level fall.

FO *Hemiplacophora semilunifera*. The first occurrence of this species is at ~143.6 m (471 ft). From this point upwards, it is present in most samples, with abundances gradually increasing, especially in the interval ~119.2-99.7 m (391-327 ft). Based on data from equatorial and Southern Hemisphere sites (Stickley et al., 2004a; Williams et al., 2004), this event has been tentatively dated between 36.00 and 41.40 Ma (36.05 to 41.20 Ma), in middle and higher latitude sites, respectively.

FO *Lentinia serrata*. This species first occurs at ~133.8 m (439 ft), although there is a short interval after this occurrence in which the taxon is not observed. This event was identified in central Italy (Brinkhuis and Biffi, 1993) sections in the lowermost Adi interval zone, which corresponds to the calcareous nannoplankton zone NP21, the planktonic foraminifera zone P18, and the top of the magnetostratigraphic chron C13r.

This agrees with an age of 33.64 Ma (33.84 Ma) assigned in equatorial latitudes (Williams et al., 2004). Although these data seem consistent, dating from the mid-latitudes in the Northern Hemisphere (Williams et al., 2004) points to an age of 40.00 Ma (39.97 Ma) for this bioevent.

LO *Areoligera sentosa*. The last occurrence of this species is clearly observed at ~124.1 m (407 ft). This event is considered synchronous and an excellent chronostratigraphic marker in the entire North Sea Basin to Norwegian-Greenland seas region (Bujak and Mudge, 1994; Costa et al., 1976; Heilmann-Clausen and Van Simaeys, 2005; Mudge and Bujak, 1996), with an age assignment in the lower part of E7 dinocyst zone and, more precisely, at the E7a/E7b sub-zone boundary (Bujak and Mudge, 1994; Mudge and Bujak, 1996), which identified this event just between NP16 and NP17 nannoplankton zones and in the lower part of planktonic foraminifera zone P14.

LO *Rottnestia borussica*. Almost all occurrences of this species at the study site are below ~137.5 m (451 ft), except for an isolated occurrence at ~110.6 m (363 ft). Although this isolated appearance may reflect patterns of ecological exclusion, interpreting it as LO event would be less consistent with the age model. Therefore, we conclude that the isolated upper occurrence represents reworking processes and constrain the range of this taxa to a short interval in the lower part of the succession (below 137.5 m). In the Hampshire Basin (Aubry, 1983, 1985) and the North Sea (Bujak and Mudge, 1994; Mudge and Bujak, 1996) this event was dated as late Bartonian, calibrated with the upper part of the dinocyst subzone E7b (Bujak and Mudge, 1994; Mudge and Bujak, 1996), nannoplankton zone NP17, and planktonic foraminifera zone P14, whilst in Italy its range is reported to extend into the lower Rupelian (Brinkhuis and Biffi, 1993). A late Bartonian age of 39.00 Ma (39.00 Ma) is consistent within the Norwegian-Greenland seas

(Eldrett et al., 2004; Eldrett and Harding, 2009) and with the southwestern margin of the Rockall Plateau, North Atlantic, where it was dated as middle Eocene and calibrated within the dinocyst zone within zone IVb (Costa and Downie, 1979); however, it is distinct from middle Priabonian age assigned in the central Danish basin (Heilmann-Clausen and Van Simaeys, 2005), calibrated with the middle part of the nannoplankton zone NP19/20; in offshore Florida (Van Mourik et al., 2001), it is found within planktonic foraminifera zone P16. Based on correlation to nannofossil biostratigraphy within the Mossy Grove core, we can constrain this event to be younger than 39.00 Ma, such that this taxa ranges into the topmost Bartonian.

LO *Hemiplacophora semilunifera*. The last occurrence of *H. semilunifera* is clearly identified at ~100.9 m (331 ft), above which the taxa is absent, except for very rare isolated and widely spaced occurrences. This event was dated in the Mediterranean (Brinkhuis and Biffi, 1993; Wilpshaar et al., 1996) with an early Oligocene age, correlated to the top of the Gse dinocyst zone (Brinkhuis and Biffi, 1993), the nannoplankton NP21, and foraminifera P18 biozones. Nevertheless, estimates from middle latitudes in the Southern Hemisphere (Williams et al., 2004) indicate that it occurred much earlier, during the NP19-20 biozone and between the P15 and P16 biozones, which an assigned age of 35.20 Ma (35.49 Ma).

FO *Achomosphaera alcicornu*. The first occurrence of this taxon at the study site was detected at ~66.8 m (219 ft), and it is consistently observed until the top of the section. Early estimates from Danish sections dated this bioevent as Danian, placing it in the upper part of the *S. inornata* subzone (Hansen, 1977). In high latitudes of the Southern Hemisphere, this event was dated at 35.70 Ma (Williams et al., 2004; 35.82 Ma). However, estimates from lower latitudes, such as the Mediterranean (Brinkhuis and Biffi,

1993; Wilpshaar et al., 1996) and the Equator (Williams et al., 2004), identified this event within the nannoplankton NP21 and foraminifera P17 biozones, and within the magnetostratigraphic chron C13r, with an assigned age varying between 33.76 (Williams et al., 2004; 33.99 Ma) and 34.00 Ma (Wilpshaar et al., 1996; 34.29 Ma).

LO *Diphyes colligerum*. This species has a relatively continuous record throughout the entire core up to ~50.9 m (167 ft). After an interval of absence (~22.0 m; 72 ft), it reappears near the top of the hole (~29.0 m; 95 ft) associated with another species of the same genus, *D. ficusoides*, which is known to have been extinct since the middle Lutetian. This suggests that the *D. colligerum* specimens found near the top of the core are most likely the result of reworking. Although the last occurrence of *D. colligerum* has been used to indicate the Eocene-Oligocene boundary worldwide (Williams, 1993), other studies record this event from the mid-Lutetian to the early Oligocene. In the southwestern margin of the Rockall Plateau, North Atlantic, this event was dated as middle Eocene and identified within zone IVb (Costa and Downie, 1979). In the North Sea it has been identified close to the Lutetian-Bartonian boundary (Bujak and Mudge, 1994; Mudge and Bujak, 1996), similar to its position in the Norwegian-Greenland seas (Eldrett et al., 2004), although later studies found it ranging up into the middle Bartonian in this area (Eldrett and Harding, 2009). In the central Danish basin it corresponds to the middle Lutetian, in the upper part of NP15 nannoplankton biozone (Heilmann-Clausen and Van Simaeys, 2005). In northwest Germany it was recorded in several samples from the lower Oligocene (Kothe, 1990). Across North America, however, some consistent younger ages were assigned for this event, from late Priabonian to early Rupelian, including offshore Canada (nannoplankton Biozone NP21) (Williams, 1975) and offshore

Florida (C13r magnetochron) (Van Mourik et al., 2001) which are both closer to the lower Rupelian age estimate of 33.27 Ma (Williams et al., 2004; 33.44 Ma).

LO *Lentinia serrata*. The last occurrence of this species at the study site is clearly observed at ~48.6 m (159.5 ft), after which only isolated occurrences are detected. In mid-latitude climatic zones in the Northern Hemisphere, the age of 33.50 Ma (Williams et al., 2004; 33.68 Ma) has been assigned to this event, whereas in equatorial regions it is estimated that this taxon persists longer, potentially up to 31.00 Ma (Williams et al., 2004).

LO *Glaphyrocysta semitecta*. This species has a fairly continuous occurrence from the base of the section upwards, becoming particularly common (up to ~9% of the dinocyst assemblage) between ~115.5 and ~92.4 m (379 and 303 ft). However, this species is again common (~4% of the dinocyst assemblage) in two upper intervals (55.8-53.3 m, 183-175 ft; and 41.2-37.5 m, 135-123 ft), which is unlikely to be a result of reworking and has a last occurrence at ~37.5 m (123 ft). The LO of *G. semitecta* has been used in central Italy to define the base of the Cin dinocyst biozone (Brinkhuis and Biffi, 1993), of Rupelian age, which is calibrated with the upper part of P18 planktonic foraminifera biozones, the upper part of NP21 nannoplankton biozones, and the C13n/C12r magnetoboundary, which is in agreement with the observations within this succession.

LO *Saturnodinium pansum*. This taxon has nearly continuous occurrence throughout the core, only being absent above ~20.4 m (67 ft). In sediments recovered from the central part of the Norwegian Sea (Williams and Manum, 1999) this extinction event is identified at the Lithostratigraphic Unit V, corresponding to the upper Rupelian and an age of 30.24 Ma.

LO *Enneadocysta arcuata*. This species occurs near continuously through almost the whole core, with highest abundances from ~105.8 m (347 ft) up to its last appearance at ~19.2 m (63 ft). A latest Priabonian age has been assigned to this bioevent in the Norwegian Sea (Manum, 1976; Manum et al., 1989), corresponding to the nannoplankton zone NP21 and the planktonic foraminifera P17/P18 boundary. However, in the Scotian Shelf and Grand Banks, offshore southeastern Canada, *E. arcuata* was an age-diagnostic species for the early Oligocene *D. heterophlycta* Assemblage Zone (Williams, 1975). At the Ocean Drilling Program (ODP) Site 1172, in the East Tasman Plateau (Brinkhuis et al., 2003b), an age estimate of 33.50 Ma (33.68 Ma) has been assigned to the unnamed *Enneadocysta* sp. A, a taxon closely related to *E. arcuata*, which is also consistent with the placement of this event in North America.

On a regional scale, some distinctive events found at Mossy Grove are very similar to those detected in five sections from southeastern Mississippi and southwestern Alabama (Jaramillo and Oboh-Ikuenobe, 1999). Graphic correlation across five sections (St. Stephens Quarry, R2089, #1 Young, #1 Wayne, and #1 Ketler) allowed age determination of the main dinocyst events, including the FO of *Dinopterygium cladoides* (33.9 Ma), the Acme of *Operculodinium centrocarpum* (33.6 Ma), the LO of *Dinopterygium cladoides* (33.5 Ma), and the LO of *Cribroperidinium tenuitabulatum* (33.2 Ma). Although these are not included in the list of the discussed bioevents above, they are all apparent in the Mossy Grove core, with depths listed in Table 2, and appear to be consistent in their age and stratigraphic position with these regional studies.

It is notable that well-preserved specimens of *Areosphaeridium diktyoplokum* were found at ~74.1 m (243 ft). The extinction of this taxa has been associated with the EOB (e.g. Head and Norris, 1989; Williams, 1975, 1977; Williams and Bujak, 1985), although

there is much discussion about the age of this event. Early publications reported late Eocene ages for the event in the Scotian Shelf and Grand Banks (Williams, 1975, 1977); and in Baffin Bay, Canada (Head and Norris, 1989), as well as in the North Sea (Bujak and Mudge, 1994; Mudge and Bujak, 1996). However, studies of central Italian successions (Brinkhuis and Biffi, 1993; Wilpshaar et al., 1996) place the LO of *A. diktyoplokum* above the hantkeninid extinction horizon, at the top of the early Oligocene Adi interval zone, calibrated against lower planktonic foraminifera P18 zone, mid nannoplankton NP21 zone, and the basal part of magnetic polarity chronozone C13n. Although previous (Costa and Manum, 1988; Stover and Williams, 1988; Williams and Bujak, 1985) and later (Bujak and Mudge, 1994; Mudge and Bujak, 1996) surveys have demonstrated the possibility that the alleged later occurrences in central Italy could be due to reworking processes, recent dinocyst bio-stratigraphies from the Norwegian-Greenland seas (Eldrett et al., 2004; Eldrett and Harding, 2009) confirmed a post-hantkeninid age for the extinction of *A. diktyoplokum*, with an age assigned of 33.47 Ma (Westerhold et al., 2014; Williams et al., 2004). Although this species is rare in the Mossy Grove succession, based on correlations to nannofossil biostratigraphy, the topmost occurrence has an estimated age of 34.12 Ma, which is very close to the EOB.

4.4.4. Integrated age model

Using these ages, we present a significantly refined age model for the Mossy Grove Core (Figure 8) based on dinocyst bioevents as discussed in the previous section (**Error! Reference source not found.**), integrated with new age constraints from calcareous nannofossil assemblages as well as existing radiometric dates. We show previously published foraminiferal-based age control for reference (Table 1).

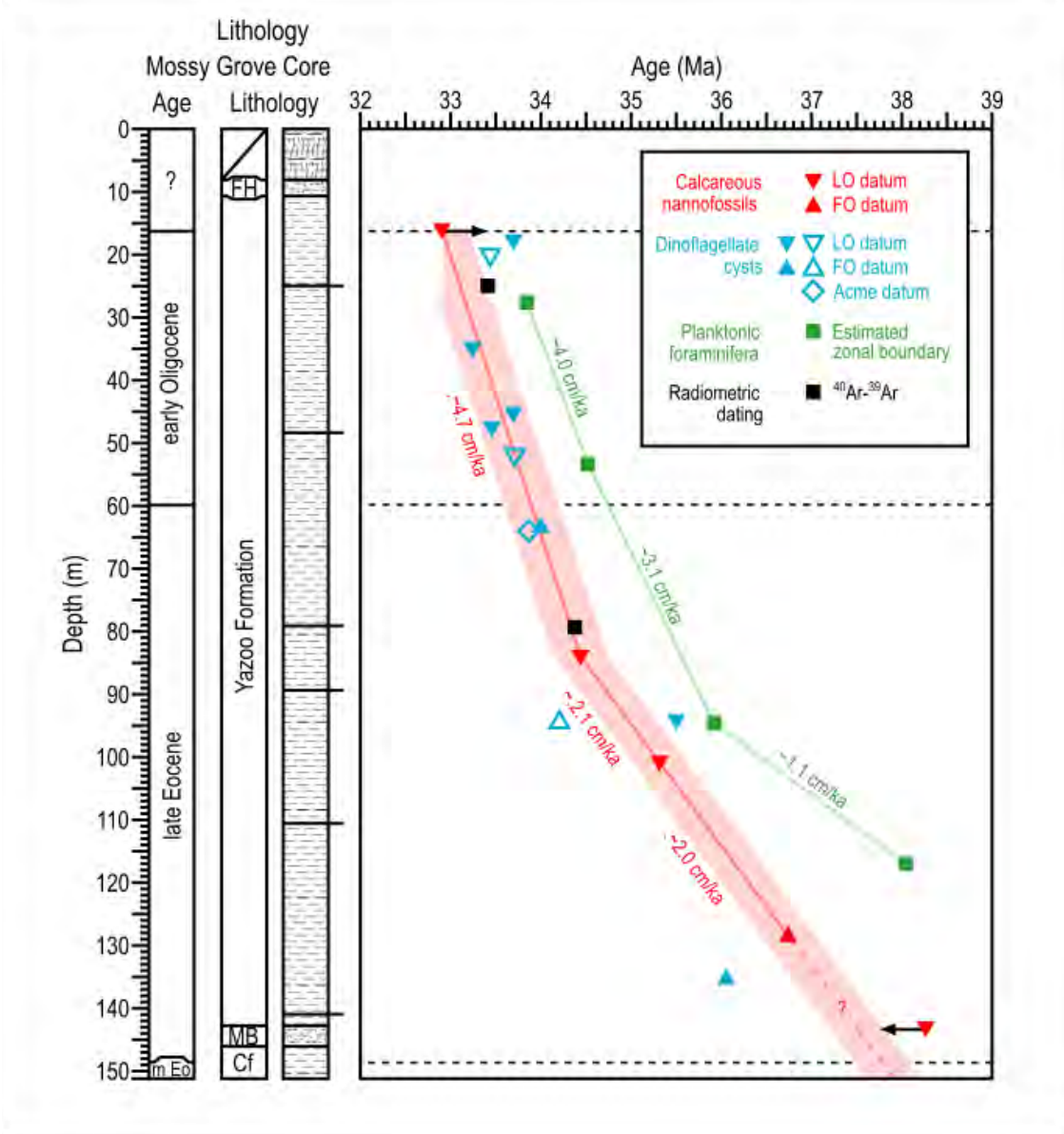


Figure 8. Refined age-depth model of the Mossy Grove Core. Lithology follows Dockery et al. (1991) and timescale follows Westerhold et al. (2014). Best fit lines for the models of Fluegeman et al. (2009) and this work are represented as green and red lines, respectively. Sedimentation rates are also indicated. The shaded area in light red reproduces an error of ~0.3 Ma, simulating the inclusion of the stated error on radiometric dating of both bentonites. Empty markers refer to bioevents regionally correlated.

This new age model can be interpreted to represent sedimentation within two intervals with distinct rates: between the bottom of the analysed section, i.e. ~152.1 m (499 ft; 37.49 Ma) and ~89.2 m (292 ft; 34.44 Ma), the sedimentation rate was 2.1 cm ka^{-1} and between ~89.2 m (292 ft; 34.44 Ma) and the top of the analysed section, i.e. ~16.8 m (55

ft; 33.05 Ma), the sedimentation rate was 4.7 cm ka^{-1}. This demonstrates that the depositional processes supplied the basin at a relatively constant rate for at least 3 million years, with a significant change only at ~34.4 Ma. This new age model also allows us to place the Priabonian-Rupelian boundary (EOB: 33.89 Ma) at ~63.4 m (208 ft) and is more consistent with radiometric dating: the bentonites previously dated at 33.40 and 34.36 Ma here are 33.11 and 34.34 Ma in age, respectively.

Another direct consequence of this model is the reassessment of the age of some dinocyst bioevents. As already mentioned, the extinction of *R. borussica,* for example, is usually correlated with a late Bartonian age in several sites of the North Sea and the Norwegian-Greenland Sea. Meanwhile, middle Priabonian ages were assigned to this event in the central Danish basin (Heilmann-Clausen and Van Simaeys, 2005), corroborating similar dating in the North Atlantic (Costa and Downie, 1979) and offshore Florida (Van Mourik et al., 2001). The last occurrence of this taxon at Mossy Grove was observed at ~36.77 Ma, consistent with a middle Priabonian age. Two other events are worth mentioning: the earliest appearance of *A. alcicornu* is similar in age to sites in the Mediterranean (Brinkhuis and Biffi, 1993; Wilpshaar et al., 1996), being an event prior to EOB; on the other hand, the extinction of *D. colligerum,* here identified in the lower Oligocene, is a post-EOB event, as suggested by several authors (e.g. Brinkhuis and Biffi, 1993; Kothe, 1990).

Comparisons with nearby sites in Mississippi and Alabama (Houben et al., 2018; Jaramillo and Oboh-Ikuenobe, 1999) (Figure 6) show a similar sequence of bioevents as the Mossy Grove section. The following key events within the Gulf Coastal Plain show a high degree of consistency (from the older to the younger): FO *D. cladoides*, LO *H. semilunifera*, FO *A. alcicornu*, LO *D. colligerum*, LO *L. serrata*, and LO *C.*

tenuitabulatum, and they are judged to be reliable biohorizons for future biozonation of the upper Eocene to lower Oligocene of the Gulf Coastal Plain.

4.5. Conclusions

The Mossy Grove core recorded a rich upper Eocene to lower Oligocene section with excellently preserved palynomorph content, including 52 genera and 70 species of dinocysts identified. Furthermore, rich diversity in other palynological groups was observed, revealing the enormous potential of the study site for the elaboration of future palynofacies models, useful in palaeobathymetric studies. High-resolution analysis (~26 ka) of the dinocyst content, integrated with calcareous nannofossil bioevents, generated a more robust age-depth model than previous models based on planktonic foraminifera alone. The new age-depth model is also more consistent with $^{40}Ar/^{39}Ar$ radiometric dating. On the basis of the new age model, the cored section spans ~5 Ma, including a ~4 Ma of the late Eocene and ~1 Ma of the earliest Oligocene, including the critical Eocene-Oligocene transition. The age model also documents a substantial increase in sedimentation rate from ~2.1 to ~4.7 cm ka^{-1} at ~34.4 Ma, indicating that the EOT climatic event caused a major change in the sedimentary regime.

CHAPTER 5: SEA-LEVEL FALL AND CARBON CYCLE PERTURBATIONS AT THE ONSET OF ANTARCTIC GLACIATION

The transition into the modern cold climate state, with the growth of continental-scale ice-sheets on Antarctica ~34 Ma, is one of the most striking examples of non-linear dynamics in the history of the Earth's climate. Coming at the end of a ~15 million-year progressive cooling trend, within ~700 thousand years the East Antarctic Ice Sheet had expanded to close to its modern extent. Although substantial modelling efforts have focused on positive feedback mechanisms associated with ice-sheet dynamics (DeConto et al., 2008; DeConto and Pollard, 2003), there are dramatic contemporaneous changes in ocean carbonate chemistry (Coxall et al., 2005; Pälike et al., 2006) and the marine biological pump (McKay et al., 2016a; Merico et al., 2008; Salamy and Zachos, 1999), the causes and effects of which are poorly known. Records of atmospheric carbon dioxide (CO_2) levels through the transition, show a transient drawdown of CO_2 closely coupled to the main phase of ice sheet expansion (Pearson et al., 2009), implicating a role for strong carbon cycle feedbacks. These feedbacks are most likely associated with the partitioning of organic and inorganic carbon burial between continental margins and the deep ocean, as well as the magnitude of nutrient trapping within shelf systems and weathering fluxes from rapidly exposed coastal environments during sea level regression. Here we present exceptional new records of sea-level dynamics through the Eocene-Oligocene Transition (EOT), which document substantial changes in shelf-ocean partitioning and nutrient/carbon fluxes very early in the EOT that represent potential carbon cycle drivers of the observed rapid transition.

Current records of the dynamics of EOT ice-sheet growth and the associated estimates of eustatic sea-level fall, are dominated by paired geochemical records of foraminiferal

test $\delta^{18}O$ and Mg/Ca. Benthic foraminifera oxygen stable isotope ($\delta^{18}O_{bf}$) records (Zachos et al., 2001, 1996) from multiple locations record a ~1.0-1.5±0.1‰ positive shift across the EOT, and represent a combination of local temperature-dependent isotopic fractionation during calcification and the isotopic composition of seawater in which the organism calcified ($\delta^{18}O_{sw}$) (Zachos et al., 2001). Changes in the $\delta^{18}O_{sw}$ composition of deep-waters is largely a function of global ice volume (Zachos et al., 2001), since the hydrological cycle concentrates ^{16}O in ice sheets, leaving the oceans more enriched in ^{18}O during glaciated climate states. Therefore, to quantify global ice volume, and from that eustatic sea level, requires an independent assessment of deep-water temperature, typically from Mg/Ca palaeothermometry (Lear et al., 2000). Through the EOT, however, deep-water foraminiferal Mg/Ca ratio are likely affected by the dramatic increase in the deep ocean carbonate saturation state (Coxall et al., 2005), which substantially reduces Mg/Ca-derived estimates of cooling (Lear et al., 2000, 2004, 2008) and makes the accurate quantification of ice growth across the EOT challenging. The best estimates to date indicate total ice-sheet expansion to a volume equivalent to 70% of the present Antarctic ice sheets (Barker et al., 1999; Bohaty et al., 2012; Cramer et al., 2011; DeConto and Pollard, 2003).

The EOT is, however, an extended interval of nearly ~700,000 years – equivalent to the duration from Marine Isotope Stage (MIS) 15 to the Holocene. MIS timescale was developed to express dating in the Quaternary and has been calibrated with Milankovitch cycles due to orbital forcing (Taylor and Aitken, 1997). High-resolution isotopic and elemental records from the eastern Equatorial Pacific clearly show orbital-scale variability through the EOT (Westerhold et al., 2014), as well as two phases of rapid (~40 ka), directional change (Coxall et al., 2005; Katz et al., 2008), during which $\delta^{18}O_{bf}$, $\delta^{13}C_{bf}$

and carbonate contents all increase (Coxall et al., 2005). These two steps, separated by a ~250 ka interval of relative stability, have been characterised as a first step (EOT-1; ~34.1 Ma) (Coxall et al., 2005; Katz et al., 2008; Westerhold et al., 2014) dominated by significant cooling (Katz et al., 2008; Miller et al., 2008; Wade et al., 2012) and isolated ice growth (DeConto et al., 2008; DeConto and Pollard, 2003; Katz et al., 2008; Lear et al., 2008), whilst the second step (EOT-2: ~33.7 Ma) (Coxall et al., 2005; Westerhold et al., 2014) represents a phase of continental-scale ice-sheet growth (DeConto and Pollard, 2003; Scher et al., 2011), a sharp increase in deep ocean carbonate saturation state (Coxall et al., 2005) and an abrupt increase in weathering flux on East Antarctica (Scher et al., 2011). The timing, magnitude and duration of these two steps may be a function of ice sheet dynamics in response to orbital forcing of high-latitude insolation (DeConto and Pollard, 2003), but given strong ice sheet – carbon cycle coupling throughout the Oligocene (Pälike et al., 2006), as well as clear evidence for major changes in the partitioning of carbon between global reservoirs through the EOT (McKay et al., 2016a; Merico et al., 2008), independent records of changing oceanic productivity regimes (Diester-Haass and Zahn, 1996; Moore et al., 2014; Plancq et al., 2014; Salamy and Zachos, 1999) and marine plankton extinctions and restructuring (Bordiga et al., 2015b; Brinkhuis and Biffi, 1993; Cotton and Pearson, 2012; Dunkley Jones et al., 2008; Houben et al., 2013a; Kamikuri and Wade, 2012; Moore et al., 2015; Pearson et al., 2008; Persico and Villa, 2004; Villa et al., 2008), it is clear that marine carbon cycle feedbacks are key to understanding the EOT. In particular, there is growing evidence for changes in the biological pump and restructuring of surface plankton communities in the earliest stages of the EOT (Dunkley Jones et al., 2008; Jones et al., 2019; Pearson et al., 2008). These events are coincident with a prominent deep ocean dissolution interval and negative

excursions in bulk- and benthic foraminiferal carbonate $\delta^{13}C$ records (Coxall et al., 2005; Westerhold et al., 2014), immediately before EOT-1.

Whereas existing paired $\delta^{18}O_{bf}$-Mg/Ca records are either subject to uncertainty from changing deep-ocean carbonate saturation state, or, for planktonic foraminiferal records, at too low a resolution to resolve the internal dynamics of the EOT (Katz et al., 2008; Lear et al., 2008; Wade and Pearson, 2008), an alternative approach to reconstruct the onset of the major phase of Antarctic ice-sheet growth and changing shelf-to-basin partitioning is through the analysis of continental margin successions that directly record micropalaeontological and geochemical markers of changing sea level (Lear et al., 2008). These successions also directly record changes in weathering, erosion, sediment and carbon flux. In many instances marginal successions through the EOT contain first-order unconformities (Gale et al., 2006; Miller et al., 2008), or large sea-level controlled facies changes that prevent the generation of the continuous high-fidelity records necessary for detailed reconstructions at the 10^4-year resolution. Here we present new records from an exceptional, ~137 m succession of mid-shelf marine clays, located within the Mississippi Embayment and recovered within the Mossy Grove Core (MGC) (Dockery III et al., 1991), drilled near Jackson, Mississippi (Figure 9), that provide a continuous record through ~4 Ma of the latest Eocene and earliest Oligocene. We present new high-resolution (~6 ka) fine-fraction (<20μm) carbonate stable oxygen ($\delta^{18}O$) and carbon ($\delta^{13}C$) isotope analyses, bulk sediment X-ray fluorescence (<10 ka) data and palynological (~26 ka) analyses to generate a multiproxy record through the late Eocene-early Oligocene. MGC is substantially expanded compared to the classic Gulf Coast Saint Stephens Quarry (SSQ) section (Miller et al., 2008) with sedimentation rates estimated to be more than ten times higher through the EOT (SSQ's ~0.4 cm ka^{-1}; MGC ~4.7 cm ka^{-}

[1]). Age constraints are based on the integrated age-depth model (see section 4.4.4) and on the timescale of Westerhold et al. (2014).

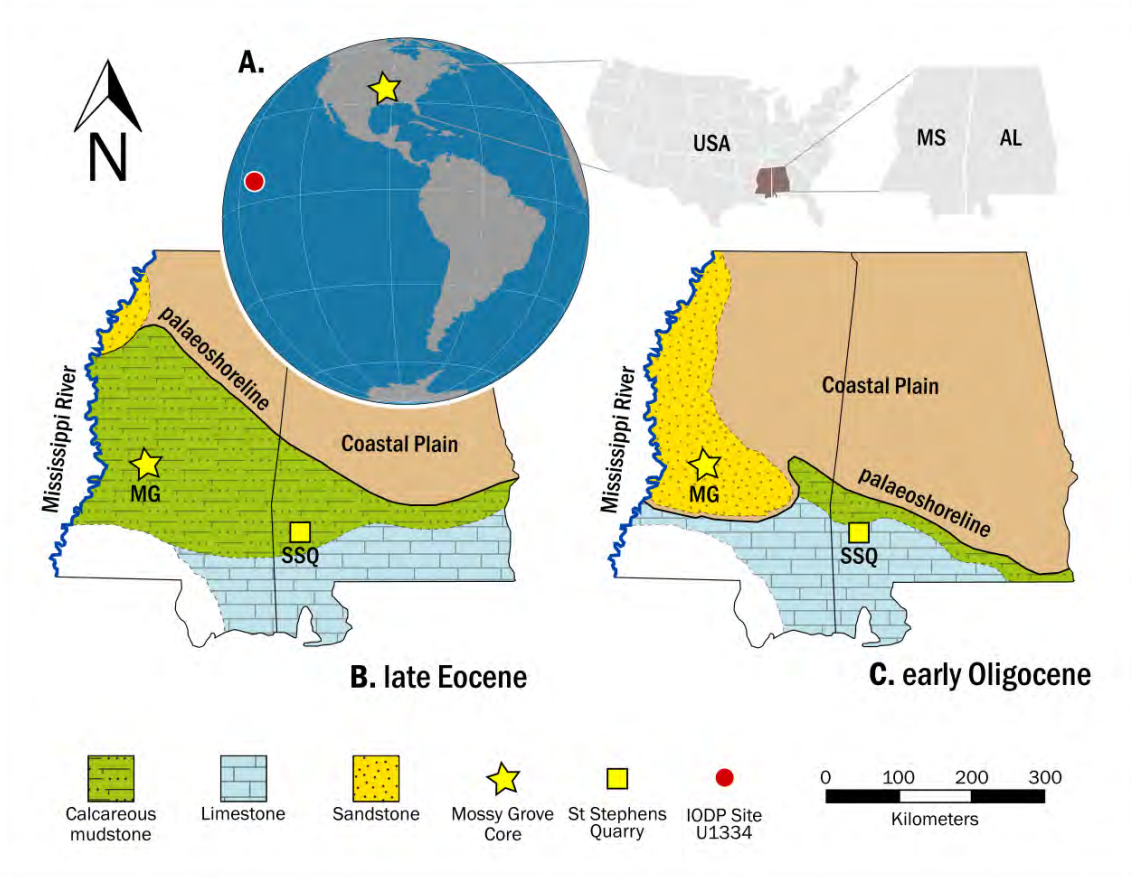


Figure 9. Palaeogeography and lithology of Mississippi and Alabama sector of the US Gulf Coastal Plain according to Tew and Mancini (1995). The Mississippi River is shown in its modern position. (A) Location of the MGC and the IODP Site U1334 (Westerhold et al., 2014). (B) Late Eocene palaeogeography of Mississippi and Alabama (Tew and Mancini, 1995). (C) Early Oligocene palaeogeography of Mississippi and Alabama (Tew and Mancini, 1995).

The key feature of the new MGC records is late Eocene stability in fine fraction $\delta^{18}O$ and $\delta^{13}C$ records that ends at ~34.5 Ma (Figure 10 and Figure 11), with standard deviation for $\delta^{18}O$ and $\delta^{13}C$ of ~0.4 and ~0.5 respectively. It is replaced by a more dynamic regime into the earliest Oligocene (standard deviation for both $\delta^{18}O$ and $\delta^{13}C$ of ~1.1). Both records have a limited dynamic range from ~37.7 to ~34.5 Ma, followed by pronounced

negative transients between ~34.4 and 34.2 Ma. Above 34.2 Ma $\delta^{18}O$ shifts to progressively more positive values, but, along with $\delta^{13}C$, has a far greater high frequency variability than in the late Eocene. Although the MGC record shows the shift to more positive $\delta^{18}O$ characteristic of most EOT records, it is of substantially smaller magnitude (~0.8‰ across the whole EOT; Figure 10 and Figure 11) than recorded in the deep ocean (Coxall et al., 2005; Westerhold et al., 2014). This diminished effect on fine fraction $\delta^{18}O$ is an additional evidence for a continent-influenced inner shelf setting. The negative transients in $\delta^{18}O$ and $\delta^{13}C$ (~34.4 and 34.2 Ma) are directly coincident with the lowest Ca/Si ratios in the record (also Ca/Fe and Ca/Ti – see SM4) – indicative of reduced biogenic carbonate content (Itambi et al., 2009) – minima in planktonic:benthic foraminifera ratios (Fluegeman et al., 2009), a drop in relative abundance of marine organic-walled dinoflagellate cysts, or dinocysts, from ~80% to ~30%, a substantial increase in relative abundance of terrestrial plant debris (e.g. plant cuticle and resin) and freshwater algae (*Pediastrum* spp.) and an increase in the proportion of low-salinity tolerant dinocysts (Sluijs et al., 2005) (Figure 10 and Figure 11). Taken together this is overwhelming evidence for an increase in freshwater versus marine components. In this context, the negative transients in $\delta^{18}O$ and $\delta^{13}C$ are best explained by an increase in the relative contribution of freshwater and terrestrially derived dissolved inorganic carbon to the surface waters of the Mississippi Embayment, most likely from the palaeo-Mississippi which, even during the late Eocene, drained a significant proportion of continental North America (Galloway et al., 2011). The $\delta^{13}C$ of dissolved inorganic carbon (DIC) in the lower modern Mississippi system is as low as -10.0‰ ($\delta^{13}C_{DIC}$) (Dubois et al., 2010), whilst $\delta^{18}O$ of Mississippi outflow waters are on the order of -6.0‰ (Myers et al., 2012; Zeigler and Whitledge, 2011), and are sufficient to lower $\delta^{18}O_{sw}$ in the surface waters of

the northern Gulf of Mexico to -8.0‰ (Tindall et al., 2010). In the late Eocene the geometry of the shallow Mississippi Embayment, enclosed to both the east and west is likely to have amplified the impact of riverine input on seawater isotopic composition.

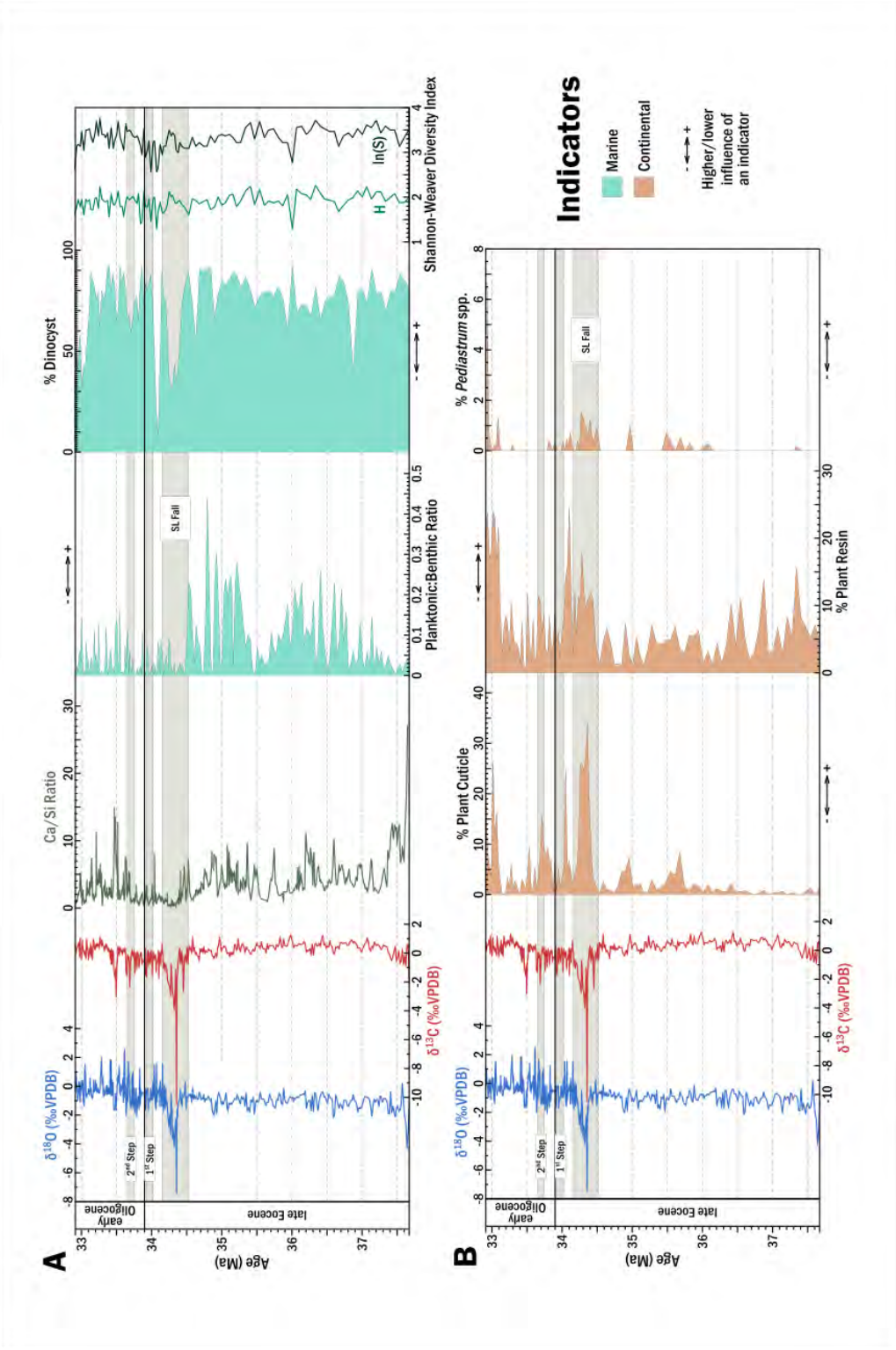


Figure 10. Geochemical and micropalaeontological records of the MGC (Part 1). (A) Bulk carbonate $\delta^{18}O$ and $\delta^{13}C$, foraminiferal planktonic:benthic ratio (Fluegeman et al., 2009), marine indicator (percentage of dinocysts), and Shannon-Weaver Diversity Index for dinocysts. (B) Bulk carbonate $\delta^{18}O$ and $\delta^{13}C$, and continental indicators (percentage of plant cuticle and resin, and freshwater algae *Pediastrum* spp.).

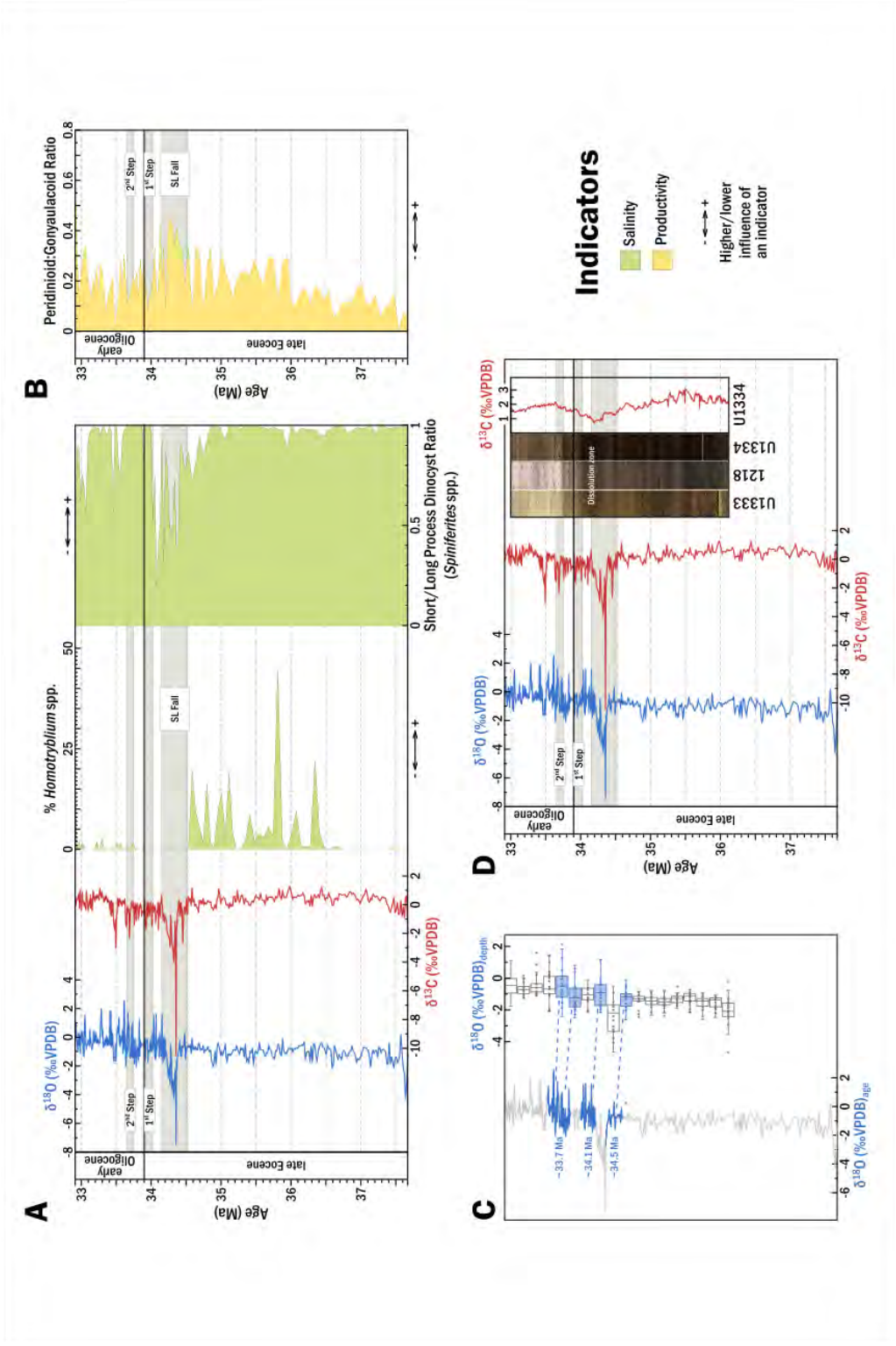


Figure 11. Geochemical and micropalaeontological records of the MGC (Part 2). (A) Bulk carbonate $\delta^{18}O$ and $\delta^{13}C$ and salinity indicators (percentage of *Homotryblium* spp. and short-long process dinocyst ratio for *Spiniferites* spp.). (B) Productivity indicator (peridinioid:gonyaulacoid ratio). (C) Box plot of bulk carbonate $\delta^{18}O$ record and marked positive steps. (D) Bulk carbonate $\delta^{18}O$ and $\delta^{13}C$ from MGC and bulk carbonate $\delta^{13}C$ from IODP Site U1334 (Westerhold et al., 2014).

Palynomorph assemblages also show a marked change at ~34.5 Ma, with an abrupt decrease in marine components (dinocysts) and an increase in continental-derived plant debris (e.g. plant cuticle and resin) and freshwater algae (*Pediastrum* spp.) (Figure 10). Further, dinocyst-based salinity reconstructions (Sluijs et al., 2005) include a marked decline in the abundance of the high-salinity preference *Homotryblium* spp. (Brinkhuis, 1994; Kothe, 1990; Pross and Schmiedl, 2002; Sluijs et al., 2005) after ~34.5 Ma, which is strong evidence for a step-change in the salinity regime and freshening of the Mississippi Embayment (Figure 11). This is supported by another salinity proxy, the ratio of short-to-long process *Spiniferites* spp., which shows a marked minimum (low salinity conditions) between ~34.5 and 34.0 Ma (Figure 11). The peridinioid/gonyaulacoid dinocyst ratio (P/G ratio) also increases between ~34.4 and 34.1 Ma, which is often used as a proxy for terrigenous-derived nutrient input to shelf surface waters (Brinkhuis et al., 1998; Crouch, 2001; Eshet et al., 1994; Harland, 1973; Van Mourik et al., 2001; van Mourik and Brinkhuis, 2000; Reichart and Brinkhuis, 2003) (Figure 11). All of these palynological results are consistent with the marked drop in the biogenic (mostly nannofossil) carbonate content within these sediments (Ca/Si ratios) and step-change in planktonic:benthic foraminifera ratios (Fluegeman et al., 2009); both consistent with a dramatic reduction in the abundance of typical open marine calcareous plankton communities during this interval (34.5 – 34.2 Ma), as would be expected from a low salinity surface ocean environment (Winter et al., 1994).

Although the interval above 34.4 Ma is clearly visible as a negative, ~200 ka, transient in both $\delta^{18}O$ and $\delta^{13}C$ it also represents a clear step-change in the behaviour of both the micropalaeontological and geochemical records, between the late Eocene interval older than 34.5 Ma, and the EOT to earliest Oligocene, younger than 34.4 Ma (Figure 10 and

Figure 11). Above this level the dynamic range of both $\delta^{18}O$ and $\delta^{13}C$ increase, more so in $\delta^{18}O$ with variability exceeding 2‰ on 10^4-year timescales. The long-term running mean values (Figure 11), however, clearly show a progressive shift towards more positive $\delta^{18}O$ values into the Oligocene, most notably with a ~0.5‰ increase between ~33.8 and 33.6 Ma, which we identify as EOT-2 (Coxall et al., 2005). The contribution of the calcareous plankton is substantially lower above 34.5 Ma – as represented by both Ca/Si and P:B ratios – and the low salinity intolerant *Homotryblium* spp. are effectively excluded above 34.5 Ma (Figure 10 and Figure 11). The concentrations of plant cuticle and resin also remain elevated above 34.5 Ma, indicating an increase in the transport of terrestrial-derived components to the site throughout the EOT and earliest Oligocene, although this is most marked across EOT-2, which accounts for ~60% of the overall increase in the abundance of these components. Within the lithostratigraphy of the MGC (Dockery III et al., 1991), the clays forming the Yazoo Formation become rich in mollusc shells and thin layers of shell hash from 33.8 Ma, directly coincident with EOT-2.

Palaeogeographic reconstructions of the late Eocene (Galloway et al., 2011; Tew and Mancini, 1995) place the MGC site on the mid-continental shelf within the Mississippi Embayment, to the south of the palaeo-Mississippi river but likely influenced by sediment supply to the prodelta sector. In response to sea-level regression, the entire delta system would advance – reducing the distance to shore from the MGC location – and erosive processes on the delta plain would accelerate, as the system adjusts to a lowered base level. It is these processes that are most consistent with the coincident surface water freshening and increase in terrestrial-derived material observed between 34.5 and 34.2 Ma in the MGC. There are strong indications that the system remains in a regressive phase into the earliest Oligocene, up to the unconformable top of the Yazoo Formation and the

overlying terrestrial lignites of the Forest Hill Formation. Within this context, we interpret the transient extreme responses in isotopic compositions, lowered abundance of marine microplankton and the flux of terrestrial debris between 34.5 and 34.2 Ma, as the timescale of delta, river and coastline adjustment to the new base-level. Over the longer timescales of the EOT and earliest Oligocene, variability in bulk carbonate $\delta^{18}O$ is consistent with the progradation, avulsion, abandonment, and submergence dynamics of a fluvial delta, which for the Holocene Mississippi River are on the order of 1,000-1,500 years with lateral movement of up to 300 km (Blum and Roberts, 2012). Such dynamics would explain variations in $\delta^{18}O$ values as the MGC location is more or less influenced by the delta front freshwater plume.

The new records from the MGC clearly demonstrate a rapid environmental change at ~34.5 Ma within the shelf environments of the Mississippi Embayment. The rates (<100 ka) and magnitude of change at this time are too large to be controlled by regional tectonics, especially on a long-term stable passive continental margin. They are also unidirectional, representing a long-term shift to substantially lowered sea levels, consistent with the major regression across the EOT. We contend that these records represent some significant component of global eustatic sea-level fall at the very start of the EOT. This challenges the view that the dynamics of the EOT are dominated by global cooling during the earliest stages, which then precondition the system to continental-scale ice-sheet expansion in the later stages (EOT-2) (DeConto and Pollard, 2003; Katz et al., 2008; Miller et al., 2008; Scher et al., 2011; Wade et al., 2012). Instead, our records demonstrate a rapid onset to the EOT, associated with sea-level fall and ice-sheet expansion at ~34.5 Ma, which is consistent with evidence for increased glacial weathering fluxes from early ice-sheet growth in the Gamburtsev Mountains (DeConto and Pollard,

2003; Rose et al., 2013), discharged via the Lambert Graben (Barrett, 1996; Hambrey et al., 1991) to Prydz Bay from ~34.5 Ma (Passchier et al., 2017). In fact, comparisons between glacioeustasy and sequence boundaries at Saint Stephens Quarry, Alabama, and the ACGS#4 Borehole, New Jersey, demonstrate that large ice sheets existed in the late Eocene (Miller, 2005; Miller et al., 2008). Furthermore, the progressive shift towards more positive $\delta^{18}O$ values into the Oligocene recorded at MGC clearly suggests that ice growth persisted through time, revealing a permanent ice-sheet inception. Based on planktonic/benthic ratio (Grimsdale and Van Morkhoven, 1955; van der Zwaan et al., 1990), we calculate in ~40-45 m the inferred sea-level drop at MGC, which is consistent with previous estimates from Saint Stephens Quarry, Alabama (Katz et al., 2008; Miller, 2005; Miller et al., 2008).

As well as defining a rapid start to the EOT controlled by ice sheet dynamics, the evidence for significant sea-level fall and substantial increases in the erosion flux of terrestrial organic matter into continental margin successions, implicates changing shelf-to-ocean carbon, carbonate and nutrient partitioning and fluxes as key drivers of previously observed carbon cycle perturbations (McKay et al., 2016a; Merico et al., 2008) and oceanic plankton extinctions (Cotton and Pearson, 2012; Kamikuri and Wade, 2012; Pearson et al., 2008) and phytoplankton community restructuring at the onset of the EOT (Jones et al., 2019). These included sharp negative excursions in bulk carbonate (Westerhold et al., 2014) and benthic foraminiferal (Coxall et al., 2005) $\delta^{13}C$ records from the eastern Equatorial Pacific, coupled to a marked low carbonate interval and calcareous microfossil dissolution characteristic of deep ocean carbonate undersaturation. This low carbonate zone in the Pacific, and global plankton extinctions, can now be tied to the observed regressive event on the US Gulf Coastal Plain. Moreover, our findings reinforce

the idea that changes in the global carbon cycle (DeConto and Pollard, 2003), rather than continental configuration (Kennett, 1977), provided the strong positive feedback mechanisms required to explain the rate of EOT climate change (McKay et al., 2016a; Merico et al., 2008). We propose that the earliest stages of the major EOT eustatic sea-level fall had a disproportionate effect on global biogeochemistry, by causing the first major incision of organic- and nutrient-rich coastal low lands that had been accreting under warm, high sea-level greenhouse conditions for tens of millions of years (Cramer et al., 2011). It is our contention, that the resultant delivery of organic carbon and nutrients to the global oceans were sufficient to trigger the observed plankton extinctions as well as perturb the marine carbon cycle through the oxidation of labile terrestrial organic carbon with strongly negative $\delta^{13}C$. This also would explain increased nutrient availability and primary production worldwide (Dunkley Jones et al., 2008).

CHAPTER 6: ECOSYSTEM RESPONSE TO LATE EOCENE CLIMATIC AND IMPACT EVENTS

6.1. Introduction

The late Eocene, or alternatively the Priabonian age (~37.8-33.9 Ma), is characterised by the build-up to a dramatic global-scale climate shift known as the Eocene-Oligocene Transition (EOT; ~34.4-33.7 Ma; Figure 1) (Zachos et al., 2001). This interval also witnessed some of the largest extra-terrestrial impact events since the Cretaceous-Paleogene (K-Pg) event (Figure 1), with late Eocene aged craters located in central Siberia (Bottomley et al., 1997; Liu et al., 2009a) and on the Atlantic margin of North America (Glass, 2002; Koeberl et al., 1996; Poag et al., 2002; Poag and Poppe, 1998). Although the quality of palaeoenvironmental records of these major events have improved in recent years (Liu et al., 2009a; Pusz et al., 2009), the long-term relationships between these events and the dynamics of late Eocene climate evolution still remain poorly understood (Coxall and Pearson, 2007; Pusz et al., 2009).

As one of the most pronounced climatic shifts of the last ~112 Ma (Friedrich et al., 2012), the EOT is a critical interval that marked the end of the warmer greenhouse climates that prevailed through the Late Cretaceous and the early Cenozoic, and the onset of the colder icehouse climate state since the Oligocene (Zachos et al., 2001, 2008). The EOT comprises a distinctive two-step positive shift in benthic foraminifera $\delta^{18}O$ records associated with the first permanent continental-scale ice sheet growth on Antarctica (Coxall et al., 2005; Zachos et al., 2001, 1996) and is widely recognized by a ~70±20 m eustatic sea-level fall (Kominz and Pekar, 2001; Miller et al., 2008; Pekar et al., 2002; Pekar and Christie-Blick, 2008), 4° C deep-sea (Cramer et al., 2011; Lear et al., 2008) and ~2.5-5° C sea-surface cooling (Liu et al., 2009b), ~1 km deepening of the calcite

compensation depth (CCD) (Coxall et al., 2005), as well as a substantial impact on terrestrial (Prothero, 1994a) and marine (Pearson et al., 2008) biotic systems, with extinction events in several groups (Coxall and Pearson, 2007; Prothero, 1994b). Although its consequences have been widely studied, the preconditioning for this event remain an object of intense debate, with continued focus on two main hypotheses: (1) substantial changes in the geometry of Southern Ocean gateways (Kennett, 1977); (2) declining atmospheric greenhouse gas concentration (DeConto and Pollard, 2003; Pagani et al., 2005). Recent studies (Coxall et al., 2018; Elsworth et al., 2017), however, proposed that changes in the late Eocene "proto-" Atlantic Meridional Overturning Circulation (AMOC) played an essential role in preconditioning the late Eocene Earth system for the greenhouse-icehouse transition.

As a major component of the modern ocean circulation system, the AMOC is responsible for the redistribution of heat on the planetary surface (Lenton et al., 2008; Rahmstorf, 2002). Since the ocean contains about fifty times more carbon than the atmosphere, AMOC also influences global carbon cycling, through changes in the physical distribution of the oceanic carbon sink, as well as influencing the strength or effectiveness of the biological pump, which transfers dissolved inorganic carbon from the surface to the deep ocean (Rahmstorf, 2002). AMOC circulation comprises the northward transport of warm and saline surface waters from the South, to Central and North Atlantic Ocean – including the warm surface Gulf Stream current. These waters progressively cool at high latitudes, to form a southward return flow of cold and salty waters to lower latitudes at intermediate to deep water depths, known as North Atlantic Deep Water (NADW) (Broecker, 1998; Broecker and Peng, 1982; Mulitza et al., 2008; Zickfeld et al., 2008). In the modern and late Neogene system, the strength of AMOC circulation depends

on a delicate balance between temperature and salinity in the surface waters of the North Atlantic (Lenton et al., 2008; Rahmstorf, 2002). Reconstructions of AMOC strength through time, indicate that it is a nonlinear system, which tends to exhibit threshold responses and multi-state dynamics (Lenton et al., 2008; Rahmstorf, 2002). The large-scale heat transport of AMOC, including from the southern to northern hemispheres, impacts surface climates not only in the North Atlantic and surrounding landmasses, but also at a global scale (Caesar et al., 2018; Lenton et al., 2008; Rahmstorf, 2002; Thornalley et al., 2018).

Although many direct continuous measurements of the AMOC have been made in recent years (Caesar et al., 2018; Thornalley et al., 2018), the longer-term dynamics of NADW formation are still poorly understood. This is especially the case in non-analogue conditions back into the early Neogene and Paleogene, when zonal transport was possible into or out from the Central Atlantic through the Panama and Tethyan tropical seaways (Goldner et al., 2014). Despite these differences from the modern system, there is strong evidence for deep water formation, analogous to NADW from at least the middle Eocene, which is likely linked to similar patterns of northward heat transport in the surface Atlantic (Vahlenkamp et al., 2018a, 2018b). Given the presence of a proto-AMOC system in the Eocene, multiproxy studies of deep water compositions in the late Eocene from both North and South Atlantic sites (Coxall et al., 2018; Elsworth et al., 2017) have inferred enhanced NADW production ~1.5 Ma before the EOT associated with a strengthened AMOC. One of these studies suggests the increased northward heat and atmospheric moisture transport associated with an intensified AMOC may have intensified silicate weathering across continental landmasses in the northern hemisphere resulting in the drawdown of atmospheric carbon dioxide and global cooling in the run-

up to continental-scale Antarctic glaciation (Elsworth et al., 2017). What controls the strength of the late Eocene AMOC, however, is an open question. Current hypotheses focus on tectonic reconfigurations of ocean gateways in either the northern or southern high latitudes (Coxall et al., 2018; Elsworth et al., 2017; Hutchinson et al., 2019). In the Southern Ocean, the deepening of the Drake Passage is a precondition for a strong Antarctic Circumpolar Current (ACC), which could have reduced the flow of warm and salty subtropical waters into regions of Southern Ocean deep water formation and initiated strong overturning circulation in the North Atlantic (Elsworth et al., 2017). Northern hemisphere hypotheses argue in two distinct pathways: (1) continued opening of subarctic gateways enabled an increased exchange across the Greenland-Scotland Ridge (GSR), with the northwards transfer of more saline and dense waters to the high latitude sites of deep water production, which strengthened the production of NADW (Coxall et al., 2018); (2) closing of the Arctic-Atlantic gateway blocked freshwater inflow from the Arctic, triggering the onset of modern-like deep water formation in the North Atlantic (Hutchinson et al., 2019). Here we seek to document potential changes in sub-tropical North Atlantic surface waters associated with the proposed late Eocene variations in AMOC, at a site on the US Gulf Coast that should be susceptible to changes in Atlantic meridional heat transport (Vahlenkamp et al., 2018a).

In addition to variations in deep water overturning, the discovery of multiple, and globally distributed impact ejecta deposits in upper Eocene sediments has raised intense speculation that the impact of extraterrestrial bodies could have triggered or enhanced global cooling and biotic turnover in the lead up to the EOT (Coccioni et al., 2009; Keller, 1986; Pusz et al., 2009; Vonhof et al., 2000). Among the impact structures now identified in upper Eocene strata, at least three are bigger than 10 km in diameter and have well-

constrained ages (error <1 Ma): the Popigai crater in central Siberia (diameter: ~100 km), and the Chesapeake Bay (diameter: ~90 km) and Toms Canyon (diameter: ~20 km) craters, on the Atlantic margin of North America. Different dating methods, including biochronology, magnetostratigraphy, and radiometric dating, have provided several age assignments for each of these events (Bottomley et al., 1997; Koeberl et al., 1996; Liu et al., 2009a; Poag, 2012; Poag et al., 2002; Pusz et al., 2009) (Table 3).

Table 3. Age assignments of the major late Eocene impact structures. Legend: Cpx – Clinopyroxene-bearing; Timescales: CK95 – Cande and Kent (1995); and adjusted to TW14 – Westerhold et al. (2014).

Impact structure	**Dating method**	**Age (Ma)**		**Reference**
		CK95	**TW14**	
Chesapeake Bay	Biochronology (breccia horizon)	35.2-36.0	35.5-36.1	Koeberl *et al.* (1996)
	Cpx microspherule layers	35.4 (±0.1)	35.6 (±0.1)	Liu *et al.* (2009)
	Magneto-stratigraphy	35.77	35.85	Poag, Plescia and Molzer (2002)
	Magneto-stratigraphy	35.43	35.65	Pusz *et al.* (2009)
	Radiometric dating (tektites)	35.2-35.5 (±0.3)	35.5-35.7 (±0.2)	Poag, Plescia and Molzer (2002)
	Various	35.3	35.6	Poag *et al.* (2012)
Popigai	Cpx microspherule layers	35.4 (±0.1)	35.6 (±0.1)	Liu *et al.* (2009)
	Magneto-stratigraphy	35.43	35.65	Pusz *et al.* (2009)
	Step-heating technique (^{40}Ar-^{39}Ar)	35.7 (±0.2)	35.8 (±0.2)	Bottomley *et al.* (1997)
Toms Canyon	Biochronology (breccia horizon)	35.2-36.0	35.5-36.1	Poag, Plescia and Molzer (2002)

	Radiometric dating (tektites)	35.2-35.5 (±0.3)	35.5-35.7 (±0.2)	Poag, Plescia and Molzer (2002)

Since these events preceded the EOT by ~1.1-1.7 Ma and are associated with only minor biotic turnover episodes (Vonhof et al., 2000), it is been widely considered that these impacts do not play a role in the onset of the EOT or the associated biosphere perturbations at this time (Coxall and Pearson, 2007). To investigate the consequences of an enhanced AMOC and these late Eocene bolide impact events, we generated a series of new high-resolution records of the surface ocean environment from a location sensitive to both Atlantic heat transport and within the ejecta strew field from the Chesapeake Bay Impact (Glass, 2002; Glass et al., 1998). These records include a ~6 ka resolution coccolith fraction (<20 μm) carbonate stable oxygen ($\delta^{18}O$) and carbon ($\delta^{13}C$) isotope record, ~26 ka resolution palynological and calcareous nannofossil assemblage records, and bulk sediment X-ray fluorescence analyses at <10 ka resolution. It is only with such records that the relative importance of these impact events, long-term climate evolution and rapid Antarctic glaciation as drivers of ecosystem change can be assessed. The timing and position of the main events mentioned in this study were constrained with an integrated age-depth model based on nannofossil and dinocyst biostratigraphy (see section 4.4.4) and all ages here follow the same geologic timescale (Westerhold et al., 2014).

6.2. Materials and Methods

The Mossy Grove Core (MGC). The study site consists of a continuously cored succession (Dockery III et al., 1991), near Jackson, Central Mississippi, US Gulf Coastal Plain. This recovered ~137 m of marine clays, spanning ~4.5 Ma through the upper

Eocene and lower Oligocene. MGC is substantially expanded compared to nearby sites, such as the Saint Stephens Quarry (SSQ) section (Miller et al., 2008), with sedimentation rates estimated to be more than ten times higher through the EOT (SSQ's ~0.4 cm ka^{-1}; MGC ~4.7 cm ka^{-1}). Therefore, it is more suitable for the detection of finer temporal-scale dynamics of ocean circulation patterns through much of the late Eocene, such as changes in the Gulf Stream, as well as the potential consequences of an impact event, especially in the Chesapeake Bay, ~1,200 km away from MGC.

Bulk stable-isotope data. A total of 444 bulk sediment samples, taken at ~30 cm spacing from the MGC, were processed at the University of Birmingham (SM1). The sediment was sieved over a 20 μm stainless steel mesh, with the fine-fraction passing through the sieve captured on ultra-fine-grade filter paper and air dried. The sediment residue was then transferred to 50 ml centrifuge tubes and organic matter within this fine fraction removed by overnight reaction with 5% sodium hypochlorite (NaClO) solution. The sample was then spun down at 4,500 rpm and the supernatant discarded. The sample was then washed 2-3 times with de-ionized water – each wash consisting of resuspension, agitation and then centrifuging and disgarding of the solution as above - until a neutral pH was established. Stable isotope measurements were performed at the NERC Isotope Geochemistry Laboratory (NIGL) at the British Geological Survey, Keyworth, on a dual inlet, triple collector, gas source mass spectrometer which is capable of simultaneously determining mass ratios 44/45 ($^{12}C/^{13}C$) and 46/44 ($^{16}O/^{18}O$). The carbonate analysis method involves reacting the carbonate sample with anhydrous phosphoric acid to liberate CO_2. All data are reported against VPDB after calibration of the in-house standard with NBS-19.

Nannofossil Assemblages. Calcareous nannofossil assemblages were quantified using polarizing light microscopy (Zeiss AxioScope) at 1250x magnification. A total of 135 simple smear slides were prepared from raw samples and within each slide individual taxa were quantified by the counting of at least 400 specimens. The relative abundance of each taxa was reported as a percentage of the total number of nannofossils observed in each sample. This work was undertaken by Dr Nursufiah Sulaiman as part of her doctoral thesis, but is unpublished and is included and re-interpreted here with the aim of providing the basis for an integrated micropalaeontological palaeoenvironmental analysis of the MGC.

Palynology. Samples were processed at Petrostrat following standard techniques. Altogether, 112 samples collected at ~1.2 m intervals from the Mossy Grove borehole between ~17.0 and 152.0 m deep were treated with 40% HCl for 30 minutes and 60% HF for 24 hours to dissolve carbonates and disaggregate the rock matrix, and sieved over a 10 µm nylon mesh to retain the HF effluent from the material. A second HCl treatment was applied to remove any precipitate formed during stage, followed by a final 10 µm sieving. The material was subjected to oxidation (70% HNO_3 for exactly 2 minutes) to remove pyrite, debris and any unstructured organic material from the palynomorphs. Another sieving was done to remove any HNO_3 effluent. A final cleaning treatment was undertaken with a combination of domestic and industrial detergents. Using a glass swirling dish and centrifugal swirling techniques, palynomorphs in each sample were then concentrated and Bismark brown was added to make them more visible with light microscopy. Finally, the samples were sieved into two size fractions, 10-30 µm (concentrating spores and pollen) and >30 µm (concentrating dinocysts), and then

mounted on separate 22x22 mm coverslips, which were glued to a glass slide using Norland optical adhesive.

Palynomorph components. In this work, only the coarse fraction content (>30 μm) of each slide was analysed. With a Zeiss transmitted light microscope (400x magnification), 200 dinocyst specimens were counted in each sample, along with the respective number of spores, pollen, algae (prasinophyceae and chlorophyceae), zoomorphs/zooclasts, phytoclasts and amorphous organic matter. Only palynomorphs that were more than 50% complete and not obscured either by air bubbles or organic debris were considered. Reworked acritarchs and amorphous organic matter were excluded from the final sum of palynomorphs and thereby from the percentage calculations (SM2, SM3).

6.3. Results

In order to provide a multiproxy-based palaeoenvironmental reconstruction of pre-EOT events, we generated a ~6 ka resolution coccolith fraction (<20 μm) carbonate stable oxygen ($\delta^{18}O$) and carbon ($\delta^{13}C$) isotope record, and bulk sediment X-ray fluorescence analyses at <10 ka resolution, combined with a ~26 ka resolution palynological and calcareous nannofossil assemblage records.

To better assess palaeoenvironmental preferences within dinocyst genera, we analysed empirically established palaeoecological affinities (Brinkhuis, 1994; Brinkhuis and Biffi, 1993; Dale, 1996; Davey and Rogers, 1975; Edwards and Andrle, 1992; Frieling and Sluijs, 2018; Harland, 1983; Kothe, 1990; Pross, 2001; De Vernal et al., 1997; Wall et al., 1977; Williams and Bujak, 1977; Zevenboom et al., 1994) of 33 genera (Table 4).

Table 4. Empirically established palaeoecological affinities of selected dinocyst genera found at MGC. Data follow different authors (Brinkhuis, 1994; Brinkhuis and Biffi, 1993; Dale, 1996; Davey and Rogers, 1975; Edwards and Andrle, 1992; Frieling and Sluijs, 2018; Harland, 1983; Kothe, 1990; Pross, 2001; De Vernal et al., 1997; Wall et al., 1977; Williams and Bujak, 1977; Zevenboom et al., 1994). See text for further explanation.

Genera	PCA Group	Davey and Rogers (1975)	Wall et al. (1977)	Williams and Bujak (1977)	Harland (1983)	Köthe (1990)	Edwards and Andrle (1992)	Brinkhuis and Biffi (1993)	Brinkhuis (1994)	Zevenboom et al. (1994)	Dale (1996)	De Vernal et al. (1997)	Pross (2001)	Frieling and Sluijs (2018)	Adopted for this study
Achomosphaera	A							C							C
Areoligera	A														?
Areosphaeridium	A			C											C
Charlesdowniea	A														?
Cleistosphaeridium	B					W		W							W
Cordosphaeridium	B														?
Cribroperidinium	A					C									C
Dapsilidinium	A														?
Deflandrea	A							W						C	?
Diphyes	A														?
Distatodinium	A							C							C
Enneadocysta	A														?
Glaphyrocysta	B					W		C							?
Hemiplacophora	B							W							W
Heteraulacacysta	B													W	W
Homotryblium	B							W	W					W	W
Horologinella	A														?
Hystrichokolpoma	A														?
Hystrichosphaeridium	A														?
Impagidinium	A							C		W					?
Lentinia	A							C						C	C
Lingulodinium	B											W			W
Minisphaeridium	A														?
Nematosphaeropsis	A									C					C
Operculodinium	A	W	C		B		B				B				B
Phthanoperidinium	A												C	C	C
Piladinium	A														?
Rhombodinium	A												C	W	C
Saturnodinium	A														?
Spiniferites	A	C					B								B
Thalassiphora	A							C							C
Turnhosphaera	A														?

When there is a single interpretation for a given genus or it is consistent between different authors, we simply followed this interpretation. However, some genera had multiple distinct assignments presented by different authors. For instance, *Rhombodinium* spp. and *Wetzeliella* spp. have been recently described as having possible warm-water affinity (Frieling and Sluijs, 2018) in Paleocene-Eocene records. On the other hand, a previous study (Pross, 2001) focused on these genera from the Oligocene of western and northwestern Europe found that warmer water masses may have led to an earlier and stronger decline of these taxa at the southernmost localities. *Deflandrea* spp., *Glaphyrocysta* spp. and *Impagidinium* spp. are equally associated with both warm and cold water palaeoenvironments (Brinkhuis and Biffi, 1993; Frieling and Sluijs, 2018; Kothe, 1990; Zevenboom et al., 1994), and on this basis here they are assigned an unknown environmental preference. Dinocyst genera preseting standard deviation <0.5 for relative abundance values were eliminated from the principal component analysis (PCA). For data treatment, the relative abundance of dinocysts were ln-transformed in order to increase the weight of the taxa with low percentages, which generally have narrow ecological preferences, and to diminish the importance of ubiquitous taxa, which often dominate the assemblages. PCA was then performed on 33 dinocyst genera from MGC, resulting in two major distinct groups, here labelled Group A and Group B (Figure 12). The application of PCA relies on the basic assumption that dinocysts co-ocurring in the samples lived in similar environments. Therefore, statistical parameters evaluate how strong a given co-occurrence is. This approach allowed us to test previous empirically established palaeoecological affinities. Our main goal was to identify which ecological parameter better controls the arrangements of our dinocyst assemblages.

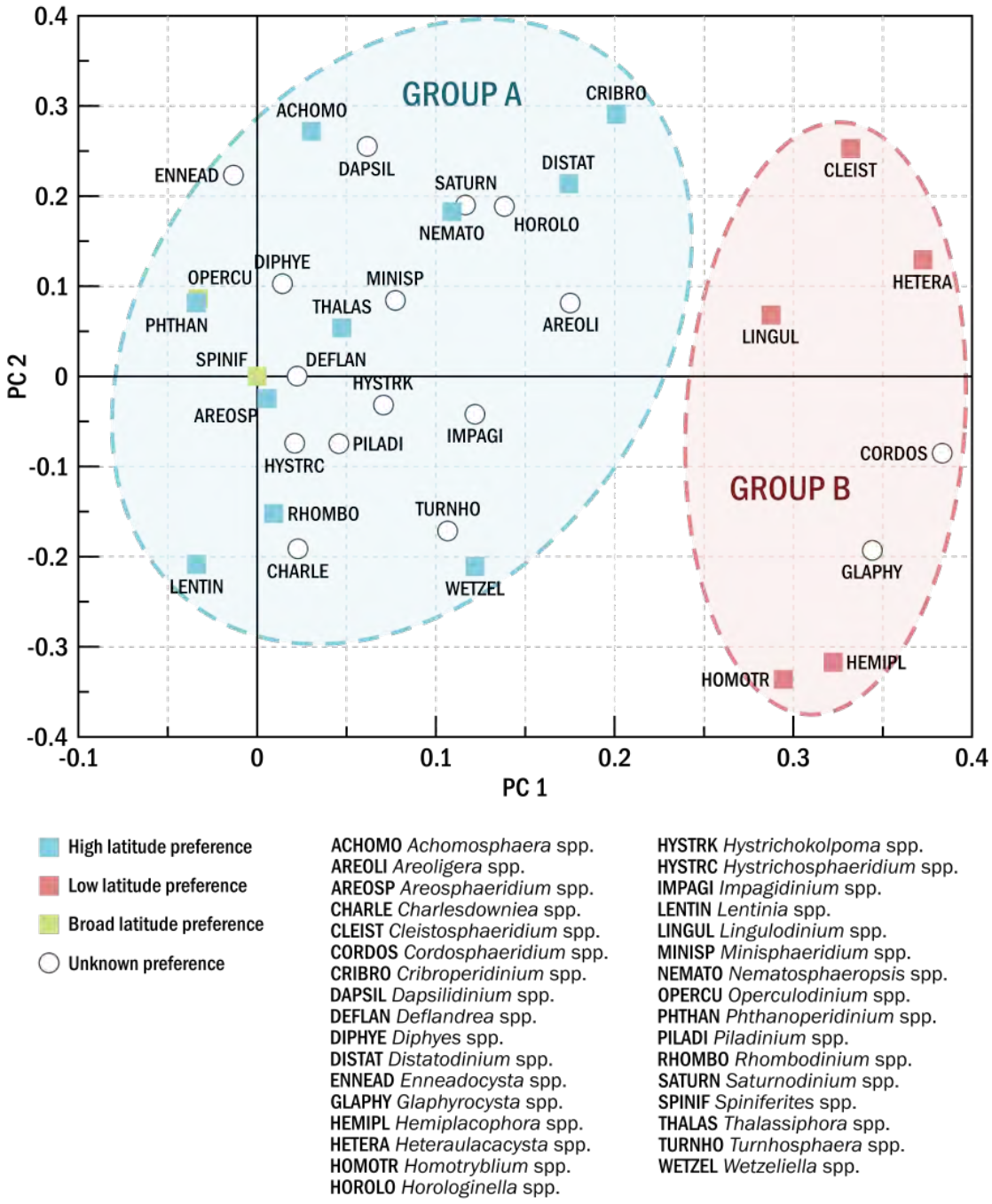


Figure 12. Scatter plot of genera ordination from principal component analysis (PCA). See text and Table 4 for literature references and methodological explanation.

A clear conclusion resulting from the distribution of species with previously assigned affinities is that sea-surface temperature is the dominant palaeoenvironmental control

being resolved in this analysis. We assumed that taxa with "unknown preference" lived with the same ecological preferences of the corresponding group. To synthesize a Warm/Cold Water Dinocyst Taxa Ratio (W/C ratio), we used relative abundances of Group B and Group A through time (Figure 13). This indicator of nearshore surface-water temperature presents a decreasing trend from the base of the record to ~36.7 Ma, when it recovers to higher values between ~36.4 and 34.7 Ma. The W/C ratio then drops abruptly, persisting in nearly zero values for ~500 ka (Figure 13).

In addition to PCA-based palaeoenvironmental assessment, we also verified the Peridinioid:Gonyaulacoid (P/G) ratio as well as three selected dinocyst taxa individually, namely *Hemiplacophora semilunifera*, *Svalbardella* spp., and *Thalassiphora* spp. Our P/G ratio shows two significant changes in its pre-EOT record: (1) a first sudden increase at ~36.0 Ma coinciding with a downward shift in Shannon diversity curve, and a significant drop in species richness of the dinocysts; and (2) a ~300 ka interval of highest values starting from ~34.4 Ma (Figure 13). Morevoer, increases in the P/G ratio tend to be coeval with falls in both the Shannon diversity curve and species richness of dinocysts (Figure 13). The range chart of *H. semilunifera* indicated that the species was relatively abundant between ~35.9 and 34.9 Ma, when it suddenly decreased towards the complete extinction, ~35.5 Ma (Figure 13). Higher abundances of *H. semilunifera* seem to be closely related to an interval of extremely low abundance of the dinocyst genus *Thalassiphora* spp. It is also noteworthy two ~2% peaks of arctic dinocyst *Svalbardella* spp. between ~34.7 and 34.5 Ma, the first of which seems coeval with a major peak in *Thalassiphora* spp. relative abundance (Figure 13).

Coccolithophores dwell and secrete coccolith plates within the photic zone (Okada and Honjo, 1973). Therefore, the chemical compositions of coccoliths record signals in the

shallow mixed layer (Dudley et al., 1980, 1986; Goodney et al., 1980). This is in agreement with comparative studies, which have demonstrated that nannofossil $\delta^{18}O$ values vary in parallel to those of planktic (Ennyu et al., 2002) and even benthic foraminifers (Bohaty and Zachos, 2003). Our $\delta^{18}O$ record show three major trends (Figure 13): (1) positive between ~37.6 and 36.2; (2) relatively stable between ~36.2 and 34.9 Ma; and (3) positive from ~34.9 Ma. In the $\delta^{13}C$ data, on the other hand, a single, conspicuous shift between ~36.4 and 36.2 Ma marks the change from a positive to a long-term negative trend (Figure 13). This event is coeval with an abrupt drop in the percentage of holococcoliths, from as much as 6-10% to <2%, suggesting increased productivity (Figure 13). Biogeographic distributions of calcareous nannofossils were inferred from the *Isthmolithus* ratio, which consists of the relative abundance of all *Isthmolithus* species divided by the sum of relative abundances of all *Isthmolithus* species, *Reticulofenestra isabellae*, *Reticulofenestra reticulate*, and holococcoliths (Villa et al., 2008). The records from MGC show a clear stepwise increase in this indicator across the late Eocene. We observed abrupt "jumps" at ~35.6 Ma, and ~34.9 Ma (Figure 13). This shift in nannofossil assemblages would be interpreted as from warm, sub-tropical oligotrophic forms, to more mid-latitude assemblages (Villa et al., 2008).

Following from a proximal-distal ecological preference of studied microfossil groups, our approach of coccolith-based records always refer to an oceanic signal, whereas dinocyst-based records are interpreted as inner-shelf indicators. Therefore, we assume here that convergent records are unequivocal evidence of sea-surface signal.

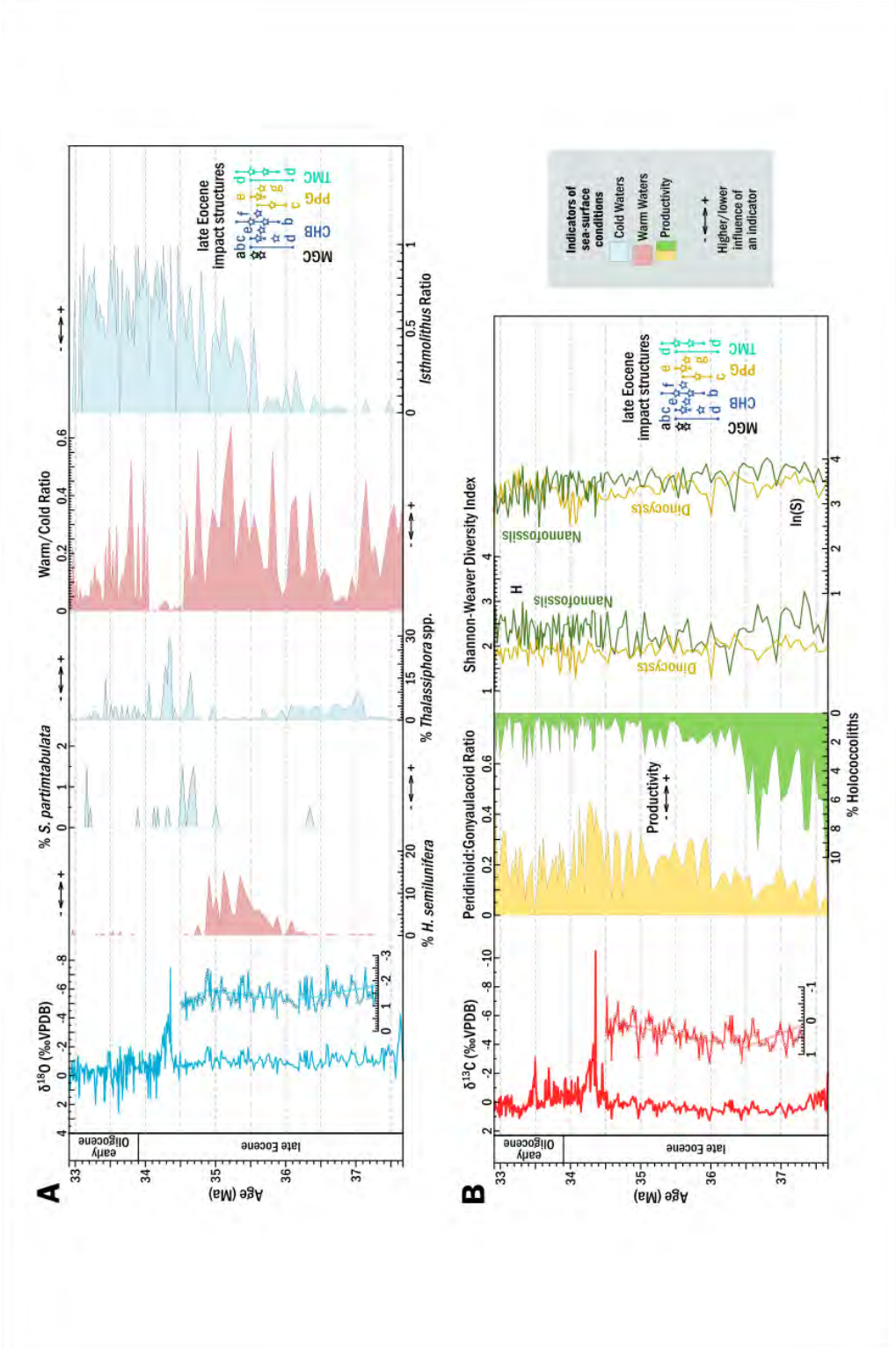


Figure 13. Geochemical and micrpalaeontological records of the MGC (Part 3). Age assignements of important late Eocene impact structures are provided. These are discussed in detail in the next section. A: High-resolution $\delta^{18}O$ record, accompanied by a specific interval of increased scale to highlight major trends; relative abundance of selected dinocyst species (*Hemiplacophora semilunifera* and *Svalbardella partimtabulata*) and genus (*Thalassiphora* spp.); dinocyst-based warm/cold sea-surface water ratio; and calcareous nannofossil-based *Isthmolithus* ratio. B: High-resolution $\delta^{13}C$ record, peridinioid:gonyaulacoid ratio, percentage of Holococcoliths and a set of Shannon-Weaver diversity indices for calcareous

nannofossils and dinocysts (H – Shannon diversity index, and ln(S) – natural logarithm of species richness). Legend of late Eocene impact structures: MGC – Mossy Grove Core, CHB – Chesapeake Bay, PPG – Popigai, TMC – Toms Canyon, a – Rymer (2019), b – Koeberl et al. (1996), c – Liu et al. (2009), d – Poag et al. (2002), e – Pusz et al. (2009), f – Poag et al. (2012), Bottomley et al. (1997).

6.4. Discussion

6.4.1. Implications for the North Atlantic circulation patterns

To assess significant palaeoceanographic changes though time, we analysed both geochemical and micropalaeontological proxies. We then established three main pre-EOT palaeoceanographic regimes (Figure 14), defined here as Regime 1 (R1: ~37.6-36.2 Ma), Regime 2 (R2: ~36.2-34.9 Ma), and Regime 3 (R3: ~34.9-34.1 Ma), the last of which overlaps the EOT-1.

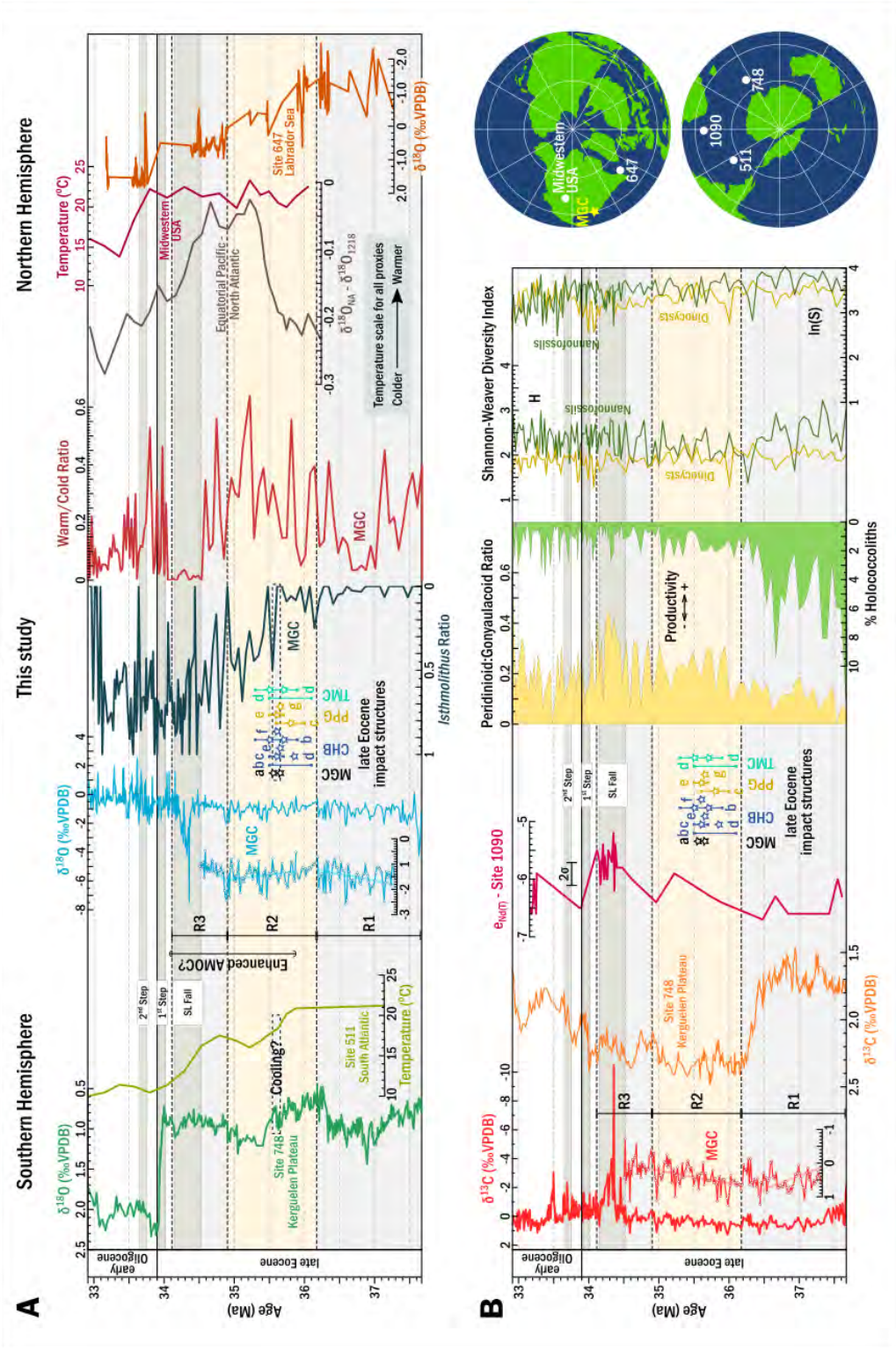


Figure 14. Late Eocene to early Oligocene geochemical and micropalaeontological records from the MGC compared to Northern and Southern Hemisphere multiproxy records. Three distinct palaeoceanographic regimes (R1, R2, R3) are shown, along with age assignments of late Eocene impact structures, potential impact-induced cooling, and proposed enhanced AMOC interval (Elsworth et al., 2017). A: Sea-surface and deep-water temperature proxies – Site 748 (Villa et al., 2008), Site 511 (Liu et al., 2009b), MGC (this study), Equatorial Pacific – North Atlantic (Elsworth et al., 2017), Midwestern USA (Zanazzi et al., 2007), Site 647 (Coxall et al., 2018). B: Productivity and diversity proxies – MGC (this study), Site 748 (Villa et

al., 2008), Site 1090 (Scher and Martin, 2006), peridinioid:gonyaulacoid ratio (this study), percentage of holococcoliths (this study), and Shannon-Weaver Diversity Index (this study). Legend of late Eocene impact structures: MGC – Mossy Grove Core, CHB – Chesapeake Bay, PPG – Popigai, TMC – Toms Canyon, a – Rymer (2019), b – Koeberl et al. (1996), c – Liu et al. (2009), d – Poag et al. (2002), e – Pusz et al. (2009), f – Poag et al. (2012), Bottomley et al. (1997).

Regime 1 (R1; ~37.6-36.2 Ma): Reconfiguration of oceanic gateways?

The first regime in our record is characterised by colder surface waters, evidenced by a ~0.5‰ increase in $\delta^{18}O$ values (Figure 14). This is in accordance with a decreasing W/C ratio, *Thalassiphora*-enriched dinocyst assemblages and scarce occurrences of *H. semilunifera* (Figure 14). *Thalassiphora* spp. has been associated with cooling of surface waters in Central Italy (Coccioni et al., 2000; Vonhof et al., 2000), whereas the absence of low latitude *H. semilunifera* was reported as a response to major cooling events (Brinkhuis and Biffi, 1993). The MGC records show consistency with a long-term sea-surface cooling trend observed at Site 748, Kerguelen Plateau, Indian sector of the Southern Ocean (Figure 14) (Bohaty and Zachos, 2003; Villa et al., 2008). Benthic $\delta^{18}O$ records from the high latitude North Atlantic Site 647, in the Southern Labrador Sea (palaeodepth ~2-3 km), present a relatively stable trend, with values as low as ours (Figure 14) (Coxall et al., 2018).

We believe that R1 represents a stage of significant surface and deep water cooling with possible buildup of small ice sheets on Antarctica (Bohaty and Zachos, 2003). This global trend initiated after the Middle Eocene Climatic Optimum (MECO; ~41 Ma), and cooled ocean temperature by ~6° C in the long-term (Bohaty and Zachos, 2003). Our $\delta^{13}C$ records, on the other hand, follows a positive trend, marked by an overall ~1‰ increase during R1 (Figure 14). This behaviour differs from high latitude records, as $\delta^{13}C$ values at Sites 647 (Southern Labrador Sea) and 748 (Kerguelen Plateau) show a long-term

stable trend throughout the same interval (Figure 14) (Bohaty and Zachos, 2003; Coxall et al., 2018; Villa et al., 2008).

Another remarkable event in this regime is the profound change in the majority of our indicators towards more R2-like conditions during the last 200 ka of R1 (Figure 14). At MGC, this transitional interval comprehends the stabilization of the $\delta^{18}O$ increasing trend, a shift from positive to negative trend in our $\delta^{13}C$ records, a dramatic decrease in the percentage of holococcoliths, and a prominent dinocyst assemblage reorganisation, with rising W/C ratio and coeval *Hemiplacophora*-enriched dinocyst assemblage (Figure 14). Our records suggest that the cooling observed in R1 is no longer the thermal condition dominating North Atlantic surface waters. Substantial changes in circulation patterns in the Southern Ocean, including a potential surface-water warming linked to a pronounced and abrupt 1‰ negative shift in fine-fraction $\delta^{13}C$ records from Site 748 (Southern Ocean) (Bohaty and Zachos, 2003; Villa et al., 2008), could have triggered the alterations observed at MGC.

One attempt to explain the palaeoceanographic alterations observed in the Southern Ocean would be the deepening and widening of the Drake Passage (Scher and Martin, 2006). Fish teeth neodymium (Nd) isotope data from Site 1090, on Agulhas Ridge, in the Atlantic sector of the Southern Ocean, revealed a strong positive trend in Nd isotope ratios ($^{143}Nd/^{144}Nd$: ε_{Nd}) at three different intervals from the middle to late Eocene (Scher and Martin, 2006). Since water masses are imprinted with the signature of Nd isotope ratios from their source region, seawater ε_{Nd} values can be used to detect Pacific seawater (ε_{Nd} = -3 to -5) in the Atlantic sector (ε_{Nd} = -10 to -11) of the Southern Ocean and, thereby, track changes in basin-to-basin water mass exchange. A pronounced ε_{Nd} increase was observed (Scher and Martin, 2006) starting at ~36.5 Ma, and coincides with high reactive

phosphorus mass accumulation rate (Pr MAR) at the same age from Site 1090 (Anderson and Delaney, 2005), a chemical proxy for organic carbon burial. This is furtherly supported by a pre-EOT onset of the Antarctic Circumpolar Current, including estimates of ~35.5 Ma for the latest shallow circulation (Barker et al., 2007).

Regime 2 (R2; ~36.2-34.9 Ma): Evidence of a late Eocene AMOC-like system?

The development of a distinct NADW in the late Eocene is marked by a strong negative $\delta^{13}C$ excursion observed in sites from the North (612, U1411, 647, 1053), Equatorial (366) and South Atlantic (1090) (Coxall et al., 2018). This excursion is largest at North Atlantic sites, probably corresponding to the southward export of Arctic-imprinted, nutrient-rich NADW (Coxall et al., 2018). To test this signal and whether it represents the contribution of the NADW to the global deep ocean, a proxy consisting of the difference between the $\delta^{18}O$ data from the North Atlantic compilation and that of the deep Pacific Ocean (ODP Site 1218) has been performed (Elsworth et al., 2017). The declining $\delta^{18}O$ gradient between the North Atlantic and deep Pacific between ~35.7 and 33.7 Ma suggests a stronger contribution of NADW to the global deep sea, consistent with the presence of a stronger AMOC (Elsworth et al., 2017). As expected, this is coeval with the negative $\delta^{13}C$ excursion mentioned above (Coxall et al., 2018). A strong AMOC-like system would trigger an enhanced Gulf Stream redistributing heat from the North Equatorial current to North Atlantic waters. The modern path of these currents follows a clockwise trajectory around the North Atlantic gyre, crossing the Gulf of Mexico, where the Gulf Stream itself arises. Palaeogeographic recontructions of the late Eocene US Gulf Coastal Plain demonstrate that the Floridian Peninsula (Galloway et al., 2011) was still an immense but submersed plateau, which could have broadened and invigorated the Gulf Stream.

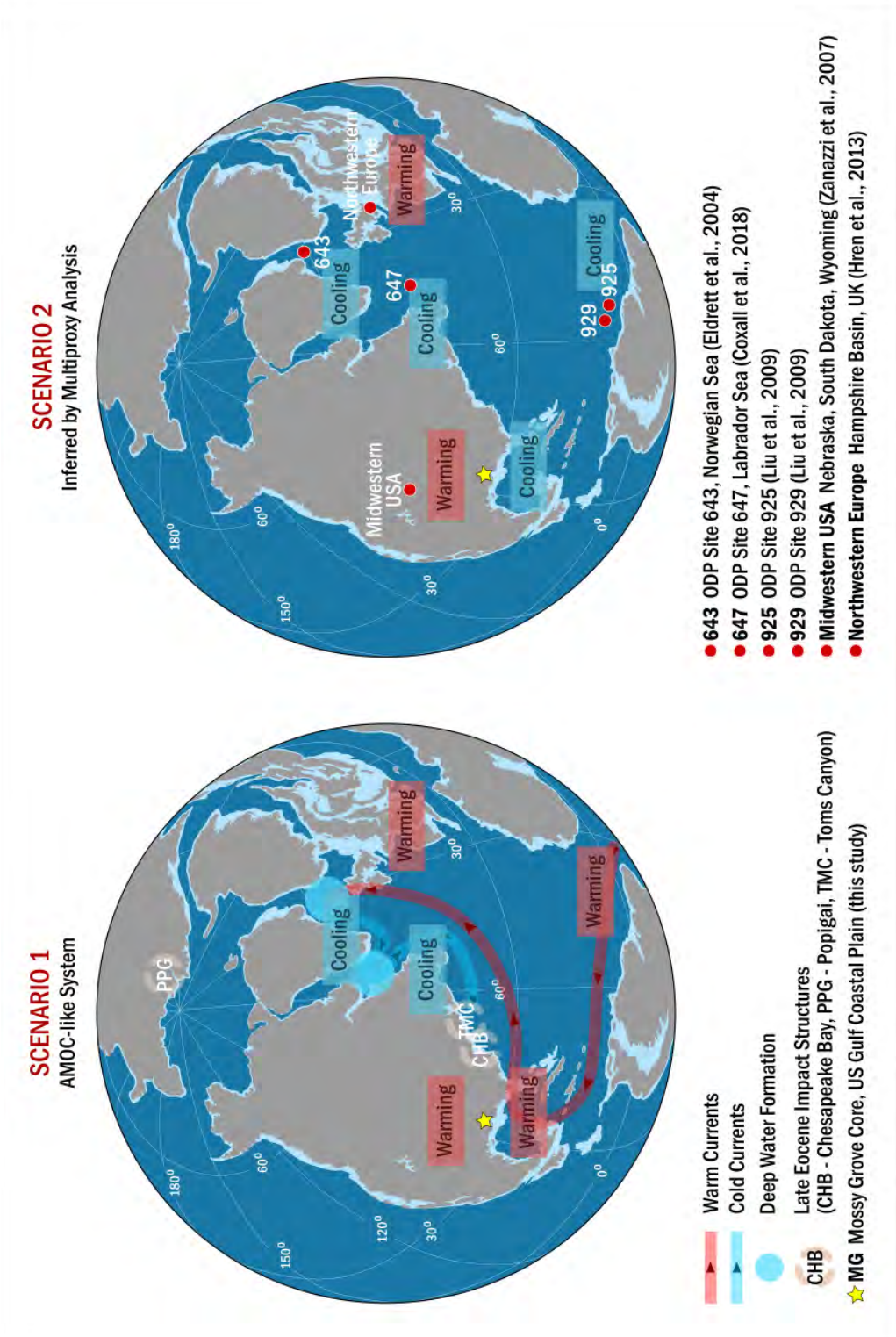


Figure 15. Palaeogeographic reconstruction of the North Atlantic showing oceanic circulation patterns and expected/inferred temperature trends under two distinct scenarios. Scenario 1: invigorated AMOC regime and expected sea-surface and continental temperature trends. Scenario 2: Sea-surface and continental

temperature trends based on multiproxy analysis from multiple sites. Palaeogeography follows Coxall et al. (2018).

At MGC, Regime 2 comprehends relatively stable $\delta^{18}O$ values within a long-term positive trend recorded in R1 and R3. Moreover, we also detected higher W/C ratio, absence of cold-water dinocyst genus *Thalassiphora* spp. and coeval *Hemiplacophora*-enriched dinocyst assemblages (Figure 14). Our $\delta^{13}C$ record shows a ~1.5 Ma negative trend, along with higher productivity patterns, as indicated by lower relative abundance of holococcoliths and higher P/G ratio. The coccolith-fraction $\delta^{18}O$ and dinocyst-based palaeoenvironmental records at MGC suggest sea-surface warming in the Gulf Coast realm. However, this diverges from our *Isthmolithus* ratio, which indicates a clear sea-surface cooling at ~35.6 Ma and is more consistent with high-latitude waters. In fact, from ~35.9 Ma surface ocean temperature from the alkenone insaturation index ($U^{K'}_{37}$) of the South Atlantic Site 511 (Falklands Plateau) and even benthic $\delta^{18}O$ from the Labrador Sea (Site 647) show evidence of progressive cooling (Coxall et al., 2018; Elsworth et al., 2017; Liu et al., 2009b).

The MGC records seem incoherent with an invigorated overturning circulation in the North Atlantic. However, if we assume that dinocyst-based records are reflecting continental-to-inner-shelf conditions and coccolith-based records are responding to changes in ocean waters, we can interprete the cooling as a trend exclusively open marine, whereas continental and nearshore settings persisted relatively warm. We believe that Regime 2 represents an interval of open ocean cooling coupled with relatively warm continental environments. Increasing runoff in coastal areas driven by precipitation may have affected the $\delta^{18}O$ records at MGC, lowering its values and, thus, cancelling out with progressively more positive figures due to sea-surface cooling. This ultimately resulted

in a long-term stable trend as observed at MGC. The dinocyst-based P/G ratio (Harland, 1973) is an excellent approach for nearshore primary productivity and strong terrigenous inputs (Brinkhuis et al., 1998; Crouch, 2001; Eshet et al., 1994; Van Mourik et al., 2001; van Mourik and Brinkhuis, 2000; Reichart and Brinkhuis, 2003). P/G ratio values at MGC shows a pronounced increase at ~36.0 Ma. Assuming that major sea-level changes did not happen before the EOT (Zachos et al., 2001), our records suggest that enchaned runoff may have occurred along with open ocean cooling (Coxall et al., 2018; Elsworth et al., 2017; Liu et al., 2009b). Our interpretation is in agreement with terrestrial records from Midwestern United States and northwestern Europe, both of which indicate sustained continental warmth until the onset of the Oligocene (Hren et al., 2013; Zanazzi et al., 2007).

Moreover, Regime 2 is marked by a ~1.5 Ma negative trend in our coccoltih-fraction $\delta^{13}C$ records, a behaviour also observed in fine fraction $\delta^{13}C$ records at Site 748, Kerguelen Plateau, Southern Ocean (Bohaty and Zachos, 2003; Villa et al., 2008). Additionally, R2 is characterised by a prominent drop in the relative abundance of holococcoliths, suggesting a large increase in open ocean primary productivity. Circulation-induced productivity increase and a coeval switch in our $\delta^{13}C$ records to more negative values are indicative of increased nutrient – and ^{13}C-depleted DIC – supply to the sub-tropical and tropical oceans. We believe that the newly created passage between the Pacific and Atlantic Oceans may have led to the enhancement of the global thermohaline circulation, increasing the export of nutrients from the Southern Ocean to the tropical and sub-tropical oceans via sub-thermocline Antarctic mode waters, and increasing marine primary production in these regions (Anderson and Delaney, 2005; Scher and Martin, 2006).

Therefore, our records do not support an AMOC-like system induced by tectonic adjustments from Northern ou Southern Hemispheres (Coxall et al., 2018; Elsworth et al., 2017; Hutchinson et al., 2019). Besides, the timing of the proposed long-term AMOC-driven warming in the North Atlantic (Coxall et al., 2018; Elsworth et al., 2017; Hutchinson et al., 2019) is not corroborated by our 3-regime-scheme, especially considering its overlap with the even colder Regime 3.

Regime 3 (R3; ~34.9-34.1 Ma): An early-stage EOT-1 sea-surface cooling?

In Regime 3, our $\delta^{18}O$ records returned to the long-term positive trend, which marked R1. Since our nearshore productivity indicator – the dinocyst-based P/G ratio – indicates sustained continental runoff, we assume that further cooling induced positive $\delta^{18}O$ to surpass continental-derived negative $\delta^{18}O$ values. This is supported by our nearshore and open ocean temperature indicators. Our W/C ratio declined gradually between ~34.9 and 34.6 Ma, until they fell almost completely between ~34.6 and 34.1 Ma, suggesting that dinocyst-assemblages were dominated by cold-water dwellers during this ~500 ka interval. A remarkable ~200-300 ka offset between decrasing coccolith-fraction $\delta^{18}O$ record and nearly zero values in W/C ratio demonstrate that the sensitivity of this biotic proxy depends on the temperature tolerances and optima of the dinocyst assemblage used, and as such it may respond nonlinearly to environmental drivers, such as changing temperature. Therefore, we believe that sea-surface cooling started at ~34.9 Ma, as suggested by the $\delta^{18}O$ curve, and only at ~34.6 Ma the temperature was low enough to trigger an ecological exclusion of Group B, reducing the W/C ratio towards zero values. This is clearly marked by the extinction of low latitude *H. semilunifera* at ~34.6 Ma, a dinocyst taxon likely associated with warm waters (Brinkhuis and Biffi, 1993).

Initial cooling in the Regime 3 (between ~34.9 and 34.6 Ma) is further supported by the analysis of individual dinocyst taxa. A sharp decline in low latitude *H. semilunifera* relative abundance and a prominent peak in the relative abundance of cold-water *Thalassiphora* spp., both of which represent cooling of surface waters (Brinkhuis and Biffi, 1993; Coccioni et al., 2000; Vonhof et al., 2000). Moreover, the ~2% peaks of high latitude dinocyst genus *Svalbardella* spp. is an additional evidence that Regime 3 is conspicuously marked by colder surface waters. This genus has been reported from high latitudes, such as the North Sea (Śliwińska and Heilmann-Clausen, 2011), Norwegian-Greenland Sea (Manum et al., 1989; van Simaeys et al., 2005; Śliwińska and Heilmann-Clausen, 2011), Labrador Sea (Head and Norris, 1989) and off western Tasmania (Brinkhuis et al., 2003a) and its appearance at tropical/subtropical realms might seem unlikely. However, some authors argue that the taxon could have migrated from the Arctic towards much lower latitudes in the Northern Hemisphere during strong cooling events (van Simaeys et al., 2005; Śliwińska and Heilmann-Clausen, 2011). Furthermore, transequatorial migration has also been proposed to explain isolated occurrences of *Svalbardella* spp. in Southern Hemisphere high latitudes (Brinkhuis et al., 2003a; van Simaeys et al., 2005). Based on modern paths of Greenland and Labrador Currents, it is not unlikely that their invigoration would have allowed migration of this taxon down the east coast of North America during cool phases. In fact, this migration event could be explained by increased late Eocene seasonality (Eldrett et al., 2009; Ivany et al., 2000; Wade et al., 2012). Modern Labrador Current shows seasonal and spatial variability, becoming strong in the autumn/winter and weak in the spring/summer (Han et al., 2008). Additionally, a second step-like increase in *Isthmolithus* ratio suggests that open ocean cooling not only maintened, but also intensified. This is consistent with sustained cooling

of surface waters observed either at high and low-latitude sites from both hemispheres (Coxall et al., 2018; Liu et al., 2009b; Wade et al., 2012). The first positive step in benthic $\delta^{18}O$ records is widely thought to be mainly driven by significant global cooling from ~34.1 Ma (Houben et al., 2018; Katz et al., 2008; Miller et al., 2008; Wade et al., 2012), with limited ice-sheet growth (Katz et al., 2008; Lear et al., 2008). Based on multiple lines of evidence, we demonstrated in previous chapter that MGC recorded profound early-stage sea-level fall likely associated with large-scale ice-sheet growth on East Antarctica (Miller et al., 2008; Passchier et al., 2017). Our records ultimately indicate that Regime 3 is characterised by cooling either in continental and nearshore settings and in open marine environments.

6.4.2. Implications for extraterrestrial impacts

The discovery of various, globally distributed impact ejecta deposits in upper Eocene sediments has raised intense speculation that the impact of extraterrestrial bodies could have triggered or enhanced global cooling and biotic turnover in the lead up to the EOT (Coccioni et al., 2009; Keller, 1986; Pusz et al., 2009; Vonhof et al., 2000). At MGC, recently discovered microspherule layers have been dated at ~35.67 and ~35.54 Ma (Rymer, 2019; Westerhold et al., 2014), which is perfectly consistent with multiple dating methods that provided well constrained age assignments for major late Eocene impact structures (Bottomley et al., 1997; Koeberl et al., 1996; Liu et al., 2009a; Poag, 2012; Poag et al., 2002; Pusz et al., 2009) (**Error! Reference source not found.**). These are so closely dated, that some authors argue for an asteroid or comet shower (Farley et al., 1998; Hut et al., 1987; Tagle and Claeys, 2004). According to our *Isthmolithus* ratio, an abrupt step-like increase is directly correlated with the microspherule layers found at

MGC (Rymer, 2019), suggesting that open ocean cooling would have followed the impact events.

Although some authors argue for a greenhouse-like warming as the longer-term consequence of bolide impacts (e.g. Kawaragi et al., 2009; MacLeod et al., 2018), it has been increasingly accepted that short-to-long-term cooling events may have been induced by extraterrestrial impacts through a sulfate-aerosol-driven climate forcing (Artemieva and Morgan, 2017). Impact events can inject large amounts of sulfur into the stratosphere, ultimately affecting the radiation budget of the Earth (Kring et al., 1996). Evidence of post-impact millennial-scale cooling have been detected in the Cretaceous-Paleogene (K-Pg) boundary (Brinkhuis et al., 1998; Galeotti et al., 2004), associated to the Chicxulub impact structure. The K-Pg and the late Eocene Popigai impact events may have injected similar amounts of sulfur into the atmosphere (Kring et al., 1996), which could explain late Eocene post-impact evidence of cooling and reorganisation of water structure (Coccioni et al., 2000; Keller, 1986; Vonhof et al., 2000).

6.4.3. Concluding remarks

Our records from the Gulf Coastal Plain show that, during Regime 1 (~37.6-36.2 Ma), the long-term cooling trend initiated after the Middle Eocene Climatic Optimum (~41 Ma) (Bohaty and Zachos, 2003) affected surface-water temperatures at a global scale, as demonstrated by consistent evidences from the Gulf of Mexico and the Indian sector of the Southern Ocean. These palaeoceanographic patterns were interrupted by a transitional interval that shifted our records into a more Regime 2-like conditions, potentially linked to a major stage in the deepening and widening process of the Drake Passage (Scher and Martin, 2006). This may have initiated oceanic flow through shallow depths. It is notable that the transitional phase at MGC (~36.4-36.2 Ma) coincides with a profound shift to

more positive $\delta^{13}C$ values in bulk (surface-ocean) carbonates from the Southern Ocean (Figure 14) (Bohaty and Zachos, 2003; Villa et al., 2008). These are strongly indicative of increased nutrient export from the surface ocean of this region.

We did not find strong evidences to support an AMOC-like system induced by tectonic adjustments, either from Northern ou Southern Hemisphere high-latitude gateways (Coxall et al., 2018; Elsworth et al., 2017; Hutchinson et al., 2019). Instead, our data revealed a strong continent-ocean thermal gradient during the late Eocene. Whereas the open ocean seetings cooled along with Northern and Southern Hemisphere high-latitudes (Coxall et al., 2018; Elsworth et al., 2017; Liu et al., 2009b), the continental interior of North America and Europe sustained warm temperatures (Hren et al., 2013; Zanazzi et al., 2007). Previous experiments in model simulations already concluded that the opening of the Drake Passage to shallow depths do not induce NADW formation (Sijp and England, 2004). Moreover, contourite-drift-based evidence suggest that the onset of northern-sourced, strongly circulating bottom water occurred in the Oligocene (Boyle et al., 2017). Some mechanisms discussed above need better age constrains, including the timing of complete deepeding and widening of Atlantic gateways and precise duration of the proposed long-term AMOC-driven warming (Coxall et al., 2018; Elsworth et al., 2017; Hutchinson et al., 2019).

We advocate that the newly created passage between the Pacific and Atlantic Oceans may have led to the enhancement of the global thermohaline circulation, increasing the export of nutrients from the Southern Ocean to the tropical and sub-tropical oceans via sub-thermocline Antarctic mode waters, and increasing marine primary production in these regions (Anderson and Delaney, 2005; Scher and Martin, 2006). The proposed circulation-induced productivity increase is coeval with the switch in our $\delta^{13}C$ records to

more negative values, again indicative of increased nutrient – and ^{13}C-depleted DIC – supply to the sub-tropical and tropical oceans. This long-term process may have led to increased sequestration of atmospheric CO_2 through an enhanced biological pump, an important link between short- and long-term carbon cycle. This mechanism, rather than enhanced weathering and CO_2 drawdown driven by invigorated overturning circulation, may have been a major factor in lowering atmospheric CO_2 during the late Eocene.

It is also possible that extraterrestrial impacts may have induced sulfate-aerosol-driven climate forcing (Artemieva and Morgan, 2017). This could have been the case of late Eocene impact events, which probably affected the radiation budget of the Earth (Kring et al., 1996), triggering post-impact millennial-scale cooling and reorganisation of water structure (Coccioni et al., 2000; Keller, 1986; Vonhof et al., 2000). We argue that the larger late Eocene impact structures found in North America and Russia (Bottomley et al., 1997; Koeberl et al., 1996; Liu et al., 2009a; Poag, 2012; Poag et al., 2002; Pusz et al., 2009) could have played an important role in ocean cooling, as recorded by coupled *Isthmolithus* ratio and microspherule layers found at MGC (Rymer, 2019). The short-term impact-induced cooling may have triggered positive feedback mechanisms such as vegetation-albedo and permafrost, that intensified and/or sustained the sea-surface cooling observed either in higher and lower latitudes from both hemispheres (Coxall et al., 2018; Liu et al., 2009b; Wade et al., 2012).

Large-scale cooling-driven changes in the distribution of vegetation in high latitudes (e.g. boreal forests replaced by tundra) increases the albedo of Arctic regions, and the reflectance of solar radiation. Permafrost deposits and other organic carbon and methane hydrate reservoirs could store growing amounts of greenhouse gases during cooling periods, particularly in high latitudes. We believe that such mechanisms (extraterrestrial

impacts and positive feedback loops) may have intensified the cooling initiated by enhanced biological pump activity. Moreover, our newly-generated geochemical and micropalaeontological records from MGC suggest that substantial sea-surface cooling preceeded sea-level fall by ~80 ka. This multiproxy evidence of enhanced cooling in surface waters agrees with multiple sites worldwide that long-term sea-surface cooling marked the late Eocene prior to the first large-scale ice-sheet expansion on Antarctica (Coxall et al., 2018; Liu et al., 2009b; Wade et al., 2012), which strongly supports atmospheric cooling and, therefore, the hypothesis that declining greenhouse gas concentration played the major role in preconditioning the Earth for the Eocene-Oligocene Transition.

CHAPTER 7: CONCLUSION

Anthropogenic carbon emissions to the atmosphere continuously grows and, unless they do not change in a dramatic way, by the end of this century CO_2 concentrations will rise to values between ~790 and 1,150 ppmv, i.e., ~2.8 to 4.1 times pre-industrial levels. The last time this happened was ~34 Ma ago, in the late Eocene, when atmospheric CO_2 concentration crossed a ~750 ppmv threshold, below which the first Cenozoic East Antarctic continental-scale ice sheets formed in the Cenozoic. A warmer ice-free Cretaceous and early Paleogene Earth underwent the typical colder climate state that prevails since the Oligocene. Although this shift has been widely studied by a multitude of sedimentological, micropalaeontological, and geochemical records, the driving mechanisms that led to this dramatic climate event remains controversial. Understanding and predicting the behaviour of the East Antarctic Ice Sheet around these thresholds of climate forcing, and its role in the wider Earth System, should provide strong cautionary evidence to support the mitigation of 21st century anthropogenic climate change.

To reconstruct the evolutionary history of tropical/subtropical realms in the late Eocene-early Oligocene, we applied coccolith-fraction (<20 μm) carbonate stable oxygen ($\delta^{18}O$) and carbon ($\delta^{13}C$) isotopes (~6 ka resolution), palynological and calcareous nannofossil assemblages (~26 ka resolution), and bulk sediment X-ray fluorescence data (<10 ka resolution). Along with a new and more robust age-depth model, these data yielded new high-resolution multiproxy record from a continuously cored (~137 m) and substantially expanded (~4.7 cm ka^{-1}) succession spanning ~5 Ma of upper Eocene-early Oligocene mid-shelf marine clays from the the Mossy Grove Core (MGC), central Mississippi, US Gulf Coastal Plain.

Our records suggest that surface-water temperatures from the Gulf Coastal Plain were probably affected by the long-term cooling trend initiated after the Middle Eocene Climatic Optimum (~41 Ma). These palaeoceanographic patterns were interrupted by a transitional interval potentially linked to a major stage in the deepening and widening process of the Drake Passage. This may have initiated oceanic flow through shallow depths, shifting $\delta^{13}C$ records either from MGC and the Southern Ocean in bulk (surface-ocean) carbonates. We did not find strong evidences to support an AMOC-like system induced by tectonic adjustments, either from Northern ou Southern Hemisphere high-latitude gateways. Instead, our data suggest a strong continent-ocean thermal gradient during the late Eocene. We advocate that the newly created passage between the Pacific and Atlantic Oceans may have led to the enhancement of the global thermohaline circulation, increasing the export of nutrients from the Southern Ocean to the tropical and sub-tropical oceans via sub-thermocline Antarctic mode waters, and increasing marine primary production in these regions. This long-term process may have led to increased sequestration of atmospheric CO_2 through an enhanced biological pump, an important link between short- and long-term carbon cycle. This mechanism, rather than enhanced weathering and CO_2 drawdown driven by invigorated overturning circulation, may have been a major factor in lowering atmospheric CO_2 during the late Eocene.

We also found evidence that extraterrestrial impacts recorded in the larger late Eocene impact structures found in North America and Russia may have played an important role in ocean cooling, by inducing sulfate-aerosol-driven climate forcing that affected the radiation budget of the Earth, and triggering post-impact millennial-scale cooling and reorganisation of water structure. This short-term impact-induced cooling may have triggered positive feedback mechanisms such as vegetation-albedo and permafrost, that

intensified and/or sustained the sea-surface cooling initiated by an enhanced biological pump activity. Moreover, our newly-generated geochemical and micropalaeontological records from MGC support the hypothesis that declining greenhouse gas concentration played the major role in preconditioning the Earth for the Eocene-Oligocene Transition.

Our new records from the MGC further revealed rapid environmental change at ~34.5 Ma within the shelf environments of the Mississippi Embayment. The rates (<100 ka) and magnitude of change at this time are too large to be controlled by regional tectonics, especially on a long-term stable passive continental margin. We contend that these records represent some significant component of global eustatic sea-level fall at the very start of the EOT. This challenges the view that the dynamics of the EOT are dominated by global cooling during the earliest stages, which then precondition the system to continental-scale ice-sheet expansion in the later stages. Furthermore, the progressive shift towards more positive $\delta^{18}O$ values into the Oligocene recorded at MGC clearly suggests that ice growth persisted through time, revealing a permanent ice-sheet inception. As well as defining a rapid start to the EOT controlled by ice sheet dynamics, the evidence for significant (~40-45 m) sea-level fall and substantial increases in the erosion flux of terrestrial organic matter into continental margin successions, implicates changing shelf-to-ocean carbon, carbonate and nutrient partitioning and fluxes as key drivers of previously observed carbon cycle perturbations, oceanic plankton extinctions, and phytoplankton community restructuring at the onset of the EOT. We propose that the earliest stages of the major EOT eustatic sea-level fall had a disproportionate effect on global biogeochemistry, by causing the first major incision of organic- and nutrient-rich coastal low lands that had been accreting under warm, high sea-level greenhouse conditions for tens of millions of years.

We finally propose as future works: [1] high-resolution record of the continental palynomorph content to generate a paired continent-ocean palaeoclimatic and palaeoceanographic record of the late Eocene tropical-subtropical realms; [2] organic geochemical records of sea-surface temperature estimates ($U^{K'}_{37}$ and TEX_{86}), and dinoflagellate cyst abundance (dinosterol); and [3] extended discussion on the carbon cycle disturbance driven during the EOT.

APPENDICES

Appendix 1 – List of Samples and Methods

The table below presents a summary of all methods applied to each sample used in this work. It also includes the name (s) of who performed each technique (NS = Dr Nursulfiah Sulaiman; MM = Marcelo Mota). It is worthy mentioning that the interval 17.1-109.4 m (2,098 intervals/samples outlined) was analysed for XRF data by Dr Tatsuhiko Yamaguchi at the core store of the Mississippi Department of Environmental Quality, in Jackson, Mississippi.

Sample	Depth		Isotopes	XRF	Palyn.	Nanno.
MG_	m	ft	NS/MM	MM	MM	NS
55	16.8	55.0			X	X
55.5	16.9	55.5				
56	17.1	56.0				
56.5	17.2	56.5	X			
57.5	17.5	57.5	X			
58	17.7	58.0				
58.5	17.8	58.5	X			
59	18.0	59.0			X	X
59.5	18.1	59.5	X			
60	18.3	60.0				
60.5	18.4	60.5				
61.5	18.7	61.5				
62	18.9	62.0				
62.5	19.1	62.5	X			
63	19.2	63.0			X	X
63.5	19.4	63.5	X			
64	19.5	64.0				
64.5	19.7	64.5	X			
65.5	20.0	65.5	X			
66	20.1	66.0				
66.5	20.3	66.5	X			
67	20.4	67.0			X	X
67.5	20.6	67.5	X			
68	20.7	68.0				
68.5	20.9	68.5	X			
69.5	21.2	69.5	X			

70	21.3	70.0				
70.5	21.5	70.5	X			
71	21.6	71.0			X	X
71.5	21.8	71.5				
72	21.9	72.0				
72.5	22.1	72.5	X			
73.5	22.4	73.5	X			
74	22.6	74.0				
74.5	22.7	74.5	X			
75	22.9	75.0			X	X
75.5	23.0	75.5				
76	23.2	76.0				
76.5	23.3	76.5	X			
77.5	23.6	77.5	X			
78	23.8	78.0				
78.5	23.9	78.5	X			
79	24.1	79.0			X	X
79.5	24.2	79.5				
80	24.4	80.0				X
80.5	24.5	80.5	X			
81.5	24.8	81.5	X			
82	25.0	82.0				
82.5	25.1	82.5	X			
83	25.3	83.0			X	X
83.5	25.5	83.5				
84	25.6	84.0				
84.5	25.8	84.5	X			
85.5	26.1	85.5	X			
86	26.2	86.0				
86.5	26.4	86.5				
87	26.5	87.0			X	X
87.5	26.7	87.5				
88	26.8	88.0				
88.5	27.0	88.5	X			
89.5	27.3	89.5	X			
90	27.4	90.0				
90.5	27.6	90.5	X			
91	27.7	91.0			X	X
91.5	27.9	91.5	X			
92	28.0	92.0				
92.5	28.2	92.5	X			
93.5	28.5	93.5				
94	28.7	94.0				
94.5	28.8	94.5	X			

95	29.0	95.0			X	X
95.5	29.1	95.5				
96	29.3	96.0				
96.5	29.4	96.5	X			
97.5	29.7	97.5	X			
98	29.9	98.0				
98.5	30.0	98.5	X			
99	30.2	99.0			X	X
99.5	30.3	99.5	X			
100	30.5	100.0				
100.5	30.6	100.5	X			
101.5	30.9	101.5	X			
102	31.1	102.0				
102.5	31.2	102.5	X			
103	31.4	103.0			X	
103.5	31.5	103.5	X			
104	31.7	104.0				
104.5	31.9	104.5	X			
105.5	32.2	105.5	X			
106	32.3	106.0				
106.5	32.5	106.5	X			
107	32.6	107.0			X	X
107.5	32.8	107.5	X			
108	32.9	108.0				
108.5	33.1	108.5	X			
109.4	33.3	109.4				
109.5	33.4	109.5	X			
110	33.5	110.0				
110.5	33.7	110.5	X			
111	33.8	111.0			X	X
111.5	34.0	111.5	X			
112	34.1	112.0				X
112.5	34.3	112.5	X			
113.5	34.6	113.5	X			
114	34.7	114.0				X
114.5	34.9	114.5	X			
115	35.1	115.0			X	
115.5	35.2	115.5	X			
116	35.4	116.0				X
116.5	35.5	116.5	X			
117.5	35.8	117.5	X			
118	36.0	118.0				
118.5	36.1	118.5	X			
119	36.3	119.0			X	X

119.5	36.4	119.5	X			
120	36.6	120.0				
120.5	36.7	120.5	X			
121.5	37.0	121.5	X			
122	37.2	122.0				
122.5	37.3	122.5	X			
123	37.5	123.0			X	X
123.5	37.6	123.5	X			
124	37.8	124.0				
124.5	37.9	124.5	X			
125.5	38.3	125.5	X			
126	38.4	126.0				
126.5	38.6	126.5	X			
127	38.7	127.0			X	X
127.5	38.9	127.5	X			
128	39.0	128.0				
128.5	39.2	128.5	X			
129.5	39.5	129.5	X			
130	39.6	130.0				
130.5	39.8	130.5	X			
131	39.9	131.0			X	X
131.5	40.1	131.5	X			
132	40.2	132.0				
132.5	40.4	132.5	X			
133.5	40.7	133.5	X			
134	40.8	134.0				
134.5	41.0	134.5	X			
135	41.1	135.0			X	X
135.5	41.3	135.5	X			
136	41.5	136.0				
136.5	41.6	136.5	X			
137.5	41.9	137.5	X			
138	42.1	138.0				
138.5	42.2	138.5	X			
139	42.4	139.0			X	X
139.5	42.5	139.5	X			
140	42.7	140.0				
140.5	42.8	140.5	X			
141.5	43.1	141.5	X			
142	43.3	142.0				
142.5	43.4	142.5	X			
143	43.6	143.0			X	X
143.5	43.7	143.5				
144	43.9	144.0				

144.5	44.0	144.5	X			
145.5	44.3	145.5	X			
146	44.5	146.0				
146.5	44.7	146.5	X			
147	44.8	147.0			X	X
147.5	45.0	147.5				
148	45.1	148.0				
148.5	45.3	148.5	X			
149.5	45.6	149.5	X			
150	45.7	150.0				X
150.5	45.9	150.5	X			
151	46.0	151.0			X	
151.5	46.2	151.5	X			
152	46.3	152.0				X
152.5	46.5	152.5	X			
153.5	46.8	153.5	X			
154	46.9	154.0				
154.5	47.1	154.5	X			
155	47.2	155.0			X	X
155.5	47.4	155.5	X			
156	47.5	156.0				
156.5	47.7	156.5	X			
157.5	48.0	157.5	X			
158	48.2	158.0				
158.5	48.3	158.5	X			
159.5	48.6	159.5	X		X	X
160	48.8	160.0				
160.5	48.9	160.5	X			
161.5	49.2	161.5	X			
162	49.4	162.0				X
162.5	49.5	162.5	X			
163	49.7	163.0			X	
163.5	49.8	163.5	X			
164	50.0	164.0				X
164.5	50.1	164.5	X			
165.5	50.4	165.5	X			
166	50.6	166.0				
166.5	50.7	166.5	X			
167	50.9	167.0			X	X
167.5	51.1	167.5	X			
168	51.2	168.0				
168.5	51.4	168.5	X			
169.5	51.7	169.5				
170	51.8	170.0				

170.5	52.0	170.5	X			
171	52.1	171.0			X	
171.5	52.3	171.5	X			
172	52.4	172.0				X
172.5	52.6	172.5	X			
173.5	52.9	173.5	X			
174	53.0	174.0				X
174.5	53.2	174.5	X			
175	53.3	175.0			X	
175.5	53.5	175.5	X			
176	53.6	176.0				
176.5	53.8	176.5	X			
177.5	54.1	177.5				
178	54.3	178.0				
178.5	54.4	178.5	X			
179	54.6	179.0			X	X
179.5	54.7	179.5				
180	54.9	180.0				
180.5	55.0	180.5	X			
181.5	55.3	181.5	X			
182	55.5	182.0				X
182.5	55.6	182.5	X			
183	55.8	183.0			X	
183.5	55.9	183.5	X			
184	56.1	184.0				X
184.5	56.2	184.5	X			
185.5	56.5	185.5	X			
186	56.7	186.0				X
186.5	56.8	186.5	X			
187	57.0	187.0			X	
187.5	57.2	187.5	X			
188	57.3	188.0				
188.5	57.5	188.5	X			
189.5	57.8	189.5	X			
190	57.9	190.0				
190.5	58.1	190.5	X			
191.5	58.4	191.5	X		X	
192	58.5	192.0				
192.5	58.7	192.5	X			
193.5	59.0	193.5	X			
194	59.1	194.0				X
194.5	59.3	194.5	X			
195	59.4	195.0			X	
195.5	59.6	195.5	X			

196	59.7	196.0				X
196.5	59.9	196.5	X			
197.5	60.2	197.5				
198	60.4	198.0				
198.5	60.5	198.5	X			
199.5	60.8	199.5	X		X	X
200	61.0	200.0				
200.5	61.1	200.5	X			
201.5	61.4	201.5	X			
202	61.6	202.0				X
202.5	61.7	202.5	X			
203	61.9	203.0			X	
203.5	62.0	203.5	X			
204	62.2	204.0				X
204.5	62.3	204.5	X			
205.5	62.6	205.5				
206	62.8	206.0				X
206.5	62.9	206.5				
207	63.1	207.0			X	
207.5	63.2	207.5				
208	63.4	208.0				X
208.5	63.6	208.5	X			
209.5	63.9	209.5	X			
210	64.0	210.0				X
210.5	64.2	210.5	X			
211	64.3	211.0			X	
211.5	64.5	211.5	X			
212	64.6	212.0				
212.5	64.8	212.5				
213.5	65.1	213.5	X			
214	65.2	214.0				
214.5	65.4	214.5	X			
215	65.5	215.0			X	
215.5	65.7	215.5	X			
216	65.8	216.0				X
216.5	66.0	216.5	X			
217.5	66.3	217.5	X			
218	66.4	218.0				X
218.5	66.6	218.5	X			
219	66.8	219.0			X	X
219.5	66.9	219.5	X			
220	67.1	220.0				
220.5	67.2	220.5				
221.5	67.5	221.5	X			

222	67.7	222.0				X
222.5	67.8	222.5	X			
223	68.0	223.0			X	
223.5	68.1	223.5	X			
224	68.3	224.0				X
224.5	68.4	224.5	X			
225.5	68.7	225.5	X			
226	68.9	226.0				X
226.5	69.0	226.5	X			
227	69.2	227.0			X	
227.5	69.3	227.5	X			
228	69.5	228.0				
228.5	69.6	228.5	X			
229.5	70.0	229.5	X			
230	70.1	230.0				X
230.5	70.3	230.5	X			
231	70.4	231.0			X	
231.5	70.6	231.5	X			
232	70.7	232.0				X
232.5	70.9	232.5	X			
233.5	71.2	233.5	X			
234	71.3	234.0				
234.5	71.5	234.5	X			
235	71.6	235.0			X	
235.5	71.8	235.5	X			
236	71.9	236.0				X
236.5	72.1	236.5	X			
237.5	72.4	237.5	X			
238	72.5	238.0				
238.5	72.7	238.5	X			
239	72.8	239.0			X	X
239.5	73.0	239.5	X			
240	73.2	240.0				
240.5	73.3	240.5	X			
241.5	73.6	241.5	X			
242	73.8	242.0				X
242.5	73.9	242.5	X			
243	74.1	243.0			X	
243.5	74.2	243.5	X			
244	74.4	244.0				X
244.5	74.5	244.5	X			
245.5	74.8	245.5	X			
246	75.0	246.0				X
246.5	75.1	246.5	X			

247	75.3	247.0				X	
247.5	75.4	247.5	X				
248	75.6	248.0					X
248.5	75.7	248.5	X				
249.5	76.0	249.5	X				
250	76.2	250.0					
250.5	76.4	250.5	X				
251	76.5	251.0				X	
251.5	76.7	251.5	X				
252	76.8	252.0					X
252.5	77.0	252.5	X				
253.5	77.3	253.5	X				
254	77.4	254.0					X
254.5	77.6	254.5	X				
255	77.7	255.0				X	
255.5	77.9	255.5	X				
256	78.0	256.0					
256.5	78.2	256.5	X				
257.5	78.5	257.5	X				
258	78.6	258.0					
258.5	78.8	258.5	X				
259	78.9	259.0				X	X
259.5	79.1	259.5	X				
260	79.2	260.0					X
260.5	79.4	260.5					
261.5	79.7	261.5					
262	79.9	262.0					
262.5	80.0	262.5	X				
263	80.2	263.0				X	X
263.5	80.3	263.5					
264	80.5	264.0					
264.5	80.6	264.5	X				
265.5	80.9	265.5					
266	81.1	266.0					X
266.5	81.2	266.5	X				
267	81.4	267.0				X	
267.5	81.5	267.5	X				
268	81.7	268.0					X
268.5	81.8	268.5	X				
269.5	82.1	269.5	X				
270	82.3	270.0					X
270.5	82.4	270.5	X				
271	82.6	271.0				X	
271.5	82.8	271.5					

272	82.9	272.0				X
272.5	83.1	272.5	X			
273.5	83.4	273.5				
274	83.5	274.0				
274.5	83.7	274.5	X			
275	83.8	275.0			X	
275.5	84.0	275.5				
276	84.1	276.0				
276.5	84.3	276.5	X			
277.5	84.6	277.5	X			
278	84.7	278.0				X
278.5	84.9	278.5	X			
279	85.0	279.0			X	X
279.5	85.2	279.5	X			
280	85.3	280.0				
280.5	85.5	280.5	X			
281.5	85.8	281.5	X			
282	86.0	282.0				X
282.5	86.1	282.5	X			
283	86.3	283.0			X	
283.5	86.4	283.5				
284	86.6	284.0				
284.5	86.7	284.5				
285.5	87.0	285.5	X			
286	87.2	286.0				
286.5	87.3	286.5	X			
287	87.5	287.0			X	
287.5	87.6	287.5	X			
288	87.8	288.0				
288.5	87.9	288.5				
289.5	88.2	289.5	X			
290	88.4	290.0				X
290.5	88.5	290.5	X			
291	88.7	291.0			X	X
291.5	88.8	291.5	X			
292	89.0	292.0				
292.5	89.2	292.5	X			
293.5	89.5	293.5	X			
294	89.6	294.0				X
294.5	89.8	294.5	X			
295	89.9	295.0			X	
295.5	90.1	295.5	X			
296	90.2	296.0				X
296.5	90.4	296.5	X			

297.5	90.7	297.5	X				
298	90.8	298.0					
298.5	91.0	298.5	X				
299	91.1	299.0				X	X
299.5	91.3	299.5	X				
300	91.4	300.0					
300.5	91.6	300.5	X				
301.5	91.9	301.5	X				
302	92.0	302.0					
302.5	92.2	302.5	X				
303	92.4	303.0				X	X
303.5	92.5	303.5	X				
304	92.7	304.0					
304.5	92.8	304.5	X				
305.5	93.1	305.5	X				
306	93.3	306.0					
306.5	93.4	306.5	X				
307	93.6	307.0				X	X
307.5	93.7	307.5	X				
308	93.9	308.0					
308.5	94.0	308.5	X				
309.5	94.3	309.5	X				
310	94.5	310.0					
310.5	94.6	310.5	X				
311	94.8	311.0				X	X
311.5	94.9	311.5	X				
312	95.1	312.0					
312.5	95.3	312.5	X				
313.5	95.6	313.5	X				
314	95.7	314.0					
314.5	95.9	314.5	X				
315	96.0	315.0				X	X
315.5	96.2	315.5	X				
316	96.3	316.0					
316.5	96.5	316.5	X				
317.5	96.8	317.5	X				
318	96.9	318.0					
318.5	97.1	318.5	X				
319	97.2	319.0				X	X
319.5	97.4	319.5	X				
320	97.5	320.0					
320.5	97.7	320.5	X				
321.5	98.0	321.5	X				
322	98.1	322.0					

322.5	98.3	322.5	X			
323	98.5	323.0			X	X
323.5	98.6	323.5	X			
324	98.8	324.0				
324.5	98.9	324.5	X			
325.5	99.2	325.5	X			
326	99.4	326.0				
326.5	99.5	326.5	X			
327	99.7	327.0			X	X
327.5	99.8	327.5	X			
328	100.0	328.0				
328.5	100.1	328.5	X			
329.5	100.4	329.5	X			
330	100.6	330.0				
330.5	100.7	330.5	X			
331	100.9	331.0			X	X
331.5	101.0	331.5	X			
332	101.2	332.0				
332.5	101.3	332.5	X			
333.5	101.7	333.5	X			
334	101.8	334.0				
334.5	102.0	334.5	X			
335	102.1	335.0			X	X
335.5	102.3	335.5	X			
336	102.4	336.0				
336.5	102.6	336.5	X			
337.5	102.9	337.5	X			
338	103.0	338.0				
338.5	103.2	338.5	X			
339	103.3	339.0			X	X
339.5	103.5	339.5	X			
340	103.6	340.0				
340.5	103.8	340.5	X			
341.5	104.1	341.5	X			
342	104.2	342.0				
342.5	104.4	342.5	X			
343	104.5	343.0			X	X
343.5	104.7	343.5	X			
344	104.9	344.0				
344.5	105.0	344.5	X			
345.5	105.3	345.5	X			
346	105.5	346.0				
346.5	105.6	346.5	X			
347	105.8	347.0			X	X

347.5	105.9	347.5	X			
348	106.1	348.0				
348.5	106.2	348.5	X			
349.5	106.5	349.5	X			
350	106.7	350.0				
350.5	106.8	350.5	X			
351	107.0	351.0			X	X
351.5	107.1	351.5	X			
352	107.3	352.0				
352.5	107.4	352.5	X			
353.5	107.7	353.5	X			
354	107.9	354.0				
354.5	108.1	354.5	X			
355	108.2	355.0			X	X
355.5	108.4	355.5	X			
356	108.5	356.0				
356.5	108.7	356.5	X			
357.5	109.0	357.5	X			
358	109.1	358.0				
358.5	109.3	358.5	X			
359	109.4	359.0			X	X
359.5	109.6	359.5	X	X		
360	109.7	360.0				
360.5	109.9	360.5	X	X		
361.5	110.2	361.5	X	X		
362	110.3	362.0				
362.5	110.5	362.5	X			
363	110.6	363.0			X	X
363.5	110.8	363.5	X	X		
364	110.9	364.0				
364.5	111.1	364.5	X	X		
365.5	111.4	365.5	X	X		
366	111.6	366.0				
366.5	111.7	366.5	X	X		
367	111.9	367.0			X	X
367.5	112.0	367.5	X	X		
368	112.2	368.0				
368.5	112.3	368.5	X	X		
369.5	112.6	369.5	X			
370	112.8	370.0				
370.5	112.9	370.5	X	X		
371	113.1	371.0			X	X
371.5	113.2	371.5	X	X		
372	113.4	372.0				

372.5	113.5	372.5	X	X		
373.5	113.8	373.5	X	X		
374	114.0	374.0				
374.5	114.1	374.5	X			
375	114.3	375.0			X	X
375.5	114.5	375.5	X			
376	114.6	376.0				
376.5	114.8	376.5	X	X		
377.5	115.1	377.5	X	X		
378	115.2	378.0				
378.5	115.4	378.5	X	X		
379	115.5	379.0			X	X
379.5	115.7	379.5	X			
380	115.8	380.0				
380.5	116.0	380.5	X	X		
381.5	116.3	381.5	X	X		
382	116.4	382.0				
382.5	116.6	382.5	X	X		
383	116.7	383.0			X	X
383.5	116.9	383.5		X		
384	117.0	384.0				
384.5	117.2	384.5	X	X		
385.5	117.5	385.5	X	X		
386	117.7	386.0				
386.5	117.8	386.5	X	X		
387	118.0	387.0			X	X
387.5	118.1	387.5	X	X		
388	118.3	388.0				
388.5	118.4	388.5	X	X		
389.5	118.7	389.5	X			
390	118.9	390.0				
390.5	119.0	390.5	X	X		
391	119.2	391.0			X	X
391.5	119.3	391.5	X	X		
392	119.5	392.0				
392.5	119.6	392.5	X			
393.5	119.9	393.5	X	X		
394	120.1	394.0				
394.5	120.2	394.5	X	X		
395	120.4	395.0			X	X
395.5	120.5	395.5		X		
396	120.7	396.0				
396.5	120.9	396.5	X	X		
397.5	121.2	397.5	X	X		

398	121.3	398.0				
398.5	121.5	398.5	X			
399	121.6	399.0			X	X
399.5	121.8	399.5	X	X		
400	121.9	400.0	X	X		
400.5	122.1	400.5		X		
401	122.2	401.0	X			
402	122.5	402.0	X			
402.5	122.7	402.5		X		
403	122.8	403.0	X	X	X	X
403.5	123.0	403.5		X		
404	123.1	404.0	X	X		
404.5	123.3	404.5		X		
405	123.4	405.0	X	X		
405.5	123.6	405.5		X		
406	123.7	406.0	X			
406.5	123.9	406.5		X		
407	124.1	407.0	X		X	X
407.5	124.2	407.5		X		
408	124.4	408.0	X	X		
408.5	124.5	408.5		X		
409	124.7	409.0	X			
409.5	124.8	409.5		X		
410	125.0	410.0	X			
410.5	125.1	410.5		X		
411	125.3	411.0	X		X	X
411.5	125.4	411.5		X		
412	125.6	412.0	X			
412.5	125.7	412.5		X		
413	125.9	413.0	X	X		
413.5	126.0	413.5		X		
414	126.2	414.0	X	X		
414.5	126.3	414.5		X		
415	126.5	415.0	X	X	X	X
415.5	126.6	415.5		X		
416	126.8	416.0	X			
416.5	126.9	416.5		X		
416.5	126.9	416.5		X		
417	127.1	417.0	X	X		
417.5	127.3	417.5		X		
418	127.4	418.0	X	X		
418.5	127.6	418.5		X		
419	127.7	419.0	X		X	X
419.5	127.9	419.5		X		

420	128.0	420.0	X	X		
420.5	128.2	420.5		X		
421	128.3	421.0	X			
421.5	128.5	421.5		X		
422	128.6	422.0	X			
422.5	128.8	422.5		X		
423	128.9	423.0	X	X	X	X
423.5	129.1	423.5		X		
424	129.2	424.0	X	X		
424.5	129.4	424.5		X		
425	129.5	425.0	X			
425.5	129.7	425.5		X		
426	129.8	426.0	X	X		
426.5	130.0	426.5		X		
427	130.1	427.0	X	X	X	X
427.5	130.3	427.5		X		
428	130.5	428.0	X			
428.5	130.6	428.5		X		
429	130.8	429.0	X	X		
429.5	130.9	429.5		X		
430	131.1	430.0	X			
430.5	131.2	430.5		X		
431	131.4	431.0	X		X	X
431.5	131.5	431.5		X		
432	131.7	432.0	X			
432.5	131.8	432.5		X		
433	132.0	433.0	X	X		
433.5	132.1	433.5		X		
434	132.3	434.0	X			
434.5	132.4	434.5		X		
435	132.6	435.0	X		X	X
435.5	132.7	435.5		X		
436	132.9	436.0	X			
436.5	133.0	436.5		X		
437	133.2	437.0	X			
437.5	133.4	437.5		X		
438	133.5	438.0	X	X		
438.5	133.7	438.5		X		
439	133.8	439.0	X	X	X	X
439.5	134.0	439.5		X		
440	134.1	440.0	X			
440.5	134.3	440.5		X		
441	134.4	441.0	X	X		
441.5	134.6	441.5		X		

442	134.7	442.0	X			
442.5	134.9	442.5		X		
443	135.0	443.0	X	X	X	X
443.5	135.2	443.5		X		
444	135.3	444.0	X	X		
444.5	135.5	444.5		X		
445	135.6	445.0	X	X		
445.5	135.8	445.5		X		
446	135.9	446.0	X			
446.5	136.1	446.5		X		
447	136.2	447.0	X		X	X
447.5	136.4	447.5		X		
448	136.6	448.0	X	X		
448.5	136.7	448.5		X		
449	136.9	449.0	X			
449.5	137.0	449.5		X		
450	137.2	450.0	X	X		
450.5	137.3	450.5		X		
451	137.5	451.0	X	X	X	X
451.5	137.6	451.5		X		
452	137.8	452.0	X			
452.5	137.9	452.5		X		
453	138.1	453.0	X			
453.5	138.2	453.5		X		
454	138.4	454.0	X			
454.5	138.5	454.5		X		
455	138.7	455.0	X	X	X	X
455.5	138.8	455.5		X		
456	139.0	456.0	X			
456.5	139.1	456.5		X		
457	139.3	457.0	X	X		
457.5	139.4	457.5		X		
458	139.6	458.0	X	X		
458.5	139.8	458.5		X		
459	139.9	459.0	X	X	X	X
459.5	140.1	459.5		X		
460	140.2	460.0	X	X		
460.5	140.4	460.5		X		
461	140.5	461.0	X			
461.5	140.7	461.5		X		
462	140.8	462.0	X			
462.5	141.0	462.5		X		
463	141.1	463.0	X	X	X	X
463.5	141.3	463.5		X		

464	141.4	464.0	X			
464.5	141.6	464.5		X		
465	141.7	465.0	X			
465.5	141.9	465.5		X		
466	142.0	466.0	X	X		
466.5	142.2	466.5		X		
467	142.3	467.0	X	X	X	X
467.5	142.5	467.5		X		
468	142.6	468.0	X			
468.5	142.8	468.5		X		
469	143.0	469.0	X			
469.5	143.1	469.5		X		
470	143.3	470.0	X			
470.5	143.4	470.5		X		
471	143.6	471.0	X		X	X
471.5	143.7	471.5		X		
472	143.9	472.0	X			
472.5	144.0	472.5		X		
473	144.2	473.0	X			
473.5	144.3	473.5		X		
474	144.5	474.0	X			
474.5	144.6	474.5		X		
475	144.8	475.0	X		X	X
475.5	144.9	475.5		X		
476	145.1	476.0	X			
476.5	145.2	476.5		X		
477	145.4	477.0	X			
477.5	145.5	477.5		X		
478	145.7	478.0	X			
478.5	145.8	478.5		X		
479	146.0	479.0	X		X	X
479.5	146.2	479.5		X		
480	146.3	480.0	X	X		
480.5	146.5	480.5		X		
481	146.6	481.0	X			
481.5	146.8	481.5		X		
482	146.9	482.0	X	X		
482.5	147.1	482.5		X		
483	147.2	483.0	X	X	X	X
483.5	147.4	483.5		X		
484	147.5	484.0	X			
484.5	147.7	484.5		X		
485	147.8	485.0	X			
485.5	148.0	485.5		X		

486	148.1	486.0	X			
486.5	148.3	486.5		X		
487	148.4	487.0	X		X	X
487.5	148.6	487.5		X		
488	148.7	488.0	X	X		
488.5	148.9	488.5		X		
489	149.0	489.0	X			
489.5	149.2	489.5		X		
490	149.4	490.0	X			
490.5	149.5	490.5		X		
491	149.7	491.0	X	X	X	X
491.5	149.8	491.5		X		
492	150.0	492.0	X			
492.5	150.1	492.5		X		
493	150.3	493.0	X	X		
493.5	150.4	493.5		X		
494	150.6	494.0	X			
494.5	150.7	494.5		X		
495	150.9	495.0	X	X	X	X
496	151.2	496.0	X			
496.5	151.3	496.5		X		
497	151.5	497.0	X			
497.5	151.6	497.5		X		
498	151.8	498.0	X			
499	152.1	499.0	X		X	X
519	158.2	519.0				X

Appendix 2 – List of Taxa

Dinocysts dominante the palynological assemblages in the studied material. In total, we identified 52 genera and 70 species. The nomenclature cited in this work followed Williams, Fensome and Macrae (2017), where all the bibliographical references mentioned in this section can be consulted. For convenience, these taxa are listed in alphabetical.

Achomosphaera alcicornu (Eisenack 1954) Roger Jack Davey and Williams 1966 (Plate 1, fig. 1)

Achomosphaera ramulifera (Deflandre 1937) Evitt 1963 (Plate 7, fig. 1)

Araneosphaera araneosa Eaton 1976 (Plate 1, fig. 2)

Areoligera sentosa Eaton 1976 (Plate 1, figs. 3, 4)

Areosphaeridium diktyoplokum (Klumpp 1953) Eaton 1971 emend. Stover and Williams 1995 (Plate 1, figs. 5, 6)

Cannosphaeropsis spp. Wetzel 1933 emend. Marheinecke 1992 (Plate 7, fig. 2)

Charlesdowniea coleothrypta (Williams and Downie 1966b) Lentin and Vozzhennikova 1989 (Plate 1, fig. 7)

Chatangiella spp. Vozzhennikova 1967 emend. Marshall 1988 (Plate 7, figs. 3, 4)

Cleistosphaeridium ancyreum (Cookson and Eisenack 1965) Eaton et al. 2001 (Plate 1, figs. 8, 9)

Cleistosphaeridium polypetellum (Islam 1983c) Stover and Williams 1995 (Plate 1, fig. 10)

Cordosphaeridium cantharellus (Brosius 1963) Gocht 1969 (Plate 1, fig. 11)

Cordosphaeridium fibrospinosum R J Davey and Williams 1966 emend. Davey 1969 (Plate 1, figs. 12, 13)

Cordosphaeridium inodes (Klumpp 1953) Eisenack 1963 emend. Sarjeant 1981 (Plate 1, figs. 14, 15)

Corrudinium incompositum (Drugg 1970) Stover and Evitt 1978 (Plate 1, figs. 16-19)

Cribroperidinium tenuitabulatum (Gerlach 1961) Helenes 1984 (Plate 1, fig. 20)

Cymososphaeridium? *phoenix* (Duxbury 1980) Fauconnier et al. 2004 (Plate 7, fig. 5)

Dapsilidinium pastielsii (R J Davey and Williams 1966) Bujak et al. 1980 (Plate 2, fig. 1)

Deflandrea heterophlycta Deflandre and Cookson 1955 (Plate 2, fig. 2)

Deflandrea phosphoritica Eisenack 1938 (Plate 2, figs. 3, 4)

Dinogymnium sibiricum (Vozzhennikova 1967) Lentin and Williams 1973 emend. Lentin and Vozzhennikova 1990 (Plate 7, fig. 6)

Dinopterygium cladoides Deflandre 1935 (Plate 2, figs. 5, 6)

Diphyes colligerum (Deflandre and Cookson 1955) Cookson 1965 emend. Goodman and Witmer 1985 (Plate 2, fig. 7)

Diphyes ficusoides Islam 1983 (Plate 2, figs. 8, 9)

Distatodinium biffii Brinkhuis et al. 1992 (Plate 2, figs. 10, 11)

Distatodinium ellipticum (Cookson 1965) Eaton 1976 (Plate 2, fig. 12)

Distatodinium paradoxum (Brosius 1963) Eaton 1976 (Plate 2, fig. 13)

Echinidinium spp. Zonneveld 1997 ex Head et al. 2001 (Plate 2, fig. 14)

Enneadocysta arcuata (Eaton 1971) Stover and Williams 1995 emend. Stover and Williams 1995 (Plate 2, figs. 15, 16)

Enneadocysta deconinckii Stover and Williams 1995 (Plate 2, fig. 17)

Glaphyrocysta laciniiformis (Gerlach 1961) Stover and Evitt 1978 (Plate 2, figs. 18, 19)

Glaphyrocysta retiintexta (Cookson 1965) Stover and Evitt 1978 (Plate 2, fig. 20)

Glaphyrocysta semitecta (Bujak et al. 1980) Lentin and Williams 1981 (Plate 3, figs. 1-4)

Hemiplacophora semilunifera Cookson and Eisenack 1965 (Plate 3, fig. 5)

Heteraulacacysta leptalea Eaton 1976 (Plate 3, fig. 6)

Heteraulacacysta porosa Bujak et al. 1980 (Plate 3, fig. 7)

Homotryblium abbreviatum Eaton 1976 (Plate 3, figs. 8, 9)

Homotryblium floripes (Deflandre and Cookson 1955) Stover 1975 (Plate 3, figs. 10-12)

Homotryblium oceanicum Eaton 1976 (Plate 3, fig. 13)

Horologinella pentagonalis Heilmann-Clausen and Van Simaeys 2005 (Plate 3, fig. 14)

Hystrichokolpoma granulatum Eaton 1976 (Plate 3, fig. 15)

"*Hystrichokolpoma pseudooceanicum*" Zevenboom 1995 (Plate 3, fig. 16)

Hystrichokolpoma rigaudiae Deflandre and Cookson 1955 (Plate 3, fig. 17)

Hystrichokolpoma salacia Eaton 1976 (Plate 3, fig. 18,19)

Hystrichosphaeridium tubiferum (Ehrenberg 1837) Deflandre 1937 emend. R J Davey and Williams 1966 (Plate 3, fig. 20)

Impagidinium paradoxum (Wall 1967) Stover and Evitt 1978 (Plate 4, figs. 1, 2)

Lejeunecysta spp. Artzner and Dörhöfer 1978 emend. Bujak et al. 1980 (Plate 4, fig. 3)

Lentinia serrata Bujak et al. 1980 (Plate 4, figs. 4, 5)

Lingulodinium "brevispinosum" Matsuoka and Bujak 1988 (Plate 4, figs. 6, 7)

Lingulodinium machaerophorum (Deflandre and Cookson 1955) Wall 1967 (Plate 4, figs. 8, 9)

Litosphaeridium siphoniphorum (Cookson and Eisenack 1960) R J Davey and Williams 1966 emend. Lucas-Clark 1984 (Plate 7, fig. 7)

Melitasphaeridium pseudorecurvatum (Morgenroth 1966a) Bujak et al. 1980 (Plate 4, fig. 10)

Minisphaeridium latirictum (Morgenroth 1966a) Fensome et al. 2009 (Plate 4, fig. 11)

Nematosphaeropsis spp. Deflandre and Cookson 1955 emend. Wrenn 1988 (Plate 4, figs. 12, 13)

Operculodinium centrocarpum (Deflandre and Cookson 1955) Wall 1967 (Plate 4, fig. 14)

Operculodinium microtriainum (Klumpp 1953) Islam 1983b (Plate 4, figs. 15, 16)

Palaeohystrichophora infusorioides Deflandre 1935 (Plate 7, fig. 8)

Phthanoperidinium comatum (Morgenroth 1966b) Eisenack and Kjellström 1972 (Plate 4, fig. 17)

Phthanoperidinium distinctum Bujak 1994 (Plate 4, fig. 18)

Piladinium columna (Michoux 1988) Williams et al. 2015 (Plate 4, fig. 19)

Rhombodinium spinula (Bujak 1979) Williams et al. 2015 (Plate 5, fig. 1)

Rhombodinium spp. Gocht 1955 emend. Fensome et al. 2009 (endocyst: Plate 4, fig. 20)

Rottnestia borrusica (Eisenack 1954) Cookson and Eisenack 1961 (Plate 5, fig. 2)

Saturnodinium pansum (Stover 1977) Brinkhuis et al. 1992 (Plate 5, figs. 3, 4)

Senegalinium spp. Jain and Millepied 1973 emend. Stover and Evitt 1978 (Plate 5, fig. 5)

Sophismatia tenuivirgula (Williams and Downie 1966b) Williams et al. 2015 (Plate 5, fig. 6)

Spiniferites bentorii (Rossignol 1964) Wall and Dale 1970 (Plate 5, fig. 7)

Spiniferites mirabilis (Rossignol 1964) Sarjeant 1970 (Plate 5, fig. 8)

Spiniferites pseudofurcatus (Klumpp 1953) Sarjeant 1970 emend. Sarjeant 1981 (Plate 5, figs. 9, 10)

Spiniferites ramosus group (Ehrenberg 1837) Mantell 1854 (Plate 5, fig. 11)

Svalbardella partimtabulata Heilmann-Clausen and Van Simaeys 2005 (Plate 6, figs. 1, 2)

Tectatodinium pellitum Wall 1967 emend. Head 1994 (Plate 5, fig. 12)

Thalassiphora fenestrata Liengjarern et al. 1980 (Plate 6, fig. 3)

Thalassiphora pelagica (Eisenack 1954) Eisenack and Gocht 1960 emend. Benedek and Gocht 1981 (Plate 6, figs. 4, 5)

Thalassiphora spinifera (Cookson and Eisenack 1965) Stover and Evitt 1978 (Plate 5, figs. 13, 14)

Turnhosphaera hypoflata (Yun 1981) Slimani 1994 (Plate 5, fig. 15)

Wetzeliella articulata Eisenack 1938 (Plate 5, fig. 16)

Appendix 3 – List of Plates and Photos

Plate 1. Illustration of taxa, sample/slide number. **1.** *Achomosphaera alcicornu* (MG55). **2.** *Araneosphaera araneosa* (MG479). **3, 4.** *Areoligera sentosa* (MG423). **5, 6.** *Areosphaeridium diktyoplokum* (MG243). **7.** *Charlesdowniea coleothrypta* (MG271). **8, 9.** *Cleistosphaeridium ancyreum* (MG55). **10.** *Cleistosphaeridium polypetellum* (MG499). **11.** *Cordosphaeridium cantharellus* (MG215). **12, 13.** *Cordosphaeridium fibrospinosum* (MG383, MG371). **14, 15.** *Cordosphaeridium inodes* (MG347). **16-19.** *Corrudinium incompositum* (MG59). **20.** *Cribroperidinium tenuitabulatum* (MG363).

Plate 2. Illustration of taxa, sample/slide number. **1.** *Dapsilidinium pastielsii* (MG391). **2.** *Deflandrea heterophlycta* (MG111). **3, 4.** *Deflandrea phosphoritica* (MG111). **5, 6.** *Dinopterygium cladoides* (MG187). **7.** *Diphyes colligerum* (MG259). **8, 9.** *Diphyes ficusoides* (MG231). **10, 11.** *Distatodinium biffii* (MG71, MG471). **12.** *Distatodinium ellipticum* (MG59). **13.** *Distatodinium paradoxum* (MG103). **14.** *Echidinium sp*. (MG59). **15, 16.** *Enneadocysta arcuata* (MG263). **17.** *Enneadocysta deconinckii* (MG127). **18, 19.** *Glaphyrocysta laciniiformis* (MG371). **20.** *Glaphyrocysta retiintexta* (MG427).

Plate 3. Illustration of taxa, sample/slide number. **1-4.** *Glaphyrocysta semitecta* (MG331). **5.** *Hemiplacophora semilunifera* (MG471). **6.** *Heteraulacacysta leptalea* (MG487). **7.** *Heteraulacacysta porosa* (MG111). **8, 9.** *Homotryblium abbreviatum* (MG319). **10-12.** *Homotryblium floripes* (MG55). **13.** *Homotryblium oceanicum* (MG59). **14.** *Horologinella pentagonalis* (MG319). **15.** *Hystrichokolpoma granulatum* (MG63). **16. "***Hystrichokolpoma pseudooceanicum"* (MG455). **17.** *Hystrichokolpoma rigaudiae* (MG59). **18, 19.** *Hystrichokolpoma salacia* (MG299, MG307). **20.** *Hystrichosphaeridium tubiferum* (MG299).

Plate 4. Illustration of taxa, sample/slide number. **1, 2.** *Impagidinium paradoxum* (MG459). **3.** *Lejeunecysta sp*. (MG411). **4, 5.** *Lentinia serrata* (MG59). **6, 7.** *Lingulodinium "brevispinosum"* (MG299, MG259). **8, 9.** *Lingulodinium machaerophorum* (MG215, MG311). **10.** *Melitasphaeridium pseudorecurvatum* (MG199.5). **11.** *Minisphaeridium latirictum* (MG275). **12, 13.** *Nematosphaeropsis sp*. (MG451). **14.** *Operculodinium centrocarpum* (MG459). **15, 16.** *Operculodinium microtriainum* (MG451). **17.** *Phthanoperidinium comatum* (MG323). **18.** *Phthanoperidinium distinctum* (MG95). **19.** *Piladinium columna* (MG55). **20.** *Rhombodinium sp. endocyst* (MG55).

Plate 5. Illustration of taxa, sample/slide number. **1.** *Rhombodinium spinula* (MG447). **2.** *Rottnestia borussica* (MG459). **3, 4.** *Saturnodinium pansum* (MG311, MG411). **5.** *Senegalinium sp*. (MG55). **6.** *Sophismatia tenuivirgula* (MG55). **7.** *Spiniferites bentorii* (MG55). **8.** *Spiniferites mirabilis* (MG259). **9, 10.** *Spiniferites pseudofurcatus* (MG459). **11.** *Spiniferites ramosus* group (MG59). **12.** *Tectatodinium pellitum* (MG59). **13, 14.** *Thalassiphora spinifera* (MG463, MG363). **15.** *Turnhosphaera hypoflata* (MG343). **16.** *Wetzeliella articulata* (MG319).

Plate 6. Illustration of taxa, sample/slide number. **1, 2.** *Svalbardella partimtabulata* (MG419). **3.** *Thalassiphora fenestrata* (MG175). **4, 5.** *Thalassiphora pelagica* (MG499).

Plate 7. Illustration of reworked taxa, sample/slide number. **1.** *Achomosphaera ramulifera* (MG363). **2.** *Cannosphaeropsis sp*. (MG 167). **3, 4.** *Chatangiella sp*. (MG283, MG271). **5.** *Cymososphaeridium? phoenix* (MG167). **6.** *Dinogymnium sibiricum* (MG371). **7.** *Litosphaeridium siphoniphorum* (MG363). **8.** *Palaeohystrichophora infusorioides* (MG275).

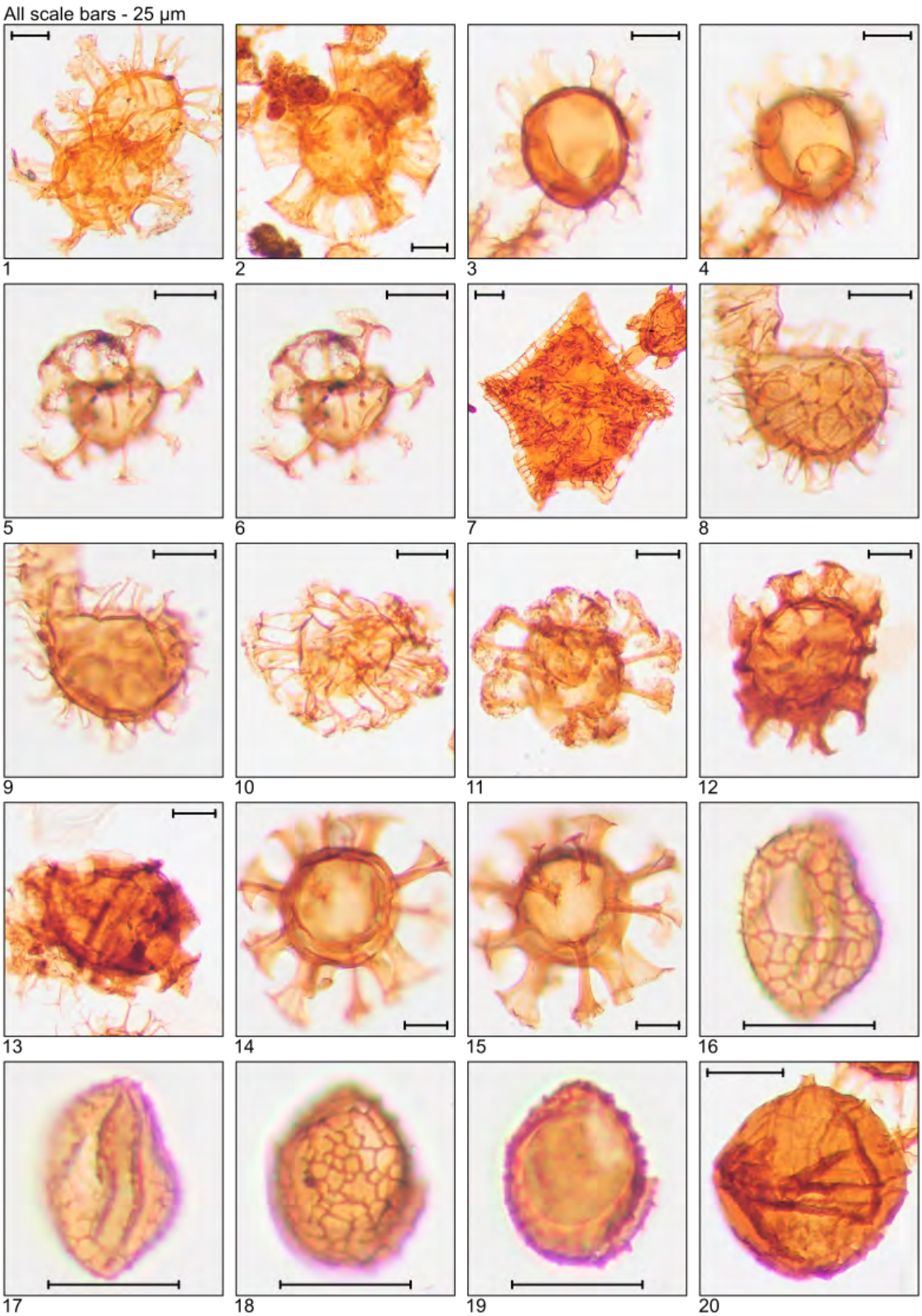


Plate 1

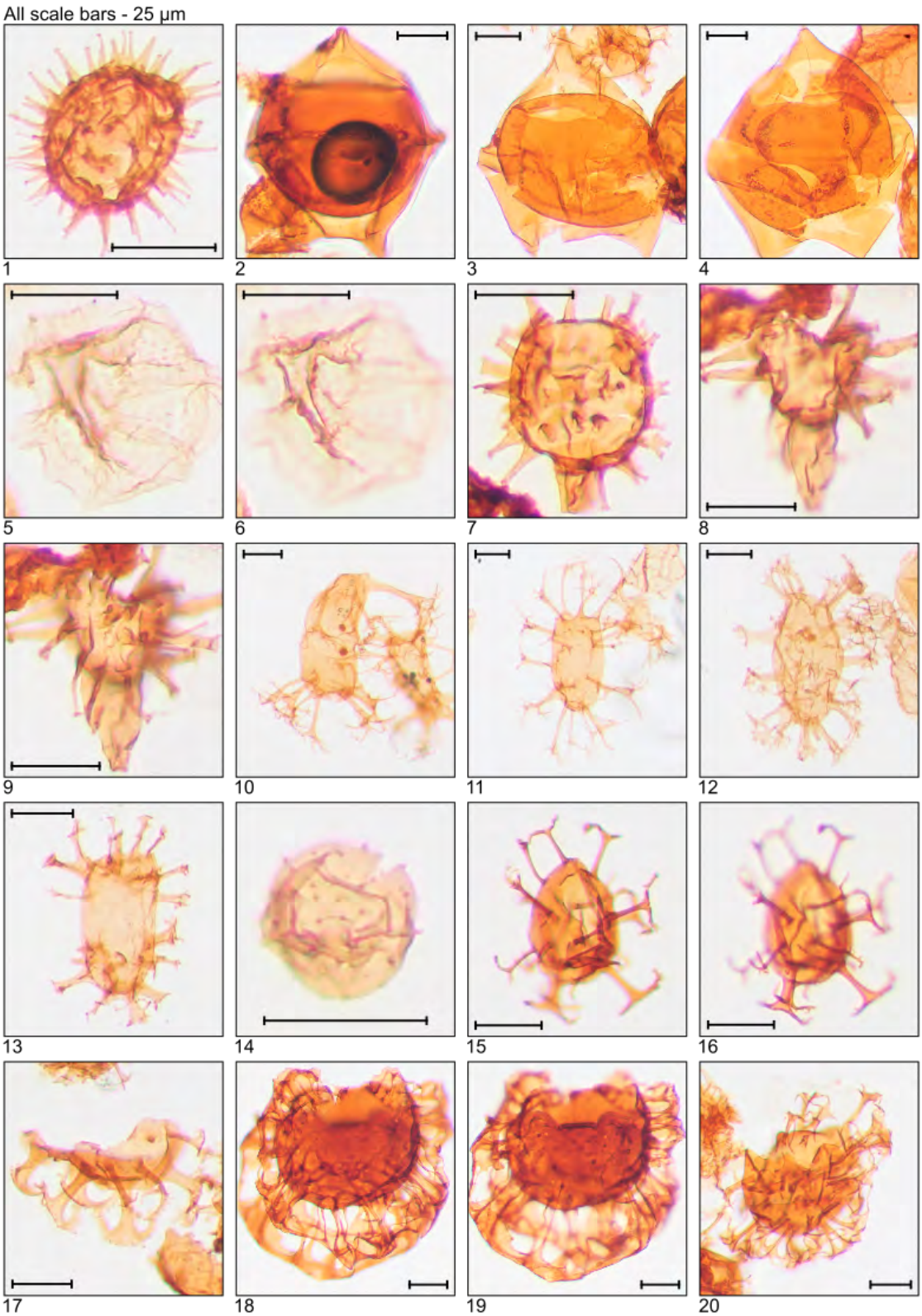


Plate 2

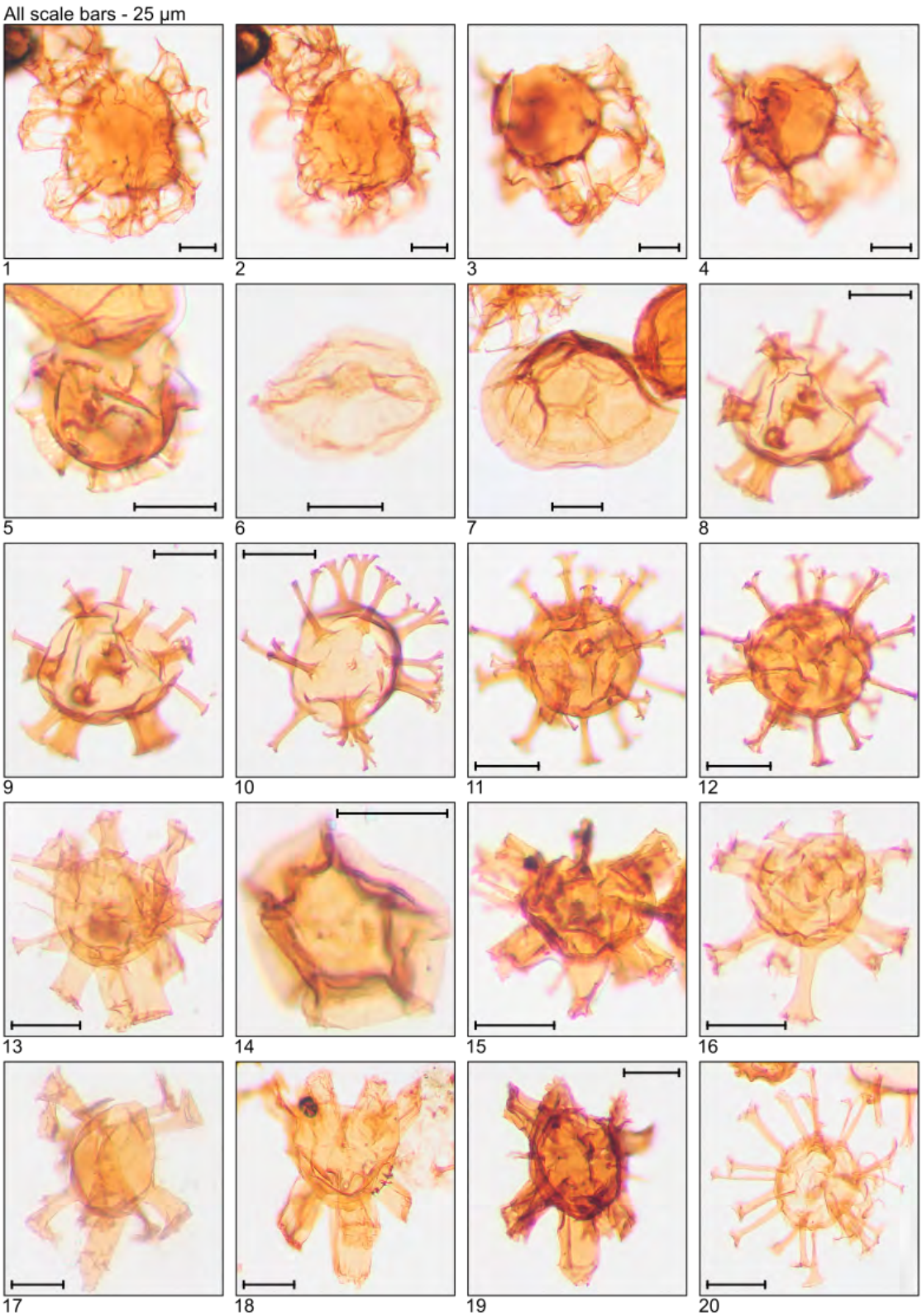


Plate 3

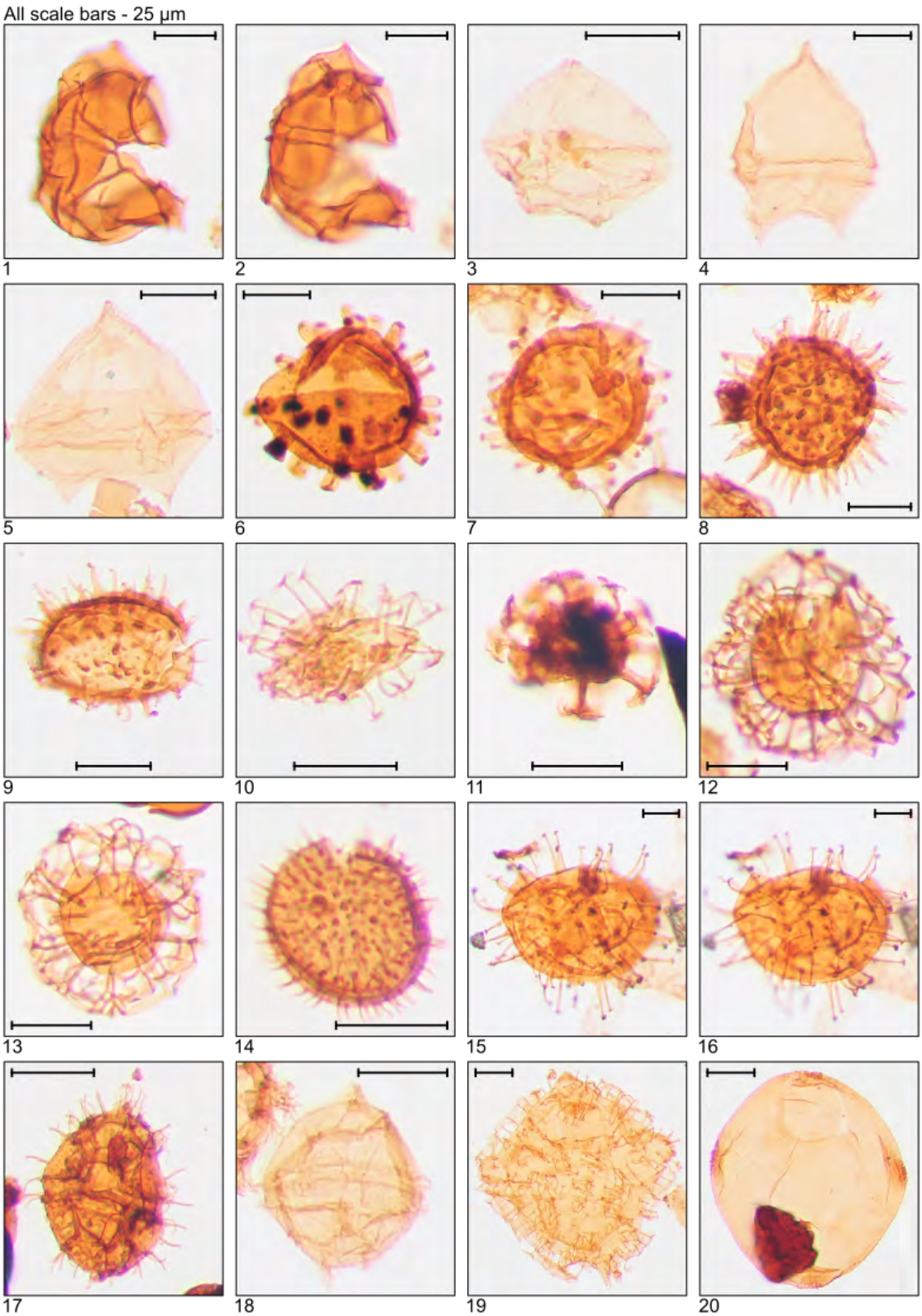


Plate 4

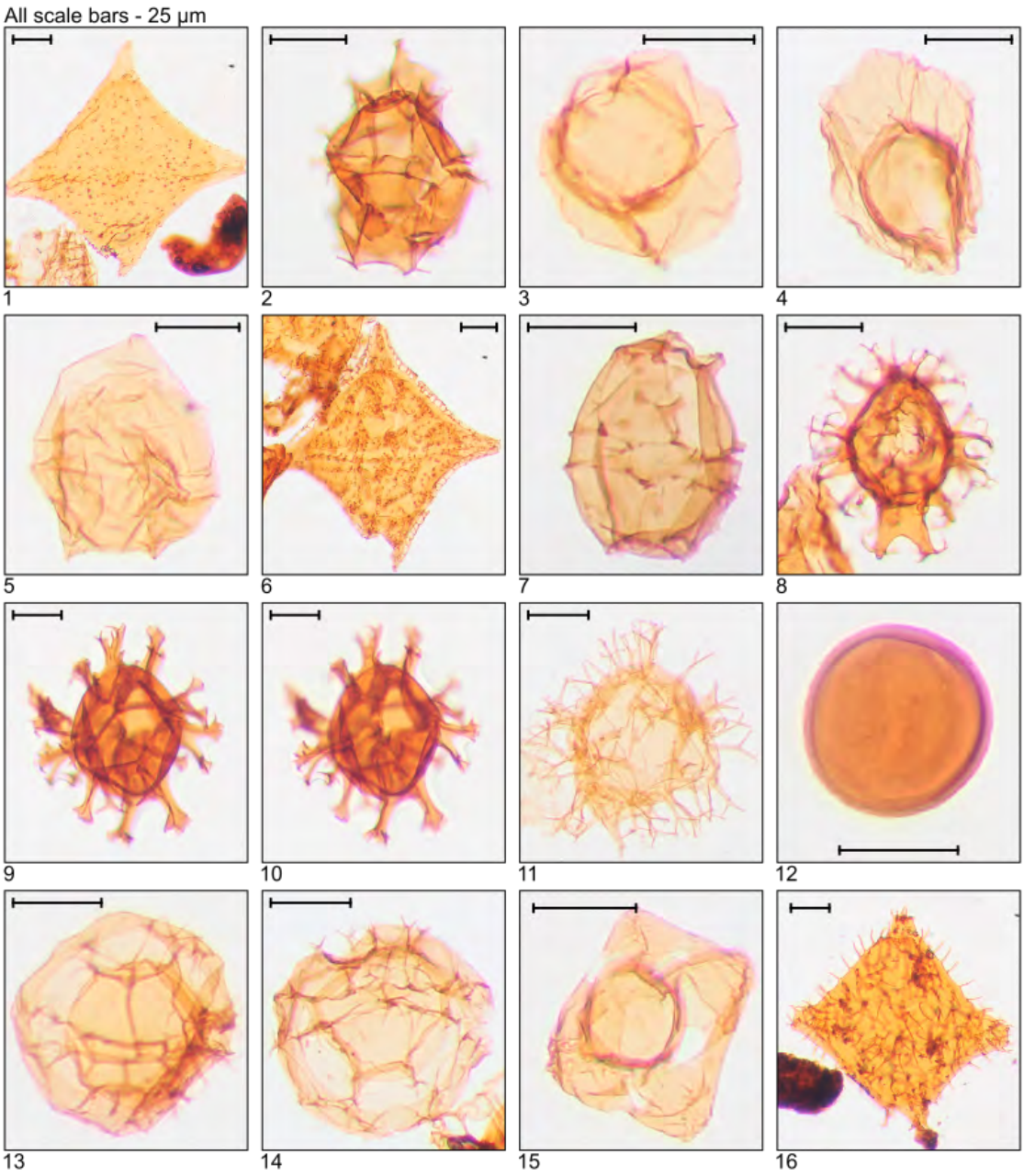


Plate 5

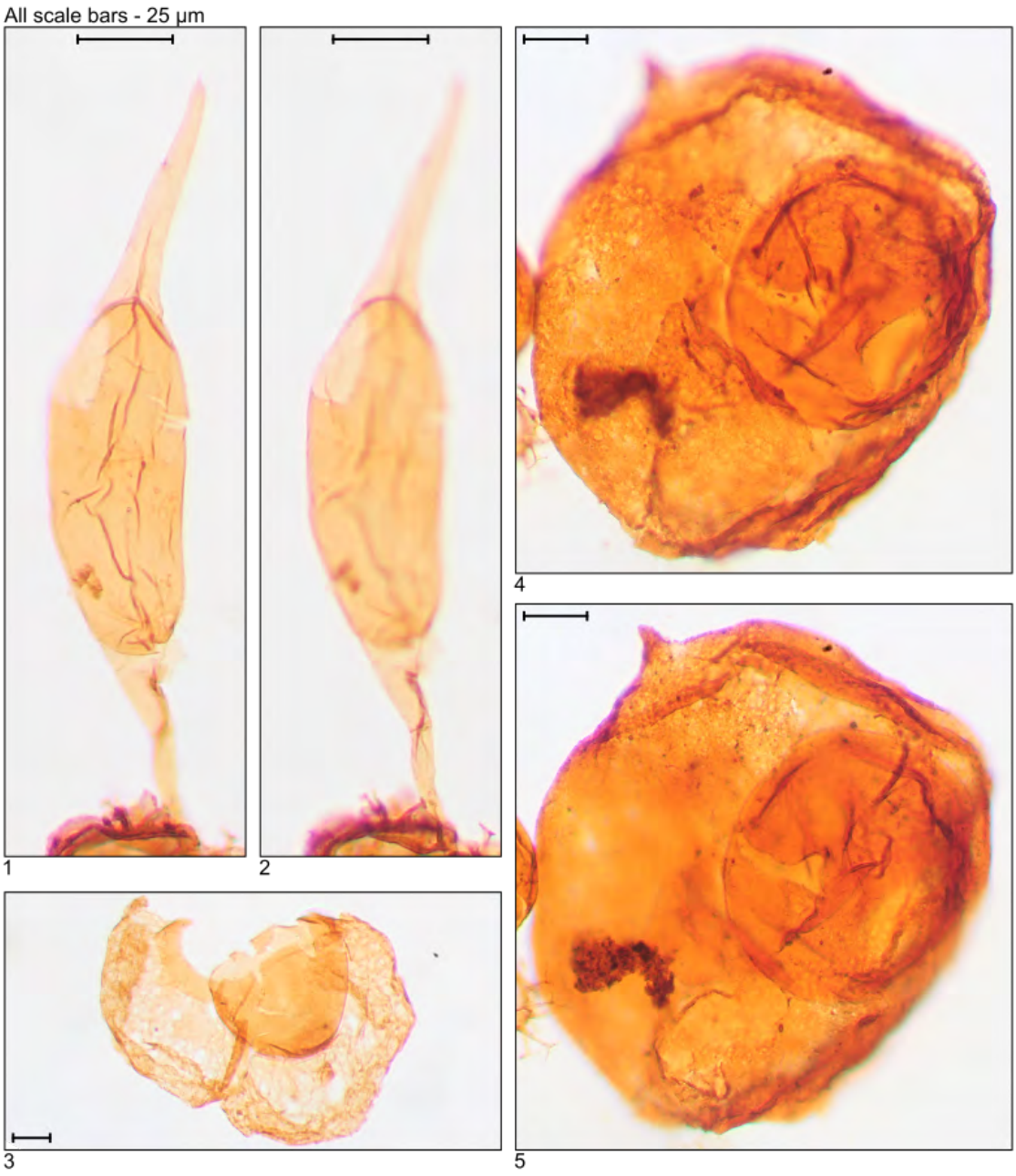


Plate 6

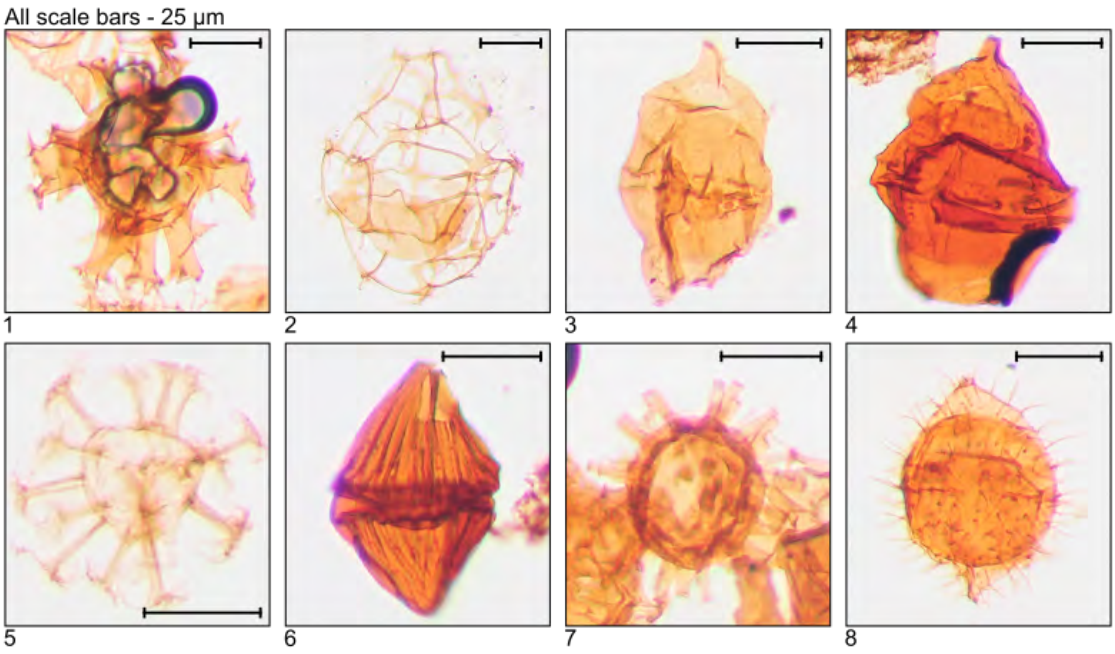


Plate 7

LIST OF REFERENCES

Adams, C. G., Butterlin, J. and Samanta, B. K.: Larger foraminifera and events at the Eocene/Oligocene boundary in the Indo-West Pacific region, in Developments in Palaeontology and Stratigraphy, vol. 9, pp. 237–252, Elsevier., 1986.

Agnini, C., Fornaciari, E., Raffi, I., Catanzariti, R., Pälike, H., Backman, J. and Rio, D.: Biozonation and biochronology of Paleogene calcareous nannofossils from low and middle latitudes, Newsletters on Stratigraphy, 47(2), 131–181, doi:10.1127/0078-0421/2014/0042, 2014.

Anagnostou, E., John, E. H., Edgar, K. M., Foster, G. L., Ridgwell, A., Inglis, G. N., Pancost, R. D., Lunt, D. J. and Pearson, P. N.: Changing atmospheric CO2 concentration was the primary driver of early Cenozoic climate, Nature, 533(7603), 380–384, doi:10.1038/nature17423, 2016.

van Andel, T. H. and Moore Jr, T. C.: Cenozoic calcium carbonate distribution and calcite compensation depth in the central equatorial Pacific Ocean, Geology, 2(2), 87–92, 1974.

Anderson, D. M., Aubrey, D. G., Tyler, M. A. and Coats, D. W.: Vertical and horizontal distributions of dinoflagellate cysts in sediments, Limnology and Oceanography, 27(4), 757–765, doi:10.4319/lo.1982.27.4.0757, 1982.

Anderson, L. D. and Delaney, M. L.: Use of multiproxy records on the Agulhas Ridge, Southern Ocean (Ocean Drilling Project Leg 177, Site 1090) to investigate sub-Antarctic hydrography from the Oligocene to the early Miocene, Paleoceanography, 20(3), 1–16, doi:10.1029/2004PA001082, 2005.

Artemieva, N. and Morgan, J.: Quantifying the Release of Climate-Active Gases by Large Meteorite Impacts With a Case Study of Chicxulub, Geophysical Research Letters, 44(20), 10,180-10,188, doi:10.1002/2017GL074879, 2017.

Aubry, M.-P.: Biostratigraphie du Paléogène épicontinental de l'Europe du Nord-Ouest:

Étude fondée sur les nannofossiles calcaires, Université Claude Bernard-Lyon I, Département des sciences de la terre., 1983.

Aubry, M.-P.: Northwestern European Paleogene magnetostratigraphy, biostratigraphy, and paleogeography: Calcareous nannofossil evidence, Geology, 13(3), 198–202, 1985.

Aubry, M.-P.: Late Paleogene calcareous nannoplankton evolution: a tale of climatic deterioration, Unknown Journal, 272–309, 1992.

Balch, W. M., Reid, P. C. and Surrey-Gent, S. C.: Spatial and Temporal Variability of Dinoflagellate Cyst Abundance in a Tidal Estuary, Canadian Journal of Fisheries and Aquatic Sciences, 40(Supplement 1), 244–261, doi:10.1139/f83-287, 1983.

Barker, P. F., Barrett, P. J., Cooper, A. . and Huybrechts, P.: Antarctic glacial history from numerical models and continental margin sediments, , 150, 247–267, 1999.

Barker, P. F., Filippelli, G. M., Florindo, F., Martin, E. E. and Scher, H. D.: Onset and role of the Antarctic Circumpolar Current, Deep-Sea Research Part II: Topical Studies in Oceanography, 54(21–22), 2388–2398, doi:10.1016/j.dsr2.2007.07.028, 2007.

Barrett, P. J.: Antarctic Palaeoenvironment through Cenozoic Times - A Review, Terra Antarctica, 3(2), 103–119, 1996.

Baum, G. R. and Vail, P. R.: Sequence stratigraphic concepts applied to Paleogene outcrops, Gulf and Atlantic basins, 1988.

Berggren, W. A. and Pearson, P. N.: A Revised Tropical To Subtropical Paleogene Planktonic Foraminiferal Zonation, The Journal of Foraminiferal Research, 35(4), 279–298, doi:10.2113/35.4.279, 2005.

Berggren, W. A., Kent, D. V., Swisher, C. C. and Aubry, M.-P.: A Revised Cenozoic Geochronology and Chronostratigraphy., 1995.

Bijl, P. K., Bendle, J. A. P., Bohaty, S. M., Pross, J., Schouten, S., Tauxe, L., Stickley, C. E., McKay, R. M., Rohl, U., Olney, M., Sluijs, A., Escutia, C., Brinkhuis, H., Klaus, A., Fehr,

A., Williams, T., Carr, S. A., Dunbar, R. B., Gonzalez, J. J., Hayden, T. G., Iwai, M., Jimenez-Espejo, F. J., Katsuki, K., Kong, G. S., Nakai, M., Passchier, S., Pekar, S. F., Riesselman, C., Sakai, T., Shrivastava, P. K., Sugisaki, S., Tuo, S., van de Flierdt, T., Welsh, K. and Yamane, M.: Eocene cooling linked to early flow across the Tasmanian Gateway, Proceedings of the National Academy of Sciences, 110(24), 9645–9650, doi:10.1073/pnas.1220872110, 2013.

Bijl, P. K., Houben, A. J. P., Bruls, A., Pross, J. and Sangiorgi, F.: Stratigraphic calibration of Oligocene-Miocene organic-walled dinoflagellate cysts from offshore Wilkes Land, East Antarctica, and a zonation proposal, Journal of Micropalaeontology, 37(1), 105–138, doi:10.5194/jm-37-105-2018, 2018.

Blum, M. D. and Roberts, H. H.: The Mississippi Delta Region: Past, Present, and Future, Annual Review of Earth and Planetary Sciences, 40(1), 655–683, doi:10.1146/annurev-earth-042711-105248, 2012.

Bohaty, S. M. and Zachos, J. C.: Significant Southern Ocean warming event in the late middle Eocene, Geology, 31(11), 1017–1020, doi:10.1130/G19800.1, 2003.

Bohaty, S. M., Zachos, J. C. and Delaney, M. L.: Foraminiferal Mg/Ca evidence for Southern Ocean cooling across the Eocene-Oligocene transition, Earth and Planetary Science Letters, 317–318, 251–261, doi:10.1016/j.epsl.2011.11.037, 2012.

Bordiga, M., Henderiks, J., Tori, F., Monechi, S., Fenero, R., Legarda-Lisarri, A. and Thomas, E.: Microfossil evidence for trophic changes during the Eocene-Oligocene transition in the South Atlantic (ODP Site 1263, Walvis Ridge), Climate of the Past, 11(9), 1249–1270, doi:10.5194/cp-11-1249-2015, 2015a.

Bordiga, M., Henderiks, J., Tori, F., Monechi, S., Fenero, R. and Thomas, E.: The Eocene–Oligocene transition at ODP Site 1263, Atlantic Ocean: decreases in nannoplankton size and abundance and correlation with benthic foraminiferal assemblages, Climate of the Past

Discussions, 11(3), 1615–1664, doi:10.5194/cpd-11-1615-2015, 2015b.

Bottomley, R., Grieve, R., York, D. and Masaltis, V.: The age of the Popigai impact event and its relation to events at the Eocene/Oligocene boundary, Nature, 388(6640), 365–368, doi:10.1038/41073, 1997.

Bown, P. R. and Young, J. .: Techniques, in Calcareous Nannofossil Biostratigraphy, edited by P. R. Bown, pp. 16–28, British Micropalaeontological Society Publications Series. Kluwer Academic, London., 1998.

Bown, P. R., Lees, J. A. and Young, J. R.: Calcareous nannoplankton evolution and diversity through time, in Coccolithophores, pp. 481–508, Springer., 2004.

Boyle, P. R., Romans, B. W., Tucholke, B. E., Norris, R. D., Swift, S. A. and Sexton, P. F.: Cenozoic North Atlantic deep circulation history recorded in contourite drifts, offshore Newfoundland, Canada, Marine Geology, 385, 185–203, doi:10.1016/j.margeo.2016.12.014, 2017.

Brinkhuis, H.: Late Eocene to Early Oligocene dinoflagellate cysts from the Priabonian type-area (Northeast Italy): biostratigraphy and paleoenvironmental interpretation, Palaeogeography, Palaeoclimatology, Palaeoecology, 107(1–2), 121–163, doi:10.1016/0031-0182(94)90168-6, 1994.

Brinkhuis, H. and Biffi, U.: Dinoflagellate cyst stratigraphy of the Eocene/Oligocene transition in central Italy, Marine Micropaleontology, 22(1–2), 131–183, doi:10.1016/0377-8398(93)90007-K, 1993.

Brinkhuis, H., Powell, A. J. and Zevenboom, D.: High-resolution dinoflagellate cyst stratigraphy of the Oligocene/Miocene transition interval in northwest and central Italy, in Neogene and Quaternary Dinoflagellate Cysts and Acritarchs, edited by M. J. Head and J. H. Wrenn, pp. 219–258, American Association of Stratigraphic Palynologists Foundation, Dallas., 1992.

Brinkhuis, H., Bujak, J. P., Smit, J., Versteegh, G. J. M. and Visscher, H.: Dinoflagellate-based sea surface temperature reconstructions across the Cretaceous-Tertiary boundary, Palaeogeography, Palaeoclimatology, Palaeoecology, 141(1–2), 67–83, doi:10.1016/S0031-0182(98)00004-2, 1998.

Brinkhuis, H., Sengers, S., Sluijs, A., Warnaar, J. and Williams, G. L.: Late Eocene-Quaternary Dinoflagellate Cysts from ODP Site 1168, off Western Tasmania, Proceedings of the Ocean Drilling Program, Scientific Results, 189(October), 1–36, 2003a.

Brinkhuis, H., Sengers, S., Sluijs, A., Warnaar, J. and Williams, G. L.: Latest Cretaceous-Earliest Oligocene and Quaternary Dinoflagellate Cysts, ODP site 1172, East Tasman Plateau, Proceedings of the Ocean Drilling Program, Scientific Results, 189(October), 1–48, 2003b.

Broecker, W. S.: Paleocean circulation during the last deglaciation: a bipolar seesaw?, Paleoceanography, 13(2), 119–121, 1998.

Broecker, W. S. and Peng, T. H.: Tracers in the Sea, Lamont-Doherty geological observatory, Lamont-Doherty Geological Observatory, Eldigo Press, New York., 1982.

Bryant, H. N.: Nimravidae, The terrestrial Eocene–Oligocene transition in North America. Cambridge University Press, Cambridge, 453–475, 1996.

Bujak, J. P. and Mudge, D. C.: A high-resolution North Sea Eocene dinocyst zonation, Journal of the Geological Society, 151(3), 449–462, doi:10.1144/gsjgs.151.3.0449, 1994.

Bujak, J. P. and Williams, G. L.: Mesozoic and Cenozoic dinoflagellates, Plankton Stratigraphy. Cambridge University Press, Cambridge, (February), 847–965, 1985.

Burgess, R.: Analysis of the palynomorph assemblage through the Eocene/Oligocene transition within the Mossy Grove core, Mississippi, University of Birmingham., 2015.

Bybell, L. M. and Poore, R. Z.: Reworked Hantkenina specimens at Little Stave Creek, Alabama: Gulf Coast Association of Geological Societies Transactions, 33, 253–256, 1983.

Caesar, L., Rahmstorf, S., Robinson, A., Feulner, G. and Saba, V.: Observed fingerprint of a weakening Atlantic Ocean overturning circulation, Nature, 556(7700), 191–196, doi:10.1038/s41586-018-0006-5, 2018.

Carvalho, M. de A., Mendonça Filho, J. G. and Menezes, T. R.: Paleoenvironmental reconstruction based on palynofacies analysis of the Aptian-Albian succession of the Sergipe Basin, Northeastern Brazil, Marine Micropaleontology, 59(1), 56–81, doi:10.1016/j.marmicro.2006.01.001, 2006.

Chateaneuf, J.-J. and Reyre, Y.: Elements de Palynologie: Applications Geologiques, Laboratoire de Paleontologie de l'Universite de Geneve., 1974.

Chu, S. P.: The Influence of the Mineral Composition of the Medium on the Growth of Planktonic Algae: Part I. Methods and Culture Media, Journal of Ecology, 30(2), 284–325, doi:10.2307/2256574, 1942.

Clowes, C. D., Crouch, E. M., Prebble, J. G. and Roncaglia, L.: Development and multi-operator calibration of a standardised palynofacies analysis technique., 2016.

Coccioni, R., Basso, D., Brinkhuis, H., Galeotti, S., Gardin, S., Monechi, S. and Spezzaferri, S.: Marine biotic signals across a late Eocene impact layer at Massignano, Italy: Evidence for long-term environmental perturbations?, Terra Nova, 12(6), 258–263, doi:10.1046/j.1365-3121.2000.00305.x, 2000.

Coccioni, R., Frontalini, F. and Spezzaferri, S.: Evidence from the Massignano global stratotype section and point (central Italy), Geological Society of America Special Paper, 452, 97–118, 2009.

Collinson, M. E.: Vegetational and floristic changes around the Eocene/Oligocene boundary in western and central Europe, Princeton University Press., 1992.

Cooper, A. K. and O'Brien, P. E.: Leg 188 synthesis: transitions in the glacial history of the Prydz Bay region, East Antarctica, from ODP drilling, in Proceedings of the Ocean Drilling

Program, Scientific Results, vol. 188, pp. 1–42, Ocean Drilling Program College Station, TX., 2004.

Costa, L. I. and Downie, C.: Cenozoic dinocyst stratigraphy of sites 403 to 406 (Rockall Plateau), IPOD, Leg 48, Initial reports of the Deep Sea Drilling project, 48, 513–529, 1979.

Costa, L. I. and Manum, S. B.: The description of the interregional zonation of the Paleogene (D1–D15) and the Miocene (D16–D20), Geologisches Jahrbuch, Reihe A, 100, 321–330, 1988.

Costa, L. I., Downie, C. and Eaton, G. L.: Palynostratigraphy of some middle Eocene sections from the Hampshire basin (England), Proceedings of the Geologists' Association, 87(3), 273–284, 1976.

Cotton, L. J. and Pearson, P. N.: Larger benthic foraminifera from the middle Eocene to Oligocene of Tanzania, Austrian Journal of Earth Sciences, 105(1), 189–199, 2012.

Coxall, H. K. and Pearson, P. N.: The Eocene-Oligocene transition, in Deep-time perspectives on climate change: Marrying the signal from computer models and biological proxies, vol. 2, pp. 351–387., 2007.

Coxall, H. K., Wilson, P. A., Pälike, H., Lear, C. H. and Backman, J.: Rapid stepwise onset of Antarctic glaciation and deeper calcite compensation in the Pacific Ocean, Nature, 433(January), 53–57, doi:10.1038/nature03186.1., 2005.

Coxall, H. K., Huck, C. E., Huber, M., Lear, C. H., Legarda-Lisarri, A., O'Regan, M., Sliwinska, K. K., Van De Flierdt, T., De Boer, A. M., Zachos, J. C. and Backman, J.: Export of nutrient rich Northern Component Water preceded early Oligocene Antarctic glaciation, Nature Geoscience, 11(3), 190–196, doi:10.1038/s41561-018-0069-9, 2018.

Cramer, B. S., Miller, K. G., Barrett, P. J. and Wright, J. D.: Late Cretaceous – Neogene trends in deep ocean temperature and continental ice volume : Reconciling records of benthic foraminiferal geochemistry (d 18 O and Mg / Ca) with sea level history, Journal of

Geophysical Research, 116, 1–23, doi:10.1029/2011JC007255, 2011.

Crisman, T. L.: Algal remains in Minnesota lake types: a comparison of modern and late-glacial distributions: With 4 figures and 1 table in the text, Verhandlungen der Internationalen Vereinigung for Theoretische und Angewandte Limnologie, 20(1), 445–451, 1978.

Cronberg, G.: Pediastrum and Scenedesmus (Chlorococcales) in sediments from lake Växjösjön, Sweden, Archiv fur Hydrobiologie Supplement, 60, 500–507, 1982.

Crouch, E. M.: Environmental Change at the Time of the Paleocene-Eocene Biotic Turnover: Met Een Samenvatting in Het Nederlands, Laboratory of Palaeobotany and Palynology Contribution Series., 2001.

Cushing, E. M., Boswell, E. H. and Hosman, R. L.: General geology of the Mississippi embayment, U.S. Geological Survey Professional Paper 448-B, 448 [online] Available from: http://pubs.er.usgs.gov/publication/pp448B, 1964.

Dale, B.: Cyst formation, sedimentation, and preservation: Factors affecting dinoflagellate assemblages in recent sediments from trondheimsfjord, Norway, Review of Palaeobotany and Palynology, 22(1), 39–60, doi:10.1016/0034-6667(76)90010-5, 1976.

Dale, B.: Dinoflagellate cyst ecology: modeling and geological applications, Palynology: principles and applications, 1249–1275, 1996.

Davey, R. J.: Non-calcareous microplankton from the Cenomanian of England, northern France and North America, Bulletins of the British Museum (Natural History), Geology, 18, 333–397, 1970.

Davey, R. J. am and Rogers, J.: Palynomorph distribution in Recent offshore sediments along two traverses off South West Africa, Marine Geology, 18(4), 213–225, 1975.

DeConto, R. M. and Pollard, D.: Rapid Cenozoic glaciation of Antarctica induced by declining atmospheric CO2, Nature, 421(6920), 245–249, doi:10.1038/nature01290, 2003.

DeConto, R. M., Pollard, D., Wilson, P. A., Pälike, H., Lear, C. H. and Pagani, M.: Thresholds for Cenozoic bipolar glaciation, Nature, 455(7213), 652–656, doi:10.1038/nature07337, 2008.

Diester-Haass, L. and Zahn, R.: Eocene-Oligocene transition in the Southern Ocean: History of water mass circulation and biological productivity, Geology, 24(2), 163–166, 1996.

Diester-Haass, L. and Zahn, R.: Paleoproductivity increase at the Eocene - Oligocene climatic transition: ODP/DSDP sites 763 and 592, Palaeogeography, Palaeoclimatology, Palaeoecology, 172(1–2), 153–170, doi:10.1016/S0031-0182(01)00280-2, 2001.

Diester-Haass, L., Robert, C. and Chamley, H.: The Eocene-Oligocene preglacial-glacial transition in the Atlantic sector of the Southern Ocean (ODP Site 690), Marine Geology, 131(3–4), 123–149, 1996.

Diester-Haass, L., Zachos, J. and Prothero, D. R.: The Eocene-Oligocene transition in the Equatorial Atlantic (ODP Site 925); paleoproductivity increase and positive δ13C excursion, Greenhouse to Icehouse: The Marine Eocene-Oligocene Transition, 397–416, 2003.

Dockery, D. T.: Lower Oligocene bivalvia of the Vicksburg group in Mississippi, 1982.

Dockery III, D. T.: Punctuated succession of Paleogene mollusks in the northern Gulf Coastal Plain, Palaios, 582–589, 1986.

Dockery III, D. T. and Lozouet, P.: Biotic patterns in Eocene-Oligocene Molluscs of the Atlantic Coastal Plain, USA, in From Greenhouse to Icehouse, edited by D. R. Prothero, L. Ivany, and E. A. Nesbitt, pp. 303–340, Columbia University Press, New York., 2003.

Dockery III, D. T., Stover, C. W., Weathersby, P., Stover Jr, C. W. and Ingram, S. L.: A continuous core through the undifferentiated Yazoo Clay (late Eocene, Jackson Group) of central Mississippi, Mississippi Geology, 12(3, 4), 21–27, 1991.

Dodge, J. D. and Harland, R.: The distribution of planktonic dinoflagellates and their cysts in the eastern and northeastern Atlantic Ocean, New Phytologist, 118(4), 593–603,

doi:10.1111/j.1469-8137.1991.tb01000.x, 1991.

Downie, C., Hussain, M. A. and Williams, G. L.: Dinoflagellate cyst and acritarch associations in the Paleogene of southeast England, Geoscience and Man, 3(1), 29–35, 1971.

Dubois, K. D., Lee, D. and Veizer, J.: Isotopic constraints on alkalinity, dissolved organic carbon, and atmospheric carbon dioxide fluxes in the Mississippi River, Journal of Geophysical Research: Biogeosciences, 115(G2), n/a-n/a, doi:10.1029/2009jg001102, 2010.

Dudley, W. C., Duplessy, J. C., Blackwelder, P. L., Brand, L. E. and Guillard, R. R. L.: Coccoliths in Pleistocene–Holocene nannofossil assemblages, Nature, 285(5762), 222–223, 1980.

Dudley, W. C., Blackwelder, P., Brand, L. and Duplessy, J. C.: Stable isotopic composition of coccoliths, Marine Micropaleontology, 10(1–3), 1–8, doi:10.1016/0377-8398(86)90021-6, 1986.

Dunkley Jones, T., Bown, P. R., Pearson, P. N., Wade, B. S., Coxall, H. K. and Lear, C. H.: Major shifts in calcareous phytoplankton assemblages through the Eocene-Oligocene transition of Tanzania and their implications for low-latitude primary production, Paleoceanography, 23(4), 1–14, doi:10.1029/2008PA001640, 2008.

Dunkley Jones, T., Bown, P. R. and Pearson, P. N.: Exceptionally well preserved upper Eocene to lower Oligocene calcareous nannofossils (Prymnesiophyceae) from the Pande Formation (Kilwa Group), Tanzania, Journal of Systematic Palaeontology, 7(4), 359–411, doi:10.1017/S1477201909990010, 2009.

Dupont-Nivet, G., Krijgsman, W., Langereis, C. G., Abels, H. A., Dai, S. and Fang, X.: Tibetan plateau aridification linked to global cooling at the Eocene-Oligocene transition, Nature, 445(7128), 635–638, doi:10.1038/nature05516, 2007.

Duxbury, S. and Vieira, M.: A Stratigraphic Review of the Late Callovian to Oxfordian Interval, Fisher Bank Basin Area (UK Sector, Central North Sea), Journal of Petroleum

Geology, 41(1), 47–65, doi:10.1111/jpg.12692, 2018.

Echols, R. J., Armentrout, J. M., Root, S. A., Fearn, L. B., Cooke, J. C., Rodgers, B. K. and Thompson, P. R.: Sequence stratigraphy of the Eocene/Oligocene boundary interval: Southeastern Mississippi, in From Greenhouse to Ice House: The Marine Eocene–Oligocene Transition, edited by D. R. Prothero, E. Nesbitt, and L. Ivany, pp. 189–222., 2003.

Edwards, L. E. and Andrle, V. A. S.: Distribution of selected dinoflagellate cysts in modern marine sediments, Neogene and Quaternary dinoflagellate cysts and acritarchs, 259–288, 1992.

Egger, L. M., Śliwińska, K. K., van Peer, T. E., Liebrand, D., Lippert, P. C., Friedrich, O., Wilson, P. A., Norris, R. D. and Pross, J.: Magnetostratigraphically-calibrated dinoflagellate cyst bioevents for the uppermost Eocene to lowermost Miocene of the western North Atlantic (IODP Expedition 342, Paleogene Newfoundland sediment drifts), Review of Palaeobotany and Palynology, 234, 159–185, doi:10.1016/j.revpalbo.2016.08.002, 2016.

Ehrmann, W. U. and Mackensen, A.: Sedimentological evidence for the formation of an East Antarctic ice sheet in Eocene/Oligocene time, Palaeogeography, Palaeoclimatology, Palaeoecology, 93(1–2), 85–112, 1992.

Eldrett, J. S. and Harding, I. C.: Palynological analyses of Eocene to Oligocene sediments from DSDP Site 338, Outer Vøring Plateau, Marine Micropaleontology, 73(3–4), 226–240, doi:10.1016/j.marmicro.2009.10.004, 2009.

Eldrett, J. S., Harding, I. C., Firth, J. V. and Roberts, A. P.: Magnetostratigraphic calibration of Eocene-Oligocene dinoflagellate cyst biostratigraphy from the Norwegian-Greenland Sea, Marine Geology, 204(1–2), 91–127, doi:10.1016/S0025-3227(03)00357-8, 2004.

Eldrett, J. S., Harding, I. C., Wilson, P. A., Butler, E. and Roberts, A. P.: Continental ice in Greenland during the Eocene and Oligocene, Nature, 446(7132), 176–179, doi:10.1038/nature05591, 2007.

Eldrett, J. S., Greenwood, D. R., Harding, I. C. and Huber, M.: Increased seasonality through the Eocene to Oligocene transition in northern high latitudes, Nature, 459(7249), 969–973, doi:10.1038/nature08069, 2009.

Ellegaard, M.: Variations in dinoflagellate cyst morphology under conditions of changing salinity during the last 2000 years in the Limfjord, Denmark, Review of Palaeobotany and Palynology, 109(1), 65–81, doi:10.1016/S0034-6667(99)00045-7, 2000.

Elsworth, G., Galbraith, E., Halverson, G. and Yang, S.: Enhanced weathering and CO 2 drawdown caused by latest Eocene strengthening of the Atlantic meridional overturning circulation, Nature Geoscience, 10(3), 213–216, doi:10.1038/ngeo2888, 2017.

Ennyu, A., Arthur, M. A. and Pagani, M.: Fine-fraction carbonate stable isotopes as indicators of seasonal shallow mixed-layer paleohydrography, Marine Micropaleontology, 46(3–4), 317–342, doi:10.1016/S0377-8398(02)00079-8, 2002.

Eshet, Y., Almogi-Labin, A. and Bein, A.: Dinoflagellate cysts, paleoproductivity and upwelling systems: A Late Cretaceous example from Israel, Marine Micropaleontology, 23(3), 231–240, doi:10.1016/0377-8398(94)90014-0, 1994.

Evitt, W. R.: Sporopollenin dinoflagellate cysts: their morphology and interpretation, American Association of Stratigraphic Palynologists Foundation, Salt Lake City., 1985.

Farley, K. A., Moǹtanari, A., Shoemaker, E. M. and Shoemaker, C. S.: Geochemical evidence for a comet shower in the late Eocene, Science, 280(5367), 1250–1253, doi:10.1126/science.280.5367.1250, 1998.

Farr, K. M., Batten, D. J. and Keen, M. C.: Palynomorph and palynodebris distributions in modern British and Irish estuarine sediments, in Northwest European Micropalaeontology and Palynology, edited by D. J. Batten and M. C. Keen, pp. 265–285, British Micropalaeontological Society Series, Ellis Horwood, Chichester., 1989.

Fluegeman, R. H.: Preliminary paleontological report on the foraminifera of the Mossy Grove

core, Hinds County, Mississippi: Mississippi Geology, 17(1), 9–15, 1996.

Fluegeman, R. H.: Late Eocene–early Oligocene benthic foraminifera in the Gulf Coastal Plain—Regional vs. global influences, From Greenhouse to Icehouse: The Marine Eocene–Oligocene Transition: Columbia University Press, New York, 283–293, 2003.

Fluegeman, R. H., Grigsby, J. D. and Hurley, J. V: Eocene-Oligocene greenhouse to icehouse transition on a subtropical clastic shelf; the Jackson-Vicksburg Groups of the eastern Gulf Coastal Plain of the United States, Special Paper - Geological Society of America, 452, 261–277, doi:10.1130/2009.2452(17), 2009.

Fordyce, R. E.: Cetacean evolution and Eocene/Oligocene environments, Eocene-Oligocene climatic and biotic evolution, 1992.

Fordyce, R. E.: Cetacean evolution and Eocene-Oligocene oceans revisited, From greenhouse to icehouse: the marine Eocene-Oligocene transition, 154–171, 2003.

Francis, J. E.: Evidence from fossil plants for Antarctic palaeoclimates over the past 100 million years, Terr. Antarct. Rep, 3, 43–52, 1999.

Francis, J. E. and Poole, I.: Cretaceous and early Tertiary climates of Antarctica: evidence from fossil wood, Palaeogeography, Palaeoclimatology, Palaeoecology, 182(1–2), 47–64, 2002.

Friedrich, O., Norris, R. D. and Erbacher, J.: Evolution of middle to late Cretaceous oceans-A 55 m.y. Record of Earth's temperature and carbon cycle, Geology, 40(2), 107–110, doi:10.1130/G32701.1, 2012.

Frieling, J. and Sluijs, A.: Towards quantitative environmental reconstructions from ancient non-analogue microfossil assemblages: Ecological preferences of Paleocene – Eocene dinoflagellates, Earth-Science Reviews, 185(August), 956–973, doi:10.1016/j.earscirev.2018.08.014, 2018.

Funakawa, S., Nishi, H., Moore, T. C. and Nigrini, C. A.: Radiolarian faunal turnover and

paleoceanographic change around Eocene/Oligocene boundary in the central equatorial Pacific, ODP Leg 199, Holes 1218A, 1219A, and 1220A, Palaeogeography, Palaeoclimatology, Palaeoecology, 230(3–4), 183–203, 2006.

Gale, A. S., Huggett, J. M., PÄlike, H., Laurie, E., Hailwood, E. A. and Hardenbol, J.: Correlation of Eocene–Oligocene marine and continental records: orbital cyclicity, magnetostratigraphy and sequence stratigraphy of the Solent Group, Isle of Wight, UK, Journal of the Geological Society, 163(2), 401–415, doi:10.1144/0016-764903-175, 2006.

Galeotti, S., Brinkhuis, H. and Huber, M.: Records of post-Cretaceous-Tertiary boundary millennial-scale cooling from the western Tethys: A smoking gun for the impact-winter hypothesis?, Geology, 32(6), 529–532, doi:10.1130/G20439.1, 2004.

Galloway, W. E., Whiteaker, T. L. and Ganey-Curry, P.: History of Cenozoic North American drainage basin evolution, sediment yield, and accumulation in the Gulf of Mexico basin, Geosphere, 7(4), 938–973, doi:10.1130/ges00647.1, 2011.

Glass, B. P.: Upper Eocene impact ejecta/spherule layers in marine sediments, Chemie der Erde-Geochemistry, 62(3), 173–196, 2002.

Glass, B. P., Koeberl, C., Blum, J. D. and Mchugh, C. M. G.: Upper Eocene tektite and impact ejecta layer on the continental slope off New Jersey, Meteoritics and Planetary Science, 33(2), 229–241, doi:10.1111/j.1945-5100.1998.tb01628.x, 1998.

Goldner, A., Herold, N. and Huber, M.: Antarctic glaciation caused ocean circulation changes at the Eocene-Oligocene transition, Nature, 511(7511), 574–577, doi:10.1038/nature13597, 2014.

Goodney, D. E., Margolis, S. V., Dudley, W. C., Kroopnick, P. and Williams, D. F.: Oxygen and carbon isotopes of recent calcareous nannofossils as paleoceanographic indicators, Marine Micropaleontology, 5, 31–42, 1980.

Gradstein, F. M., Kristiansen, I. L., Loemo, L. and Kaminski, M. A.: Cenozoic foraminiferal

and dinoflagellate cyst biostratigraphy of the central North Sea, Micropaleontology, 38(2), 101–137, doi:10.2307/1485991, 1992.

Grimes, S. T., Hooker, J. J., Collinson, M. E. and Mattey, D. P.: Summer temperatures of late Eocene to early Oligocene freshwaters, Geology, 33(3), 189–192, 2005.

Grimsdale, T. F. and Van Morkhoven, F. P. C. M.: 4. The Ratio between Pelagic and Benthonic Foraminifera as a Means of Estimating Depth of Deposition of Sedimentary Rocks, in 4th World Petroleum Congress, World Petroleum Congress, Rome., 1955.

Habib, D.: Sedimentation rate dependent distribution of organic matter in the North Atlantic Jurassic-Cretaceous, in Initial Reports of the Deep Sea Drilling Project, in Initial Reports of the Deep Sea Drilling Project, vol. 76, edited by R. E. Sheridan and F. M. Gradstein, pp. 781–794, U.S. Government Printing Office, Washington, DC., 1983.

Hambrey, M. J., Ehrmann, W. U. and Larsen, B.: Cenozoic Glacial Record of the Prydz Bay Continental Shelf, East Antarctica, Proceedings of the Ocean Drilling Program, 119 Scientific Results, 119(2), 77–132, doi:10.2973/odp.proc.sr.119.200.1991, 1991.

Han, G., Lu, Z., Wang, Z., Helbig, J., Chen, N. and de Young, B.: Seasonal variability of the Labrador Current and shelf circulation off Newfoundland, Journal of Geophysical Research: Oceans, 113(10), doi:10.1029/2007JC004376, 2008.

Hansen, J. M.: Dinoflagellate stratigraphy and echinoid distribution in Upper Maastrichtian and Danian deposits from Denmark, Bulletin of the Geological Society of Denmark, 26, 1–26, 1977.

Harland, R.: Dinoflagellate cysts and acritarchs from the Bearpaw Formation (Upper Campanian) of southern Alberta, Canada, Palaeontology, 16(4), 665–706, 1973.

Harland, R.: Distribution maps of recent dinoflagellate cysts in bottom sediments from the North Atlantic Ocean and adjacent seas, Palaeontology, 26(2), 321–387, 1983.

Hays, J. D., Imbrie, J. and Shackleton, N. J.: Variations in the earth's orbit: Pacemaker of the

ice ages, Science, 194(4270), 1121–1132, doi:10.1126/science.194.4270.1121, 1976.

Head, M. J.: Modern dinoflagellate cysts and their biological affinities, edited by J. Jansonius and D. C. McGregor, Palynology: Principles and Applications. American Association of Stratigraphic Palynologists Foundation, Dallas, TX, 3(November), 1197–1248 [online] Available from: http://scholar.google.com/scholar?hl=en&btnG=Search&q=intitle:Chapter+30+MODERN+DINOFLAGELLATE+CYSTS+AND+THEIR+BIOLOGICAL+AFFINITIES#0, 1996.

Head, M. J. and Norris, G.: Palynology and Dinocyst Stratigraphy of the Eocene and Oligocene in ODP Leg 105, Hole 647A, Labrador Sea, in Proceedings of the Ocean Drilling Program, Scientific Results, vol. 105, pp. 515–550., 1989.

Heilmann-Clausen, C. and Van Simaeys, S.: Dinoflagellate cysts from the Middle Eocene to ?lowermost Oligocene succession in the Kysing research borehole, central Danish basin, Palynology, 29(1), 143–204, doi:10.1080/01916122.2005.9989606, 2005.

Hickman, C. S.: Evidence for Abrupt Eocene-Oligocene, From greenhouse to icehouse: The marine Eocene-Oligocene transition, 71, 2003.

Hosman, R. L.: Regional stratigraphy and subsurface geology of Cenozoic deposits, Gulf Coastal Plain, south-central United States., 1996.

Houben, A. J. P., van Mourik, C. A., Montanari, A., Coccioni, R. and Brinkhuis, H.: The Eocene-Oligocene transition: Changes in sea level, temperature or both?, Palaeogeography, Palaeoclimatology, Palaeoecology, 335–336, 75–83, doi:10.1016/j.palaeo.2011.04.008, 2012.

Houben, A. J. P., Bijl, P. K., Pross, J., Bohaty, S. M., Passchier, S., Stickley, C. E., Röhl, U., Sugisaki, S., Tauxe, L., van de Flierdt, T., Olney, M., Sangiorgi, F., Sluijs, A., Escutia, C., Brinkhuis, H. and Scientists, E. 318: Reorganization of Southern Ocean Plankton Ecosystem at the Onset of Antarctic Glaciation, Science, 340, 341–344, doi:10.1126/science.1223646, 2013a.

Houben, A. J. P., Bijl, P. K., Pross, J., Bohaty, S. M., Passchier, S., Stickley, C. E., Rohl, U., Sugisaki, S., Tauxe, L., van de Flierdt, T., Olney, M., Sangiorgi, F., Sluijs, A., Escutia, C. and Brinkhuis, H.: Reorganization of Southern Ocean Plankton Ecosystem at the Onset of Antarctic Glaciation, Science, 340(6130), 341–344, doi:10.1126/science.1223646, 2013b.

Houben, A. J. P., Quaijtaal, W., Wade, B. S., Schouten, S. and Brinkhuis, H.: Quantitative organic-walled dinoflagellate cyst stratigraphy across the Eocene-Oligocene Transition in the Gulf of Mexico: A record of climate- and sea level change during the onset of Antarctic glaciation, Newsletters on Stratigraphy, (September), doi:10.1127/nos/2018/0455, 2018.

Hren, M. T., Sheldon, N. D., Grimes, S. T., Collinson, M. E., Hooker, J. J., Bugler, M. and Lohmann, K. C.: Terrestrial cooling in Northern Europe during the Eocene-Oligocene transition, Proceedings of the National Academy of Sciences of the United States of America, 110(19), 7562–7567, doi:10.1073/pnas.1210930110, 2013.

Huber, M., Brinkhuis, H., Stickley, C. E., Döös, K., Sluijs, A., Warnaar, J., Schellenberg, S. A. and Williams, G. L.: Eocene circulation of the Southern Ocean: Was Antarctica kept warm by subtropical waters?, Paleoceanography, 19(4), 1–12, doi:10.1029/2004PA001014, 2004.

Hultberg, S. U.: Palynological evidence for a diachronous low-salinity event in the C–T boundary clay at Stevns Klint, Denmark, Journal of Micropalaeontology, 6(2), 35–40, doi:10.1144/jm.6.2.35, 1987.

Hut, P., Alvarez, W., Elder, W. P., Hansen, T. A., Kauffman, E. G., Keller, G., Shoemaker, E. M. and Weissman, P. R.: Comet showers as possible causes of stepwise mass extinctions, Nature, 329(September), 118–126, 1987.

Hutchinson, D. K., Coxall, H. K., O′Regan, M., Nilsson, J., Caballero, R. and de Boer, A. M.: Arctic closure as a trigger for Atlantic overturning at the Eocene-Oligocene Transition, Nature Communications, 10(1), 3797, doi:10.1038/s41467-019-11828-z, 2019.

Hutchinson, G. E.: A treatise on limnology, Introduction to Lake biology and the

limnoplankton, Wiley, New York., 1967.

Hutchison, J. H.: Western North American reptile and amphibian record across the Eocene/Oligocene boundary and its climatic implications, Eocene–Oligocene climatic and biotic evolution, 451–463, 1992.

Ingram, W. C., Meyers, S. R., Brunner, C. A. and Martens, C. S.: Late Pleistocene-Holocene sedimentation surrounding an active seafloor gas-hydrate and cold-seep field on the Northern Gulf of Mexico Slope, Marine Geology, 278(1–4), 43–53, doi:10.1016/j.margeo.2010.09.002, 2010.

IPCC: Climate Change 2013: The Physical Science Basis. Contribution of Working Group I to the Fifth Assessment Report of the Intergovern- mental Panel on Climate Change, edited by T. F. Stocker, D. Qin, G.-K. Plattner, M. Tignor, S. K. Allen, J. Boschung, A. Nauels, Y. Xia, V. Bex, and P. M. Midgley, Cambridge University Press, Cambridge, United Kingdom and New York, NY, USA., 2013.

Itambi, A. C., Von Dobeneck, T., Mulitza, S., Bickert, T. and Heslop, D.: Millennial-scale northwest African droughts related to Heinrich events and Dansgaard-Oeschger cycles: Evidence in marine sediments from offshore Senegal, Paleoceanography, 24(1), 1–16, doi:10.1029/2007PA001570, 2009.

Ivany, L. C., Patterson, W. P. and Lohmann, K. C.: Cooler winters as a possible cause of mass extinctions at the Eocene/Oligocene boundary., Nature, 407(6806), 887–890, doi:10.1038/35038044, 2000.

Jaramillo, C., Rueda, M. J., Mora, G. and Margalit, A.: Cenozoic Plant Diversity in the Neotropics, Science, 311(March), 1893–1896, 2006.

Jaramillo, C. A. and Oboh-Ikuenobe, F. E.: Sequence stratigraphic interpretations from palynofacies, dinocyst and lithological data of upper eocene-lower oligocene strata in southern Mississippi and Alabama, U.S. Gulf Coast, Palaeogeography, Palaeoclimatology,

Palaeoecology, 145(4), 259–302, doi:10.1016/S0031-0182(98)00126-6, 1999.

Jones, A. P., Dunkley Jones, T., Coxall, H., Pearson, P. N., Nala, D. and Hoggett, M.: Low-Latitude Calcareous Nannofossil Response in the Indo-Pacific Warm Pool Across the Eocene-Oligocene Transition of Java, Indonesia, Paleoceanography and Paleoclimatology, 34(11), 1833–1847, doi:10.1029/2019PA003597, 2019.

Joughin, I., Smith, B. E. and Medley, B.: Marine Ice Sheet Collapse Potentially Under Way for the Thwaites Glacier Basin, West Antarctica, Science, 344(May), 735–739, 2014.

Kamikuri, S. and Wade, B. S.: Radiolarian magnetobiochronology and faunal turnover across the middle/late Eocene boundary at Ocean Drilling Program Site 1052 in the western North Atlantic Ocean, Marine Micropaleontology, 88, 41–53, 2012.

Kaminski, M. A.: The utility of Deep-Water Agglutinated Foraminiferal acmes for correlating Eocene to Oligocene abyssal sediments in the North Atlantic and Western Tethys, Studia Geologica Polonica, 124, 325–339, 2005.

Katz, M. E., Miller, K. G., Wright, J. D., Wade, B. S., Browning, J. V., Cramer, B. S. and Rosenthal, Y.: Stepwise transition from the Eocene greenhouse to the Oligocene icehouse, Nature Geoscience, 1(5), 329–334, doi:10.1038/ngeo179, 2008.

Kawaragi, K., Sekine, Y., Kadono, T., Sugita, S., Ohno, S., Ishibashi, K., Kurosawa, K., Matsui, T. and Ikeda, S.: Direct measurements of chemical composition of shock-induced gases from calcite: an intense global warming after the Chicxulub impact due to the indirect greenhouse effect of carbon monoxide, Earth and Planetary Science Letters, 282(1–4), 56–64, doi:10.1016/j.epsl.2009.02.037, 2009.

Keller, G.: Stepwise mass extinctions and impact events: Late Eocene to early Oligocene, Marine Micropaleontology, 10(4), 267–293, doi:10.1016/0377-8398(86)90032-0, 1986.

Kemp, E. M.: Tertiary climatic evolution and vegetation history in the southeast Indian Ocean region, Palaeogeography, Palaeoclimatology, Palaeoecology, 24(3), 169–208, 1978.

Kennett, J. P.: Cenozoic evolution of Antarctic glaciation, the circum-Antarctic Ocean, and their impact on global paleoceanography, Journal of Geophysical Research, 82(27), 3843–3860, doi:10.1029/JC082i027p03843, 1977.

Kennett, J. P. and Shackleton, N. J.: Oxygen isotopic evidence for the development of the psychrosphere 38 Myr ago, Nature, 260(5551), 513–515, doi:10.1038/260513a0, 1976.

Kobashi, T., Grossman, E. L., Yancey, T. E. and Dockery, D. T.: Reevaluation of conflicting Eocene tropical temperature estimates: Molluskan oxygen isotope evidence for warm low latitudes, Geology, 29(11), 983–986, doi:10.1130/0091-7613(2001)029<0983:ROCETT>2.0.CO;2, 2001.

Koeberl, C., Poag, C. W., Reimold, W. U. and Brandt, D.: Impact Origin of the Chesapeake Bay Structure and the Source of the North American Tektites KOEBERL et al 1996, , 271(March), 1–4 [online] Available from: http://www.univie.ac.at/geochemistry/koeberl/publikation_list/103-Chesapeake-crater-confirmed-Science1996.pdf%0Afile:///Users/paulrichardson/Dropbox/Library.papers3/Files/83/839E29A4-14D7-4612-BEFF-77E319B85605.pdf%0Apapers3://publication/uuid/8EF0D123-2A, 1996.

Kohn, M. J., Josef, J. A., Madden, R., Kay, R., Vucetich, G. and Carlini, A. A.: Climate stability across the Eocene-Oligocene transition, southern Argentina, Geology, 32(7), 621–624, doi:10.1130/G20442.1, 2004.

Kokinos, J. P. and Anderson, D. M.: Morphological development of resting cysts in cultures of the marine dinoflagellate Lingulodinium polyedrum (= L. Machaerophorum), Palynology, 19(1), 143–166, doi:10.1080/01916122.1995.9989457, 1995.

Kominz, M. A. and Pekar, S. F.: Oligocene eustasy from two-dimensional sequence stratigraphic backstripping, Geological Society of America Bulletin, 113(3), 291–304,

doi:10.1130/0016-7606(2001)113<0291:OEFTDS>2.0.CO;2, 2001.

Korde, N. V: Biostratification and Classification of Russian Sapropels, National Lending Library for Science and Technology (now British Library Document Supply Centre), Boston Spa, UK., 1960.

Kothe, A.: Paleogene dinoflagellates from Northwest Germany: biostratigraphy and paleoenvironments, Geologisches Jahrbuch, 118, 3–111, 1990.

Kring, D. A., Melosh, H. J. and Hunten, D. M.: Impact-induced perturbations of atmospheric sulfur, Earth and Planetary Science Letters, 140(1–4), 201–212, doi:10.1016/0012-821X(96)00050-7, 1996.

Kump, L. R. and Arthur, M. A.: Global chemical erosion during the Cenozoic: Weatherability balances the budgets, in Tectonic uplift and climate change, pp. 399–426, Springer., 1997.

Larsen, H. C., Saunders, A. D., Clift, P. D., Beget, J., Wei, W. and Spezzaferri, S.: Seven Million Years of Glaciation in Greenland, Science, 264(May), 952–955, 1994.

Larsson, S. G.: Baltic amber: a palaeobiological study, 1st ed., Entomonograph, Scandinavian Science Press, Klampenborg, Denmark., 1978.

Latimer, J. C. and Filippelli, G. M.: Eocene to Miocene terrigenous inputs and export production: geochemical evidence from ODP Leg 177, Site 1090, Palaeogeography, Palaeoclimatology, Palaeoecology, 182(3–4), 151–164, 2002.

Lear, C. H., Elderfield, H. and Wilson, P. A.: Cenozoic deep-sea temperatures and global ice volumes from Mg/Ca in benthic foraminiferal calcite, Science, 287(5451), 269–272, doi:10.1126/science.287.5451.269, 2000.

Lear, C. H., Elderfield, H. and Wilson, P. A.: A Cenozoic seawater Sr/Ca record from benthic foraminiferal calcite and its application in determining global weathering fluxes, Earth and Planetary Science Letters, 208(1–2), 69–84, doi:10.1016/S0012-821X(02)01156-1, 2003a.

Lear, C. H., Rosenthal, Y. and Wright, J. D.: The closing of a seaway: Ocean water masses and global climate change, Earth and Planetary Science Letters, 210(3–4), 425–436, doi:10.1016/S0012-821X(03)00164-X, 2003b.

Lear, C. H., Rosenthal, Y., Coxall, H. K. and Wilson, P. A.: Late Eocene to early Miocene ice sheet dynamics and the global carbon cycle, Paleoceanography, 19(4), 1–11, doi:10.1029/2004PA001039, 2004.

Lear, C. H., Bailey, T. R., Pearson, P. N., Coxall, H. K. and Rosenthal, Y.: Cooling and ice growth across the Eocene-Oligocene transition, Geology, 36(3), 251–254, doi:10.1130/G24584A.1, 2008.

Lenton, T. M., Held, H., Kriegler, E., Hall, J. W., Lucht, W., Rahmstorf, S. and Schellnhuber, H. J.: Tipping elements in the Earth's climate system, Proceedings of the National Academy of Sciences, 105(6), 1786–1793, doi:10.1073/pnas.0705414105, 2008.

Leopold, E. B., Gengwu, L. and Clay-Poole, C.: Low-biomass vegetation in the Oligocene? in Eocene-Oligocene climatic and biotic evolution, 1992.

Lewis, J. and Hallett, R.: Lingulodinium polyedrum (gonyaulux polyedra) a blooming dinoflagellate, Oceanography and Marine Biology, 35, 97–162, 1997.

Lewis, J., Rochon, A. and Harding, I.: Preliminary observations of cyst-theca relationships in spiniferites ramosus and spiniferites membranaceus (dinophyceae), Grana, 38(2–3), 113–124, doi:10.1080/00173139908559220, 1999.

Liu, S., Glass, B. ., Kyte, F. T. and Bohaty, S. M.: The late Eocene clinopyroxene-bearing spherule layer: New sites, nature of the strewn field, Ir data, and discovery of coesite and shocked quartz, edited by C. Koeberl and A. Montanari, The Late Eocene Earth - Hothouse, Icehouse, and Impacts, Special Pa, 37–70, doi:10.1130/2009.2452(04), 2009a.

Liu, Z., Pagani, M., Zinniker, D., Deconto, R. M., Huber, M., Brinkhuis, H., Shah, S. R., Leckie, R. M. and Pearson, A.: Global Cooling During the Eocene-Oligocene Climate

Transition, Science, 970(February), 1187–1190, 2009b.

Loutit, T. S., Hardenbol, J., Vail, P. R. and Baum, G. R.: Condensed sections: the key to age determination and correlation of continental margin sequences, 1988.

MacLeod, K. G., Quinton, P. C., Sepúlveda, J. and Negra, M. H.: Postimpact earliest Paleogene warming shown by fish debris oxygen isotopes (El Kef, Tunisia), Science, 360(6396), 1467–1469, doi:10.1126/science.aap8525, 2018.

Mancini, E. A.: Eocene-Oligocene boundary in southwest Alabama: Gulf Coast Association of Geological Societies Transactions, Mancini28229Gulf Coast Association of Geological Societies Transactions1979, 29, 282–286, 1979.

Mancini, E. A. and Tew, B. H.: Relationships of Paleogene stage and planktonic foraminiferal zone boundaries to lithostratigraphic and allostratigraphic contacts in the eastern Gulf Coastal Plain, The Journal of Foraminiferal Research, 21(1), 48–66, 1991.

Manning, E. M.: The Eocene/Oligocene transition in marine vertebrates of the Gulf Coastal Plain, From Greenhouse to Icehouse, The Marine Eocene-Oligocene Transition. Columbia University Press, New York, 366–385, 2003.

Manum, S. B.: Dinocysts in Tertiary Norwegian-Greenland Sea sediments (Deep Sea Drilling Project Leg 38), with observations on palynomorphs and palynodebris in relation to environment, Initial Reports of the Deep Sea Drilling Project, 38, 897–919, 1976.

Manum, S. B., Boulter, M. C., Gunnarsdottir, H., Rangnes, K. and Scholze, A.: Eocene to Miocene Palynology of the Norwegian Sea (ODP Leg 104), in Proceedings of the Ocean Drilling Program, vol. 104, pp. 61–74, Ocean Drilling Program., 1989.

Margalef, R.: Life-forms of phytoplankton as survival alternatives in an unstable environment, Oceanologica Acta, 1, 493–509, 1978.

Martini, E.: Standard Tertiary and Quaternary calcareous nannoplankton zonation, in Proc. II Planktonic Conference, Roma 1970, Roma, Tecnoscienza, vol. 2, pp. 739–785., 1971.

Mayr, G.: The Paleogene fossil record of birds in Europe, Biological Reviews of the Cambridge Philosophical Society, 80(4), 515–542, doi:10.1017/S1464793105006779, 2005.

McGowran, B. and Beecroft, A.: Foraminiferal biofacies in a silica-rich neritic sediment, Late Eocene, South Australia, Palaeogeography, Palaeoclimatology, Palaeoecology, 52(3–4), 321–346, doi:10.1016/0031-0182(86)90053-2, 1986.

McGowran, B., Moss, G. and Beecroft, A.: Late Eocene and early Oligocene in southern Australia: local neritic signals of global oceanic changes, Eocene–Oligocene Climatic and Biotic Evolution, 178–201, 1992.

McKay, D. I. A., Tyrrell, T. and Wilson, P. A.: Global carbon cycle perturbation across the Eocene-Oligocene climate transition, Paleoceanography, (31), 311–329, doi:10.1002/2015PA002818.Received, 2016a.

McKay, R. M., Barrett, P. J., Levy, R. S., Naish, T. R., Golledge, N. R. and Pyne, A.: Antarctic Cenozoic climate history from sedimentary records: ANDRILL and beyond, Philosophical Transactions of the Royal Society A: Mathematical, Physical and Engineering Sciences, 374(2059), 1–18, doi:10.1098/rsta.2014.0301, 2016b.

McMinn, A.: Recent dinoflagellate cyst distribution in eastern Australia, Review of Palaeobotany and Palynology, 65(1–4), 305–310, 1990.

Meng, J. and McKenna, M. C.: Faunal turnovers of Palaeogene mammals from the Mongolian Plateau, Nature, 394(6691), 364–367, doi:10.1038/28603, 1998.

Merico, A., Tyrrell, T. and Wilson, P. A.: Eocene/Oligocene ocean de-acidification linked to Antarctic glaciation by sea-level fall, Nature, 452(7190), 979–982, doi:10.1038/nature06853, 2008.

Mertens, K. N., Verhoeven, K., Verleye, T., Louwye, S., Amorim, A., Ribeiro, S., Deaf, A. S., Harding, I. C., De Schepper, S., González, C., Kodrans-Nsiah, M., De Vernal, A., Henry, M., Radi, T., Dybkjaer, K., Poulsen, N. E., Feist-Burkhardt, S., Chitolie, J., Heilmann-

Clausen, C., Londeix, L., Turon, J. L., Marret, F., Matthiessen, J., McCarthy, F. M. G., Prasad, V., Pospelova, V., Kyffin Hughes, J. E., Riding, J. B., Rochon, A., Sangiorgi, F., Welters, N., Sinclair, N., Thun, C., Soliman, A., Van Nieuwenhove, N., Vink, A. and Young, M.: Determining the absolute abundance of dinoflagellate cysts in recent marine sediments: The Lycopodium marker-grain method put to the test, Review of Palaeobotany and Palynology, 157(3–4), 238–252, doi:10.1016/j.revpalbo.2009.05.004, 2009.

Miller, K. G.: The Phanerozoic Record of Global Sea-Level Change, Science, 310(5752), 1293–1298, doi:10.1126/science.1116412, 2005.

Miller, K. G., Fairbanks, R. G. and Mountain, G. S.: Tertiary Oxygen Isotope Synthesis, Sea Level History, and Continental Margin Erosion, Paleoceanography, 2(1), 1–19, 1987.

Miller, K. G., Thompson, P. R. and Kent, D. V.: Integrated Late Eocene-Oligocene Stratigraphy of the Alabama Coastal Plain: Correlation of Hiatuses and Stratal Surfaces to Glacioeustatic Lowerings, Paleoceanography, 8(2), 313–331, doi:10.1029/93PA00203, 1993.

Miller, K. G., Browning, J. V, Aubry, M. P., Wade, B. S., Katz, M. E., Kulpecz, A. A. and Wright, J. D.: Eocene-Oligocene global climate and sea-level changes: St. Stephens Quarry, Alabama, Bulletin of the Geological Society of America, 120(1–2), 34–53, doi:10.1130/B26105.1, 2008.

Miller, K. G., Wright, J. D., Katz, M. E., Wade, B. S., Browning, J. V, Cramer, B. S., Rosenthal, Y., Benjamin, S. and Cramer, B. S.: Climate threshold at the Eocene-Oligocene transition: Antarctic ice sheet influence on ocean circulation, Geological Society of America Special Papers, 452(303), 169–178, doi:10.1130/2009.2452(11)., 2009.

Mohr, B. A. R.: Eocene and Oligocene sporomorphs and dinoflagellate cysts from Leg 113 drill sites, Weddell Sea, Antarctica, in Proceedings of the Ocean Drilling Program, Scientific Results, vol. 113, pp. 595–612, US Government Printing Office College Station, Texas., 1990.

Moore, M. J. and Jansen, R. K.: Molecular evidence for the age, origin, and evolutionary history of the American desert plant genus Tiquilia (Boraginaceae), Molecular Phylogenetics and Evolution, 39(3), 668–687, doi:10.1016/j.ympev.2006.01.020, 2006.

Moore, T. C., Wade, B. S., Westerhold, T., Erhardt, A. M., Coxall, H. K., Baldauf, J. and Wagner, M.: Equatorial Pacific productivity changes near the Eocene-Oligocene boundary, Paleoceanography, 29(9), 825–844, doi:10.1002/2014PA002656, 2014.

Moore, T. C., Kamikuri, S. ichi, Erhardt, A. M., Baldauf, J., Coxall, H. K. and Westerhold, T.: Radiolarian stratigraphy near the Eocene-Oligocene boundary, Marine Micropaleontology, 116, 50–62, doi:10.1016/j.marmicro.2015.02.002, 2015.

van Mourik, C. A. and Brinkhuis, H.: Data report: organic walled dinoflagellate cyst biostratigraphy of the latest middle to late Eocene at Hole 1053A (Subtropical Atlantic Ocean), in Proceedings of the Ocean Drilling Program. Scientific Results, vol. 171, pp. 1–25., 2000.

Van Mourik, C. A. and Brinkhuis, H.: The Massignano Eocene-Oligocene golden spike section revisited, Stratigraphy, 2(1), 13–29, 2005.

Van Mourik, C. A., Brinkhuis, H. and Williams, G. L.: Mid- to Late Eocene organic-walled dinoflagellate cysts from ODP Leg 171B, offshore Florida, Geological Society, London, Special Publications, 183(1), 225–251, doi:10.1144/GSL.SP.2001.183.01.11, 2001.

Mudge, D. C. and Bujak, J. P.: Eocene stratigraphy of the North Sea basin, Marine and Petroleum Geology, 11(2), 166–181, 1994.

Mudge, D. C. and Bujak, J. P.: An integrated stratigraphy for the Paleocene and Eocene of the North Sea, Geological Society, London, Special Publications, 101(101), 91–113, doi:10.1144/GSL.SP.1996.101.01.06, 1996.

Mudie, P., Rochon, A., Richards, K., Ferguson, S. and Warny, S.: Spiniferites cruciformis, Pterocysta cruciformis and Galeacysta etrusca: morphology and palaeoecology, Palynology,

42(sup1), 135–161, doi:10.1080/01916122.2018.1465737, 2018.

Mulitza, S., Prange, M., Stuut, J. B., Zabel, M., Von Dobeneck, T., Itambi, A. C., Nizou, J., Schulz, M. and Wefer, G.: Sahel megadroughts triggered by glacial slowdowns of Atlantic meridional overturning, Paleoceanography, 23(4), 1–11, doi:10.1029/2008PA001637, 2008.

Muller, J.: Palynology of Recent Orinoco delta and shelf sediments; reports of the Orinoco shelf expedition, Micropaleontology, 5(1), 1–32, 1959.

Murchison, D. G. and Jones, J. M.: Resinite in bituminous coals, in Advances in Organic Geochemistry, edited by U. Colombo and G. D. Hobson, pp. 49–69, Pergamon Press, Oxford., 1964.

Myers, D. J., Whitledge, G. W. and Whiles, M. R.: Evaluation of δD and δ18O as natural markers of invertebrate source environment and dispersal in the middle Mississippi River-floodplain ecosystem, River research and applications, 28(2), 135–142, doi:10.1002/rra, 2012.

Naish, T., Woolfe, K. J., Barrett, P., Wilson, G. S., Atkins, C., Bohaty, S. M., Bücker, C. J., Claps, M., Davey, F. J., Dunbar, G. B., Dunn, A. G., Fielding, C. R., Florindo, F., Hannah, M., Harwood, D., Henrys, S. A., Krissek, L. A., Lavelle, M., van Der Meer, J., McIntosh, W., Niessen, F., Passchier, S., Powell, R., Roberts, A. P., Sagnotti, L., Scherer, R. P., Strong, C. P., Talarico, F., Verosub, K. L., Villa, G., Watkins, D. K., Webb, P. N. and Wonik, T.: Orbitally induced oscillations in the East Antarctic ice sheet at the Oligocene/Miocene boundary, Nature, 413(6857), 719–23, doi:10.1038/35099534, 2001.

Nesbitt, E. A.: Changes in Shallow-Marine Faunas from the Northeastern Pacific Margin Across the, From Greenhouse to Icehouse: The Marine Eocene-Oligocene Transition, 57, 2003.

Nilsen, E. B., Anderson, L. D. and Delaney, M. L.: Regional differences in pelagic productivity in the late Eocene to early Oligocene - A comparison of southern high latitudes

and lower latitudes, Paleoceanography, 18(3), 1–11, doi:10.1029/2002PA000804, 2003.

Nocchi, M., Monechi, S., Coccioni, R., Madile, M., Monaco, P., Orlando, M., Parisi, G. and Premoli Silva, I.: The extinction of the Hantkeninidae as a marker for recognizing the Eocene–Oligocene boundary: a proposal, The Eocene–Oligocene Boundary in the Marche–Umbria Basin (Italy). International Union of Geological Sciences Commission on Stratigraphy, 249–252, 1988.

Nong, G. T., Najjar, R. G., Seidov, D. and Peterson, W. H.: Simulation of ocean temperature change due to the opening of Drake Passage, Geophysical Research Letters, 27(17), 2689–2692, doi:10.1029/1999GL011072, 2000.

Oboh-Ikuenobe, F. E. and Jaramillo, C. A.: Palynological Patterns in the Uppermost Eocene to Lower Oligocene Sedimentary, in From Greenhouse to Icehouse: The Marine Eocene-Oligocene Transition, p. 269, Columbia University Press., 2003.

Obradovich, J. D. and Dockery III, D. T.: Revisions to the geochronology of the uppermost Yazoo Formation, central Mississippi, and a new estimate for the age of the Eocene, Oligocene boundary: Journal of the Mississippi Academy of Sciences, 41(1), 54, 1996.

Obradovich, J. D., Dockery III, D. T. and Swisher III, C. C.: 40Ar-39Ar ages of bentonite beds in the upper part of the Yazoo Formation (Upper Eocene), west-central Mississippi, Mississippi Geology, 14(1), 1–9 [online] Available from: http://pubs.er.usgs.gov/publication/70018289, 1993.

Okada, H. and Honjo, S.: Distribution of Oceanic Coccolithophorids in the Pacific., Deep Sea Res, 20(4), 355–374, doi:10.1016/0011-7471(73)90059-4, 1973.

Olivarez Lyle, A. and Lyle, M. W.: Missing organic carbon in Eocene marine sediments: Is metabolism the biological feedback that maintains end-member climates?, Paleoceanography, 21(2), doi:10.1029/2005PA001230, 2006.

Olney, M. P., Scherer, R. P., Bohaty, S. M. and Harwood, D. M.: Eocene–Oligocene

paleoecology and the diatom genus Kisseleviella Sheshukova-Poretskaya from the Victoria Land Basin, Antarctica, Marine Micropaleontology, 58(1), 56–72, 2005.

Opdyke, B. N. and Wilkinson, B. H.: Surface area control of shallow cratonic to deep marine carbonate accumulation, Paleoceanography, 3(6), 685–703, 1988.

Pagani, M., Zachos, J. C., Freeman, K. H., Tipple, B. and Bohaty, S.: Atmospheric science: Marked decline in atmospheric carbon dioxide concentrations during the Paleogene, Science, 309(5734), 600–603, doi:10.1126/science.1110063, 2005.

Pagani, M., Huber, M., Liu, Z., Bohaty, S. M., Henderiks, J., Sijp, W., Krishnan, S. and DeConto, R. M.: The role of carbon dioxide during the onset of antarctic glaciation, Science, 334(6060), 1261–1264, doi:10.1126/science.1203909, 2011.

Pälike, H.: Using the GENIE Earth System Model to investigate steady-state behavior of the CCD in the Greenhouse and Icehouse equatorial Pacific, in AGU Fall Meeting Abstracts., 2012.

Pälike, H., Norris, R. D., Herrle, J. O., Wilson, P. A., Coxall, H. K., Lear, C. H., Shackleton, N. J., Tripati, A. K. and Wade, B. S.: The Heartbeat of the Oligocene Climate System, Science, 314(5807), 1894–1898, doi:10.1126/science.1133822, 2006.

Pasley, M. A. and Hazel, J. E.: Revised sequence stratigraphic interpretation of the Eocene-Oligocene boundary interval, Mississippi and Alabama, Gulf Coast Basin, USA, Journal of Sedimentary Research, 65(1), 1995.

Passchier, S., Ciarletta, D. J., Miriagos, T. E., Bijl, P. K. and Bohaty, S. M.: An antarctic stratigraphic record of stepwise ice growth through the eocene-oligocene transition, Bulletin of the Geological Society of America, 129(3–4), 318–330, doi:10.1130/B31482.1, 2017.

Pearson, P. N.: Oxygen Isotopes in Foraminifera: Overview and Historical Review, The Paleontological Society Papers, 18, 1–38, doi:10.1017/S1089332600002539, 2012.

Pearson, P. N. and Palmer, M. R.: Atmospheric carbon dioxide concentrations over the past

60 million years, Nature, 406(6797), 695–699, doi:10.1038/35021000, 2000.

Pearson, P. N., Premec-Fucek, V. and Premoli Silva, I.: Taxonomy, biostratigraphy, and phylogeny of Eocene Turborotalia, Atlas of Eocene planktonic foraminifera. Cushman Foundation Special Publication, 41, 433–460, 2006.

Pearson, P. N., McMillan, I. K., Wade, B. S., Jones, T. D., Coxall, H. K., Bown, P. R. and Lear, C. H.: Extinction and environmental change across the Eocene-Oligocene boundary in Tanzania, Geology, 36(2), 179–182, doi:10.1130/G24308A.1, 2008.

Pearson, P. N., Foster, G. L. and Wade, B. S.: Atmospheric carbon dioxide through the Eocene–Oligocene climate transition, Nature, 461(7267), 1110–1113, doi:10.1038/nature08447, 2009.

Pekar, S. F. and Christie-Blick, N.: Resolving apparent conflicts between oceanographic and Antarctic climate records and evidence for a decrease in pCO2 during the Oligocene through early Miocene (34-16 Ma), Palaeogeography, Palaeoclimatology, Palaeoecology, 260(1–2), 41–49, doi:10.1016/j.palaeo.2007.08.019, 2008.

Pekar, S. F., Christie-Blick, N., Kominz, M. A. and Miller, K. G.: Calibration between eustatic estimates from backstripping and oxygen isotopic records for the Oligocene, Geology, 30(10), 903–906, doi:10.1130/0091-7613(2002)030<0903:CBEEFB>2.0.CO;2, 2002.

Pentecost, A.: Introduction to freshwater algae, Richmond Publishing, Richmond., 1984.

Perch-Nielsen, K., Bybell, L. M., Backman, J., Madile, M., Monechi, S., Mueller, C., Nagymarosy, A. and Steurbaut, E.: Calcareous nannofossil events at the Eocene/Oligocene boundary, in Developments in Palaeontology and Stratigraphy, vol. 9, pp. 275–282, Elsevier., 1986.

Persico, D. and Villa, G.: Eocene-Oligocene calcareous nannofossils from Maud Rise and Kerguelen Plateau (Antarctica): Paleoecological and paleoceanographic implications, Marine

Micropaleontology, 52(1–4), 153–179, doi:10.1016/j.marmicro.2004.05.002, 2004.

Plancq, J., Mattioli, E., Pittet, B., Simon, L. and Grossi, V.: Productivity and sea-surface temperature changes recorded during the late Eocene-early Oligocene at DSDP Site 511 (South Atlantic), Palaeogeography, Palaeoclimatology, Palaeoecology, 407, 34–44, doi:10.1016/j.palaeo.2014.04.016, 2014.

Poag, C. W.: Foraminiferal repopulation of the late Eocene Chesapeake Bay impact crater, Micropaleontology, 58(1–2), 1–206, 2012.

Poag, C. W. and Poppe, L. J.: The Toms Canyon structure, New Jersey outer continental shelf: A possible late Eocene impact crater, Marine Geology, 145(1–2), 23–60, doi:10.1016/S0025-3227(97)00113-8, 1998.

Poag, C. W., Plescia, J. B. and Molzer, P. C.: Ancient impact structures on modern continental shelves: The Chesapeake Bay, Montagnais, and Toms Canyon craters, Atlantic margin of North America, Deep-Sea Research Part II: Topical Studies in Oceanography, 49(6), 1081–1102, doi:10.1016/S0967-0645(01)00144-8, 2002.

Pollard, D. and DeConto, R. M.: Hysteresis in Cenozoic Antarctic ice-sheet variations, Global and Planetary Change, 45(1-3 SPEC. ISS.), 9–21, doi:10.1016/j.gloplacha.2004.09.011, 2005.

Powell, A. J.: Dinoflagellate cysts of the Tertiary System, in A Stratigraphic Index of Dinoflagellate Cysts, edited by A. J. Powell, pp. 155–251, Chapman & Hall., 1992.

Powell, A. J., Dodge, J. D. and Lewis, J.: Late Neogene to Pleistocene palynological facies of the Peruvian continental margin upwelling, Leg 112, in Proceedings of the Ocean Drilling Program, Scientific Result, vol. 112, edited by E. Suess and R. von Huene, pp. 297–321, College Station, TX (Ocean Drilling Program)., 1990.

Premoli Silva, I. and Jenkins, D. G.: Decision on the Eocene-Oligocene boundary stratotype, Episodes, 16(3), 379–382, 1993.

Prescott, G. W.: Algae of the Western great lakes area: exclusive of desmids and diatoms, Cranbrook Institute of Science Bulletin., 1951.

Prescott, G. W. and Vinyard, W. C.: Ecology of Alaskan freshwater algae V. Limnology and flora of Malikpuk Lake, Transactions of the Ameri- can Microscopical Society, 84(4), 427–478, 1965.

Priddy, R. R.: Madison County Geology, Mississippi State Geological Survey., 1960.

Pross, J.: Paleo-oxygenation in tertiary epeiric seas: Evidence from dinoflagellate cysts, Palaeogeography, Palaeoclimatology, Palaeoecology, 166(3–4), 369–381, doi:10.1016/S0031-0182(00)00219-4, 2001.

Pross, J. and Brinkhuis, H.: Organic-walled dinoflagellate cysts as paleoenvironmental indicators in the Paleogene ; a synopsis of concepts, Paläontologische Zeitschrift, 79, 53–59, 2005.

Pross, J. and Schmiedl, G.: Early Oligocene dinoflagellate cysts from the Upper Rhine Graben (SW Germany): Paleoenvironmental and paleoclimatic implications, Marine Micropaleontology, 45(1), 1–24, doi:10.1016/S0377-8398(01)00046-9, 2002.

Pross, J., Houben, A. J. P., van Simaeys, S., Williams, G. L., Kotthoff, U., Coccioni, R., Wilpshaar, M. and Brinkhuis, H.: Umbria-Marche revisited: A refined magnetostratigraphic calibration of dinoflagellate cyst events for the Oligocene of the Western Tethys, Review of Palaeobotany and Palynology, 158(3–4), 213–235, doi:10.1016/j.revpalbo.2009.09.002, 2010.

Prothero, D. R.: The Eocene-Oligocene Transition: Paradise Lost, Columbia University Press., 1994a.

Prothero, D. R.: The Late Eocene-Oligocene Extinctions, Annual Review Earth Planet, 22, 145–165, 1994b.

Pusz, A. E., Miller, K. G., Wright, J. D., Katz, M. E., Cramer, B. S. and Kent, D. V: Stable

isotopic response to late Eocene extraterrestrial impacts, in Eos, Transactions, American Geophysical Union, vol. 88, pp. 1–13., 2009.

Quaijtaal, W. and Brinkhuis, H.: Pentadinium alabamensis: A new, unusual dinoflagellate from the early Oligocene of the Gulf Coast, Alabama, USA, Review of Palaeobotany and Palynology, 175, 47–54, doi:10.1016/j.revpalbo.2012.03.002, 2012.

Rabosky, D. L. and Sorhannus, U.: Diversity dynamics of marine planktonic diatoms across the Cenozoic, Nature, 457(7226), 183–186, doi:10.1038/nature07435, 2009.

Rage, J.-C.: The Amphibians and Reptiles at the Eocene-Oligocene Transition in Western Europe: An Outline of the Faunal Alterations., in Developments in Palaeontology and Stratigraphy, vol. 9, pp. 309–310, Elsevier., 1986.

Rahmstorf, S.: Ocean circulation and climate during the past 120,000 years, Nature, 419(6903), 207–214, doi:10.1038/nature01090, 2002.

Raine, R., White, M. and Dodge, J. D.: The summer distribution of net plankton dinoflagellates and their relation to water movements in the NE Atlantic Ocean, west of Ireland, Journal of Plankton Research, 24(11), 1131–1147, doi:10.1093/plankt/24.11.1131, 2002.

Rau, G. H., Riebesell, U. and Wolf-Gladrow, D.: A model of photosynthetic 13C fractionation by marine phytoplankton based on diffusive molecular CO2 uptake, Marine Ecology Progress Series, 133, 275–285, 1996.

Raup, D. M. and Sepkoski, J. J.: Mass extinctions in the marine fossil record, Science, 215(4539), 1501–1503, 1982.

Ravizza, G. and Peucker-Ehrenbrink, B.: The marine 187Os/188Os record of the Eocene-Oligocene transition: The interplay of weathering and glaciation, Earth and Planetary Science Letters, 210(1–2), 151–165, doi:10.1016/S0012-821X(03)00137-7, 2003.

Rea, D. K. and Lyle, M. W.: Paleogene calcite compensation depth in the eastern subtropical

Pacific: Answers and questions, Paleoceanography, 20(1), 1–19, doi:10.1029/2004PA001064, 2005.

Reichart, G. J. and Brinkhuis, H.: Late Quaternary Protoperidinium cysts as indicators of paleoproductivity in the northern Arabian Sea, Marine Micropaleontology, 49(4), 303–315, doi:10.1016/S0377-8398(03)00050-1, 2003.

Reynolds, C. S.: Phytoplankton assemblages and their periodicity in stratifying lake systems, Holarctic Ecology, 3(3), 141–159, 1980.

Reynolds, C. S.: The ecology of freshwater phytoplankton, Cambridge University Press., 1984.

Reynolds, C. S. and Allen, S. E.: Changes in the phytoplankton of Oak Mere, following the introduction of base-rich water, British Phycological Bulletin, 3(3), 451–462, doi:10.1080/00071616800650041, 1968.

Ridgwell, A. and Edwards, U.: Geological carbon sinks., 2009.

Robert, C. and Kennett, J. P.: Antarctic continental weathering changes during Eocene-Oligocene cryosphere expansion: Clay mineral and oxygen isotope evidence, Geology, 25(7), 587–590, doi:10.1130/0091-7613(1997)025<0587:ACWCDE>2.3.CO;2, 1997.

Robinson, E.: Zoning the White Limestone Group of Jamaica using larger foraminiferal genera: a review and proposal, Cainozoic Research, 3(1–2), 39-75., 2004.

Rohling, E. J., Sluijs, A., Dijkstra, H. A., Köhler, P., Van De Wal, R. S. W., Von Der Heydt, A. S., Beerling, D. J., Berger, A., Bijl, P. K., Crucifix, M., Deconto, R., Drijfhout, S. S., Fedorov, A., Foster, G. L., Ganopolski, A., Hansen, J., Hönisch, B., Hooghiemstra, H., Huber, M., Huybers, P., Knutti, R., Lea, D. W., Lourens, L. J., Lunt, D., Masson-Demotte, V., Medina-Elizalde, M., Otto-Bliesner, B., Pagani, M., Pälike, H., Renssen, H., Royer, D. L., Siddall, M., Valdes, P., Zachos, J. C. and Zeebe, R. E.: Making sense of palaeoclimate sensitivity, Nature, 491(7426), 683–691, doi:10.1038/nature11574, 2012.

Rose, K. C., Ferraccioli, F., Jamieson, S. S. R., Bell, R. E., Corr, H., Creyts, T. T., Braaten, D., Jordan, T. A., Fretwell, P. T. and Damaske, D.: Early East Antarctic Ice Sheet growth recorded in the landscape of the Gamburtsev Subglacial Mountains, Earth and Planetary Science Letters, 375, 1–12, doi:10.1016/j.epsl.2013.03.053, 2013.

Rossignol, M.: Analyse pollinique de sédiments marins quaternaires en Israël. 1. Sediments recents, Pollen et Spores, 3, 303–324, 1961.

Rossignol, M.: Sedimentation palynologique dans le domaine marin quaternaire de Palestine: etude de pal eo-environnement, Museum National d'Histoire Naturelle, Paris., 1969.

Rothwell, R. G.: Twenty years of XRF core scanning marine sediments: what do geochemical proxies tell us?, in Micro-XRF Studies of Sediment Cores, pp. 25–102, Springer., 2015.

Rymer, E.: Impact Events and Climate Change in the Late Eocene and Early Oligocene, University of Birmingham., 2019.

Salamy, K. A. and Zachos, J. C.: Latest Eocene - early Oligocene climate change and southern Ocean fertility: inferences from sediment accumulation and stable isotope data, Palaeogeogr. Palaeoclimatol. Palaeoecol., 145, 61–77, doi:10.1016/S0031-0182(98)00093-5, 1999.

Sarmiento, J. L. and Gruber, N.: Sinks for anthropogenic carbon, Physics Today, 55(8), 30, doi:10.1063/1.1510279, 2002.

Schellenberg, S. A.: Ecological and evolutionary response of deep-sea ostracodes to the Eocene-Oligocene transition: High-resolution data from ODP Site 744, Kerguelen Plateau, in GSA Annual Meeting Abstracts with Programs, p. A-286., 1998.

Scher, H. D. and Martin, E. E.: Timing and Climatic Consequences of the Opening of Drake Passage, Science, 312(5772), 428–430, doi:10.1126/science.1120044, 2006.

Scher, H. D., Bohaty, S. M., Zachos, J. C. and Delaney, M. L.: Two-stepping into the icehouse : East Antarctic weathering during progressive ice-sheet expansion at the Eocene –

Oligocene transition, Geology, 39(4), 383–386, doi:10.1130/G31726.1, 2011.

Schouten, S., Eldrett, J., Greenwood, D. R., Harding, I., Baas, M. and Damsté, J. S. S.: Onset of long-term cooling of Greenland near the Eocene-Oligocene boundary as revealed by branched tetraether lipids, Geology, 36(2), 147–150, 2008.

Shackleton, N. J. and Kennett, J. P.: Paleotemperature history of the Cenozoic and the initiation of Antarctic glaciation: oxygen and carbon isotope analyses in DSDP Sites 277,279, and 281, Initial Reports of Deep Sea Drilling Project, 29, 743–756, 1975.

Shackleton, N. J., Backman, J., Zimmerman, H., Kent, D. V., Hall, M. A., Roberts, D. G., Schnitker, D., Baldauf, J. G., Desprairies, A., Homrighausen, R., Huddleston, P., Keene, J. B., Kaltenback, A. J., Krumsiek, K. A. O., Morton, A. C., Murray, J. W., Westberg-Smith, J. and We: Oxygen isotope calibration of the onset of ice-rafting and history of glaciation in the North Atlantic region, Nature, 307(February), 620–623, 1984.

Sheldon, N. D.: Nonmarine records of climatic change across the Eocene-Oligocene transition, in The Late Eocene Earth—Hothouse, Icehouse, and Impacts, vol. 452, edited by C. Koeberl and A. Montanari, pp. 241–248, The Geological Society of America., 2009.

Sijp, W. P. and England, M. H.: Effect of the drake passage throughflow on global climate, Journal of Physical Oceanography, 34(5), 1254–1266, doi:10.1175/1520-0485(2004)034<1254:EOTDPT>2.0.CO;2, 2004.

van Simaeys, S., Brinkhuis, H., Pross, J., Williams, G. L. and Zachos, J. C.: Arctic dinoflagellate migrations mark the strongest Oligocene glaciations, Geology, 33(9), 709–712, doi:10.1130/G21634.1, 2005.

Skinner, L.: A long view on climate sensitivity, Science, 337(6097), 917–919, doi:10.1126/science.1224011, 2012.

Śliwińska, K. K. and Heilmann-Clausen, C.: Early Oligocene cooling reflected by the dinoflagellate cyst Svalbardella cooksoniae, Palaeogeography, Palaeoclimatology,

Palaeoecology, 305(1–4), 138–149, doi:10.1016/j.palaeo.2011.02.027, 2011.

Śliwińska, K. K., Abrahamsen, N., Beyer, C., Brünings-Hansen, T., Thomsen, E., Ulleberg, K. and Heilmann-Clausen, C.: Bio- and magnetostratigraphy of Rupelian-mid Chattian deposits from the Danish land area, Review of Palaeobotany and Palynology, 172, 48–69, doi:10.1016/j.revpalbo.2012.01.008, 2012.

Sluijs, A., Pross, J. and Brinkhuis, H.: From greenhouse to icehouse; organic-walled dinoflagellate cysts as paleoenvironmental indicators in the Paleogene, Earth-Science Reviews, 68(3–4), 281–315, doi:10.1016/j.earscirev.2004.06.001, 2005.

Squires, R. L.: Turnovers in marine gastropod faunas during the Eocene-Oligocene transition, west coast of the United States, From Greenhouse to Icehouse: The Marine Eocene–Oligocene Transition. Columbia University Press, New York, 14–35, 2003.

Stehlin, H. G.: Remarques sur les faunules de mammifères des couches éocènes et oligocènes du Bassin de Paris, Bull Soc Géol France, 19, 488–520, 1909.

Stickley, C. E., Brinkhuis, H., McGonigal, K. L., Chaproniere, G. C. H., Fuller, M., Kelly, D. C., Nürnberg, D., Pfuhl, H. A., Schellenberg, S. A., Schoenfeld, J., Suzuki, N., Touchard, Y., Wei, W., Williams, G. L., Lara, J. and Stant, S. A.: Late Cretaceous-Quaternary Biomagnetostratigraphy of ODP Sites 1168, 1170, 1171, and 1172, Tasmanian Gateway, Proceedings of the Ocean Drilling Program, Scientific Results, 189(August), 1–57 [online] Available from: http://www-odp.tamu.edu/publications/189_SR/VOLUME/CHAPTERS/111.PDF, 2004a.

Stickley, C. E., Brinkhuis, H., Schellenberg, S. A., Sluijs, A., Röhl, U., Fuller, M., Grauert, M., Huber, M., Warnaar, J. and Williams, G. L.: Timing and nature of the deepening of the Tasmanian Gateway, Paleoceanography, 19(4), n/a-n/a, doi:10.1029/2004PA001022, 2004b.

Stover, L. E. and Williams, G. L.: Morphology and stratigraphy of the the Paleogene dinoflagellate genus Areosphaeridium Eaton, 1971, in Proc. 7th Int. Palynol. Conf., Brisbane

(Abstracts), p. 157., 1988.

Stover, L. E., Brinkhuis, H., Damassa, S. P., De Verteuil, L., Helby, R. J., Monteil, E., Partridge, A. D., Powell, A. J., Riding, J. B. and Smelror, M.: Mesozoic-Tertiary dinoflagellates, acritarchs and prasinophytes, Palynology: principles and applications, 2(January), 641–750, 1996.

Sulaiman, N. B.: Late Eocene palaeoenvironment and palaeoclimate of the US Gulf Coast, University of Birmingham., 2017.

Tagle, R. and Claeys, P.: Comet or asteroid shower in the late eocene?, Science, 305(5683), 492, doi:10.1126/science.1098481, 2004.

Taylor, R. E. and Aitken, M. J.: Chronometric Dating in Archaeology, edited by R. E. Taylor and M. J. Aitken, Springer US, Boston, MA., 1997.

Tew, B. H.: Sequence stratigraphy, lithofacies relationships, and paleogeography of Oligocene strata in southeastern Mississippi and southwestern Alabama, Geological Survey of Alabama, Stratigraphy and Paleontology Division., 1992.

Tew, B. H. and Mancini, E. A.: An Integrated Stratigraphic Method for Paleogeographic Reconstruction: Examples from the Jackson and Vicksburg Groups of the Eastern Gulf Coastal Plain, Palaios, 10(2), 133–153, doi:10.2307/3515179, 1995.

Thomas, E. and Gooday, A. J.: Cenozoic deep-sea benthic foraminifers: Tracers for changes in oceanic productivity?, Geology, 24(4), 355–358, doi:10.1130/0091-7613(1996)024<0355:CDSBFT>2.3.CO;2, 1996.

Thomsen, E., Abrahamsen, N., Heilmann-Clausen, C., King, C. and Nielsen, O. B.: Middle Eocene to earliest Oligocene development in the eastern North Sea Basin: Biostratigraphy, magnetostratigraphy and palaeoenvironment of the Kysing-4 borehole, Denmark, Palaeogeography, Palaeoclimatology, Palaeoecology, 350–352, 212–235, doi:10.1016/j.palaeo.2012.06.034, 2012.

Thornalley, D. J. R., Oppo, D. W., Ortega, P., Robson, J. I., Brierley, C. M., Davis, R., Hall, I. R., Moffa-Sanchez, P., Rose, N. L., Spooner, P. T., Yashayaev, I. and Keigwin, L. D.: Anomalously weak Labrador Sea convection and Atlantic overturning during the past 150 years, Nature, 556(7700), 227–230, doi:10.1038/s41586-018-0007-4, 2018.

Tindall, J., Flecker, R., Valdes, P., Schmidt, D. N., Markwick, P. and Harris, J.: Modelling the oxygen isotope distribution of ancient seawater using a coupled ocean-atmosphere GCM: Implications for reconstructing early Eocene climate, Earth and Planetary Science Letters, 292(3–4), 265–273, doi:10.1016/j.epsl.2009.12.049, 2010.

Toggweiler, J. R. and Bjornsson, H.: Drake passage and palaeoclimate, Journal of Quaternary Science, 15(4), 319–328, doi:10.1002/1099-1417(200005)15:4<319::AID-JQS545>3.0.CO;2-C, 2000.

Toon, O. B., Zahnle, K., Turco, R. P. and Covey, C.: Environmental perturbations caused by impacts, in Hazards due to comets and asteroids, edited by T. Gehrels, pp. 791–826, University of Arizona Press, Tucson., 1994.

Traverse, A.: Paleopalynology, Springer Netherlands, Dordrecht., 2007.

Tripati, A. K., Eagle, R. A., Morton, A., Dowdeswell, J. A., Atkinson, K. L., Bahé, Y., Dawber, C. F., Khadun, E., Shaw, R. M. H., Shorttle, O. and Thanabalasundaram, L.: Evidence for glaciation in the Northern Hemisphere back to 44 Ma from ice-rafted debris in the Greenland Sea, Earth and Planetary Science Letters, 265(1–2), 112–122, doi:10.1016/j.epsl.2007.09.045, 2008.

Tripati, A. K., Roberts, C. D. and Eagle, R. A.: Coupling of CO2 and Ice sheet stability over major climate transitions of the last 20 million years, Science, 326(5958), 1394–1397, doi:10.1126/science.1178296, 2009.

Tyler, M. A., Coats, D. W. and Anderson, D. M.: Encystment in a dynamic environment: deposition of dinoflagellate cysts by a frontal convergence, Marine Ecology Progress Series,

163–178, 1982.

Tyson, R. V: Sedimentary Organic Matter, Springer Netherlands, Dordrecht., 1995.

Vahlenkamp, M., Niezgodzki, I., De Vleeschouwer, D., Bickert, T., Harper, D., Kirtland Turner, S., Lohmann, G., Sexton, P., Zachos, J. and Pälike, H.: Astronomically paced changes in deep-water circulation in the western North Atlantic during the middle Eocene, Earth and Planetary Science Letters, 484, 329–340, doi:10.1016/j.epsl.2017.12.016, 2018a.

Vahlenkamp, M., Niezgodzki, I., De Vleeschouwer, D., Lohmann, G., Bickert, T. and Pälike, H.: Ocean and climate response to North Atlantic seaway changes at the onset of long-term Eocene cooling, Earth and Planetary Science Letters, 498, 185–195, doi:10.1016/j.epsl.2018.06.031, 2018b.

Varol, O.: Palaeogene, Calcareous nannofossil biostratigraphy, 200–224, 1998.

de Vernal, A. and Giroux, L.: Distribution of organic walled microfossils in Recent sediments from the Estuary and Gulf of St. Lawrence: some aspects of the organic matter fluxes, Canadian Special Publication of Fisheries and Aquatic Sciences, 113(January), 189–199, 1991.

de Vernal, A. and Marret, F.: Chapter Nine Organic-Walled Dinoflagellate Cysts: Tracers of Sea-Surface Conditions, Developments in Marine Geology, 1(07), 371–408, doi:10.1016/S1572-5480(07)01014-7, 2007.

de Vernal, A., Eynaud, F., Henry, M., Limoges, A., Londeix, L., Matthiessen, J., Marret, F., Pospelova, V., Radi, T., Rochon, A., Van Nieuwenhove, N. and Zaragosi, S.: Distribution and (palaeo)ecological affinities of the main spiniferites taxa in the mid-high latitudes of the Northern Hemisphere, Palynology, 42(sup1), 182–202, doi:10.1080/01916122.2018.1465730, 2018.

De Vernal, A., Rochon, A., Turon, J.-L. and Matthiessen, J.: Organic-walled dinoflagellate cysts: palynological tracers of sea-surface conditions in middle to high latitude marine

environments, Geobios, 30(7), 905–920, 1997.

Vieira, M., Mahdi, S. and Osterloff, P.: New Early Paleocene (Danian) dinoflagellate cyst species from the Ormen Lange Field, Møre Basin, Norwegian Continental Shelf, Palynology, 42(2), 180–198, doi:10.1080/01916122.2017.1314390, 2018.

Villa, G., Fioroni, C., Pea, L., Bohaty, S. and Persico, D.: Middle Eocene-late Oligocene climate variability: Calcareous nannofossil response at Kerguelen Plateau, Site 748, Marine Micropaleontology, 69(2), 173–192, doi:10.1016/j.marmicro.2008.07.006, 2008.

Vonhof, H. B., Smit, J., Brinkhuis, H., Montanari, A. and Nederbragt, A. J.: Global cooling accelerated by early late Eocene impacts?, Geology, 28(8), 687–690, doi:10.1130/0091-7613(2000)28<687:GCABEL>2.0.CO, 2000.

Wade, B. S. and Pearson, P. N.: Planktonic foraminiferal turnover, diversity fluctuations and geochemical signals across the Eocene/Oligocene boundary in Tanzania, Marine Micropaleontology, 68(3–4), 244–255, doi:10.1016/j.marmicro.2008.04.002, 2008.

Wade, B. S., Pearson, P. N., Berggren, W. A. and Pälike, H.: Review and revision of Cenozoic tropical planktonic foraminiferal biostratigraphy and calibration to the geomagnetic polarity and astronomical time scale, Earth-Science Reviews, 104(1–3), 111–142, doi:10.1016/j.earscirev.2010.09.003, 2011.

Wade, B. S., Houben, A. J. P., Quaijtaal, W., Schouten, S., Rosenthal, Y., Miller, K. G., Katz, M. E., Wright, J. D. and Brinkhuis, H.: Multiproxy record of abrupt sea-surface cooling across the Eocene-Oligocene transition in the Gulf of Mexico, Geology, 40(2), 159–162, doi:10.1130/G32577.1, 2012.

Wall, D., Dale, B., Lohmann, G. P. and Smith, W. K.: The environmental and climatic distribution of dinoflagellate cysts in modern marine sediments from regions in the North and South Atlantic Oceans and adjacent seas, Marine micropaleontology, 2, 121–200, 1977.

Westerhold, T., Röhl, U., Pälike, H., Wilkens, R., Wilson, P. A. and Acton, G.: Orbitally

tuned timescale and astronomical forcing in the middle Eocene to early Oligocene, Climate of the Past, 10(3), 955–973, doi:10.5194/cp-10-955-2014, 2014.

White, A. W. and Lewis, C. M.: Resting cysts of the toxic, red tide dinoflagellate Gonyaulax excavate in Bay of Fundy sediments, Canadian Journal of Fisheries and Aquatic Sciences, 39(8), 1185–1194, 1982.

Whitehead, J. M.: Cenozoic history of antarctic benthic diatoms, Alcheringa, 29(1), 151–169, doi:10.1080/03115510508619565, 2005.

Wild, M., Folini, D., Schär, C., Loeb, N., Dutton, E. G. and König-Langlo, G.: The global energy balance from a surface perspective, Climate Dynamics, 40(11–12), 3107–3134, doi:10.1007/s00382-012-1569-8, 2013.

Williams, G. L.: Dinoflagellate and spore stratigraphy of the Mesozoic-Cenozoic, offshore eastern Canada, Geological Survey of Canada, Paper, 74(30), 2, 1975.

Williams, G. L.: Dinocysts: their classification, biostratigraphy and palaeoecology, Oceanic Micropalaeontology. Academic Press, London, 2, 1231–1325, 1977.

Williams, G. L.: Morphology and stratigraphic ranges of selected Mesozoic-Cenozoic dinoflagellate taxa in the Northern Hemisphere, Geol. Surv. Can. Pap., 92, 137, 1993.

Williams, G. L. and Bujak, J. P.: Distribution patterns of some North Atlantic Cenozoic dinoflagellate cysts, Marine Micropaleontology, 2(C), 223–233, doi:10.1016/0377-8398(77)90012-3, 1977.

Williams, G. L. and Bujak, J. P.: Mesozoic and Cenozoic Dinoflagellates, in Plankton Stratigraphy: Volume 2, Radiolaria, Diatoms, Silicoflagellates, Dinoflagellates and Ichthyoliths, edited by H. M. Bolli, J. B. Saunders, and K. Perch-Nielsen, pp. 847–964, Cambridge Earth Science Series., 1985.

Williams, G. L. and Manum, S. B.: Oligocene – early Miocene dinocyst stratigraphy of Hole 985A (Norwegian Sea), Proceedings of the Ocean Drilling Program, Scientific results, 162,

99–109, 1999.

Williams, G. L., Brinkhuis, H., Pearce, M. A., Fensome, R. A. and Weegink, J. W.: Southern Ocean and global dinoflagellate cyst events compared: index events for the Late Cretaceous–Neogene, in Proceedings of the Ocean Drilling Program, Scientific Results, vol. 189, pp. 1–98., 2004.

Williams, G. L., Fensome, R. A. and Macrae, R. A.: THE LENTIN AND WILLIAMS INDEX OF FOSSIL DINOFLAGELLATES 2017 EDITION AASP Contributions Series Number 48, American Association of Stratigraphic Palynologists Contributions Series, 48(48), 1–1097, 2017.

Wilpshaar, M., Santarelli, A., Brinkhuis, H. and Visscher, H.: Dinoflagellate cysts and mid-Oligocene chronostratigraphy in the central Mediterranean region, Journal of the Geological Society, 153(4), 553–561, doi:10.1144/gsjgs.153.4.0553, 1996.

Wilson, G. J.: Paleocene and Eocene dinoflagellate cysts from Waipawa, Hawkes Bay, New Zealand, New Zealand Geological Survey., 1988.

Winter, A., Jordon, R. W. and Rot, P. H.: Biogeography of living coccolithophores in ocean waters, in Coccolithophores, edited by A. Winter and W. G. Siesser, pp. 161–177, Cambridge University Press, Cambridge., 1994.

Wolfe, J. A.: Climatic, floristic and vegetational changes near the Eocene/Oligocene boundary in North America, Eocene-Oligocene climatic and biotic evolution, 1992.

Wolfe, J. A.: Tertiary climatic changes at middle latitudes of western North America, Palaeogeography, Palaeoclimatology, Palaeoecology, 108(3–4), 195–205, 1994.

Wolfe, J. A.: Paleoclimatic estimates from Tertiary leaf assemblages, Annu. Reviews Earth Planetary Science, 23, 119–142, 1995.

Xiao, G. Q., Abels, H. A., Yao, Z. Q., Dupont-Nivet, G. and Hilgen, F. J.: Asian aridification linked to the first step of the Eocene-Oligocene climate Transition (EOT) in obliquity-

dominated terrestrial records (Xining Basin, China), Climate of the Past, 6(4), 501–513, doi:10.5194/cp-6-501-2010, 2010.

Yamaguchi, T., Norris, R. D. and Dockery, D. T.: Shallow-marine ostracode turnover during the Eocene-Oligocene transition in Mississippi, the Gulf Coast Plain, USA, Marine Micropaleontology, 106, 10–21, doi:10.1016/j.marmicro.2013.11.003, 2014.

Yancey, T. E., Elsik, W. C. and Sancay, R. H.: The palynological record of late Eocene climate change, northwest Gulf of Mexico, From Greenhouse to Icehouse: The Marine Eocene–Oligocene Transition: Columbia University Press, New York, 252–268, 2003.

Zachos, J., Pagani, M., Sloan, L., Thomas, E. and Billups, K.: Trends, Rhythms, and Aberrations in Global Climate 65 Ma to Present, Science, 292(5517), 686–693, doi:10.1126/science.1059412, 2001.

Zachos, J. C. and Kump, L. R.: Carbon cycle feedbacks and the initiation of Antarctic glaciation in the earliest Oligocene, Global and Planetary Change, 47(1), 51–66, doi:10.1016/j.gloplacha.2005.01.001, 2005.

Zachos, J. C., Breza, J. R., Wise, S. W. and Cruz, S.: Early Oligocene ice-sheet expansion on Antarctica: Stable isotope and sedimentological evidence from Kerguelen Plateau, southern Indian Ocean, Geology, 20(6), 569–573, doi:10.1130/0091-7613(1992)020<0569, 1992.

Zachos, J. C., Stott, L. D. and Lohmann, K. C.: Evolution of Early Cenozoic marine temperatures, Paleoceanography, 9(2), 353–387, doi:10.1029/93PA03266, 1994.

Zachos, J. C., Quinn, T. M. and Salamy, K. A.: High-resolution (104 years) deep-sea foraminiferal stable isotope records of the Eocene-Oligocene climate transition, Paleoceanography, 11(3), 251–266, doi:10.1029/96PA00571, 1996.

Zachos, J. C., Opdyke, B. N., Quinn, T. M., Jones, C. E. and Halliday, A. N.: Early cenozoic glaciation, antarctic weathering, and seawater 87 Srr 86 Sr: is there a link?, Chemical Geology, 161, 165–180 [online] Available from: www.elsevier.comrlocaterchemgeo, 1999.

Zachos, J. C., Dickens, G. R. and Zeebe, R. E.: An early Cenozoic perspective on greenhouse warming and carbon-cycle dynamics, Nature, 451(7176), 279–283, doi:10.1038/nature06588, 2008.

Zanazzi, A., Kohn, M. J., MacFadden, B. J. and Terry, D. O.: Large temperature drop across the Eocene-Oligocene transition in central North America, Nature, 445(7128), 639–642, doi:10.1038/nature05551, 2007.

Zeigler, J. M. and Whitledge, G. W.: Otolith trace element and stable isotopic compositions differentiate fishes from the Middle Mississippi River, its tributaries, and floodplain lakes, Hydrobiologia, 661(1), 289–302, doi:10.1007/s10750-010-0538-7, 2011.

Zevenboom, D., Brinkhuis, H. and Visscher, H.: Dinoflagellate cysts palaeoenvironmental analysis of the Oligocene/Miocene transition in northwest and central Italy, in Gior. Geol., vol. 56, edited by R. Coccioni, A. Montanari, and G. S. Odin, pp. 155–169., 1994.

Zhang, Y. G., Pagani, M., Liu, Z., Bohaty, S. M. and Deconto, R.: A 40-million-year history of atmospheric CO 2, Philosophical Transactions of the Royal Society A: Mathematical, Physical and Engineering Sciences, 371(2001), doi:10.1098/rsta.2013.0096, 2013.

Zickfeld, K., Eby, M. and Weaver, A. J.: Carbon-cycle feedbacks of changes in the Atlantic meridional overturning circulation under future atmospheric CO2, Global Biogeochemical Cycles, 22(3), 1–14, doi:10.1029/2007GB003118, 2008.

van der Zwaan, G. J., Jorissen, F. J. and de Stigter, H. C.: The depth dependency of planktonic/benthic foraminiferal ratios: Constraints and applications, Marine Geology, 95(1), 1–16, doi:10.1016/0025-3227(90)90016-D, 1990.